UNIVERSIDAD NACIONAL AUTÓNOMA DE MÉXICO
POSGRADO EN CIENCIAS FÍSICAS
INSTITUTO DE FÍSICA

Large-distance behavior of the density-density correlation functions and pair wave function throughout the BEC-BCS crossover

TESIS
QUE PARA OPTAR POR EL GRADO DE

Doctor en Ciencias (Física)

PRESENTA:

Juan Carlos Obeso Jureidini

Tutor principal
Dr. Víctor Manuel Romero Rochín
Instituto de Física

Miembros del comité tutor
Dra. Rosario Paredes Gutiérrez
Instituto de Física

Dr. Octavio Héctor Castaños Garza
Instituto de Ciencias Nucleares

Ciudad Universitaria, CD. MX., agosto de 2023

1. Datos del alumno
   Obeso
   Jureidini
   Juan Carlos
   UNAM
   Instituto de Física

2. Datos del tutor principal
   Doctor
   Víctor Manuel
   Romero
   Rochín

3. Datos de tutora 1
   Doctora
   Rosario
   Paredes
   Gutiérrez

4. Datos de tutor 2
   Doctor
   Octavio Héctor
   Castaños
   Garza

5. Datos del sinodal 1
   Doctor
   Víctor Manuel
   Romero
   Rochín

6. Datos del sinodal 2
   Doctor
   Chumin
   Wang
   Chen

7. Datos del sinodal 3
   Doctor
   Santiago Francisco
   Caballero
   Benítez

8. Datos del sinodal 4
   Doctor
   Miguel Angel
   Bastarrachea
   Magnani

9. Datos del sinodal 5
   Doctor
   Freddy Jackson
   Poveda
   Cuevas

Con mucho cariño a mi mamá, Laila,
y a mi hermano gemelo, Víctor.

Agradecimientos

Siempre estaré muy agradecido con el Dr. Víctor Manuel Romero Rochín por todo el apoyo que me brindó para mi desarrollo académico. Agradezco todas sus enseñanzas y discusiones que nos llevaron por buen camino. Realmente admiro la profundidad con la que aborda las actividades de investigación, desde plantemientos de problemas hasta los estilos de comunicación de ideas. Aprecio su actitud de entusiasmo y optimismo durante la investigación. También quiero destacar el gran esfuerzo que hizo para que mantengamos el ritmo de trabajo durante la pandemia.

Un agradecimiento especial a la Dra. Rosario Paredes Gutiérrez, por su apoyo y comentarios que han tenido un buen impacto en mi desarrollo académico. Aprecio mucho el intercambio de ideas que me ha brindado. Admiro su actitud de compromiso y entrega en las actividades académicas.

Agradezco al Dr. Gustavo Alexis Domínguez Castro por su amistad y por siempre contagiarme su buena actitud académica. Agradezco las inumerables discusiones de física, de las cuales aprendí mucho.

Agradezco al Dr. Octavio Héctor Castaños Garza por sus comentarios y observaciones al revisar este trabajo.

Agradezco al Dr. Chumin Wang Chen por la revisión de este trabajo y por ayudarme a aclarar algunos conceptos.

Agradezco al Dr. Santiago Francisco Caballero Benítez por la revisión de este trabajo y por las pláticas de Física que me han permitido tener otro enfoque. Agradezco la oportunidad de ser su ayudante de profesor.

Agradezco al Dr. Miguel Angel Bastarrachea Magnani por la revisión de este trabajo y por las observaciones constructivas, además de sus buenas preguntas.

Agradezco al Dr. Freddy Jackson Poveda Cuevas por la revisión de este trabajo y por compartirme su experiencia y puntos de vista en el campo de la investigación.

Agradezco a mi mamá y a mi hermano por su apoyo emocional y cariño, por siempre escucharme y aconsejarme, por todas las cosas que hemos vivido. ¡Les quiero mucho!

Agradezco a mis colegas y colaboradores cercanos: Eleazar Neri, Christian Madroñero, Manuel Mendoza, Ignacio Reyes, Roberto Zamora, Luis Antonio González, Grover Andrade, Daniela Olascoaga, Saúl Sánchez.

Un agradecimiento especial al Dr. Arturo Camacho Guardian por el apoyo en las etapas finales de mis estudios de doctorado.

Un agradecimiento a mis amistades y personas que me acompañaron durante el doctorado, principalmente del Instituto de Física, por su tiempo y pláticas. En especial a (una disculpa si

omito a alguien):
León García, Izamar Tapia, Rodolfo Ferro, Gustavo Ávalos, Mitzi Ordóñez, Alain Acevedo, Yadira Salazar, Jorge Acosta, Gabriel Mercado, Osmany González, Fabián Camas, Darby Paez, Dante Gómez, Brahyam Ríos, Alejandro Cásares, Ulises Barajas, Jorge Seman, Eduardo Padilla, Diego Hernández, Alejandra del Río, Oscar Gutiérrez, Ernesto Alba, Miguel Hernández, Julio Romo, Brandon Reyes, Leonardo Navarro, Jaspe Martínez, Katherin Eraso, Saúl Herrera, Elias Andrade.

Agradezco a mis amistades de la prepa (y secundaria) por las pláticas y su invaluable amistad: Luis Escalera, Jorge Name, Oscar Hernández y Mayra Castro.

Agradezco al CONACYT por la beca de posgrado, al Proyecto CONACYT 255573 y también al proyecto UNAM PAPIIT-IN105217, UNAM PAPIIT-IN108620, UNAM PAPIIT-IN117623.

Agradezco al Posgrado en Ciencias Físicas y a la UNAM por brindar un ambiente académico favorable para el desarrollo científico. Al personal del Posgrado en Ciencias Físicas y del Instituto de Física.

Abstract

In this thesis we investigate the ground state properties of an homogeneous balanced Fermi gas of two components. We describe an ultracold atomic gas where there is a unique experimental control over the effective interaction between fermions of different component by means of a magnetic field. The modulation of the interaction allows us to obtain a crossover between a Bardeen-Cooper-Schrieffer (BCS) state and a Bose-Einstein condensate state (BEC). As an approach we consider the mean-field method, which includes the BCS-Leggett variational method. We consider three cases: two-dimensional case with a contact interaction, three-dimensional case with a contact interaction, and three-dimensional case with finite-range interactions. For these three cases we analyze the spatial structure contained in three functions: density-density correlation function between same components, density-density correlation function between different components, and the variational pair wave function. The main contribution of this work is to analyze their large-distance behavior, which is given by an exponential decay that modulates an oscillatory behavior. Importantly, we found that the exponential decay is determined by a binding energy that arises as a many-body effect. For the three-dimensional case we found that the relation between the large-distance exponential decay and the binding energy is universal, in the sense that it does not depend on the details of the interaction between fermions within the mean-field approach. The large-distance exponential decay determines in an original way the characteristic size of local density fluctuations and the size of pairs of fermions that describe the ground state. For the two-dimensional case we present analytical expressions for the density-density correlation functions, which explicitly exhibit the spatial structure of the gas.

Resumen

En esta tesis se investigan las propiedades del estado base de un gas de Fermi de dos componentes homogéneo y balanceado. Se describe un gas atómico ultrafrío donde hay un control experimental único sobre la interacción efectiva entre fermiones de componente distinta por medio de un campo magnético. La modulación de la interacción permite obtener un cruce entre un estado Bardeen-Cooper-Schrieffer (BCS) y un estado de condensado de Bose-Einstein (BEC). Como aproximación se considera el método de campo medio, que incluye el método variacional de BCS-Leggett. Se consideran tres casos: caso dos dimensional con interacción de contacto, caso tres dimensional con interacción de contacto y caso tres dimensional con interacciones de alcance finito. Para los tres casos se analiza la estructura espacial contenida en tres funciones: función de correlación densidad-densidad entre componentes iguales, función de correlación densidad-densidad entre componentes distintas y función de onda variacional del par. La contribución principal de este trabajo es el análisis del comportamiento a grandes distancias, que está dado por un decaimiento exponencial que modula un comportamiento oscilatorio. Importantemente, se encontró que el decaimiento

exponencial está determinado por una energía de amarre que surge como un efecto de muchos cuerpos. Para el caso tres dimensional se encontró que la relación entre el decaimiento a grandes distancias y la energía de amarre es universal, en el sentido de que no depende de los detalles de la interacción entre fermiones en la aproximación de campo medio. El decaimiento exponencial a grandes distancias determina de manera original el tamaño característico de las fluctuaciones locales de la densidad y el tamaño de pares de fermiones que describen al estado base. Para el caso dos dimensional se presentan expresiones analíticas de las funciones de correlación densidad-densidad, que exhiben de manera explícita la estructura espacial del gas.

Contents

Chapter 1

Introduction

The challenge to understand quantum many-body systems has become a problem of general relevance [1]. It encompasses technological and basic-research interests. Recently, technological developments like laser cooling [2, 3], angle-resolved photoemission spectroscopy [4], magneto optical traps [3], RF spectroscopy [5], and chemical vapor deposition [6], have allowed us to explore a wide amount of physical situations where we can test our theoretical models for the quantum many-body problem [2, 7, 8, 9, 10, 11]. Such is the case of ultracold atoms, where we can modulate the interaction between atoms in different internal states by means of a magnetic field. This mechanism for tuning the interaction is the so-called Feshbach resonance [3]. This unique experimental advantage has allowed the observation of superfluidity in ultracold clouds [2, 12]. Another remarkable aspect of ultracold gases is that they can be considered as bosons or fermions, depending on the total number of fermions that compose the atom[1]. A model that explains the emergence of superfluidity in fermionic-type gases is the so-called BEC-BCS crossover [2, 8, 12, 13, 14]. In this work we will consider a homogeneous Fermi gas of two components which has an attractive interaction between fermions of different component [13]. When we modulate the interaction strength we can obtain a weakly interacting gas, which can be described by overlapping pairs of fermions using the theory of Bardeen, Cooper and Schrieffer (BCS) [15]. As we increase the interaction we find a continuum of quantum states that connect the weakly interacting regime (BCS regime) to the strongly interacting regime. This continuum of quantum states is known as the crossover region, due to the smooth evolution from one regime to the other [8, 9, 12]. The strongly interacting regime is dominated by the presence of bosonic molecules (composed of two fermions). At zero temperature these bosonic molecules can macroscopically occupy their zero wave vector state forming a Bose-Einstein condensate (BEC). Then we will refer to the strongly interacting regime as the BEC regime [16].

We address a many-body system which consists of a low-density two-component Fermi gas in the low-energy regime, at zero temperature. We will consider the homogeneous case, invariant under translations and rotations. Also we address a balanced system, where there are the same amount of fermions in each of the two internal components. The low-energy regime allows us to simplify the description of such a complicated system by neglecting terms that are estimated to be not so relevant in this regime [8, 12]. Then we will use a BCS Hamiltonian, which considers interactions between fermions of different component with opposite wave vectors [8, 12]. In this work we

[1] A simple way is to count the number of neutrons. If there is an even number, then the atom is a boson. If there is an odd number, the atom is a fermion. For instance, ^{6}Li has $Z = 3$ protons, $Z = 3$ electrons, and $N = 3$ neutrons, so it is a fermion. On the other hand, ^{7}Li has $Z = 3$ and $N = 4$, so it is a boson.

analyze three cases, depending on the spatial dimension and type of interaction between fermions: two-dimensional case (2D) with a contact interaction [17], three-dimensional case (3D) with a contact interaction [18], and three-dimensional case with finite-range interactions (four potentials) [19]. In general the interaction between fermions requires a suitable complicated model. However, the low-density regime allows us to focus on properties that should be independent of the details of the interaction [13], or at least weakly dependent. Hence, when choosing different interaction potentials we should look for properties that remain qualitatively invariant. As we have mentioned, in the work presented here we have chosen the structureless contact interaction for the 2D and 3D cases [13, 20]. The contact interaction (delta potential) corresponds to a potential represented by a Dirac delta function in position space, or to a constant in wave vector space. It is adequate for modeling scattering process without knowing the details of the interaction potential, enabling an easier way to perform theoretical calculations. The strength of the contact interaction can be determined by the s-wave scattering length by means of a renormalization process [8, 12]. We have explored four potentials in the 3D case [19], which are: the square well, exponential potential, Yukawa potential, and Van der Waals type potential. To characterize the interaction strength we should use a generic parameter that can be associated to any of the interaction potentials. For the models used in this work it is enough to consider their respective s-wave scattering length [21], although there are other situations where p-wave or d-wave can be considered [16, 22]. Then the BEC-BCS crossover will be parametrized by this characteristic length.

We will study the ground state properties of the Fermi gas throughout the BEC-BCS crossover. In general the ground state is not known [23], so we need to use an approximation. The approach we will use is the BCS-Leggett variational method [13, 15], which consists in using the variational wave function of BCS to minimize the grand potential energy, within the grand canonical ensemble [12], since the BCS wave function does not have a fixed number of fermions (it is not an eigenfunction of the number operator) [2]. This ingenious wave function collapses the description of a many-body system into the behavior of a two-particle wave function (pair wave function) [13]. This so-called pair wave function is a state of fermions of opposite component in a superposition where they both have opposite wave vectors. Then, this variational approach describes the many-body system with the formation of pairs of fermions. Another approach that is equivalent to the BCS-Leggett variational approach, for describing ground state properties, is the mean-field method [24]. This method consists in approximating the interaction term by another one which also emphasizes the formation of pairs with opposite momentum and different component, giving rise to a pairing mechanism that allows the formation of Cooper pairs in the BCS limit, or molecules in the BEC limit. Additionally, the mean-field approach also allows us to consider excited states, since it gives us a grand potential operator in diagonal form [12, 24].

The pairing mechanism that arises in both approaches, mean-field and BCS-Leggett variational method, can be analyzed by means of density-density correlation functions between different components [8, 15]. These functions exhibit the formation of so-called Cooper pairs in the weakly interacting BCS limit [15], while in the strongly interacting BEC limit they show the formation of molecules [8]. However, another two-body distribution that shows the evolution of the spatial structure of pairs of fermions throughout the BEC-BCS crossover is the density-density correlation function of same components [9]. In the weakly interacting regime this function exhibits the dominance of Pauli blocking effect (two fermions of the same component are unlikely to be found

close to each other), while in the strongly interacting regime we see that this blockade becomes negligible due to the formation of bosonic molecules which can be close to each other. The variational pair wave function also exhibits the evolution of pairs of fermions throughout the BEC-BCS crossover [13]. Then, it has been interesting to understand the pairing mechanism by analyzing pair distributions in position space [2, 8, 9, 12, 25].

An interesting quantity that has been addressed throughout the BEC-BCS crossover is the binding energy of pairs. The most common one is the condensation energy [16], which is the difference between the ground state energy of the non-interacting gas and the ground state energy of the interacting gas, all divided by the number of pairs [26]. However, in the work presented here we will focus on ultracold gases, where we can take advantage of the hyperfine structure of atoms, such that we can consider a gas of two components, and we can change the internal state of an atom into a third one [2, 14]. The minimum energy required for this process is what we will call the threshold energy required to break a pair, since in this process we leave an unpaired fermion. Hence, we can identify this as a binding energy that arises from the many-body system, not from the individual interaction between fermions and we will focus our attention on it.

In general, the main contribution of the work presented here is the analysis of the large-distance behavior of three functions that determine the two-body distributions of the BEC-BCS crossover in the mean-field approach, or BCS-Legett variational approach. These are the density-density correlation function between same components, the density-density correlation function between different components, and the variational pair wave function. We addressed the 2D case with a contact interaction [17], 3D case with a contact interaction [18], and 3D case with finite-range interactions (square well, exponential potential, Yukawa potential, and Van der Waals type potential) [19]. For each case, we found that the large-distance behaviors are given by an exponential decay and an oscillatory function.

The exponential decay that we found defines a large-distance correlation length for each two-body distribution[2]. For measuring a local homogeneous density in two different positions we have to ensure that those two measurements are statistically independent. When we increase the distance between those two positions the density-density correlation functions become negligible, allowing us to consider statistically independent variables. Then, the large-distance exponential decay sets a minimum separation for measuring homogeneous densities at different points, allowing us to define the size of a bulk. So we need an experimental system bigger than a characteristic box given in terms of the large-distance correlation length to have an homogeneous system that can be described by the BCS-Leggett model of an homogeneous system [18][3]. The establishment of a minimum size of a system by means of a large-distance correlation length was addressed in the original BCS theory only for the opposite spins correlation function (equivalent to the weakly interacting limit of the crossover) [15], where they obtained the Pippard's coherence length, that gives a minimum

[2]The adjective large-distance had to be added since there is another well-known distance called correlation length [8]. These lengths contribute to the characterization of pairs of different component, since both lengths give a characteristic radius that allow to determine if the local density values are statistically independent.

[3]Also, the density-density correlation functions can be written as expectation values of operators which determine average local density fluctuations, as will be shown in equation (5.15). These density fluctuations (like the Cooper pairs) have to be contained well inside the experimental system.

size for Cooper pairs (see the appendix D of Ref. [15]). Also, Leggett observed that in the BEC limit (strongly interacting limit) the gap equation becomes a Schrödinger equation of a bound state. Then, its solution, that determines the density correlation function between different components, has an exponential decay given by the s-wave scattering length [13]. A similar behavior was expected for the variational pair wave function using the Bethe-Peierls boundary condition [9, 27], which gives an exponential decay of the pair wave function in terms of a positive s-wave scattering length. Also, several research groups have addressed the determination of characteristic lengths of the BEC-BCS crossover, like Giancarlo Calvanese Strinati [8], Andrea Perali [28], Pierbiagio Pieri [8], Mohit Randeria [16], Gerardo Ortiz and Jorge Dukelsky [26]. Mainly the lengths that have been studied are the correlation length ξ_{pair} (also called coherence length) and the healing length ξ_{phase}. The correlation length ξ_{pair} gives a characteristic distance between (correlated) fermions of different components, while the healing length characterizes the distance between pairs of fermions. Also, the characteristic length of the variational pair wave function has been addressed [26], showing a different behavior between the variational pair wave function and the density-density correlation functions of different component in the BCS limit [26]. However, the exponential decay of density-density correlation functions and the pair wave function was not reported throughout the crossover region. The work presented here reports an exponential decay, not only of the opposite spins correlation function (we recover the Pippard's coherence length in the BCS limit and the scattering length in the BEC limit, as will be shown in equations (5.28) and (5.30)) but of the same spins correlation function and the variational pair wave function. Even more, for the two-dimensional and three-dimensional cases with contact interaction we extract from analytical results the exponential decay.

The large-distance correlation length also determines the characteristic size of Cooper pairs in the BCS limit and of the bosonic molecules in the BEC limit, as expected [9, 15]. However, an important result of the work presented here is that the aforementioned threshold energy required to break a pair (a many-body binding energy) determines the large-distance exponential decay of the correlation functions and the pair wave function. For the 3D case we found that this relation is a universal property of the mean-field approach (or BCS-Leggett variational method) since it holds for different potential models[4]. While we were unable to clearly define the origin of this behavior, we believe it might be related to the fact that the BCS wave function is determined by a two-body distribution, the pair wave function. This wave function has to exhibit the binding properties of the system, so it acquires an exponential decay. Then, the pair wave function determines the behavior of density-density correlation functions endowing them with the same exponential decay.

The wave vectors that characterize the oscillatory behavior of the density-density correlation functions and of the pair wave function were calculated analytically for the 2D case, while for the 3D cases, with a contact interaction and with finite range interactions, they were calculated numerically. We were not able to relate the behavior of the wave vectors to another physical quantity. Nevertheless, in agreement with Ref. [29], we also believe that, for the 3D cases, the wave vectors that characterize the spatial oscillations are determined by the many-body distribution in wave vector space. In general, for the 3D cases, the wave vectors (of the density correlation functions and pair wave function) are given by the Fermi wave number (determined by the density

[4]We speculate that depending on the beyond mean-field technique the exponential decay can be lost. This happens for the opposite spins correlation (coherence length) $\xi_{\text{pair}} = \xi_{\uparrow\downarrow}$ [8].

of the system) on the BCS side and they decrease to zero in the BEC limit. The 2D case turned to have a different behavior from the 3D case. The wave vectors that characterize the 2D oscillations are constants throughout the crossover, given by the Fermi wave number.

The analysis of the large-distance behavior allowed us to find explicit expressions of the density-density correlation functions for the 2D case with a contact interaction [17]. These expressions offer the opportunity to view how the thermodynamic quantities determine the formation of Cooper pairs in the BCS limit and the formation of molecules in the BEC limit. We want to reemphasize that these expressions also show the short-distance behavior and are valid for any region of the crossover. Nevertheless, we expect a drastic change in these results when including beyond mean-field corrections that are important for the 2D case [30].

Given that the large-distance correlation lengths offer a novel way of characterizing the size of density fluctuations we can compare their behavior with the conventional correlation length (coherence length for the opposite spins correlation function) defined as a second moment (average) of the density correlation functions and squared norm of the pair wave function. This comparison was made for the 2D case with a contact interaction [17] and for the 3D case with a contact interaction [18].

The work presented here has been reported in the following references:

- J. C. Obeso-Jureidini and V. Romero-Rochín, Density correlation functions and the spatial structure of the two-dimensional BEC-BCS crossover, Phys. Rev. A 105, 043307 (2022) [17].
- J. C. Obeso-Jureidini and V. Romero-Rochín, Spatial structure of the pair wave function and the density correlation functions throughout the BEC-BCS crossover, Phys. Rev. A 101, 033619 (2020) [18].
- J. C. Obeso-Jureidini, G. A. Dominguez-Castro, E. Neri, R. Paredes, and V. Romero-Rochín, Universal correlations along the BEC-BCS crossover, arXiv preprint arXiv:2211.03832 (2022) [19].

The structure of the thesis is as follows:

- In Chapter 2 we give a brief account of the physical systems where BEC-BCS crossover models have been implemented. Particularly, we describe the theoretical ingredients found in ultracold gases that allow to test the crossover model. That is, two fermionic components and the ability to tune the interaction between fermions of different component.
- In Chapter 3 we present the two-body scattering problem in 2D and in 3D. We introduce the concept of s-wave scattering length, which allows us to characterize the interaction strength between two particles in the low energy regime. We show that the contact interaction is an ill-defined potential which has divergent physical properties. Those divergent properties will allow us to renormalize the theory of the many-body problem. Also, we calculate the s-wave scattering lengths of the finite-range interactions for the 3D case.

- In Chapter 4 we introduce the BEC-BCS crossover model in the mean-field approach. We also present the variational approach introduced by Leggett. We calculate the relevant thermodynamic properties for determining the ground state of the many-body system. We consider the 2D case with a contact interaction, the 3D case with a contact interaction, and the 3D case with finite-range potentials. Also, we present the threshold energy required to break a pair, which determines the large-distance behavior of the density-density correlation functions and pair wave function.

- In Chapter 5 we analyze the density-density correlation functions and the pair wave function for the three cases presented in Chapter 4. Here we present their large-distance behavior and include the pair wave function. The 2D case is discussed in detail, since explicit expressions of the correlation functions were obtained. We show that the exponential decay is determined by the threshold energy required to break a pair. For the 3D case we argue that the relationship between the large-distance exponential decay and a pair-binding energy is universal.

- In Chapter 6 we present the final remarks of this work. We elaborate further on the exponential decay of the density-density correlation functions, and we elaborate on some perspectives for future work.

Chapter 2

Overview of the BEC-BCS crossover

In this chapter we briefly describe some of the developments of the BEC-BCS crossover model that are particularly relevant to the work presented here. The general physical model is an interacting Fermi gas [13, 31], which exhibits different phases depending on the interaction strength between the fermions [8], the number of components [32, 33, 34], the temperature [35, 36], and the confining potential [34], even we can consider the system in the relativistic regime [37]. In the particular case we will address, which is the homogeneous two-component Fermi gas, we can use the Bardeen, Cooper and Schrieffer (BCS) state to describe the ground state of the interacting fermions. We can describe a smooth evolution from the weakly interacting regime, known as BCS limit, to the strongly interacting regime, known as Bose-Einstein condensate (BEC) regime, where fermions form molecules that behave like bosons. The continuum of quantum states that connect the BEC and BCS limits is known as the crossover. In the past decades it acquired relevance with the realization of ultracold quantum gases [38], since unprecedented experimental control has been achieved in those systems [2, 39]. However, it is a model that can be used to describe other systems such as proton-neutron mixtures and neutron-neutron mixtures in the crust of neutron stars [40], electrons in a solid [41], and it might be observed in Quantum Chromodynamics [42].

2.1 The BEC-BCS crossover

One of the first works to propose a BEC-BCS crossover was due to Eagles, trying to decribe superconductivity in $SrTiO_3$ doped with Zr [31]. However, in a seminal work [13], Leggett addressed the superfluid properties of Helium-3 with the main motivation of describing Cooper pairs as diatomic molecules [43]. In a sense, he generalized the BCS theory to consider strong interactions, opening a new way to study the many-body problem, which we will follow in the work presented here. Later, Nozières and Schmitt-Rink generalized the model to consider finite temperatures [35], especially they calculated the critical temperature for the normal to superfluid phase transition. The BCS description of a superconductor (superfluid) is based on the formation of pairs of fermions of different component, so a natural question was the effect of imbalance between components [8]. Ground states with an imbalance were proposed soon after the formulation of BCS theory. For example, there is a generalization of the BCS state where, instead of considering a Fermi sphere, the fermions are distributed forming a structure of concentric shells centered at zero in wave vector space. This state is known as the Sarma state [44]. More exotic ground states were proposed, like the Fulde-Ferrell-Larkin-Ovchinnikov (FFLO) state [45, 46]. Differently from the Sarma state, in the FFLO state the shells formed by fermions in wave vector space can be displaced from the

concentric position. Nevertheless, superconductivity was found in different materials which the original BCS model was unable to describe. For instance it has been found in the so-called cuprate superconductors (like YBCO) [47, 48], FeSe systems [49], magic angle twisted bilayer graphene [50], and layer nitrides [51]. At the moment there are no complete explanations of all superconductors. Simplified models to address superconductivity are BEC-BCS crossover models, where differently from the original BCS approach, the electrons (and holes) can have stronger interactions. The strength of the interactions does not form electron molecules that can be considered as bosons, but the characteristic size of pairs is reduced so we can consider the formation of smaller pairs than in the original BCS model [52, 53]. Very recently two-band superconductors have been studied experimentally and theoretically with the hope of finding new mechanisms to enhance superconductivity [54]. Some theoretical models are of the BEC-BCS crossover type like the one reported in Ref. [54], where they find a non-zero critical temperature for superconductivity in a quasi-one-dimensional superconductor (modeled by a BEC-BCS crossover with a Feshbach-like resonance) coupled to a BCS superconductor in 3D (or quasi-2D) [54, 55, 56]. Then there is a general interest in understanding BEC-BCS crossover models, which mark the context of the work presented here. In the following we will not focus on superconductivity in solids, rather in ground states which are necessary for superfluidity in homogeneous gases, such as those realized in ultracold gases [2, 7, 8]. Also, we have to mention again that there is the possibility of finding a BEC-BCS crossover in neutron-neutron mixtures in the crust of neutron stars [12, 40].

The theoretical understanding of ultracold gases has become a recent topic [7, 8, 12]. Mainly, these gases give the opportunity to observe the behavior of quantum many-body systems, since those experiments can be performed within the conditions where theoretical simplifications are valid. Research in quantum gases has become such an important topic that some of the projects in this field have been receiving funding from a huge project launched by the European Union, which is the Quantum Flagship [1]. It is expected that this investment will accelerate technological developments. In Mexico, there are also laboratories dedicated to the development of state-of-the-art research in quantum systems, such as the Laboratorio Nacional de Materia Cuántica [57]. Particularly, the Laboratorio de Materia Ultrafría at the Institute of Physics at UNAM explores novel phenomena in ultracold gases, such as Faraday waves [57].

A breakthrough that allowed the emergence of ultracold atoms came when sophisticated techniques allowed us to trap and cool atoms in gaseous form [58]. Then the excitement increased with the ability to observe a Bose-Einstein condensate effect in these quantum gases [59]. Importantly for the context of this work, a major achievement was the realization of an ultracold Fermi gas [38]. This milestone gave the physics community the opportunity to enrich our understanding by being able to find analogues between our description of superconductivity in solids and our description of superfluidity in quantum gasses [7, 60]. It is in these fermionic gases where the BEC-BCS crossover has been analyzed with great experimental detail [2, 61]. Also, with the development of new techniques for the creation of quantum gases in different confinement configurations (some of them resemble electrons in a solid) other theoretical many-body models and effects were tested, such as Bose-Hubbard models [62], tight-binding models [63], Anderson localization [64, 65], Bose-Polaron [66], Fermi-Polaron [67]. See Refs. [2, 7, 10, 61, 68, 69, 70] for many other models and effects that have been addressed in ultracold atom experiments.

A common interest in all the variants of the BEC-BCS crossover (from the theoretical and experimental approach) is the characterization of the size of superconducting pairs. In the work presented here we will address a more general aspect, which is the characterization of the size of density fluctuations. This focus contains the size of superconducting pairs, since pairs need to be within the local density fluctuations. However, we will consider the most simple version of the BEC-BCS crossover, which is BCS-Leggett approach with s-wave pairing at the mean-field level [13], which we will present in Chapter 4.

2.2 Ultracold Fermi gases

As we have mentioned, the BCS-Leggett model, to be presented in Chapter 4, is a simplified model that can describe qualitatively the experiments in ultracold gases. In this section we will present some properties that allow to link the model with the experiments. A nice presentation of the experimental details required to achieve an ultracold gas can be found in Ref. [3] and in the references therein. Further details about the design and implementation of sophisticated experimental techniques can be found in Refs. [11, 71].

The BCS-Leggett model requires of a Fermi gas of two components. Then we will show that the hyperfine splitting of the electron states in atoms allows us to obtain a two-component ultracold gas. As an example we will focus on Lithium-6 [3]. In vacuum the presence of a magnetic field $\vec{B}$ splits the hyperfine states of an atom. The splitting is given by the Hamiltonian [71, 72, 73]

$$\hat{H}_{\rm hf} = \Delta E_{\rm hf} \vec{I}\cdot\vec{J} - g_J \mu_B \vec{J}\cdot\vec{B} - g_I \mu_B \vec{I}\cdot\vec{B} \tag{2.1}$$

where we will restrict to the particular case of $J = 1/2$ so that we have introduced the difference between hyperfine states in the absence of magnetic field $\Delta E_{\rm hf}$. Also we will consider the spin of the nucleus to be $I = 1$ [73]. We have introduced the Bohr magneton $\mu_B = e\hbar/(2m_e)$ and the respective Landé factors of the electron g_J and of the nucleus g_I, which have to be measured for each atom[1]. The operator $\vec{I}$ denotes the spin of the nucleus and the electronic total angular momentum is given by $\vec{J}$. For the case of total angular momentum $J = 1/2$ Breit and Rabi found an explicit equation for the eigenvalues of the Hamiltonian $\hat{H}_{\rm hf}$ of equation (2.1) for intermediate values of the magnetic field [75]. A nice derivation of this result is given in Ref. [76]. The restriction of $J = 1/2$ allows us to consider a block diagonal representation of $\hat{H}_{\rm hf}$ where the eigenvalues can be obtained straightforwardly. The qualitative behavior of the states $2^2S_{1/2}$ that we will consider for ^{6}Li is shown in Figure 2.1 [5, 71]. In experiments the ^{6}Li atoms can be prepared in the lowest energy states shown in Figure 2.1: $|1\rangle$ and $|2\rangle$, which correspond to the two components of the gas which we can arbitrarily denote $|\downarrow\rangle$ and $|\uparrow\rangle$. Figure 2.1 is to illustrate the hyperfine splitting at intermediate magnetic fields. However, the experiments are carried at higher magnetic fields, known as the Paschen-Back regime. Importantly, in this regime the energy separation between the states $|1\rangle$, $|2\rangle$, and $|3\rangle$ becomes constant (independent of the field), which allow to implement imaging techniques to analyze these systems [71].

[1] For ^{6}Li we can use $g_I = -0.0004476540$ and $g_J = 2.0023010$ [71, 73, 74].

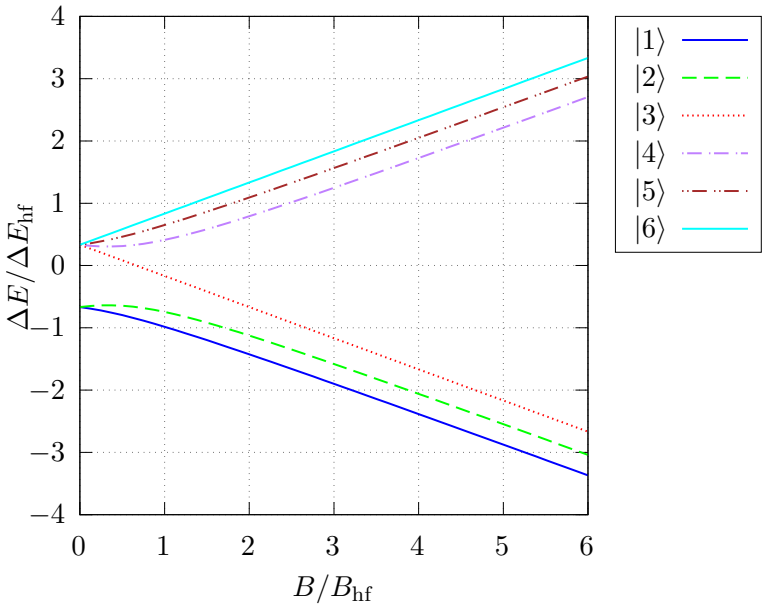

Figure 2.1: Energies of the hyperfine states as functions of the magnetic field B of the Hamiltonian given in equation (2.1) for the case $2^2S_{1/2}$. Each energy belongs to a state denoted by $|i\rangle$ for $i = 1, ..., 6$. We can use the eigenvalues found by Breit and Rabi [75]. For Lithium-6 the energy splittings are scaled with the energy difference in absence of magnetic field $\Delta E_{\rm hf}/\hbar = 228.2$ MHz [71, 73, 74] and we have defined $B_{\rm hf} = \Delta E_{\rm hf}/[(g_J - g_I)\mu_B]$, see the text for the definitions of constants. We can arbitrarily denote $|\downarrow\rangle = |1\rangle$ and $|\uparrow\rangle = |2\rangle$.

One of the techniques developed in ultracold gases is the ability to tune the effective interaction strengths between atoms by means of so-called Feshbach resonances. Basically, the atoms are prepared in low-energy states, like $|1\rangle$ and $|2\rangle$ of Figure 2.1, which have different effective interactions for different values of the magnetic field B. These effective interactions allow us to set the system in the different regions of the crossover at will. The interaction strengths have been characterized experimentally by means of an s-wave scattering length for different atomic gases [71, 77, 78].

Let us give a general picture of the interaction between atoms. Since the atoms are moving slowly, we can use the Born-Oppenheimer approximation to obtain potential energy curves [79], the same curves used for estimating the stable nuclear separation in the model of the rigid molecule [79]. For the two lowest hyperfine states, $|1\rangle$ and $|2\rangle$ of Figure 2.1, it is enough to consider the curves given by the triplet ${}^3\Sigma_u$ and the singlet ${}^1\Sigma_g$, where we are using molecular spectroscopic notation [79]. An illustration of these curves can be found in Ref. [77]. These curves are used to describe the interaction between atoms in the low energy regime using a two-channel model for scattering. The coupling between channels comes from the hyperfine coupling between the spins of the atoms and the spins of the nuclei, which is independent of the magnetic field [80]. However, the energy difference between the two potential curves ${}^3\Sigma_u$ and ${}^1\Sigma_g$ depends on the external magnetic field [80]. A "Feshbach resonance" occurs when the bound state of the singlet potential ${}^1\Sigma_g$ approaches the low-energy scattering, which is formally called a potential resonance. A pedagogical presentation of the potential resonance that occurs in this two-channel model can be found in Ref. [81].

In Fig. 2.2 we show a model of the scattering length as function of the magnetic field for ^{6}Li [82]. This model was determined by fitting measurements, as reported in [82], and is given by

$$a(B) = a_b\left(1 + \frac{\Delta_B}{B - B_0}\right)[1 + \alpha(B - B_0)], \tag{2.2}$$

where the parameters are $a_b = -1405a_0$, $B_0 = 83.4149$ mT, $\Delta_B = 30.0$ mT, and $\alpha = 0.0040(\text{ mT})^{-1}$, with $a_0 \approx 5.292^{-11}$ m the Bohr radius [82][2]. Although it is not necessary for the theoretical calculations shown further below, this plot shows that there is an experimental control of the effective interactions in ^{6}Li by means of a magnetic field B. There are more accurate models for the Feshbach resonance that have been obtained from more precise measurements [3]. That is, we have the ability to tune the strength of the interactions between fermions, an important ingredient for having a BEC-BCS crossover.

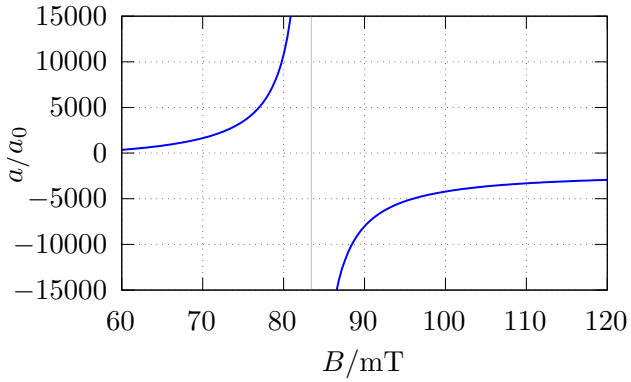

Figure 2.2: Approximate behavior of the s-wave scattering length a scaled with Bohr radius a_0 as function of the magnetic field B in units of militesla (mT). The parametrization is given in equation (2.2) as reported in [82] for the states $|1\rangle$ and $|2\rangle$ of ^{6}Li shown in Figure 2.1. The vertical line at $B_0 = 83.4149$ mT is where the resonance approximately occurs.

[2]In similar models it is enough to consider the first two factors of equation (2.2), where the width $\Delta_B = \Gamma_0/\delta\mu$ contains the information of the atoms, being $\delta\mu$ a difference between the magnetic moment of the atoms separated and the magnetic moment of the bound state in the closed channel and Γ_0 is determined by the coupling between open and closed channels. For further details see [77].

Chapter 3

Atomic scattering at low energies

Choosing a potential to model the interaction between particles is a difficult task [83, 84]. In principle, the interaction can be inferred by measuring differential cross sections with a huge amount of data [85]. However, it is easier to fit a model interaction with a few parameters that can reproduce the experimental results [83, 86]. Typically, a structureless contact interaction is chosen, which is adequate to model processes where the details of the interaction are irrelevant. Nevertheless, the lack of structure introduces divergences that have to be identified and removed by means of renormalization. The main purpose of this chapter is to present the required equations for the renormalization of the many-body problem when using a contact interaction. Also, we will briefly define the phase shifts in two and three dimensions. In particular we will emphasize the determination of the s-wave scattering length of finite-range potentials for the three dimensional case.

3.1 The T matrix of two-body scattering in 2D and 3D

In this section we consider two particles of mass m_1 and m_2 in the center-of-mass coordinate system, with relative positions given by the vector $\vec{r}$, interacting in the vacuum by a potential that depends on the relative distance $U(\vec{r}) = U(|\vec{r}|)$. The three-dimensional case $D = 3$ and the two-dimensional case $D = 2$ will be considered simultaneously. Then we are considering two interacting particles in the vacuum at zero temperature. The time-independent Schrödinger equation is [83, 87]

$$-\frac{\hbar^2}{2m_r}\nabla^2\psi(\vec{r}) + U(\vec{r})\psi(\vec{r}) = E\psi(\vec{r}), \tag{3.1}$$

where $m_r = m_1 m_2/(m_1 + m_2)$ is the reduced mass, and the proper energy is $E = \hbar^2 k^2/(2m_r)$. For the scattering problem the wave function $\psi(\vec{r})$ should have the boundary condition

$$\psi(\vec{r}) = e^{i\vec{k}\cdot\vec{r}} + \psi_{sc}(\vec{r}), \tag{3.2}$$

where the first term is a plane wave that represents the incidence, and whose wave vector $\vec{k}$ is fixed. The second term represents the scattered wave. Since the time-independent Schrödinger equation can be expressed as a Helmholtz equation this scattered wave can be written generally as [23, 87, 88][1]

$$\psi_{sc}(\vec{r}) = \int d^D x\, G_0(\vec{r} - \vec{x}, E^+)U(\vec{x})\psi(\vec{x}), \tag{3.3}$$

[1]For many integrals and sums the domain will correspond to all the space $\mathbb{R}^D$, for $D = 2, 3$.

where we have introduced the free Green's function of an outgoing wave $G_0(\vec{r}-\vec{x}, E^+)$. This function satisfies the differential equation[2]:

$$\frac{\hbar^2}{2m_r}(k^2 + \nabla^2_{\vec{r}})G_0(\vec{r}-\vec{x}, E^+) = \delta^{(D)}(\vec{r}-\vec{x}). \tag{3.4}$$

To find the free Green's functions it is convenient to change to wave vector space in equation (3.4), solve the resulting equation, and return to space representation. However, other general way is to use the equations defined by the operators and calculate the matrix elements. The operator representation of (3.4) is

$$(E - \hat{H}_0)\hat{G}_0(E) = \hat{\mathbb{I}}, \tag{3.5}$$

where we have defined the kinetic energy operator $\hat{H}_0 = \hat{p}^2/(2m_r)$ and the identity operator $\hat{\mathbb{I}}$. Then the free Green's function is given by

$$\hat{G}_0(z) = (z - \hat{H}_0)^{-1}, \tag{3.6}$$

where z can be a complex number. This operator has singularities at the proper energies of $\hat{H}_0$, which are located on the real axis. However, approaching those points as a limit is useful for calculations. In fact, for positive energies, approaching from above the real axis gives a Green's function of an outgoing wave (+), while approaching from below gives the one of an incoming wave (−). To take this limit, and make a difference between outgoing and incoming waves, let us introduce the following notation:

$$\hat{G}_0(z^\pm) = \lim_{\delta\to 0^+} (z - \hat{H}_0 \pm i\delta)^{-1}, \tag{3.7}$$

where we are using the convention $\delta > 0$ so that the case $+\delta$ allows us to approach from above the real axis (outgoing), while the $-\delta$ case is for approaching from below (incoming). For the 3D case we have [23, 88]

$$\langle\vec{r}\,|\,\hat{G}_0^{3D}(E^+)\,|\vec{x}\rangle = G_0^{3D}(\vec{r}-\vec{x}, E^+) = -\frac{m_r e^{ik|\vec{r}-\vec{x}|}}{2\pi\hbar^2|\vec{r}-\vec{x}|}, \tag{3.8}$$

where we are taking expectation values with eigenstates of the position operator which we denote by $|\vec{x}\rangle$ and $|\vec{r}\rangle$. For the 2D case we have [88, 90]

$$\langle\vec{r}\,|\,\hat{G}_0^{2D}(E^+)\,|\vec{x}\rangle = G_0^{2D}(\vec{r}-\vec{x}, E^+) = -\frac{im_r}{2\hbar^2}H_0^{(1)}(k|\vec{r}-\vec{x}|). \tag{3.9}$$

To obtain equations (3.8) and (3.9) it is enough to use the completeness relations

$$\mathbb{I} = \int d^D x\,|\vec{x}\rangle\langle\vec{x}| \quad , \quad \mathbb{I} = \frac{1}{(2\pi)^D}\int d^D k\,|\vec{k}\rangle\langle\vec{k}|, \tag{3.10}$$

with $\langle\vec{x}|\vec{k}\rangle = e^{i\vec{k}\cdot\vec{x}}$. For later convenience we will use a tilde to indicate that a function is being written in wave vector representation using the following definitions:

$$\tilde{f}(\vec{k}) = \int d^D r\, e^{-i\vec{k}\cdot\vec{r}} f(\vec{r}) \quad , \quad f(\vec{r}) = \frac{1}{(2\pi)^D}\int d^D k\, e^{i\vec{k}\cdot\vec{r}}\tilde{f}(\vec{k}). \tag{3.11}$$

[2] Another convention to define the Green's function is with a minus sign on the right side of equation (3.4). Also the units $\hbar^2/(2m_r)$ can vary in the definition [89], but the definition presented here is also commonly used [23, 83].

Also, a useful relation is

$$\int d^D k \, e^{i\vec{k}\cdot\vec{r}} = (2\pi)^D \delta^{(D)}(\vec{r}). \tag{3.12}$$

Similarly, we can define a complete Green's function using the complete Hamiltonian $\hat{H} = \hat{H}_0 + \hat{U}$, where $\hat{U}$ is the operator of the potential. This Green's function is given by

$$\hat{G}(z^{\pm}) = \lim_{\delta \to 0^+} (z - \hat{H} \pm i\delta)^{-1}. \tag{3.13}$$

A relation between the free Green's function G_0 and the complete Green's function G can be obtained by means of the following identity [85]:

$$\hat{A}^{-1} = \hat{B}^{-1} + \hat{B}^{-1}(\hat{B} - \hat{A})\hat{A}^{-1}, \tag{3.14}$$

where $\hat{A}$ and $\hat{B}$ are well defined operators. If we choose $\hat{A}^{-1} = \hat{G}(z)$ and $\hat{B}^{-1} = \hat{G}_0(z)$, using equations (3.7) and (3.13), we get the Dyson equation [23, 85]

$$\hat{G}(z) = \hat{G}_0(z) + \hat{G}_0(z)\hat{U}\hat{G}(z). \tag{3.15}$$

In the same way, if we choose $\hat{A}^{-1} = \hat{G}_0(z)$ and $\hat{B}^{-1} = \hat{G}(z)$, we get

$$\hat{G}(z) = \hat{G}_0(z) + \hat{G}(z)\hat{U}\hat{G}_0(z). \tag{3.16}$$

Equations (3.15) and (3.16) have the complete Green's function in both sides. We can introduce an identity operator and rename the operators that do not involve G_0 to avoid writting $G(z)$ on the right hand side. Hence, we have

$$\begin{aligned} \hat{G}(z) &= \hat{G}_0(z) + \hat{G}_0(z)\hat{U}\hat{G}(z) \\ &= \hat{G}_0(z) + \hat{G}_0(z)\hat{U}\hat{G}(z)\hat{G}_0^{-1}(z)\hat{G}_0(z) \\ &= \hat{G}_0(z) + \hat{G}_0(z)\hat{T}(z)\hat{G}_0(z), \end{aligned} \tag{3.17}$$

where in the first equality we used equation (3.15), in the second we introduced the identity $\mathbb{I} = \hat{G}_0^{-1}(z)\hat{G}_0(z)$ and in the last one we defined the T matrix operator (short for transition matrix [83]). It can be noticed that it is analogous to a self-energy in the many-body problem [23]. A quick view at equation (3.17) reveals that the T matrix contains all the information about the interaction because $\hat{G}_0$ is independent of the potential. Comparing equation (3.17) with equations (3.15) and (3.16) we find that

$$\hat{T}(z) = \hat{G}_0^{-1}(z)\hat{G}(z)\hat{U} = \hat{U}\hat{G}(z)\hat{G}_0^{-1}(z). \tag{3.18}$$

From this equation we can see that [83]

$$\begin{aligned} \hat{T}(z) - \hat{U} &= \hat{G}_0^{-1}(z)\hat{G}(z)\hat{U} - \hat{U} \\ &= [\hat{G}_0^{-1}(z)\hat{G}(z) - \mathbb{I}]\hat{U} \\ &= \hat{U}\hat{G}(z)\hat{U}, \end{aligned} \tag{3.19}$$

where in the first equality we used equation (3.18), in the second we factored $\hat{U}$, and in the last one we used (3.15). Then we get a relation between the T matrix and the complete Green's function, which in general is unknown,

$$\hat{T}(z) = \hat{U} + \hat{U}\hat{G}(z)\hat{U}. \tag{3.20}$$

However, we can use equation (3.18) to obtain a relation analogous to equations (3.15) and (3.16) for the T matrix:

$$\hat{T}(z) = \hat{U} + \hat{U}\hat{G}_0(z)\hat{T}(z). \tag{3.21}$$

Following an extensive part of the literature, we will refer to this equation as the Lippmann-Schwinger equation [10, 85, 91], although other equations have the same name [83, 89, 92]. We can calculate the matrix elements of the T matrix in wave vector representation. Especially we are interested in evaluating it in the fixed energy $E = \hbar^2 k^2/(2m_r)$ and calculating $T(\vec{k}', \vec{k}, E) = \langle \vec{k}'|\hat{T}(E)|\vec{k}\rangle$, where the wave vector $\vec{k}$ is also fixed by the energy E. From equation (3.21) it is found that

$$T(\vec{k}', \vec{k}, E) = \tilde{U}(\vec{k} - \vec{k}') + \frac{1}{(2\pi)^D}\int d^D k'' \tilde{U}(\vec{k}'' - \vec{k}')\frac{1}{E - E_{k''} + i\delta}T(\vec{k}'', \vec{k}, E). \tag{3.22}$$

To obtain the last term have used the completeness relation for the wave vector basis given in equation (3.10) to get

$$\begin{aligned}\left\langle \vec{k}'\right| \hat{U}\hat{G}_0(E)\hat{T}(E) \left|\vec{k}'\right\rangle &= \frac{1}{(2\pi)^D}\int d^D p\, d^D l\, \langle \vec{k}'|\hat{U}\left|\vec{p}\right\rangle \left\langle \vec{p}\right| \hat{G}_0(E)|\vec{l}\rangle\langle \vec{l}|\hat{T}(E)|\vec{k}'\rangle \\ &= \frac{1}{(2\pi)^D}\int d^D p\, d^D l\, \tilde{U}(\vec{p} - \vec{k}')\left[E - \frac{\hbar^2 p^2}{2m_r} + i\delta\right]^{-1}(2\pi)^D \delta^{(D)}(\vec{p} - \vec{l})T(\vec{l}, \vec{k}, E),\end{aligned} \tag{3.23}$$

where in the first equality we introduced completeness relations and in the last equality we identified matrix elements. It is straightforward to obtain the matrix element $\langle \vec{p}|\hat{G}_0(E)|\vec{l}\rangle$ using equation (3.7), from where we obtain the dirac delta $\delta^{(D)}(\vec{p} - \vec{l})$. Equation (3.22) is well defined as long as the potential $\tilde{U}(\vec{q})$ remains physically acceptable. The advantage of introducing the T matrix is that we can work with the scattered wave $\psi_{sc}(\vec{r})$ leaving aside the incident plane wave. This can be seen by expressing the general solution, given in equation (3.2), with bra-ket notation:

$$|\psi\rangle = |\vec{k}\rangle + \hat{G}_0(E^+)\hat{U}\,|\psi\rangle\,, \tag{3.24}$$

where we have the wave function $\psi(\vec{r}) = \langle \vec{r}|\psi\rangle$, and $\langle \vec{r}|\vec{k}\rangle = e^{i\vec{k}\cdot\vec{r}}$. Also we can identify the scattered wave $\psi_{sc}(\vec{r}) = \langle \vec{r}|\psi_{sc}\rangle$ by means of equation (3.3),

$$|\psi_{sc}\rangle = \hat{G}_0(E^+)\hat{U}\,|\psi\rangle\,. \tag{3.25}$$

From equation (3.24) we find

$$|\psi\rangle = [\hat{\mathbb{I}} - \hat{G}_0(E^+)\hat{U}]^{-1}|\vec{k}\rangle, \tag{3.26}$$

where on the right side we have known quantities, but it is operationally impractical. Using equations (3.15) and (3.16) it can be shown that $[\hat{\mathbb{I}} - \hat{G}_0(E^+)\hat{U}][\hat{\mathbb{I}} + \hat{G}(E^+)\hat{U}] = \hat{\mathbb{I}}$, so we can identify the inverse function of $\hat{\mathbb{I}} - \hat{G}_0(E^+)\hat{U}$ that we can substitute in equation (3.26),

$$|\psi\rangle = [\hat{\mathbb{I}} + \hat{G}(E^+)\hat{U}]|\vec{k}\rangle. \tag{3.27}$$

Besides, from equation (3.18) we have $\hat{G}(E^+)\hat{U} = \hat{G}_0(E^+)\hat{T}(E^+)$ that allows us to get an expression for the state $|\psi\rangle$ in terms of the T matrix,

$$|\psi\rangle = [\hat{\mathbb{I}} + \hat{G}_0(E^+)\hat{T}(E)]|\vec{k}\rangle. \tag{3.28}$$

Comparing equation (3.24) with equation (3.28) we find that the scattered state $|\psi_{sc}\rangle$ can be determined by calculating the matrix elements of $\hat{G}_0(E^+)\hat{T}(E)$ because

$$|\psi_{sc}\rangle = \hat{G}_0(E^+)\hat{T}(E)|\vec{k}\rangle. \tag{3.29}$$

Notice that the matrix elements of $\hat{G}_0(E^+)\hat{T}(E)$ appear naturally in equation (3.22), a particular case of the Lippmann-Schwinger equation. Hence the solution to the scattering problem can be found by determining the T matrix. The problem is still difficult, but the T matrix allows a versatile formulation in which some approximations can be done. As an example, in the following we will consider a contact interaction.

3.1.1 *s*-wave scattering from a delta potential

Regarding the difficulties that emerge when modeling the interaction between particles, it is common to use a structureless potential known as contact interaction (delta potential), which is ill-defined, as we will show. The operator of the contact interaction is defined by

$$\hat{U}\left|\vec{x}\right\rangle = g\delta^{(D)}(\vec{x})\left|\vec{x}\right\rangle, \tag{3.30}$$

where g is the interaction strength. From the Lippmann-Schwinger equation (3.21) we can find an expression for the T matrix, provided the inverse of $(\mathbb{I} - \hat{U}\hat{G}_0(z))$ or $(\mathbb{I} - \hat{G}_0(z)\hat{U})$ exists. Then we get

$$\hat{T}(z) = \hat{U}(\mathbb{I} - \hat{G}_0(z)\hat{U})^{-1}. \tag{3.31}$$

We can iterate the T matrix in equation (3.21) or use the definition of a geometric series in equation (3.31) to find the Born series [85]:

$$\hat{T}(z) = \hat{U}[\mathbb{I} + \hat{G}_0(z)\hat{U} + \hat{G}_0(z)\hat{U}\hat{G}_0(z)\hat{U} + \hat{G}_0(z)\hat{U}\hat{G}_0(z)\hat{U}\hat{G}_0(z)\hat{U} + ...]. \tag{3.32}$$

In this equation it is easier to calculate the matrix elements than in equation (3.31). Equivalently we can iterate the T matrix in equation (3.22). In the following we will consider the particular case where the s-wave component of the T matrix is the dominant term. If we were to consider other components, like p-wave or d-wave, we would have to follow a more careful analysis[3]. For a contact interaction it is found that

$$T(\vec{k}', \vec{k}, E) = g\left[1 + \frac{g}{(2\pi)^D}\int d^D k'' \frac{1}{E - E_{k''} + i\delta} + \left(\frac{g}{(2\pi)^D}\int d^D k'' \frac{1}{E - E_{k''} + i\delta}\right)^2 + ...\right]. \tag{3.33}$$

It can be seen that the integrals in each term are divergent, since for large wave vectors the integrand goes like $k''^{D-1}/E_{k''}$. In a more explicit way we have a behavior of the form

$$\int^{\infty} dk'' \, \frac{k''^{D-1}}{k''^2} = \begin{cases} k'' \to \infty & \text{for 3D,} \\ \ln(k'') \to \infty & \text{for 2D.} \end{cases} \tag{3.34}$$

[3] In general we would have to expand the T matrix and the potential $\tilde{U}(\vec{q} - \vec{q}')$ of equation (3.22) in terms of partial waves. See for instance Ref. [16] for the 2D case, and Ref. [22] for the 3D case. Then we would have to use equation (3.22) for each partial wave. Depending on the spatial dimension, more assumptions have to be made on the interaction potential $\tilde{U}(\vec{q} - \vec{q}')$ than the ones we are considering here [16, 22].

Then we have a divergent expression for the T matrix, which implies an ill-defined Green's function G and a scattered wave without physical meaning. However, we can see that this divergence arises from our election of a structureless contact interaction. A well-defined interaction should allow the integrals to converge[4]. Then we can identify the interaction strength g as a non-physical quantity which we adjust arbitrarily to ensure convergence. This is done by introducing a parameter known as regulator Λ which controls the integration limits and the interaction strength, allowing $g \to 0$ when $\Lambda \to \infty$ [94]. Using an identity for the geometric series we have [94]

$$T(\vec{k}', \vec{k}, E) = g(\Lambda)\left[1 - \frac{g(\Lambda)}{(2\pi)^D}\int^{\Lambda} d^D k'' \frac{1}{E - E_{k''} + i\delta}\right]^{-1}. \tag{3.35}$$

This equation can be rearranged to find the interaction strength g in terms of the T matrix plus a divergent term that will allow us to cancel another divergence that arises in the many-body problem[5], due to the contact interaction,

$$\frac{1}{g(\Lambda)} = \frac{1}{T(\vec{k}', \vec{k}, E)} + \frac{1}{(2\pi)^D}\int^{\Lambda} d^D k'' \frac{1}{E - E_{k''} + i\delta}. \tag{3.36}$$

This equation became important in the literature because it allows us to use a contact interaction in the many-body problem [8, 12, 23, 91]. The use of a contact interaction enables an easier theoretical treatment, but at the cost of having divergences that need to be removed by renormalizing the theories[6].

We can readily use equation (3.36) to renormalize the interaction strength in the many-body problem[7]. However we might notice that the basis used here, for an homogeneous space, differs from the one commonly used in the many-body problem, where we use periodic boundary conditions with an auxiliary box whose size is taken to infinity at the end of calculations. We can still find an analogous equation but we cannot use directly the Lippmann-Schwinger equation (3.21) because the normalization of the free waves with periodic boundary conditions is not adequate to describe a scattering process, unless a different definition for the T matrix is used [89][8]. The free waves with periodic boundary conditions are of the form

$$\langle \vec{r} | \vec{k} \rangle = \frac{e^{i\vec{k}\cdot\vec{r}}}{L^{D/2}}, \tag{3.37}$$

where L^D is the size of the box in two dimensions $D = 2$ or in three dimensions $D = 3$ [96]. The equation used to renormalize the theory using explicitly the periodic boundary conditions is

$$\frac{1}{g(\Lambda)} = \frac{1}{T(\vec{k}', \vec{k}, E)} + \frac{1}{L^D}\sum_{\vec{k}''}^{\Lambda} \frac{1}{E - E_{k''} + i\delta}. \tag{3.38}$$

[4] Further discussion about the form of the potentials can be found in quantum scattering books like [85, 93].

[5] It might be tempting to consider that the T matrix is zero in equation (3.35), but this possibility is discarded since the T matrix is different from zero whenever there is an interaction, as seen in equation (3.21).

[6] A nice presentation of the renormalization procedure used in this work can be found in [95].

[7] We must mention that there are other schemes for renormalizing the models with a contact interaction, such as a direct use of a renormalized contact interaction with a partial derivative [9].

[8] The important aspect is to find a solution to Schrödinger's equation of the form given by equation (3.2), regardless of the normalization.

In this section we have introduced the T matrix, whose determination allows to solve the scattering problem, as shown in equation (3.29). For the contact interaction we were only able to say that it should be a finite quantity, by means of equation (3.35). As we are interested in using an interaction adequate for the low-energy and dilute regime, we expect the T matrix to be given approximately by a physical property belonging to this regime. In the following we will show that a good approximation is given by the s-wave component of the total scattering cross section, which can be determined considering only the respective s-wave scattering length.

3.2 Scattering from a finite-range potential in 2D

In the last section we considered a general formulation for the scattering problem from a potential that depends on the relative distance between particles. In this section we will consider the determination of the phase shifts for potentials that have a radius such that for distances larger than this radius the potential can be neglected, which we call finite-range potentials. While the steps to define and determine the phase shifts are similar between 2D and 3D, it is not common to find a treatment of this topic in 2D. In this section we will follow closely Refs. [97] and [90] for the presentation of the scattering, although we are mainly interested in obtaining an expression for the T matrix in terms of the s-wave scattering length. We will start from equation (3.1), where we can use separation of variables in polar coordinates $\psi(\vec{r}) = R(r)\Theta(\theta)$. Then we get two coupled equations. One corresponds to the angular momentum equation,

$$\frac{\hbar^2}{2m_r}\frac{d^2\Theta}{d\theta^2} = -\frac{\hbar^2 m_\theta^2}{2m_r}\,\Theta, \tag{3.39}$$

while the other one is the radial equation,

$$r^2\frac{d^2R}{dr^2} + r\frac{dR}{dr} + \left[\frac{2m_r}{\hbar^2}\Big(E - U(r)\Big)r^2 - m_\theta^2\right]R = 0. \tag{3.40}$$

The angular momentum equation can be solved generally to find the two independent solutions, $\Theta_1(\theta) = \exp(im_\theta\theta)$ and $\Theta_2(\theta) = \exp(-im_\theta\theta)$. However, the wave function must have a unique value in each point in space and in this case the transformation $\theta \to 2\pi+\theta$ leaves invariant the system. Thus, we find that the angular momentum quantum number must have integer values $m_\theta = 0, \pm1, \pm2, ...$ For the scattering problem we can choose $\theta = 0$ as the angle of incidence, see Figure 3.1. For a radial potential we expect that the direction of incidence defines a reflection symmetry, so we require $\Theta(\theta) = \Theta(-\theta)$. Then, it is enough to consider the following linear combinations:

$$\Theta(\theta) = \cos(l\theta), \tag{3.41}$$

with $l = 0, 1, 2, 3, ...$ Outside the range of the potential, where we can neglect it, the radial equation (3.40) becomes the well-known Bessel differential equation, whose solution is a linear combination of Bessel's functions $J_l(kr)$ and Neumann's functions $N_l(kr)$, both of order l [88]. Then, the wave function $\psi(\vec{r})$ is given as

$$\psi(r,\theta) = \sum_{l=0}^{\infty} \varepsilon_l[a_l J_l(kr) + b_l N_l(kr)]\cos(l\theta), \tag{3.42}$$

where a_l and b_l are linear coefficients and we have introduced [97]

$$\varepsilon_l = \begin{cases} 1 \text{ if } l = 0, \\ 2 \text{ if } l \neq 0, \end{cases} \tag{3.43}$$

so as to compare this expression with the one of the incident plane wave, given by [97]

$$e^{i\vec{k}\cdot\vec{r}} = e^{ikr\cos(\theta)} = \sum_{l=0}^{\infty} \varepsilon_l J_l(kr)\cos(l\theta)e^{il\pi/2}. \tag{3.44}$$

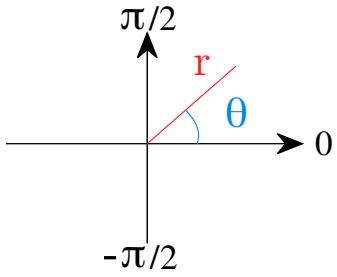

Figure 3.1: Illustration of the conventions used for the polar coordinates. The direction of incidence will be taken in the direction $\theta = 0$. The upper half plane corresponds to $\theta > 0$, while the lower one to $\theta < 0$.

For large distances we can use the following approximations for the Bessel and Neumann functions [88]:

$$J_l(kr) \to \sqrt{\frac{2}{\pi kr}}\cos\left(kr - \frac{l\pi}{2} - \frac{\pi}{4}\right), \tag{3.45}$$

$$N_l(kr) \to \sqrt{\frac{2}{\pi kr}}\text{sen}\left(kr - \frac{l\pi}{2} - \frac{\pi}{4}\right). \tag{3.46}$$

Then at large distances the wave function $\psi(r,\theta)$ given in equation (3.42) behaves like

$$\psi(r,\theta) \approx \sum_{l=0}^{\infty} \sqrt{\frac{2}{\pi kr}} B_l\varepsilon_l[\cos(\beta_l(kr))\cos(\delta_l) - \text{sen}(\beta_l(kr))\text{sen}(\delta_l)]\cos(l\theta), \tag{3.47}$$

where we have defined $\beta_l(kr) = kr - l\pi/2 - \pi/4$ and we have introduced the phase shifts δ_l defined by the linear coefficients, $a_l = B_l\cos(\delta_l)$ and $b_l = -B_l\text{sen}(\delta_l)$. Notice that the phase shifts are not defined uniquely, there can be others differing by multiples of 2π. Using the trigonometric identity $\cos(\beta_l(kr) + \delta_l) = \cos(\beta_l(kr))\cos(\delta_l) - \text{sen}(\beta_l(kr))\text{sen}(\delta_l)$ we get $\psi(r,\theta)$

$$\psi(r,\theta) = \sum_{l=0}^{\infty} \sqrt{\frac{2}{\pi kr}}\, B_l\, \varepsilon_l\, \cos\left(kr - \frac{l\pi}{2} - \frac{\pi}{4} + \delta_l\right)\cos(l\theta). \tag{3.48}$$

Then we see the meaning of δ_l. At large distances it is the shift of the circular wave due to the presence of the finite-range potential. If there was no potential, the radial equation (3.40) would become Bessel's differential equation. Then the linear coefficients b_l of equation (3.42) would have to be zero because the Neumann function has a logarithmic divergence at the origin (a wave

function cannot diverge), so this implies $\delta_l = 0$.

Let us return to the problem of determining the scattered wave function $\psi_{sc}(\vec{r})$. Far from the origin we expect the scattered wave to behave like a circular wave, so we have the asymptotic behavior

$$\psi(r,\theta) = e^{i\vec{k}\cdot\vec{r}} + \psi_{sc}(r,\theta) \approx e^{i\vec{k}\cdot\vec{r}} + \frac{f(\theta)e^{ikr}}{\sqrt{r}}, \tag{3.49}$$

where we have defined a scattering amplitude $f(\theta)$ following Ref. [97][9]. We can use equations (3.44) and (3.48) to find an expression for $f(\theta)$,

$$\begin{aligned} f(\theta) &= \left(\frac{\sqrt{r}}{e^{ikr}}\right)[\psi(\vec{r}) - e^{i\vec{k}\cdot\vec{r}}] \\ &= \frac{e^{-i\pi/4}}{\sqrt{2\pi k}} \sum_{l=0}^{\infty} \varepsilon_l \cos(l\theta)\{e^{i2\delta_l} - 1\}, \end{aligned} \tag{3.50}$$

where we had to set $B_l = e^{i\delta_l}e^{il\pi/2}$ in equation (3.48) because each term $\cos(l\theta)$ is linearly independent. Then we can identify a differential scattering cross section $|f(\theta)|^2$ [90] and a total cross section λ given by

$$\lambda = \int_{-\pi}^{\pi} |f(\theta)|^2 d\theta = \frac{4}{k}\sum_{l=0}^{\infty} \varepsilon_l \operatorname{sen}^2(\delta_l) = \frac{4}{k}\sum_{l=0}^{\infty} \varepsilon_l \frac{1}{\cot^2(\delta_l) + 1}. \tag{3.51}$$

The total scattering cross section λ is a measure of the probability of a particle of mass m_r being scattered by the potential in any way by the potential $U(r)$ [93], while the differential cross section $|f(\theta)|^2$ is the probability of being scattered towards the angle θ. These are observable quantities that could be measured, provided we have achieve a two-dimensional confinement. In the low energy regime that concerns us the scattering cross sections are determined by the s-wave phase shift. The anti-symmetry of the complete wave function (including spin) requires to consider an anti-symmetric scattering amplitude when the particles are indistinguishable. If we consider spin 1/2 fermions the amplitude is given by [98]

$$f_A(\theta) = f(\theta) \pm f(\pi - \theta), \tag{3.52}$$

where the upper sign is for a singlet and the lower for the triplet states. Considering only the s-wave component in the case of triplet states (same spin projection) gives a zero scattering amplitude, since $f(\theta)$ is independent of the angle θ,

$$f(\theta)|_{s\text{-wave}} = \frac{e^{-i\pi/4}}{\sqrt{2\pi k}}[e^{i2\delta_0} - 1]. \tag{3.53}$$

In this sense fermions with same quantum numbers behave as non-interacting particles, since $f_A(\theta) \approx 0$. However, the next partial wave contribution $l = 1$ should be taken into account for the

[9] It is also common to find different conventions, such as [90]

$$\psi(r,\theta) \approx e^{i\vec{k}\cdot\vec{r}} + \frac{e^{i\pi/4}f(\theta)e^{ikr}}{\sqrt{kr}},$$

where $f(\theta)$ is a scattering amplitude.

triplet states, where we would find a smaller value of $|f_A(\theta)|$ than for the case of scattering in the singlet state.

We are interested in characterizing the interaction strength for a generic finite-range potential $U(r)$ in equation (3.40). Then in the next subsection we will analyze the behavior of the phase shifts and find that the s-wave contribution $l = 0$ dominates the scattering solution at low energies, given in equation (3.48). From the s-wave phase shift we will be able to define an s-wave scattering length which gives information about the interaction strength.

3.2.1 s-wave scattering length in 2D

For finite-range potentials, that satisfy $U(r) < 0$, we can divide the domains of the radial equation in two, at least. We will denote the solution "inside" the potential with a subindex I and the solutions "outside" with II. Then, we can proceed in the standard way. We solve the radial equation in each domain and then we find the general solution by using the physical boundary conditions. That is, continuity of the wave function and its derivative. For the scattering problem it is enough to consider the continuity of the logarithmic derivative,

$$\left.\frac{R_I'(r)}{R_I(r)}\right|_{r=r_0} = \left.\frac{R_{II}'(r)}{R_{II}(r)}\right|_{r=r_0}. \tag{3.54}$$

In region II, "outside", we have the condition

$$\alpha_{\rm sc} = r_0 \left.\frac{R_{II}'(r)}{R_{II}(r)}\right|_{r=r_0} = \frac{kr_0[\cot(\delta_l)J_l'(kr_0) - N_l'(kr_0)]}{[\cot(\delta_l)J_l(kr_0) - N_l(kr_0)]}, \tag{3.55}$$

where we used equation (3.42), taking into account that each term is linearly independent. Also we have defined a value for the boundary condition $\alpha_{\rm sc}$, which depends on the details of the potential (and on the angular momentum by means of the index l) because it is also determined by the solution "inside",

$$\alpha_{\rm sc} = r_0 \left.\frac{R_I'(r)}{R_I(r)}\right|_{r=r_0}. \tag{3.56}$$

Then, $\alpha_{\rm sc}$ represents the structure of the potential in the scattering problem, therefore the "sc" label. Hence, we can solve equation (3.55) to find

$$\cot(\delta_l) = \frac{\alpha_{\rm sc}N_l(kr_0) - kr_0N_l'(kr_0)}{[\alpha_{\rm sc}J_l(kr_0) - kr_0J_l'(kr_0)]}. \tag{3.57}$$

Observing the functional form of the cross section in equation (3.51) we can notice that a s-wave scattering resonance occurs when $\cot(\delta_0) = 0$. The wave vector k at which this condition occurs determines the energy of s-wave scattering resonance $E_{\rm res}$, as shown in Figure 3.2 for a circular potential illustrated in the inset. In the low energy limit we expect that $\alpha_{\rm sc}$ becomes a constant that depends on the details of the potential $\alpha_{\rm sc}^{(0)}$. Then we can find a low-energy (or short-range)

approximation for equation (3.57) using well-known asymptotic expansions for the Bessel and Neumann functions [88]:

$$J_l(x) \approx \frac{1}{\Gamma(l+1)}\left(\frac{x}{2}\right)^l, \tag{3.58}$$

$$N_l(x) \approx \begin{cases} \frac{2}{\pi}[\ln(x) + \gamma - \ln(2)] & \text{for } l = 0, \\ -\frac{(l-1)!}{\pi}\left(\frac{2}{x}\right)^l & \text{for } l > 0, \end{cases} \tag{3.59}$$

where we are restricting to integer values of $l \geq 0$. From this asymptotic expansions it can be seen that the s-wave $\cot(\delta_0)$ is the dominant term at low energies in the total scattering cross section λ, see equation (3.51), because it has a logarithmic behavior[10], given by

$$\cot(\delta_0) \approx -\frac{2}{\pi\alpha_{sc}^{(0)}} + \frac{2\gamma}{\pi} - \frac{2}{\pi}\ln(2) + \frac{2}{\pi}\ln(kr_0). \tag{3.60}$$

Finally, we can introduce an identity function in the form of a composition $\ln \circ \exp$ to write everything in one logarithm [16],

$$\begin{aligned} \cot(\delta_0) &\approx \frac{1}{\pi}\left\{\ln[(kr_0)^2] + \ln\left[\exp\left(-\frac{2}{\alpha_{sc}^{(0)}} + 2\gamma - 2\ln(2)\right)\right]\right\} \\ &= \frac{1}{\pi}\ln\left[\frac{(kr_0)^2}{4\exp\left(\frac{2}{\alpha_{sc}^{(0)}} - 2\gamma\right)}\right] \\ &= \frac{1}{\pi}\ln\left(\frac{E}{E_a}\right). \end{aligned} \tag{3.61}$$

In the last equality we defined the energy E_a, which is the approximate energy where a scattering resonance would occur[11]. It is given by

$$E_a = 4\left(\frac{\hbar^2}{2m_r r_0^2}\right)\exp\left(\frac{2}{\alpha_{sc}^{(0)}} - 2\gamma\right). \tag{3.62}$$

From the energy E_a we can define the s-wave scattering length a_{2D}, as a characteristic length of scattering at low energies[12]. Here we will adopt the convention (for equal mass particles m, the reduced mass is $m_r = m/2$):

$$E_a = \frac{\hbar^2}{2m_r a_{2D}^2}. \tag{3.63}$$

[10] For $l > 0$ we have $\cot(\delta_l) \approx c_1(kr_0)^{-2l}$, where c_1 is independent of kr_0.

[11] For this interpretation we must obtain equation (3.61) using $r_0 \ll 1$ while leaving free the wave vector k.

[12] In the literature there are different conventions to define the scattering length, but they differ by constants [30, 99].

Then, we can express the phase shift in terms of the s-wave scattering length:

$$\cot(\delta_0) = \frac{2}{\pi}\ln(ka_{2D}) \tag{3.64}$$

For a fixed wave vector k, the quantity that modulates the s-wave component in the cross-section is a dimensionless logarithm $\ln(ka_{2D})$. Then the scattering length does not have the same geometrical interpretation as the 3D scattering length, it does not shift directly the wave function, since it is inside the logarithm. It is counter intuitive that the cross section diverges at low energies, for $k \to 0$. However, this can be thought to be related to the appearance of a bound state for the potentials we have been discussing, finite-range potentials with no divergences. For example, in 2D a circular potential, as illustrated in the inset of Figure 3.2, always has a bound state. This is different from the 3D case, where shallow potentials do not have a bound state. In Appendix A.1 we determine the equations for finding the bound state of the circular potential, and show that the approximation $|E_{\text{bound}}| \approx E_a$ is valid for shallow circular potentials.

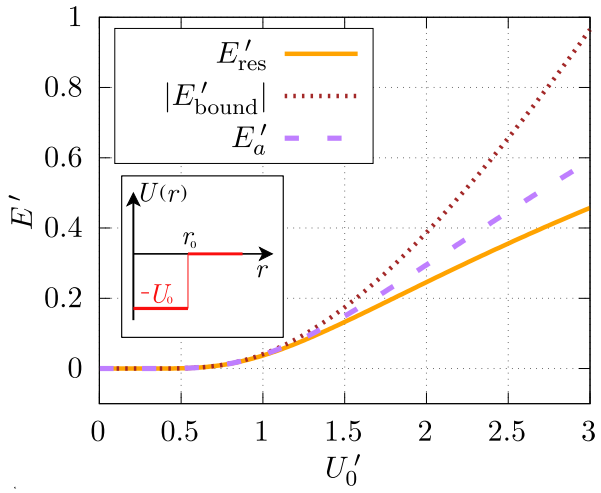

Figure 3.2: For a 2D circular potential of depth U_0 and radius r_0, shown in the inset, we show the behaviors of the energy of s-wave scattering resonance E_{res} (solid line), the energy of the first bound state E_{bound} (dotted line) and the approximate energy E_a (dashed line) given in equation (3.63), as funcions of the depth. Primed variables indicate dimensionless form, for example $E'_a = 2m_r r_0^2 E_a/\hbar^2$.

Let us remind that we want to find the T matrix in terms of the phase shifts. From equation (3.29) we can calculate the wave vector representation of the scattered wave,

$$\begin{aligned}\tilde{\psi}_{sc}(\vec{k}') &= \left\langle \vec{k}' \middle| \hat{G}_0(E^+)\hat{T}(E) \middle| \vec{k} \right\rangle \\ &= \frac{1}{E - \dfrac{\hbar^2 k'^2}{2m_r} + i\delta} T(\vec{k}', \vec{k}, E),\end{aligned} \tag{3.65}$$

where we used the completeness relations (3.10). Then, we can calculate its space representation, where we can make approximations to find the large-distance behavior of the scattered wave $\psi_{sc}(\vec{r})$.

Hence we will be able to find a relation between the scattering amplitude $f(\theta)$ and the T matrix at low energies, and therefore the T matrix in terms of the phase shifts. So we have

$$\psi_{sc}(\vec{r}) = \frac{1}{(2\pi)^2}\int d^2k'\; e^{i\vec{k}'\cdot\vec{r}}\frac{1}{E-\dfrac{\hbar^2k'^2}{2m_r}+i\delta}T(\vec{k}',\vec{k},E). \tag{3.66}$$

In the large distance regime $r \gg 1$ we can approximate the integrand by first assuming[13] that the T matrix depends on the magnitude of the wave vector $\vec{k}'$, $T(\vec{k}',\vec{k},E) = T(|\vec{k}'|,\vec{k},E)$. This allows us to write the Fourier transform of equation (3.66) as a Hankel transform, introducing a Bessel function $J_0(k'r)$. Then, we can use the asymptotic form for the Bessel function given in equation (3.45), which allows for an extension of the integral to the complex plane, where we can close an integration contour and use Cauchy's theorem. The final approximation is

$$\psi_{sc}(\vec{r}) \approx -\frac{1}{4}\sqrt{\frac{2}{\pi kr}}e^{i\pi/4}e^{ikr}T(k,\vec{k},E), \tag{3.67}$$

which is valid for small wave vector k. Then we can compare this expression for the scattered wave with its functional form at large distances, given in equation (3.49). This expression allows us to find an approximate relation between the T matrix and the s-wave phase shift. We have, for small wave vector k,

$$f(\theta) \approx -\frac{m_r}{2\pi\hbar^2}\sqrt{\frac{2\pi}{k}}e^{i\pi/4}T(k,\vec{k},E) \tag{3.68}$$

Using the s-wave term of the scattering amplitude, given in equation (3.50) we find

$$\begin{aligned} T(k,\vec{k},E) &\approx \frac{2\hbar^2}{m_r}\left[\frac{1}{-\cot(\delta_0)+i}\right] \\ &= \frac{2\hbar^2}{m_r}\left[\frac{1}{\frac{2}{\pi}\ln(1/ka_{2D})+i}\right] \\ &= \frac{2\hbar^2}{m_r}\left[\frac{1}{-\frac{1}{\pi}\ln(E/E_a)+i}\right] \end{aligned} \tag{3.69}$$

where we used

$$\frac{e^{i2\delta_0}-1}{2i} = \frac{1}{\cot(\delta_0)-i}, \tag{3.70}$$

and the relation between the phase shift and the s-wave scattering length, given in equation (3.64). Another strange property is that in the low energy limit $k \to 0$ the s-wave approximation of the T matrix, given in equation (3.69), vanishes, since the denominator diverges as $\ln(E) \to \infty$. The vanishing T matrix gives the impression that the particles become non-interacting. However, this is not the case, since the T matrix cannot be zero when there is a potential $\hat{U}$, as seen in equation (3.21). After obtaining equation (3.69) we have acquired the basic elements for performing the renormalization procedure in the many-body problem[14]. That is, we can substitute equation (3.69)

[13] This condition is not necessary, but it makes easier the demonstration. For a more general dependence we can follow the 3D arguments of Ref. [98], modifying them for the 2D case.

[14] We can consider the scattering of particles in a medium using a many-body t-matrix, which is one method for including beyond mean-field terms [8, 12].

into equation (3.36). We need to emphasize that this result has been obtained from a two-body problem and we want to use it in the many-body problem. To do so, we need to consider a dilute system, so that the structure of the interaction can be disregarded.

3.3 Scattering from a finite-range potential in 3D

In this section we will consider the determination of the phase shifts for finite-range potentials, the ones that have a radius such that for distances larger than this radius the potential can be neglected. It has to be mentioned that this is not the case for a Coulomb potential because it decays very slow with the distance [83]. It is more common to find nice discussions about scattering in 3D, see for instance [83, 85, 89, 93, 98, 100]. Then we will give a general overview of the phase shifts, the cross section and its relation to the low energy approximation of the T matrix.

We can use separation of variables in Schrödinger equation (3.1) with $\psi(\vec{r}) = R(r)Y(\theta,\varphi)$ to obtain a radial equation and the angular equation. However, for scattering from central potentials we can set the polar angle $\theta = 0$ in the direction of the incident wave vector $\vec{k}$ and notice that there should be a rotational symmetry around the direction of incidence. Then we can restrict ourselves to the plane where scattering occurs [98], equivalent to fixing the azimuth angle φ. Hence we have the radial equation:

$$\frac{1}{r^2}\frac{d}{dr}\left(r^2\frac{dR}{dr}\right) + \left[k^2 - \frac{2m_r}{\hbar^2}U(r) - \frac{l(l+1)}{r^2}\right]R = 0 \tag{3.71}$$

and the angle equation

$$\frac{d}{d\theta}\left(\sin(\theta)\frac{d\Theta}{d\theta}\right) + l(l+1)\sin(\theta) = 0, \tag{3.72}$$

where θ is the angle between $\vec{k}$ and $\vec{r}$ [98]. A general solution is given by [83]

$$\psi(r,\theta) = \sum_{l=0}^{\infty} B_l(2l+1)i^l R_l(r)P_l(\cos(\theta)). \tag{3.73}$$

For finite-range potentials, the radial equation (3.71) is satisfied by the spherical Bessel functions when the potential becomes negligible $U(r) \approx 0$. The spherical Bessel function of the first kind is defined by [88]

$$j_l(x) = \sqrt{\frac{\pi}{2x}}J_{l+1/2}(x), \tag{3.74}$$

while the spherical Bessel function of the second kind is given by [88]

$$n_l(x) = \sqrt{\frac{\pi}{2x}}N_{l+1/2}(x). \tag{3.75}$$

Then, the radial function $R_l(r)$ is a linear combination of the two solutions, such that far from the center of the potential, where $kr \gg 1$, we have the asymptotic limit:

$$R_l(r) \approx \frac{\sin(kr - \pi l/2 + \delta_l)}{kr}, \tag{3.76}$$

where we have introduced the phase shift δ_l that has information about the linear combination of $j_l(kr)$ and $n_l(kr)$. Let us remember the expansion of a free plane wave in terms of partial waves [83]:

$$e^{i\vec{k}\cdot\vec{r}} = \sum_{l=0}^{\infty}(2l+1)i^l j_l(kr)P_l(\cos(\theta)). \tag{3.77}$$

Then, we can substitute equations (3.73), (3.76), and (3.77) into equation (3.2), which has the following asymptotic limit at large distances:

$$\psi(\vec{r}) = e^{i\vec{k}\cdot\vec{r}} + \frac{f(\theta)}{r}e^{ikr}, \tag{3.78}$$

where $f(\theta)$ is known as the scattering amplitude. We find $f(\theta)$ to be given in terms of the phase shifts:

$$f(\theta) = \frac{1}{k}\sum_{l=0}^{\infty}(2l+1)\sin(\delta_l)\, e^{i\delta_l}\, P_l(\cos(\theta)), \tag{3.79}$$

where we had to set $B_l = e^{i\delta_l}$ in equation (3.73) because each Legendre polynomial is linearly independent. Then we can calculate the total cross section

$$\sigma = \int_0^{2\pi} d\varphi \int_0^{\pi} d\theta\, \sin(\theta)\, |f(\theta)|^2 = \frac{4\pi}{k^2}\sum_{l=0}^{\infty}(2l+1)\sin^2(\delta_l). \tag{3.80}$$

From this sum we can identify the s-wave contribution to the total cross section, which can be the dominant term at low energies, unless the antisymmetry of the wave function cancels those terms, as discussed in equations (3.52) (3.53). That is, for fermions with spin $s = 1/2$ the scattering amplitude is given by [98]

$$f_A(\theta) = f(\theta) \pm f(\pi - \theta), \tag{3.81}$$

where the upper sign is for a singlet and the lower for the triplet states. Considering only the s-wave component in the case of triplet states (same spin projection) gives a zero scattering amplitude, since $f(\theta)$ is independent of the angle θ,

$$f(\theta)|_{s\text{-wave}} = \frac{\sin(\delta_l)e^{i\delta_l}}{k}. \tag{3.82}$$

Given that we will consider interactions between fermions of different spin, we need to characterize the general behavior of the s-wave contribution for any finite-range interaction potential. For this purpose we will find that it is adequate to define the s-wave scattering length, which we will introduce in the next subsection.

3.3.1 s-wave scattering length in 3D

For the simplified potentials that we are considering, which are spherical and of finite range (can be considered zero outside a characteristic radius), the information about the structure of the potential is contained in the phase shifts δ_l. At low energies the dominant term of a spatially symmetric wave functions is the one that characterizes the most spherically symmetric component

with $l = 0$. However, this is not the general case. For example, depending on the anti-symmetry of the wave function the first dominant term can be with $l = 1$ [98].

Like for the 2D case, we can divide the interval of the radial equation into two parts, inside (Region I) and outside the potential (Region II), where the solutions of the radial equation (3.71) behave like

$$R_{II}(r) \propto \cos(\delta_l) j_l(kr) - \sin(\delta_l) n_l(kr). \tag{3.83}$$

Then, the continuity of the wave function and its derivatives at the boundaries can be joined in one condition, the continuity of the logarithmic derivative,

$$\left.\frac{R_I'(r)}{R_I(r)}\right|_{r=r_0} = \left.\frac{R_{II}'(r)}{R_{II}(r)}\right|_{r=r_0}. \tag{3.84}$$

We can define the boundary condition inside the potential as

$$\alpha_{\text{sc}} = r_0 \left.\frac{R_I'(r)}{R_I(r)}\right|_{r=r_0}, \tag{3.85}$$

while outside, where we can neglect the potential, the solution $R_{II}(r)$ is such that

$$r_0 \left.\frac{R_{II}'(r)}{R_{II}(r)}\right|_{r=r_0} = \frac{kr_0[\cot(\delta_l) j_l'(kr_0) - n_l'(kr_0)]}{[\cot(\delta_l) j_l(kr_0) - n_l(kr_0)]}. \tag{3.86}$$

Using equations (3.85) and (3.86) we can determine the phase shift, up to a term involving the periodicity,

$$\cot(\delta_l) = \frac{\alpha_{\text{sc}} n_l(kr_0) - kr_0 n_l'(kr_0)}{[\alpha_{\text{sc}} j_l(kr_0) - kr_0 j_l'(kr_0)]}. \tag{3.87}$$

In the low energy regime, $kr_0 \ll 1$, we can use the small argument behavior of the spherical Bessel functions, $j_l(x) \propto x^l$ and $n_l(x) \propto x^{-l-1}$, to convince ourselves[15] that the dominant phase shift is the one with $l = 0$, the s-wave term, assuming a constant behavior of α_{sc} when $k \to 0$. Then we will be interested in calculating its low-energy behavior. Taking the limit $k \to 0$ we can see that the following limit defines a characteristic length of the scattering process:

$$\lim_{k\to 0} k \cot(\delta_0) = -\frac{1}{a}, \tag{3.88}$$

where we have defined the s-wave scattering length a, which depends on the details of the potential by means of α_{sc}. Then, the s-wave scattering length represents the shift of the scattered wave function $\psi_{sc}(\vec{r})$ in equation (3.2) for the 3D case. Basically, it represents the strength of the potential. When it has a change of sign it indicates the availability of a bound state in the potential. While the limit shown in equation (3.88) is correct, it is numerically difficult to calculate the scattering length using equations (3.87) and (3.88). Also we have avoided giving an expression

[15] For the Van der Waals potential of equation (3.97) this behavior is not quite general, but it is enough for arguing that the s-wave contribution is the dominant term. For more general expressions of the phase shifts see [77, 101].

for the range of the potential r_0, which can also be infinite (as a limit) [92]. For determining the s-wave scattering length we will follow Ref. [86] and use the definition:

$$a = \lim_{r\to 0}\left[r - \frac{u(r)}{u'(r)}\right]_{k=0}, \tag{3.89}$$

where $u(r)$ is given in terms of the solution to the radial equation (3.71) as $u(r) = rR(r)$. To use equation (3.89) we can first solve the radial equation, with $k = 0$, in terms of $u(r)$ with the boundary conditions $u(0) = 0$ and $u'(0) = 1$ [86]. This can be done with a Runge-Kutta method [102], which allows us to compute $u(r)$ and $u'(r)$ numerically [19, 86, 92]. We will not give a rigorous demonstration of equation (3.89), but we will argue its validity. Far from the center of the potential $r \gg 1$ (in region II) we can write the s-wave solution to the radial equation like

$$R_{II}(r) \propto \cot(\delta_0) j_0(kr) - n_0(kr). \tag{3.90}$$

For low energies $k \to 0$ we can use the well-known behaviors $j_0(kr) \approx 1$ and $n_0(kr) \approx -1/(kr)$ [88]. Hence

$$R_{II}(r) \propto \frac{1}{k}\left(k\cot(\delta_0) + \frac{1}{r}\right) \propto \mathcal{N}\left(-\frac{1}{a} + \frac{1}{r}\right), \tag{3.91}$$

where we have factored $1/k$ and we have made an early substitution of the s-wave scattering length, using equation (3.88). Also we have written a normalization factor $\mathcal{N}$. We can use this asymptotic behavior in the definition of $u(r)$ to verify the limit given in equation (3.89). We can notice that the normalization constant $\mathcal{N}$ does not determine the value of a.

Further below we will model the interaction between fermions using representative potentials of finite-range interactions, following the previous work reported in Refs. [92, 103, 104]. We will characterize the deepness of the potentials by a constant V_0, and the range of the potential by a length R_0 (not to be confused with r_0 in our previous discussion). The potentials are [92]:

- The well-known square well, also known as finite spherical well [87]:

$$U_{\mathrm{SW}}(r) = \begin{cases} -V_0 & r \le R_0 \\ 0 & r \ge R_0, \end{cases} \tag{3.92}$$

  This potential has been a nice model for interactions because it can be solved explicitly [83, 87]. Also it is a simplified model for the scattering properties that should be obtained from a coupled-channels scattering problem [105], which are relevant for collision between atoms in ultracold gases. An important feature of this potential is that it is exactly zero outside the radius R_0 and it has a discontinuity at the same radius R_0. When the mass of the particles is the same $m_1 = m_2 = m$, the s-wave scattering length of this potential is given by [103]

$$a = R_0\left\{1 - \left(\frac{mV_0R_0^2}{\hbar^2}\right)^{-1/2}\tan\left[\left(\frac{mV_0R_0^2}{\hbar^2}\right)^{1/2}\right]\right\} \tag{3.93}$$

  The behavior of the s-wave scattering length is shown in Figure 3.3 (a).

- The exponential potential:

$$U_{\text{exp}}(r) = -V_0 e^{-r/R_0}, \tag{3.94}$$

This potential was used by William Rarita and R. D. Present to model the interaction between nuclei [106]. Also this potential was used in previous analysis of the BEC-BCS crossover [92, 103, 104]. The exponential function is an analytic function (it is smooth) in all space $r \in [0, \infty)$, which is one of the main properties that seem attractive of this potential. Its s-wave scattering length, when the mass of the particles is the same $m_1 = m_2 = m$, is given by [103]

$$a = -2R_0\left\{\frac{\pi}{2}\frac{N_0\left[\left(\frac{4mV_0R_0^2}{\hbar^2}\right)^{1/2}\right]}{J_0\left[\left(\frac{4mV_0R_0^2}{\hbar^2}\right)^{1/2}\right]} - \ln\left[\left(\frac{mV_0R_0^2}{\hbar^2}\right)^{1/2}\right] - \gamma\right\}, \tag{3.95}$$

where γ is the Euler-Mascheroni constant. The behavior of the s-wave scattering length is shown in Figure 3.3 (b).

- The Yukawa potential:

$$U_{\text{Yuk}}(r) = -V_0\frac{R_0}{r}e^{-r/R_0}\,. \tag{3.96}$$

This potential appeared as an approximation in many models. For example it can be regarded as a screened Coulomb potential. It seems to be used by van der Waals long before Yukawa proposed it for modeling the neutron-proton interaction [107]. Actually there are more accurate potentials to describe interactions between nucleons [8, 77]. Nevertheless, its divergence at the origin is the main feature that we want to test in the many-body system. The s-wave scattering length was calculated numerically as explained in equation (3.89). The numerical calculations are shown in Figure 3.3 (c) [86].

- A Van der Waals type potential [103]:

$$U_{\text{VdW}}(r) = \begin{cases} 0 & r \le R_0 \\ -V_0R_0^6/r^6 & r \ge R_0, \end{cases} \tag{3.97}$$

Within the Born-Oppenheimer approximation of static nuclei, the interaction between two atoms goes like r^{-6} due to the mutually induced dipoles in the atoms [93]. Then this potential is of relevance for ultracold gases, where we expect a slow motion of the atoms [77]. The main feature of this potential is that it has an algebraic decay. In Figure 3.3 (d) we show the s-wave scattering length calculated numerically as explained in equation (3.89) [86].

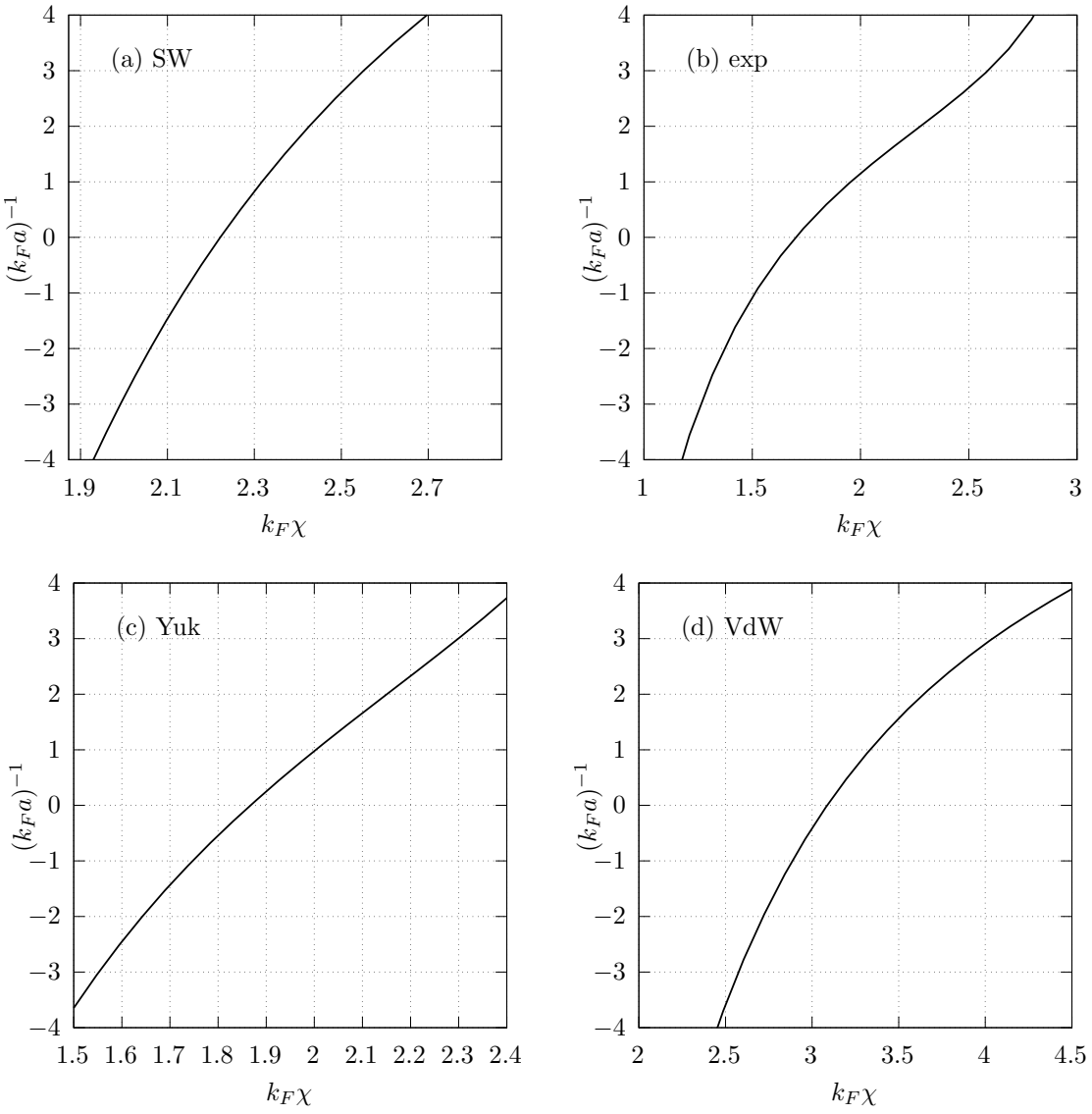

Figure 3.3: Examples of the behavior of the inverse of the scattering length a^{-1}, scaled with the Fermi wave number k_F, as function of a parameter $k_F\chi$ that represents the "depth" of the potentials, given by $k_F\chi = k_F R_0 \sqrt{V_0/\varepsilon_F}$, with the Fermi energy given by $\varepsilon_F = \hbar^2 k_F^2/(2m)$. In all plots we use $k_F R_0 = 0.1$. In (a) we have an example of the square well (3.92). (b) corresponds to the exponential potential (3.94). (c) is an example of the Yukawa potential (3.96). (d) shows the one of the Van der Waals type potential (3.97). These calculations were performed following Refs. [103] and [86].

In Figure 3.3 we show the scattering lengths a of the finite-range potentials calculated with equation (3.89). We have introduced the Fermi wave number k_F given by the density of a non-interacting homogeneous gas $n = k_F^3/(3\pi^2)$ for using these calculations in the many-body problem. Also we introduced the Fermi energy $\varepsilon_F = \hbar^2 k_F^2/(2m)$. The behaviors of the inverse scattering lengths shown in Figure 3.3 tells us that an increase of $(k_F a)^{-1}$ from negative to positive values corresponds to an increase in the strength of the interaction. These calculations are for simplified models of two-particle interactions. As we have commented, the real interactions between atoms are more complicated, but in the low-energy regime they can be characterized by the s-wave

scattering length. Also, in experiments of ultracold gases the interactions are characterized by the scattering lengths, like the model shown in Figure 2.2. Hence, in the following it will be adequate to parametrize the interaction strength with the s-wave scattering length.

After having introduced models for the interaction between particles we can use them in the many-body problem. A general observation is that we cannot avoid using two-body physics to set an adequate interaction between particles. For our particular models under consideration the s-wave scattering length characterizes the interaction strength between particles at low energies. Then, in the many-body problem we can use an ill-defined contact interaction with a non-physical interaction strength, where we would find an ultraviolet divergence due to the contact potential. Since we know the origin of the divergence in the two-body scattering problem we can remove it using the s-wave scattering length using equations (3.36) and (3.38). This process is the so-called renormalization of the theory.

3.4 Remarks on differences and similarities between 2D and 3D

As can be seen, there have been many similarities between the scattering in 2D and 3D. However, we will give a brief list of similarities between the scattering in 2D and 3D that we want to emphasize:

- Notice that the phase shifts δ_l in both dimensions are not defined uniquely, there can be others differing by multiples of 2π.
- In both dimensions, at low energies $k \to 0$, we have restricted to the case of interactions without spin, and then we take into account the spin states. For interaction between fermions in a singlet state ($s = 1/2$), the dominant terms in the total cross sections λ in equation (3.51) and σ in equation (3.80) correspond to the s-wave terms $l = 0$. However we could consider other spin configurations or some other potentials, where the dominant terms are not the s-wave terms [16, 22].
- When considering only the s-wave contribution to the scattering amplitudes in equations (3.53) and (3.82) we can neglect the interaction between fermions in the same quantum state.

Some differences that we want to remark between 2D and 3D are:

- The definitions of the scattering length in each dimension are different. In 2D it is a coefficient for finite wave vector k, as seen in equation (3.64), while in 3D it is the low energy limit, as defined in equation (3.88).
- Differently from the 3D case, the scattering length has to be a positive quantity because it is inside a logarithm.
- Regarding the different definitions of the s-wave scattering length, in 3D it is easy to see that in general the phase shift remains finite when $k \to 0$. From equation (3.88) we have $\delta_0 \approx -ka$, while in 2D the logarithm gives a divergent expression as seen in equation (3.64).

- Also, as shown in Figure 3.2 a 2D circular potential has an *s*-wave bound state for any depth, while in 3D there is a minimum depth required for a bound state.

Chapter 4

BEC-BCS crossover of ultracold Fermi gases

In this chapter we will present the main aspects of the BEC-BCS crossover. We will follow the work of Leggett [13], who had the idea to extend the pairing mechanism of Bardeen, Cooper and Schrieffer (BCS) to describe an homogeneous system with stronger interactions, where fermions form molecules that are described by a Bose-Einstein condensate (BEC) at zero temperature. The model we will consider is a homogeneous gas of fermions with two components, where we can tune the attractive interaction between fermions of different component. When modulating the strength of the interaction we can obtain a weakly interacting regime, which corresponds to the BCS limit, where the formation of Cooper pairs poses the conditions for the existence of superfluidity. On the other hand, we can tune the strength to the strongly interacting regime, where we obtain the formation of molecules made of two fermions of different component. These molecules are represented by an operator which satisfies bosonic commutation relations. Then, the strongly interacting regime is known as the Bose regime [30]. In the following we will focus on the zero temperature case, so we will refer to the strongly interacting limit as Bose-Einstein condensate regime (BEC), although there is no macroscopic occupation of the ground state at a non-zero temperature in an ideal 2D bose gas [108].

4.1 The BCS Hamiltonian

Let us begin with the mathematical description of our simplified model. We are considering an homogeneous gas of two-component fermions with the same mass m. For brevity we will label the components as spins $\uparrow$, $\downarrow$. The form of a second quantization Hamiltonian adequate for the low energy and low density gas is given by [13, 103, 109]:

$$\hat{H} = \sum_{\vec{k}\sigma} \varepsilon_{\vec{k}} c^{\dagger}_{\vec{k}\sigma} c_{\vec{k}\sigma} + \frac{1}{2L^D} \sum_{\vec{k}_1,\vec{k}_2,\vec{Q}} \sum_{\sigma_1,\sigma_2} \tilde{U}_{\sigma_1\sigma_2}(|\vec{k}_1 - \vec{k}_2|)\, c^{\dagger}_{\vec{k}_1,\sigma_1} c^{\dagger}_{\vec{Q}-\vec{k}_1,\sigma_2} c_{\vec{Q}-\vec{k}_2,\sigma_2} c_{\vec{k}_2,\sigma_1}, \tag{4.1}$$

where $\varepsilon_{\vec{k}} = \hbar^2 k^2/(2m)$ is the kinetic energy of a fermion of mass m, $c_{\vec{k}\sigma}$ and $c^{\dagger}_{\vec{k}\sigma}$ are annihilation and creation operators of fermions with momentum $\vec{k}$ and spin σ in an auxiliary box of size L^D with periodic boundary conditions. The vector $\vec{Q}$ can be regarded as the total wave vector of the interacting pairs. The interaction potential in wave vector space is denoted by $\tilde{U}_{\sigma_1\sigma_2}(\vec{k})$. The algebra of the annihilation and creation operators is given by

$$[c_{\vec{k}\sigma}, c^{\dagger}_{\vec{q}\sigma'}]_+ = \mathbb{I}\delta_{\vec{k}\vec{q}}\delta_{\sigma\sigma'}, \tag{4.2}$$

$$[c_{\vec{k}\sigma}, c_{\vec{q}\sigma'}]_+ = [c^{\dagger}_{\vec{k}\sigma}, c^{\dagger}_{\vec{q}\sigma'}]_+ = 0, \tag{4.3}$$

where we have defined the anticommutator $[c, c']_+ = cc' + c'c$ and the delta symbols $\delta_{\vec{k}\vec{q}}$ are zero when $\vec{k} \neq \vec{q}$, and equal to one when $\vec{k} = \vec{q}$. Also these operators have their own vacuum state $|0\rangle$, defined by

$$c_{\vec{k}\sigma}|0\rangle = 0. \tag{4.4}$$

In analogy with the non-interacting Fermi gas, we have used creation and annihilation operators of free particles with periodic boundary conditions. This is necessary since we want to determine densities of particles or energy. If we had used the basis of free particles, without the auxiliary volume, like in equation (3.11), we would find a problem defining a Fermi surface, since the infinite number of particles of the system does not allow us to fill a finite Fermi sphere. Then it is adequate to use periodic boundary conditions with an auxiliary box whose size will be taken to infinity at the end of calculations $L^D \to \infty$.

The Hamiltonian of equation (4.1) does not have an explicit solution, so theoretical tools have been developed to calculate observable properties, which try to capture the relevant features [13, 15, 23, 110]. Here we will follow the works of Bardeen, Cooper and Schrieffer [15] and Leggett [13] to describe a gas near its ground state. Then, we can remove some interaction terms based on scattering properties. As pointed out in equations (3.52) and (3.81), we will neglect interactions between same spins, and keep an interaction between opposite spins. This is because the interaction between same spins is given by a p-wave term which is negligible in comparison to the s-wave term. Also we will assume that the fermions move so slowly that we can neglect the interaction of pairs of fermions moving with a wave vector $\vec{Q} \neq \vec{0}$. Hence we propose the BCS Hamiltonian [15][1]

$$\hat{H}_{\text{BCS}} = \sum_{\vec{k}\sigma} \varepsilon_{\vec{k}} c^\dagger_{\vec{k}\sigma} c_{\vec{k}\sigma} + \frac{1}{2L^D} \sum_{\vec{k}_1,\vec{k}_2} \sum_{\sigma_1} \tilde{U}_{\sigma_1,-\sigma_1}(|\vec{k}_1 - \vec{k}_2|)\, c^\dagger_{\vec{k}_1,\sigma_1} c^\dagger_{-\vec{k}_1,-\sigma_1} c_{-\vec{k}_2,-\sigma_1} c_{\vec{k}_2,\sigma_1}. \tag{4.5}$$

We can make the sum over the spin σ_1 and notice that we can join the two terms by making a change of variables in the wave vectors $\vec{k}_1 \to -\vec{k}_1$, $\vec{k}_2 \to -\vec{k}_2$. This can be done for our radial potential because $\tilde{U}_{\sigma_1,-\sigma_1}(|\vec{k}_1 - \vec{k}_2|) = \tilde{U}_{-\sigma_1,\sigma_1}(|\vec{k}_2 - \vec{k}_1|)$. Then we obtain the final form of the Hamiltonian that we will use:

$$\hat{H}_{\text{BCS}} = \sum_{\vec{k}\sigma} \varepsilon_{\vec{k}} c^\dagger_{\vec{k}\sigma} c_{\vec{k}\sigma} + \frac{1}{L^D} \sum_{\vec{k}_1,\vec{k}_2} \tilde{U}(|\vec{k}_1 - \vec{k}_2|)\, c^\dagger_{\vec{k}_1\uparrow} c^\dagger_{-\vec{k}_1\downarrow} c_{-\vec{k}_2\downarrow} c_{\vec{k}_2\uparrow}, \tag{4.6}$$

where we dropped the spin labels of the potential. For the BCS-Leggett variational approach we can use this Hamiltonian to estimate the ground state energy [13]. However, we are also interested in calculating excitation properties. This can be done using the Mean-Field method [111, 112, 113][2], where we will substitute the interaction by a decomposed version of it using averages of operators in the following form:

$$c^\dagger_{\vec{k}_1\uparrow} c^\dagger_{-\vec{k}_1\downarrow} c_{-\vec{k}_2\downarrow} c_{\vec{k}_2\uparrow} \to \langle c^\dagger_{\vec{k}_1\uparrow} c^\dagger_{-\vec{k}_1\downarrow}\rangle c_{-\vec{k}_2\downarrow} c_{\vec{k}_2\uparrow} + c^\dagger_{\vec{k}_1\uparrow} c^\dagger_{-\vec{k}_1\downarrow} \langle c_{-\vec{k}_2\downarrow} c_{\vec{k}_2\uparrow}\rangle - \langle c^\dagger_{\vec{k}_1\uparrow} c^\dagger_{-\vec{k}_1\downarrow}\rangle \langle c_{-\vec{k}_2\downarrow} c_{\vec{k}_2\uparrow}\rangle. \tag{4.7}$$

[1] We could work with the removed terms and make the Mean-field approach, where we would get Hartree and Fock terms. If we consider an interaction that does not depend on the spin, they affect the gap equation. If we consider a contact interaction, those terms are removed when renormalizing the theory, since they would be proportional to the (non-physical) strength $g \to 0^-$.

[2] We approximate an operator of the form $\hat{A}\hat{B}$ by small deviations $(\hat{d},\ \hat{e})$ around their expectation value of the ground state $\hat{A} = \hat{d} + \langle\hat{A}\rangle$, $\hat{B} = \hat{e} + \langle\hat{B}\rangle$ and neglect quadratic deviations $\hat{d}\hat{e}$ [111].

The operator on the right side will be the interaction term of the mean-field approximation of the BCS Hamiltonian. This approximation can be regarded as an approximation to a correlation [111, 114]:

$$\langle c^\dagger_{\vec{k}_1\uparrow} c^\dagger_{-\vec{k}_1\downarrow} c_{-\vec{k}_2\downarrow} c_{\vec{k}_2\uparrow}\rangle \approx \langle c^\dagger_{\vec{k}_1\uparrow} c^\dagger_{-\vec{k}_1\downarrow}\rangle\langle c_{-\vec{k}_2\downarrow} c_{\vec{k}_2\uparrow}\rangle. \tag{4.8}$$

The equality in equation (4.8) is not always a good approximation so there are many beyond-mean-field techniques that have been developed in past years [23, 110, 115]. Nevertheless, the mean-field approach gives a good qualitative description and it is a starting point for improving the physical descriptions. For example, Gaussian fluctuations use a small deviation around the mean-field values [115].

After making the mean-field approximation, given in equation (4.7), we are left with a Hamiltonian that is easier to analyze. We will follow Bogoliubov [112] and Valatin [113] and define a Grand potential operator which we can diagonalize by means of a Bogoliubov transformation. The following is based on the nice presentation of Tinkham [24]. We have the mean-field approximation of the Grand potential operator $\hat{\Omega}_M = \hat{H}_M - \mu\hat{N}$

$$\hat{\Omega}_M = \sum_{\vec{k}\sigma} \xi_{\vec{k}} c^\dagger_{\vec{k}\sigma} c_{\vec{k}\sigma} + \frac{1}{L^D}\sum_{\vec{k}_1}\sum_{\vec{k}_2} \tilde{U}(|\vec{k}_1 - \vec{k}_2|)\,(c^\dagger_{\vec{k}_1\uparrow} c^\dagger_{-\vec{k}_1\downarrow} b_{\vec{k}_2} + b^*_{\vec{k}_1} c_{-\vec{k}_2\downarrow} c_{\vec{k}_2\uparrow} - b^*_{\vec{k}_1} b_{\vec{k}_2}), \tag{4.9}$$

where $b_{\vec{k}} = \langle c_{-\vec{k}\downarrow} c_{\vec{k}\uparrow}\rangle$ and $\xi_{\vec{k}} = \varepsilon_{\vec{k}} - \mu$. In the grand canonical ensemble, assuming that we have the same amount of spin up particles as spin down $N_\uparrow = N_\downarrow$, we have to introduce a number equation, which determines the average number of particles [116]. For our homogeneous case we have to work with the density because we will take the thermodynamic limit ($N \to \infty$ and $L^D \to \infty$ keeping a finite density N/L^D):

$$\frac{\langle\hat{N}\rangle}{L^D} = \frac{1}{L^D}\sum_{\vec{k}\sigma}\langle c^\dagger_{\vec{k}\sigma} c_{\vec{k}\sigma}\rangle. \tag{4.10}$$

We can notice that there is a scalar quantity in the interaction term of equation (4.9) that can be grouped by defining the so-called gap $\Delta_{\vec{k}}$. Hence, the gap is a quantity defined in terms of the interaction and the expectation value $\langle c_{-\vec{k}\downarrow} c_{\vec{k}\uparrow}\rangle$. The gap emphasizes the presence of pairs of fermions, introducing a pairing mechanism that will allow the formation of Cooper pairs or molecules. We define the gap equation in the following way:

$$\Delta_{\vec{k}} = -\frac{1}{L^D}\sum_{\vec{k}_1} \tilde{U}(\vec{k}_1 - \vec{k})\langle c_{-\vec{k}_1\downarrow} c_{\vec{k}_1\uparrow}\rangle. \tag{4.11}$$

In accordance with our previous assumptions of the scattering potentials, we will consider a gap that depends on the norm of the wave vector $|\vec{k}|$, although we will keep the wave vector in the subscript. Then, using equations (4.11) and (4.9), the Grand potential $\hat{\Omega}_M$ is given by[3]

$$\hat{\Omega}_M = \sum_{\vec{k}\sigma} \xi_{\vec{k}} c^\dagger_{\vec{k}\sigma} c_{\vec{k}\sigma} - \sum_{\vec{k}_1} (\Delta_{\vec{k}_1} c^\dagger_{\vec{k}_1\uparrow} c^\dagger_{-\vec{k}_1\downarrow} + \Delta^*_{\vec{k}_1} c_{-\vec{k}_1\downarrow} c_{\vec{k}_1\uparrow} - \Delta_{\vec{k}_1} b^*_{\vec{k}_1}). \tag{4.12}$$

[3]Sometimes the last term is dropped in the sense that it is just a shift in energy. However, it is important to keep it for calculating the ground state energy. Also for considering phase transitions it might be important [33].

To diagonalize the grand potential operator we can perform a Bogoliubov transformation [112]. We have two types of fermions ($\uparrow$, $\downarrow$), so we need to introduce two operators that will create different quasiparticles $\gamma_{\vec{k}}$ and $\alpha_{\vec{k}}$. We define the transformation in the following way [24]:

$$c_{\vec{k}\uparrow} = u^*_{\vec{k}}\gamma_{\vec{k}} + v_{\vec{k}}\alpha^\dagger_{\vec{k}} \tag{4.13}$$

$$c_{-\vec{k}\downarrow} = -v_{\vec{k}}\gamma^\dagger_{\vec{k}} + u^*_{\vec{k}}\alpha_{\vec{k}}, \tag{4.14}$$

We are interested in defining a canonical transformation to preserve the fermionic anti-commuting relations, else we would have to deal with complicated anti-conmutators. Hence, we impose a condition that allows us to continue using a fermionic algebra of the operators [23]

$$|u_{\vec{k}}|^2 + |v_{\vec{k}}|^2 = 1. \tag{4.15}$$

Then we have the fermionic algebra

$$[\alpha_{\vec{k}}, \alpha_{\vec{q}}]_+ = [\gamma_{\vec{k}}, \gamma_{\vec{q}}]_+ = [\alpha_{\vec{k}}, \gamma^\pm_{\vec{q}}]_+ = 0, \tag{4.16}$$

and

$$[\alpha_{\vec{k}}, \alpha^\dagger_{\vec{q}}]_+ = [\gamma_{\vec{k}}, \gamma^\dagger_{\vec{q}}]_+ = \mathbb{I}\delta_{\vec{k}\vec{q}}, \tag{4.17}$$

where we are using the anticonmutator $[\alpha, \gamma]_+ = \alpha\gamma + \gamma\alpha$. After the transformation, the grand potential operator in the mean-field approximation is given by

$$\begin{aligned}
\hat{\Omega}_M = &\sum_{\vec{k}} \xi_{\vec{k}}\Big[|u_{\vec{k}}|^2\gamma^\dagger_{\vec{k}}\gamma_{\vec{k}} + u_{\vec{k}}v_{\vec{k}}\underline{\gamma^\dagger_{\vec{k}}\alpha^\dagger_{\vec{k}}} + v^*_{\vec{k}}u^*_{\vec{k}}\underbrace{\alpha_{\vec{k}}\gamma_{\vec{k}}} + |v_{\vec{k}}|^2 - |v_{\vec{k}}|^2\alpha^\dagger_{\vec{k}}\alpha_{\vec{k}}\Big] \\
&+ \sum_{\vec{k}} \xi_{\vec{k}}\Big[|v_{\vec{k}}|^2 - |v_{\vec{k}}|^2\gamma^\dagger_{\vec{k}}\gamma_{\vec{k}} - v^*_{\vec{k}}u^*_{\vec{k}}\underbrace{\gamma_{\vec{k}}\alpha_{\vec{k}}} - u_{\vec{k}}v_{\vec{k}}\underline{\alpha^\dagger_{\vec{k}}\gamma^\dagger_{\vec{k}}} + |u_{\vec{k}}|^2\alpha^\dagger_{\vec{k}}\alpha_{\vec{k}}\Big] \\
&+ \sum_{\vec{k}} \Big[(\Delta_{\vec{k}}u_{\vec{k}}v^*_{\vec{k}} + \Delta^*_{\vec{k}}u^*_{\vec{k}}v_{\vec{k}})(\gamma^\dagger_{\vec{k}}\gamma_{\vec{k}} + \alpha^\dagger_{\vec{k}}\alpha_{\vec{k}} - 1) + (\Delta_{\vec{k}}v^{*2}_{\vec{k}} - \Delta^*_{\vec{k}}u^{*2}_{\vec{k}})\underbrace{\alpha_{\vec{k}}\gamma_{\vec{k}}} \\
&+ (\Delta^*_{\vec{k}}v^2_{\vec{k}} - \Delta_{\vec{k}}u^2_{\vec{k}})\underline{\gamma^\dagger_{\vec{k}}\alpha^\dagger_{\vec{k}}} + \Delta_{\vec{k}}b^*_{\vec{k}}\Big],
\end{aligned} \tag{4.18}$$

where we have indicated the non-diagonal terms, whose coefficients should be zero. This condition allows us to determine the parameters $u_{\vec{k}}$ and $v_{\vec{k}}$,

$$\xi_{\vec{k}}v_{\vec{k}}u_{\vec{k}} + \xi_{\vec{k}}v_{\vec{k}}u_{\vec{k}} + (\Delta^*_{\vec{k}}v^2_{\vec{k}} - \Delta_{\vec{k}}u^2_{\vec{k}}) = 0. \tag{4.19}$$

Rearranging terms we have

$$2\xi_{\vec{k}}v_{\vec{k}}u_{\vec{k}} + (\Delta^*_{\vec{k}}v^2_{\vec{k}} - \Delta_{\vec{k}}u^2_{\vec{k}}) = 0. \tag{4.20}$$

Multiplying by $\Delta^*_{\vec{k}}/u^2_{\vec{k}}$ we get

$$\left(\Delta^*_{\vec{k}}\frac{v_{\vec{k}}}{u_{\vec{k}}}\right)^2 + 2\xi_{\vec{k}}\Delta^*_{\vec{k}}\frac{v_{\vec{k}}}{u_{\vec{k}}} - |\Delta_{\vec{k}}|^2 = 0. \tag{4.21}$$

Below we will see that we can divide by $u_{\vec{k}}$ because it will turn out to be different from zero. We can identify equation (4.21) with a quadratic polynomial in the variable $\Delta^*_{\vec{k}} v_{\vec{k}}/u_{\vec{k}}$ whose solutions lead us to:

$$\frac{v_{\vec{k}}}{u_{\vec{k}}} = \frac{-\xi_{\vec{k}} \pm \sqrt{\xi^2_{\vec{k}} + |\Delta_{\vec{k}}|^2}}{\Delta^*_{\vec{k}}} = \frac{-\xi_{\vec{k}} \pm E_{\vec{k}}}{\Delta^*_{\vec{k}}}, \tag{4.22}$$

where we have defined

$$E_{\vec{k}} = \sqrt{\xi^2_{\vec{k}} + |\Delta_{\vec{k}}|^2}. \tag{4.23}$$

In equation (4.22) we have two possibilities for the term $v_{\vec{k}}/u_{\vec{k}}$, which are rarely discussed. If we were to choose the negative sign, the quantity $|v_{\vec{k}}|^2$ would not be integrable over all the momentum space. Then, when calculating the expectation value of the number operator $\langle \hat{N} \rangle$, we would get a divergent density $\langle \hat{N} \rangle / L^D \to \infty$, which contradicts our hypothesis of a finite density. Then we have[4]

$$\frac{v_{\vec{k}}}{u_{\vec{k}}} = \frac{E_{\vec{k}} - \xi_{\vec{k}}}{\Delta^*_{\vec{k}}}. \tag{4.24}$$

Using the unitarity condition (4.15) we have

$$|v_{\vec{k}}|^2 = \frac{1}{2}\left(1 - \frac{\xi_{\vec{k}}}{E_{\vec{k}}}\right) \quad , \quad |u_{\vec{k}}|^2 = \frac{1}{2}\left(1 + \frac{\xi_{\vec{k}}}{E_{\vec{k}}}\right), \tag{4.25}$$

Hence the Bogoliubov transformation (4.13)-(4.14) is determined by the gap $\Delta_{\vec{k}}$ and the chemical potential μ. Consistently, we verify that $u_{\vec{k}}$ is different from zero because its norm is positive (then it can be in denominators). Also, we find that $|v_{\vec{k}}|^2 \to 0$ when $k \to \infty$ [allowing us to get a well defined density in equation (4.10)]. Another observation that has to be made is that in some steps we have divided by the gap $\Delta_{\vec{k}}$, so we would not expect it to be zero. However, a careful view at the steps, for example in equations (4.19) and (4.22), shows that the parameters $v_{\vec{k}}$ and $u_{\vec{k}}$ can be defined with their analytic continuation[5] when $\Delta_{\vec{k}} \to 0$. This important aspect is relevant for the case of finite-range interactions that we will discuss in subsection 4.4.3, since $\Delta_{\vec{k}}$ be zero at some points $\vec{k}$. Also we have verified numerically a good behavior of the gap when it has an oscillatory behavior, having nodes [103] [6]. Using the relations in (4.25) it can be verified that

$$\xi_{\vec{k}} |u_{\vec{k}}|^2 - \xi_{\vec{k}} |v_{\vec{k}}|^2 = \frac{\xi^2_{\vec{k}}}{E_{\vec{k}}}, \tag{4.26}$$

[4] If we had started with the BCS-Leggett variational method we would have identified $v_{\vec{k}}/u_{\vec{k}}$ as the Fourier transform of the pair wave function, which has to be a square-integrable function, making natural the election of the plus sign.

[5] An example of analytic continuation is given by the sinc function. We can show that

$$\lim_{x \to 0} x^{-1} \sin(x) = 1.$$

Then we can define the $\mathrm{sinc}(x)$ function as

$$\mathrm{sinc}(x) = \begin{cases} x^{-1}\sin(x) \text{ for} & x \neq 0 \\ 1 \text{ if} & x = 0 \end{cases}$$

[6] By hypothesis the system always has an interaction between fermions. In the mean-field approach a solution with the gap equal to zero [no interaction term, see equation (4.12)] indicates that the approximations may not be strictly valid.

$$\xi_{\vec{k}}|u_{\vec{k}}|^2 + \xi_{\vec{k}}|v_{\vec{k}}|^2 = \xi_{\vec{k}}, \tag{4.27}$$

and

$$\Delta^*_{\vec{k}} u^*_{\vec{k}} v_{\vec{k}} = \frac{|\Delta_{\vec{k}}|^2}{2E_{\vec{k}}}. \tag{4.28}$$

With those relations we can simplify the grand potential operator $\hat{\Omega}_M$ in equation (4.18), where we already know that non-diagonal terms are zero. Then we obtain

$$\hat{\Omega}_M = \sum_{\vec{k}} \left\{ E_{\vec{k}} \gamma^\dagger_{\vec{k}} \gamma_{\vec{k}} + E_{\vec{k}} \alpha^\dagger_{\vec{k}} \alpha_{\vec{k}} + \xi_{\vec{k}} - E_{\vec{k}} + \frac{|\Delta_{\vec{k}}|^2}{2E_{\vec{k}}} \right\}. \tag{4.29}$$

This diagonal form allows us to identify the eigenvalues of the grand potential operator, particularly the ground state value Ω_0, given by

$$\Omega_0 = \sum_{\vec{k}} \xi_{\vec{k}} - E_{\vec{k}} + \frac{|\Delta_{\vec{k}}|^2}{2E_{\vec{k}}}. \tag{4.30}$$

In this case, the absence of quasiparticles corresponds to the ground state[7] because when we create one ($\gamma_{\vec{k}}$ or $\alpha_{\vec{k}}$) we increase the energy by $E_{\vec{k}} > 0$. Also this form allows us to generate a complete basis, by using the quasiparticle creation operators over their vacuum, which we will show to be given by the BCS state $|\Psi_{\text{BCS}}\rangle$. To calculate the expectation values of equations (4.10) and (4.11) we can substitute the free fermion operators using quasiparticle operators $\alpha_{\vec{k}}$ and $\gamma_{\vec{k}}$ to obtain expressions given in terms of $v_{\vec{k}}$ and $u_{\vec{k}}$. Then we can use equation (4.25) to express the number equation (4.10) and the gap equation (4.11) in terms of the chemical potential μ and the gap $\Delta_{\vec{k}}$, as we will show in section 4.4.

4.2 The BCS-Leggett variational approach

We can define a grand potential operator $\hat{\Omega}$ using the BCS Hamiltonian (4.6), without using the mean-field approach [shown in equation (4.7)] and follow the generalized BCS approach made by Leggett [13] and Eagles [31] to describe a strongly interacting regime. The BCS wave function is

$$|\Psi_{\text{BCS}}\rangle = \prod_{\vec{k}} (u_{\vec{k}} + v_{\vec{k}} c^\dagger_{\vec{k}\uparrow} c^\dagger_{-\vec{k}\downarrow}) |0\rangle, \tag{4.31}$$

where we are using the vacuum of free fermions $|0\rangle$ given in equation (4.4). Also, $u_{\vec{k}}$ and $v_{\vec{k}}$ are the variational parameters, which are complex numbers in genral, that satisfy the normalization condition

$$|u_{\vec{k}}|^2 + |v_{\vec{k}}|^2 = 1. \tag{4.32}$$

This relation is useful for the calculation of any expectation value. It turns out that these parameters are the same that determine the Bogoliubov transformation, given in equations (4.13)

[7] In general the ground state is not the vacuum of the quasiparticles, as can be found if we considered an imbalance between up and down spins $N_\uparrow \neq N_\downarrow$ [33].

and (4.14). Hence it is enough to calculate the expectation value of the grand potential operator

$$\hat{\Omega} = \sum_{\vec{k}\sigma}(\varepsilon_{\vec{k}} - \mu)c^{\dagger}_{\vec{k}\sigma}c_{\vec{k}\sigma} + \frac{1}{L^D}\sum_{\vec{k}_1,\vec{k}_2}\tilde{U}(|\vec{k}_1 - \vec{k}_2|)\, c^{\dagger}_{\vec{k}_1\uparrow}c^{\dagger}_{-\vec{k}_1\downarrow}c_{-\vec{k}_2\downarrow}c_{\vec{k}_2\uparrow}, \tag{4.33}$$

which is given by [109]

$$\Omega_0 = 2\sum_{\vec{k}}(\varepsilon_{\vec{k}} - \mu)|v_{\vec{k}}|^2 + \frac{1}{L^D}\sum_{\vec{k}_1}\tilde{U}(\vec{0})|v_{\vec{k}_1}|^2 + \frac{1}{L^D}\sum_{\vec{k}_1}\sum_{\vec{k}_2\neq\vec{k}_1}\tilde{U}(|\vec{k}_1 - \vec{k}_2|)v^*_{\vec{k}_1}u_{\vec{k}_1}v_{\vec{k}_2}u^*_{\vec{k}_2} \tag{4.34}$$

Without loss of generality we will restrict the parameters to real values $u_{\vec{k}},\ v_{\vec{k}} \in \mathbb{R}$ to facilitate the discussion of the minimization procedure [8], which is given by

$$\frac{\partial\langle\hat{\Omega}\rangle}{\partial v_{\vec{k}}} = 0\ ,\ \frac{\partial^2\langle\hat{\Omega}\rangle}{\partial v^2_{\vec{k}}} > 0, \tag{4.35}$$

The first equality is satisfied[9] when the parameters obey the so-called gap equation:

$$2u_{\vec{k}}v_{\vec{k}}E_{\vec{k}} = -\frac{1}{L^D}\sum_{\vec{k}_2}\tilde{U}(|\vec{k} - \vec{k}_2|)u_{\vec{k}_2}v_{\vec{k}_2}, \tag{4.36}$$

where $E_{\vec{k}} = [(\varepsilon_{\vec{k}} - \mu)^2 + \Delta^2_{\vec{k}}]^{1/2}$. We can notice the appearance of the terms $u_{\vec{k}}v_{\vec{k}}$ in equations (4.34) and (4.36), which come from the expectation values $\langle c^{\dagger}_{\vec{k}\uparrow}c^{\dagger}_{-\vec{k}\downarrow}\rangle$ and $\langle c_{-\vec{k}\downarrow}c_{\vec{k}\uparrow}\rangle$ (we are considering $u_{\vec{k}},\ v_{\vec{k}} \in \mathbb{R}$). Then the BCS-Leggett variational approach also emphasizes the presence of pairs. The form of equation (4.36) leads us to define a quantity that represents the interaction between fermions, known as the gap $\Delta_{\vec{k}}$ (which is also a real number). Then we have

$$\Delta_{\vec{k}} = 2u_{\vec{k}}v_{\vec{k}}E_{\vec{k}}. \tag{4.37}$$

Before analyzing the inequality in equation (4.35), let us mention that the number equation, that arises from the grand canonical ensemble [116], is given by the expectation value

$$\frac{\langle\hat{N}\rangle}{L^D} = \frac{1}{L^D}\sum_{\vec{k}\sigma}\langle c^{\dagger}_{\vec{k}\sigma}c_{\vec{k}\sigma}\rangle = \frac{1}{L^D}\sum_{\vec{k}\sigma}v^2_{\vec{k}}, \tag{4.38}$$

where we have used the BCS wave function of equation (4.31). Then, $v^2_{\vec{k}}$ has to be integrable. Using the normalization condition we obtain the expected relation for the variational parameters, given in equation (4.25),

$$v^2_{\vec{k}} = \frac{1}{2}\left(1 - \frac{\xi_{\vec{k}}}{E_{\vec{k}}}\right)\ ,\quad u^2_{\vec{k}} = \frac{1}{2}\left(1 + \frac{\xi_{\vec{k}}}{E_{\vec{k}}}\right), \tag{4.39}$$

[8] In general the parameters would have the form $v_{\vec{k}} = e^{i\phi_v(\vec{k})}|v_{\vec{k}}|$, $u_{\vec{k}} = e^{i\phi_u(\vec{k})}|u_{\vec{k}}|$. Then the minimization would be given by finding the critical points and analyzing the determinant of the Hessian matrix of $\Omega(|v_{\vec{k}}|, \phi_v(\vec{k}), \phi_u(\vec{k}))$. However, since the imaginary part of the grand potential Ω_0 in equation (4.34) is zero, we can argue that for a general interaction potential $\tilde{U}(|\vec{q}|)$ the phases $\phi_v(\vec{k})$, $\phi_u(\vec{k})$ are constant.

[9] When deriving we use the following identity:

$$\frac{\partial v_{\vec{k}_1}}{\partial v_{\vec{k}}} = \delta_{\vec{k},\vec{k}_1}$$

Let us return to the inequality in equation (4.35). It turns out to be satisfied by means of the gap equation (4.36) and with the aid of the thermodynamic limit. It is found

$$\frac{\partial^2\langle\hat{\Omega}\rangle}{\partial v_{\vec{k}}^2} = 4\frac{E_{\vec{k}}}{1-v_{\vec{k}}^2} > 0. \tag{4.40}$$

Let us overemphasize that the thermodynamic limit in equation (4.40) allows us to drop another term that involves the interaction potential explicitly $\tilde{U}(|\vec{k}|)$. Also, to justify that the second derivative is positive we can interpret $v_{\vec{k}}^2$ as the occupation of states in wave vector space, see equation (4.38), and use equations (4.39). Then we can convince ourselves that $1-v_{\vec{k}}^2 > 0$, which can be verified numerically in Figure 5.1. Although the mean-field approach is easier and contains the variational method, it is interesting to go through the algebra of calculating the expectation value $\langle\hat{\Omega}\rangle$, because in this way we see explicitly how we can force the expectation value of the interaction to have its mean-field value, given in equation (4.8). We require to use the thermodynamic limit during the calculations, else we would have to carry a huge amount of terms. Now we can see that the BCS state is the vacuum of the quasiparticles obtained in the mean-field approach (4.13)-(4.14). For example:

$$\begin{aligned}
\alpha_{\vec{q}}\,|\Psi_{\mathrm{BCS}}\rangle =&(v_{\vec{q}}c_{\vec{q}\uparrow}^{\dagger} + u_{\vec{q}}c_{-\vec{q}\downarrow})\prod_{\vec{k}}(u_{\vec{k}} + v_{\vec{k}}c_{\vec{k}\uparrow}^{\dagger}c_{-\vec{k}\downarrow}^{\dagger})\,|0\rangle \\
=&\left[\prod_{\vec{k}\neq\vec{q}}(u_{\vec{k}} + v_{\vec{k}}c_{\vec{k}\uparrow}^{\dagger}c_{-\vec{k}\downarrow}^{\dagger})\right](v_{\vec{q}}c_{\vec{q}\uparrow}^{\dagger} + u_{\vec{q}}c_{-\vec{q}\downarrow})(u_{\vec{q}} + v_{\vec{q}}c_{\vec{q}\uparrow}^{\dagger}c_{-\vec{q}\downarrow}^{\dagger})\,|0\rangle \\
=&\left[\prod_{\vec{k}\neq\vec{q}}(u_{\vec{k}} + v_{\vec{k}}c_{\vec{k}\uparrow}^{\dagger}c_{-\vec{k}\downarrow}^{\dagger})\right](v_{\vec{q}}u_{\vec{q}}c_{\vec{q}\uparrow}^{\dagger} + v_{\vec{q}}^2c_{\vec{q}\uparrow}^{\dagger}c_{\vec{q}\uparrow}^{\dagger}c_{-\vec{q}\downarrow}^{\dagger} + u_{\vec{q}}^2c_{-\vec{q}\downarrow} + u_{\vec{q}}v_{\vec{q}}c_{-\vec{q}\downarrow}c_{\vec{q}\uparrow}^{\dagger}c_{-\vec{q}\downarrow}^{\dagger})\,|0\rangle \\
=&\left[\prod_{\vec{k}\neq\vec{q}}(u_{\vec{k}} + v_{\vec{k}}c_{\vec{k}\uparrow}^{\dagger}c_{-\vec{k}\downarrow}^{\dagger})\right][v_{\vec{q}}u_{\vec{q}}c_{\vec{q}\uparrow}^{\dagger} + v_{\vec{q}}^2c_{\vec{q}\uparrow}^{\dagger}c_{\vec{q}\uparrow}^{\dagger}c_{-\vec{q}\downarrow}^{\dagger} + u_{\vec{q}}^2c_{-\vec{q}\downarrow} - u_{\vec{q}}v_{\vec{q}}c_{\vec{q}\uparrow}^{\dagger}(\mathbb{I} - c_{-\vec{q}\downarrow}^{\dagger}c_{-\vec{q}\downarrow})]\,|0\rangle \\
=&0.
\end{aligned} \tag{4.41}$$

In the fist equality we introduced the definition of the BCS state. In the second equality we moved all the operators which have $\vec{k} \neq \vec{q}$ to the left. In the third equality we expanded the product of operators. In the fourth we used anticommutation relations, so we can see that like terms cancel, and Pauli exclusion principle makes zero one of the terms. In the same way we can verify that

$$\gamma_{\vec{q}}\,|\Psi_{\mathrm{BCS}}\rangle = 0. \tag{4.42}$$

Then we have verified that the BCS state is the vacuum of the quasiparticle operators (4.13)-(4.14).

Since we have a variational wave function, it is interesting to discuss its functional form. We can see that this wave function belongs to the Fock space because it is a linear combination of states with different number of particles. To see this we can perform the product of operators in the BCS state (4.31) to identify terms with fixed number of particles. This product has to be made

using an arbitrary order of the wave vectors $\vec{k}$. Then we have [109, 117]

$$|\Psi_{\rm BCS}\rangle = \Bigg[\prod_{\vec{k}} u_{\vec{k}} + \sum_{\vec{k}_1}\Bigg(\prod_{\vec{k}\neq\vec{k}_1} u_{\vec{k}}\Bigg)v_{\vec{k}_1}\beta^\dagger_{\vec{k}_1} + \sum_{\vec{k}_1}\sum_{\vec{k}_2>\vec{k}_1}\Bigg(\prod_{\vec{k}\neq\vec{k}_1,\vec{k}_2} u_{\vec{k}}\Bigg)v_{\vec{k}_1}v_{\vec{k}_2}\beta^\dagger_{\vec{k}_1}\beta^\dagger_{\vec{k}_2}$$
$$+ \sum_{\vec{k}_1}\sum_{\vec{k}_2>\vec{k}_1}\sum_{\vec{k}_3>\vec{k}_2}\Bigg(\prod_{\vec{k}\neq\vec{k}_1,\vec{k}_2,\vec{k}_3} u_{\vec{k}}\Bigg)v_{\vec{k}_1}v_{\vec{k}_2}v_{\vec{k}_3}\beta^\dagger_{\vec{k}_1}\beta^\dagger_{\vec{k}_2}\beta^\dagger_{\vec{k}_3} + \ldots + \sum_{\vec{k}_\infty>\vec{k}_1}\Bigg(\prod_{\vec{k}\neq\vec{k}_1,\ldots,\vec{k}_\infty} u_{\vec{k}}\Bigg)v_{\vec{k}_1}\ldots v_{\vec{k}_\infty}\beta^\dagger_{\vec{k}_1}\ldots\beta^\dagger_{\vec{k}_\infty}\Bigg]|0\rangle\,, \tag{4.43}$$

where we have defined $\beta^\dagger_{\vec{k}} = c^\dagger_{\vec{k}\uparrow}c^\dagger_{-\vec{k}\downarrow}$, and the inequalities on the sums are to indicate that we should keep the arbitrary order of the wave vectors. We can factorize a product of the parameters $u_{\vec{k}}$ to obtain[10]

$$|\Psi_{\rm BCS}\rangle = \Bigg(\prod_{\vec{k}} u_{\vec{k}}\Bigg)\Bigg[1 + \sum_{\vec{k}_1}\frac{v_{\vec{k}_1}}{u_{\vec{k}_1}}\beta^\dagger_{\vec{k}_1} + \sum_{\vec{k}_1}\sum_{\vec{k}_2>\vec{k}_1}\frac{v_{\vec{k}_1}}{u_{\vec{k}_1}}\frac{v_{\vec{k}_2}}{u_{\vec{k}_2}}\beta^\dagger_{\vec{k}_1}\beta^\dagger_{\vec{k}_2}$$
$$+ \sum_{\vec{k}_1}\sum_{\vec{k}_2>\vec{k}_1}\sum_{\vec{k}_3>\vec{k}_2}\frac{v_{\vec{k}_1}}{u_{\vec{k}_1}}\frac{v_{\vec{k}_2}}{u_{\vec{k}_2}}\frac{v_{\vec{k}_3}}{u_{\vec{k}_3}}\beta^\dagger_{\vec{k}_1}\beta^\dagger_{\vec{k}_2}\beta^\dagger_{\vec{k}_3} + \ldots + \sum_{\vec{k}_\infty>\vec{k}_1}\frac{v_{\vec{k}_1}}{u_{\vec{k}_1}}\ldots\frac{v_{\vec{k}_\infty}}{u_{\vec{k}_\infty}}\beta^\dagger_{\vec{k}_1}\ldots\beta^\dagger_{\vec{k}_\infty}\Bigg]|0\rangle\,, \tag{4.44}$$

where on each sum we had to complete the product of $u_{\vec{k}}$, so we had to divide by the missing parameters. We can remove the restricted (arbitrary) order of the wave vectors by noting that terms of the form $\beta^\dagger_{\vec{k}}\beta^\dagger_{\vec{k}}|0\rangle = 0$ because of Pauli exclusion principle (using the same creation operator twice over the vacuum gives zero). It can be shown that $[\beta^\dagger_{\vec{k}},\beta^\dagger_{\vec{q}}] = 0$. So that we can remove the restriction over the sums and take into account that each combination of wave vectors $\vec{k}_i$ will be repeated $M!$ times in the term with M pairs,

$$|\Psi_{\rm BCS}\rangle = \Bigg(\prod_{\vec{k}} u_{\vec{k}}\Bigg)\Bigg[1 + \sum_{\vec{k}_1}\frac{v_{\vec{k}_1}}{u_{\vec{k}_1}}\beta^\dagger_{\vec{k}_1} + \frac{1}{2!}\sum_{\vec{k}_1}\sum_{\vec{k}_2}\frac{v_{\vec{k}_1}}{u_{\vec{k}_1}}\frac{v_{\vec{k}_2}}{u_{\vec{k}_2}}\beta^\dagger_{\vec{k}_1}\beta^\dagger_{\vec{k}_2}$$
$$+ \frac{1}{3!}\sum_{\vec{k}_1}\sum_{\vec{k}_2}\sum_{\vec{k}_3}\frac{v_{\vec{k}_1}}{u_{\vec{k}_1}}\frac{v_{\vec{k}_2}}{u_{\vec{k}_2}}\frac{v_{\vec{k}_3}}{u_{\vec{k}_3}}\beta^\dagger_{\vec{k}_1}\beta^\dagger_{\vec{k}_2}\beta^\dagger_{\vec{k}_3} + \ldots + \frac{1}{M_\infty!}\sum_{\vec{k}_\infty,\ldots,\vec{k}_1}\frac{v_{\vec{k}_1}}{u_{\vec{k}_1}}\ldots\frac{v_{\vec{k}_\infty}}{u_{\vec{k}_\infty}}\beta^\dagger_{\vec{k}_1}\ldots\beta^\dagger_{\vec{k}_\infty}\Bigg]|0\rangle\,. \tag{4.45}$$

We can identify the series of the exponential function to get

$$|\Psi_{\rm BCS}\rangle = \Bigg(\prod_{\vec{k}} u_{\vec{k}}\Bigg)\exp\Bigg(\sum_{\vec{k}}\frac{v_{\vec{k}}}{u_{\vec{k}}}\beta^\dagger_{\vec{k}}\Bigg)|0\rangle\,. \tag{4.46}$$

[10] Another more direct way is to note that

$$|\Psi_{\rm BCS}\rangle = \prod_{\vec{k}} u_{\vec{k}}\Bigg(1 + \frac{v_{\vec{k}}}{u_{\vec{k}}}\beta^\dagger_{\vec{k}}\Bigg)|0\rangle$$
$$= \prod_{\vec{q}} u_{\vec{q}}\prod_{\vec{k}}\Bigg(1 + \frac{v_{\vec{k}}}{u_{\vec{k}}}\beta^\dagger_{\vec{k}}\Bigg)|0\rangle$$

Hence we can project to a state with fixed particle number in space representation. We get an antisymmetric wave function,

$$\langle \vec{x}_1, ..., \vec{x}_N | \Psi_{\mathrm{BCS}} \rangle = \left(\prod_{\vec{k}} u_{\vec{k}} \right) \frac{1}{(N/2)!} \sum_{\vec{k}_1,...,\vec{k}_{N/2}} \frac{v_{\vec{k}_1}}{u_{\vec{k}_1}} ... \frac{v_{\vec{k}_{N/2}}}{u_{\vec{k}_{N/2}}} \langle \vec{x}_1, ..., \vec{x}_N | \beta^\dagger_{\vec{k}_1} ... \beta^\dagger_{\vec{k}_{N/2}} |0\rangle . \tag{4.47}$$

We can identify the antisymmetric product of free fermions:

$$\langle \vec{x}_1, ..., \vec{x}_N | \beta^\dagger_{\vec{k}_1} ... \beta^\dagger_{\vec{k}_{N/2}} |0\rangle = \langle \vec{x}_1, ..., \vec{x}_N | c^\dagger_{\vec{k}_1\uparrow} c^\dagger_{-\vec{k}_1\downarrow} ... c^\dagger_{\vec{k}_{N/2}\uparrow} c^\dagger_{-\vec{k}_{N/2}\downarrow} |0\rangle$$

$$= \begin{vmatrix} e^{i\vec{k}_1\cdot\vec{x}_1}\chi_\uparrow(1) & e^{-i\vec{k}_1\cdot\vec{x}_1}\chi_\downarrow(1) & ... & e^{i\vec{k}_{N/2}\cdot\vec{x}_1}\chi_\uparrow(1) & e^{-i\vec{k}_{N/2}\cdot\vec{x}_1}\chi_\downarrow(1) \\ e^{i\vec{k}_1\cdot\vec{x}_2}\chi_\uparrow(2) & e^{-i\vec{k}_1\cdot\vec{x}_2}\chi_\downarrow(2) & ... & e^{i\vec{k}_{N/2}\cdot\vec{x}_2}\chi_\uparrow(2) & e^{-i\vec{k}_{N/2}\cdot\vec{x}_2}\chi_\downarrow(2) \\ \vdots & ... & \ddots & ... & \vdots \\ e^{i\vec{k}_1\cdot\vec{x}_{N-1}}\chi_\uparrow(N-1) & e^{-i\vec{k}_1\cdot\vec{x}_{N-1}}\chi_\downarrow(N-1) & ... & e^{i\vec{k}_{N/2}\cdot\vec{x}_{N-1}}\chi_\uparrow(N-1) & e^{-i\vec{k}_{N/2}\cdot\vec{x}_{N-1}}\chi_\downarrow(N-1) \\ e^{i\vec{k}_1\cdot\vec{x}_N}\chi_\uparrow(N) & e^{-i\vec{k}_1\cdot\vec{x}_N}\chi_\downarrow(N) & ... & e^{i\vec{k}_{N/2}\cdot\vec{x}_N}\chi_\uparrow(N) & e^{-i\vec{k}_{N/2}\cdot\vec{x}_N}\chi_\downarrow(N) \end{vmatrix}, \tag{4.48}$$

where we defined the one-particle spin function χ_σ which has spin $\sigma = \uparrow, \downarrow$. When substituting equation (4.48) into (4.47) we find an antisymmetric product which can be written in terms of a two-particle wave function:

$$\phi(i, j) = \phi_{\mathrm{BCS}}(\vec{x}_i - \vec{x}_j)\chi_\uparrow(i)\chi_\downarrow(j), \tag{4.49}$$

where we have separated the spatial dependence, which we will call the pair wave function[11]:

$$\phi_{\mathrm{BCS}}(\vec{r}) = \frac{1}{L^D} \sum_{\vec{k}} e^{i\vec{k}\cdot\vec{r}} \frac{v_{\vec{k}}}{u_{\vec{k}}}. \tag{4.50}$$

For one pair (two fermions) we have

$$\langle \vec{x}_1, \vec{x}_2 | \Psi_{\mathrm{BCS}} \rangle = L^D \left(\prod_{\vec{k}} u_{\vec{k}} \right) [\phi(1, 2) - \phi(2, 1)]. \tag{4.51}$$

For two pairs (four fermions) we have

$$\begin{aligned} \langle \vec{x}_1, \vec{x}_2, \vec{x}_3, \vec{x}_4 | \Psi_{\mathrm{BCS}} \rangle = L^{2D} \left(\prod_{\vec{k}} u_{\vec{k}} \right) [&\phi(4,3)\phi(2,1) - \phi(3,4)\phi(2,1) - \phi(4,2)\phi(3,1) + \phi(2,4)\phi(3,1) \\ &+\phi(3,2)\phi(4,1) - \phi(2,3)\phi(4,1) - \phi(4,3)\phi(1,2) + \phi(3,4)\phi(1,2) + \phi(4,1)\phi(3,2) \\ &-\phi(1,4)\phi(3,2) - \phi(3,1)\phi(4,2) + \phi(1,3)\phi(4,2) + \phi(4,2)\phi(1,3) - \phi(2,4)\phi(1,3) \\ &-\phi(4,1)\phi(2,3) + \phi(1,4)\phi(2,3) + \phi(2,1)\phi(4,3) - \phi(1,2)\phi(4,3) - \phi(3,2)\phi(1,4) \\ &+\phi(2,3)\phi(1,4) + \phi(3,1)\phi(2,4) - \phi(1,3)\phi(2,4) - \phi(2,1)\phi(3,4) + \phi(1,2)\phi(3,4)]. \end{aligned} \tag{4.52}$$

Then we can conclude that the BCS variational wave function is a sum of terms with different particle numbers. Each term is given by an anti-symmetric product of two-particle wave functions denoted by [7]

$$\langle \vec{x}_1, ..., \vec{x}_N | \Psi_{\mathrm{BCS}} \rangle \propto \mathcal{A}[\phi(1, 2)...\phi(N-1, N)], \tag{4.53}$$

[11] In the literature it is usual to refer to the Fourier transform of $u_{\vec{k}} v_{\vec{k}}$ as the pair wave function.

where $\mathcal{A}$ is to denote an antisymmetry operation.

Although we have not analyzed the behavior of the variational parameters $u_{\vec{k}}$ and $v_{\vec{k}}$, we will mention that the BCS wave function resembles a coherent state of bosons [7]

$$|\Psi_{\text{BCS}}\rangle = C_{\text{BCS}} \exp(\alpha b_{\vec{0}}^{\dagger})\,|0\rangle\,, \tag{4.54}$$

where [7]

$$C_{\text{BCS}} = \exp\Big[-\frac{1}{2}\sum_{\vec{k}} \ln(1+|v_{\vec{k}}/u_{\vec{k}}|^2)\Big], \tag{4.55}$$

and we have introduced a creation operator

$$b_{\vec{0}}^{\dagger} = \sum_{\vec{k}} \frac{v_{\vec{k}}}{\alpha u_{\vec{k}}} \beta_{\vec{k}}^{\dagger}. \tag{4.56}$$

The constant α is defined[12] such that

$$\langle\Psi_{\text{BCS}}|\, b_{\vec{0}}^{\dagger} b_{\vec{0}}\,|\Psi_{\text{BCS}}\rangle = \frac{N}{2}. \tag{4.57}$$

That is, the expectation value of the number operator associated to $b_{\vec{0}}$ is the number of pairs $N/2$. However, this operator has the following commutation relations [2, 12]:

$$[b_{\vec{0}}, b_{\vec{0}}] = 0 \tag{4.58}$$

$$[b_{\vec{0}}, b_{\vec{0}}^{\dagger}] = \sum_{\vec{k}} \frac{v_{\vec{k}}^2}{\alpha^2 u_{\vec{k}}^2}(\mathbb{I} - c_{\vec{k}\uparrow}^{\dagger} c_{\vec{k}\uparrow} - c_{\vec{k}\downarrow}^{\dagger} c_{\vec{k}\downarrow}), \tag{4.59}$$

where $\mathbb{I}$ is the identity operator. The relation in equation (4.59) is not of a boson operator, but what can be shown is that in the BEC limit the parameters behave in such a way that

$$\sum_{\vec{k}} \frac{v_{\vec{k}}^2}{\alpha^2 u_{\vec{k}}^2}\bigg|_{\text{BEC}} \approx 1. \tag{4.60}$$

Also, it is argued that the number operators have a negligible value in this limit [2][13]. Then we can neglect the two last terms in equation (4.59) to obtain a bosonic commutation relation $[b_{\vec{0}}, b_{\vec{0}}^{\dagger}] \approx \mathbb{I}$. However, in general we have to analyze all the matrix elements of $[b_{\vec{0}}, b_{\vec{0}}^{\dagger}]$, but the orthogonality of the eigenvectors of $\hat{\Omega}$ allows us to restrict to a few of them. As a representative case we will analyze the following matrix element for the contact interaction cases (2D and 3D):

$$\langle\Psi_{\text{BCS}}|[b_{\vec{0}}, b_{\vec{0}}^{\dagger}]|\Psi_{\text{BCS}}\rangle = \sum_{\vec{k}} \frac{v_{\vec{k}}^2}{\alpha^2 u_{\vec{k}}^2}(1 - 2v_{\vec{k}}^2), \tag{4.61}$$

[12] Being careful with the thermodynamic limit we can set $\alpha = (N/2)^{1/2}$.

[13] We can argue that the weighted sums of number operators in equation can be neglected when considering a restricted region of quantum states in the thermodynamic limit, or when operating over $|\Psi_{\text{BCS}}\rangle$. See Fig. 5.1 (d) for the number occupation, although the arbitrary normalization hides the low values that they have.

where the term $2v_{\vec{k}}^2$ comes from the terms $c_{\vec{k}\sigma}^\dagger c_{\vec{k}\sigma}$ in equation (4.59). In the BEC limit, we will show that $-\mu \gg \Delta$. Then we can make the following approximation:

$$v_{\vec{k}}^2 = \frac{1}{2}\left(1-\frac{\varepsilon_{\vec{k}}-\mu}{\sqrt{(\varepsilon_{\vec{k}}-\mu)^2+\Delta^2}}\right) = \frac{1}{2}\left[1-\frac{1}{\sqrt{1+\Delta^2/(\varepsilon_{\vec{k}}-\mu)^2}}\right] \approx \frac{1}{2}\left[1-\left(1-\frac{\Delta^2}{2(\varepsilon_{\vec{k}}-\mu)^2}\right)\right] = \frac{\Delta^2}{4(\varepsilon_{\vec{k}}-\mu)^2}, \quad (4.62)$$

where the first equality is the exact form of $v_{\vec{k}}^2$, in the second equality we divided by Δ in the second term, in the third equality we used a Taylor series, and in the last equality we simplified terms. For the Taylor series we have used that $-\mu \gg \Delta$, then $\varepsilon_{\vec{k}}-\mu \gg \Delta$, so that $1 \gg \Delta/(\varepsilon_{\vec{k}}-\mu)$. Finally, we can argue that

$$1 - 2v_{\vec{k}}^2 \approx 1 - \frac{\Delta^2}{2(\varepsilon_{\vec{k}}-\mu)^2} \approx 1. \quad (4.63)$$

Then, we can approximate the expectation value in equation (4.61),

$$\langle \Psi_{\text{BCS}} | [b_{\vec{0}}, b_{\vec{0}}^\dagger] | \Psi_{\text{BCS}} \rangle \approx \sum_{\vec{k}} \frac{v_{\vec{k}}^2}{\alpha^2 u_{\vec{k}}^2}. \quad (4.64)$$

With similar arguments as those given in equation (4.62) we can show that in the BEC limit

$$\left(\frac{v_{\vec{k}}}{u_{\vec{k}}}\right)^2 = \frac{\Delta}{\sqrt{(\varepsilon_{\vec{k}}-\mu)^2+\Delta^2}+(\varepsilon_{\vec{k}}-\mu)} \approx \left(\frac{\Delta}{2(\varepsilon_{\vec{k}}-\mu)}\right)^2. \quad (4.65)$$

Then, from the number equation (4.38) we have

$$N = 2\sum_{\vec{k}} v_{\vec{k}}^2 \approx 2\sum_{\vec{k}} \frac{v_{\vec{k}}^2}{u_{\vec{k}}^2}, \quad (4.66)$$

where the approximation is obtained using equations (4.62) and (4.65). Hence, we can use equations (4.64) and that $\alpha^2 = N/2$, which comes from equation (4.57), to conclude that

$$\langle \Psi_{\text{BCS}} | [b_{\vec{0}}, b_{\vec{0}}^\dagger] | \Psi_{\text{BCS}} \rangle \approx 1. \quad (4.67)$$

Then, we have argued that we can neglect the number operators in equation (4.59) in the strongly interacting regime, which allows us to consider a gas of composite bosons. It remains to confirm that in the BEC limit $-\mu \gg \Delta$, which will be shown in Section 4.4.

4.3 Binding energy of a pair

The methods we have presented are for an interacting Fermi gas of two components. However in ultracold gases the structure of the atoms allows us to consider a third state $|3\rangle$ that can be considered as empty. For Lithium-6 we show the low energy states in Figure 2.1. Then, we can extend our Hamiltonian to consider this third non-interacting state [2]:

$$\hat{H}_a = \hat{H}_{\text{BCS}} + \sum_{\vec{k}} \varepsilon_{\vec{k}}^{(3)} c_{\vec{k},3}^\dagger c_{\vec{k},3}, \quad (4.68)$$

where we are using the BCS Hamiltonian of equation (4.6) and we have introduced creation and annihilation operators of the third state $c^\dagger_{\vec{k},3}$, $c_{\vec{k},3}$. The kinetic energy is $\varepsilon^{(3)}_{\vec{k}} = \hbar^2k^2/(2m)$.

We are interested in calculating the energy difference between the variational ground state $|\Psi_{\text{BCS}}\rangle$ and a state where we remove a spin σ with wave vector $\vec{k}$ and put it on the third unoccupied state. That is, the state given by $c^\dagger_{\vec{k},3}c_{\vec{k}\sigma}|\Psi_{\text{BCS}}\rangle$. This corresponds to an experimental process in which we transfer an atom in any of the states $|\uparrow\rangle$ or $|\downarrow\rangle$ into the third state $|3\rangle$ by means of a radio-frequency pulse [14]. Then we want to consider excited states, which we will analyze in the mean-field approach using Bogoliubov quasiparticles (the BCS-Leggett variational approach is not enough for analyzing excited states). For consistency we will use the grand potential operator $\hat{\Omega}_a = \hat{H}_a - \mu\hat{N} - \mu_3\hat{N}_3$, where we are using the restriction $N_\uparrow = N_\downarrow$ and we have introduced a chemical potential for the third state μ_3. Since we will not consider any particles in that state we have $\mu_3 = 0$, being a Fermi energy of the third state (in the absence of particles there is no Fermi sphere). Using the Bogoliubov transformation given in equations (4.13) and (4.14) we have

$$c^\dagger_{\vec{k},3}c_{\vec{k}\uparrow}|\Psi_{\text{BCS}}\rangle = v_{\vec{k}}c^\dagger_{\vec{k},3}\alpha^\dagger_{\vec{k}}|\Psi_{\text{BCS}}\rangle. \tag{4.69}$$

and

$$c^\dagger_{\vec{k},3}c_{\vec{k}\downarrow}|\Psi_{\text{BCS}}\rangle = -v_{\vec{k}}c^\dagger_{\vec{k},3}\gamma^\dagger_{\vec{k}}|\Psi_{\text{BCS}}\rangle. \tag{4.70}$$

We can identify that these are eigenstates of the gran potential operator $\hat{\Omega}_a$, so we know that their grand potential energy is $\Omega_0 + E_{\vec{k}} + \varepsilon^{(3)}_{\vec{k}}$, where Ω_0 is the ground state grand potential given in equation (4.30), $E_{\vec{k}}$ is the energy of a quasiparticle, given in equation (4.23) and, $\varepsilon^{(3)}_{\vec{k}} = \hbar^2k^2/(2m)$ is the energy of a free particle. Although we can calculate the difference in energy of the grand potential $\Delta\Omega$, we are interested in the internal energy difference $\Delta\bar{E}$, when we do not change the number of particles. We can calculate it by

$$\Delta\bar{E} = \Delta\Omega + \mu\Delta N + \mu_3\Delta N_3. \tag{4.71}$$

For the process we are interested (removing one particle of spin $\uparrow$ or $\downarrow$ and putting it on the third state) we have $\Delta N = -1$. Since the chemical potential μ_3 is zero we can forget about the last term in equation (4.71). Hence we have

$$\Delta\bar{E} = E_{\vec{k}} + \varepsilon^{(3)}_{\vec{k}} - \mu. \tag{4.72}$$

This energy difference depends on the wave vector $\vec{k}$. From the expressions of the quasiparticle energies $E_{\vec{k}}$ and $\varepsilon^{(3)}_{\vec{k}}$ we can notice that there is a minimum energy for this process to occur. Since we are considering a state of paired fermions given by the pair wave function $\phi_{\text{BCS}}(\vec{r})$, see equations (4.49), (4.50) and (4.53), we will identify this threshold energy as the energy required to break a pair $\varepsilon_{\text{spec}}$. This energy has been discussed in experimental works of radio-frequency spectroscopy [2, 14], so we decided to use the subindex "spec". In general it will be given by

$$\varepsilon_{\text{spec}} = \min_{\vec{k}}\{E_{\vec{k}} + \varepsilon^{(3)}_{\vec{k}} - \mu\}. \tag{4.73}$$

We have assumed that the third state has the energy $\varepsilon^{(3)}_{\vec{k}}$, but in general it can have a shift $\varepsilon^{(3)}_{\vec{k}} + \varepsilon_3$. This shift does not change our previous arguments, but it would shift the threshold energy $\varepsilon_{\text{spec}}$, so we can redefine the threshold energy to get equation (4.73), removing the energy shift that does

not affect the components ↑ and ↓. For the contact interaction the minimum can be easily found using derivatives [2, 14, 17, 18]. It is found that the threshold is when $k = 0$. For finite-range potentials this value could be different due to the gap being a function of k. However, we found that the minimum is still at $k = 0$ for the potentials given in equations (3.92)-(3.97) [19]. Then, for any of the interactions and dimensions considered in this work we found

$$\varepsilon_{\text{spec}} = \sqrt{\mu^2 + \Delta_0^2} - \mu, \tag{4.74}$$

where Δ_0 is the value of the gap at $k = 0$, for the contact interactions $\Delta_0 = \Delta$. We will return to this result further below. Let us mention that the energy $\varepsilon_{\text{spec}}$ also determines the critical velocity for superfluidity on the BCS side [2]. For the contact interaction it is given by [2]

$$v_c|_{\text{BCS}} = \frac{\varepsilon_{\text{spec}}}{m}. \tag{4.75}$$

This property is independent of the third state $|3\rangle$.

It has been very difficult to measure this threshold energy required to break a pair $\varepsilon_{\text{spec}}$ for the 2D case [118] and for the 3D case [119]. In the simplified Hamiltonian (4.68) we are considering a non-interacting third state $|3\rangle$, but in experiments they can interact with the other components.

4.4 Thermodynamic properties

For the zero temperature case we can calculate the value of the grand canonical potential using the BCS-Leggett variational approach by means of an expectation value of the grand potential operator, as we did in equation (4.33). Also we can use the mean-field method that we have presented in the previous section, which also allows us to consider finite temperatures, since it gives an approximation to the spectrum of excited states.

Mainly, the thermodynamic properties that we will present are the gap $\Delta_{\vec{k}}$ and the chemical potential μ, which are required to determine the ground state properties, since they determine the parameters $u_{\vec{k}}$ and $v_{\vec{k}}$, as shown in equations (4.25) and (4.39):

$$v_{\vec{k}}^2 = \frac{1}{2}\left(1 - \frac{\varepsilon_{\vec{k}} - \mu}{\sqrt{(\varepsilon_{\vec{k}} - \mu)^2 + \Delta_{\vec{k}}^2}}\right) \quad , \quad u_{\vec{k}}^2 = \frac{1}{2}\left(1 + \frac{\varepsilon_{\vec{k}} - \mu}{\sqrt{(\varepsilon_{\vec{k}} - \mu)^2 + \Delta_{\vec{k}}^2}}\right).$$

Also we will show the threshold energy required to break a pair $\varepsilon_{\text{spec}}$, given in equation (4.74). For the contact interaction cases in 2D and 3D we will show the ground state energies E_0, the Tan's contact C (thermodynamic variable associated to the interaction between fermions [120]) and the isothermal compressibility κ_T. For the finite-range interactions we will only show the gaps and chemical potentials, together with the threshold energy required to break a pair $\varepsilon_{\text{spec}}$. For a complete analysis of the thermodynamic aspects of the 3D finite-range interactions see Refs. [92] and [103].

For the contact interaction we will encounter an ultraviolet divergence due to the structureless potential. We will remove the divergence by means of a renormalization procedure. However, for well-defined finite range interactions we do not need the renormalization procedure.

4.4.1 Two dimensions

Although it has been argued that the mean-field method in the two-dimensional case 2D should be less accurate than in the three-dimensional case, it turns that for the contact interaction case many observable quantities can be calculated explicitly [16, 20, 121], some integrals are well known. This allows us to view explicitly the evolution of thermodynamic quantities throughout the crossover.

In both approaches, mean-field or variational method, we obtained the number and gap equations [20]:

$$n = \frac{\langle \hat{N} \rangle}{L^2} = \frac{1}{L^2} \sum_{\vec{k}} \left(1 - \frac{\varepsilon_{\vec{k}} - \mu}{E_{\vec{k}}} \right), \tag{4.76}$$

$$\Delta_{\vec{k}} = -\frac{1}{L^2} \sum_{\vec{k}_1} \frac{\tilde{U}(\vec{k}_1 - \vec{k}) \Delta_{\vec{k}_1}}{2E_{\vec{k}_1}}, \tag{4.77}$$

where $E_{\vec{k}} = \sqrt{(\varepsilon_{\vec{k}} - \mu)^2 + \Delta_{\vec{k}}^2}$, and in the number equation we have made the sum over the spin. Also we have made use of the relations given in equation (4.25), where we are neglecting a possible complex phase in the gap[14]. For the two-dimensional case we will consider the contact interaction given by

$$\tilde{U}(\vec{k}) = g, \tag{4.78}$$

where g is the interaction strength, which is a non-physical quantity. If we introduce this potential in the gap equation (4.77) we find that the sum on the right side diverges. If the gap increases with $|\vec{k}|$ the sum would go like $\Delta_{\vec{k}}/\Delta_{\vec{k}} \approx 1$ which diverges. And, even if the gap goes to zero fast enough, the left side depends on $\vec{k}$, while the right side of equation (4.77) does not, so that the gap must be a constant $\Delta_{\vec{k}} = \Delta$. Again we find a divergent sum which goes like $1/\varepsilon_{\vec{k}}$. Thus we are left with a divergent expression, associated to the use of a contact interaction [16], so we can set the interaction strength as a (non-physical) parameter which allows us to obtain a well-defined gap equation[15]

$$1 = -\frac{g(\Lambda)}{L^2} \sum_{\vec{k}_1}^{\Lambda} \frac{1}{2E_{\vec{k}_1}}, \tag{4.79}$$

where we have introduced a cutoff Λ to regularize the sum (parameter that defines the integration limits) such that $g(\Lambda) \to 0^-$ when $\Lambda \to \infty$. Notice that $g(\Lambda)$ has to be negative to agree with the positive left side of equation (4.79), given that $E_{\vec{k}} > 0$. To remove the interaction strength and replace it with a physical quantity we use the two-body scattering problem, which we presented in Chapter 3. There we found a divergent expression for the T matrix in terms of the interaction strength g, as shown in equations (3.36) and (3.38). We can use those equations to remove $g(\Lambda)$ obtaining a renormalized theory which now depends on the scattering length a_{2D} instead of the interaction strength g. Dividing equation (4.79) by $g(\Lambda)$ and using equation (3.38) we find

$$\frac{1}{T(k, \vec{k}, 2z)} + \frac{1}{L^2} \sum_{\vec{k}''}^{\Lambda} \frac{1}{E - E_{k''} + i\delta} = \frac{1}{g(\Lambda)} = -\frac{1}{L^2} \sum_{\vec{k}_1}^{\Lambda} \frac{1}{2E_{\vec{k}_1}}, \tag{4.80}$$

[14] The relative phase between $u_{\vec{k}}$ and $v_{\vec{k}}$ is the phase of the gap $\Delta_{\vec{k}}$ which is relevant for the Josephson effect [24].
[15] We might call this the regularized gap equation.

where the left side corresponds to equation (3.38) and the right side to equation (4.79). Also, we are using the low energy behavior of the T matrix with $|\vec{k}| \to 0$, given in equation (3.69) and we have introduced the variable $z = \hbar^2 k^2/(2m)$ [so that $E = 2z$ in equations (3.36), (3.38) and (3.69)]. In the following we will give more details on how to take the thermodynamic limit in equation (4.80). Then, the renormalized gap equation is [16, 20]

$$\frac{1}{T(k,\vec{k},2z)} = -\frac{1}{L^2}\sum_{\vec{k}_1}\frac{1}{2(z-\varepsilon_{\vec{k}_1}+i\delta)} - \frac{1}{L^2}\sum_{\vec{k}_1}\frac{1}{E_{\vec{k}_1}}, \tag{4.81}$$

Taking explicitly the limit $L \to \infty$ we obtain an integral over the wave vector components $\vec{k}_1 = (k_x, k_y)$ on the right side of equation (4.81). We can make changes of variable to use polar coordinates (θ, k). We can perform the angular integral over θ. We can make a last change of variables to use a variable of energy $\varepsilon = \hbar^2 k^2/(2m)$. Then we find

$$\frac{m}{2\hbar^2}[-\cot(\delta_0(2z)) + i] = \frac{m}{(2\pi)\hbar^2}\int_0^\infty d\varepsilon\left[\frac{1}{(\varepsilon - z - i\delta)} - \frac{1}{\sqrt{(\varepsilon-\mu)^2+\Delta^2}}\right], \tag{4.82}$$

Using the low-energy approximation of the phase shift, given in equations (3.64) and (3.69) we have

$$\frac{m}{2\hbar^2}\left[-\frac{1}{\pi}\ln\left(\frac{2z}{E_a}\right) + i\right] = \frac{m}{(2\pi)\hbar^2}\int_0^\infty d\varepsilon\left[\frac{1}{(\varepsilon - z - i\delta)} - \frac{1}{\sqrt{(\varepsilon-\mu)^2+\Delta^2}}\right]. \tag{4.83}$$

In this expression we have a dependence on z in both sides that should cancel, as we will show. The first integral on the right hand side can be integrated directly, giving a logarithm. The second term can also be integrated and identified with an inverse hyperbolic sine $\sinh^{-1}(x) = \ln[x + (1+x)^{1/2}]$ [122]. Then we have

$$\begin{aligned}\frac{m}{2\hbar^2}\left[-\frac{1}{\pi}\ln\left(\frac{2z}{E_a}\right) + i\right] &= \frac{m}{(2\pi)\hbar^2}\left[-\ln\left(\sqrt{(x-\mu)^2+\Delta^2}+x-\mu\right) + \ln(x - z - i\delta)\right]_{x=0}^{x=\infty} \\ &= \frac{m}{(2\pi)\hbar^2}\left\{-\ln(2) - \left(-\ln\left(\sqrt{\mu^2+\Delta^2}-\mu\right) + \ln(-z-i\delta)\right)\right\},\end{aligned} \tag{4.84}$$

where in the last equality we evaluated the limits. The upper limit was evaluated using the natural logarithm for complex values[16] in the following way:

$$\begin{aligned}&\lim_{x\to\infty} -\ln\left(\sqrt{(x-\mu)^2+\Delta^2}+x-\mu\right) + \ln(x - z - i\delta) \\ &= \lim_{x\to\infty} -\ln\left(\sqrt{(x-\mu)^2+\Delta^2}+x-\mu\right) + \ln(|x - z - i\delta|) + i\arg(x - z - i\delta) \\ &= \lim_{x\to\infty} -\ln\left(x\left(\sqrt{(1-\mu/x)^2+\Delta^2/x^2}+1-\mu/x\right)\right) + \ln(x|1 - z/x - i\delta/x|) + i\arg(x - z - i\delta) \\ &= \lim_{x\to\infty} -\ln(x) - \ln\left(\sqrt{(1-\mu/x)^2+\Delta^2/x^2}+1-\mu/x\right) + \ln(x) + \ln(|1 - z/x - i\delta/x|) + i\arg(x - z - i\delta),\end{aligned} \tag{4.85}$$

[16] The logarithm $\ln : \mathbb{C}\setminus\{0\} \to \mathbb{C}$ is defined as [123]

$$\ln(z) = \ln|z| + i\,\arg(z),$$

where arg is the argument function which takes values in the arbitrary interval $[y_0, y_0 + 2\pi]$ and $|z|$ is the norm of an element $z \in \mathbb{C}\setminus\{0\}$. To recover the usual definition for real numbers we should use the convention $\arg(z) = 0$ when $z \in \mathbb{R}$ and $z > 0$, for z in the lower half plane $\arg(z) < 0$, and for z in the upper half plane $\arg(z) > 0$.

where in the first equality we substituted the definition of the natural logarithm for complex values, in the second we factorized the variable x inside each logarithm. In the third equality we used the property of the logarithm $\ln(ab) = \ln(a) + \ln(b)$. In the last equality we can see that the first and third term cancel between them, the second term can be evaluated to give $-\ln(2)$, the fourth term is zero because we obtain $\ln(1) = 0$. The last term is zero in the convention of the logarithm that we are using ($\arg(z) = 0$ for $z \in \mathbb{R}$ and $z > 0$). As we will find, the imaginary part on the left side in equation (4.84) will be canceled with terms on the right side. For this we need to use again the definition of the natural logarithm to evaluate the last term [123]. Then we have

$$\frac{m}{2\hbar^2}\left[-\frac{1}{\pi}\ln\left(\frac{2z}{E_a}\right)+i\right] = -\frac{m}{(2\pi)\hbar^2}\ln(2) + \frac{m}{(2\pi)\hbar^2}\ln\left(\sqrt{\mu^2+\Delta^2}-\mu\right) - \frac{m}{(2\pi)\hbar^2}\Big[\ln(|z+i\delta|) + i\arg(-z-i\delta)\Big]. \tag{4.86}$$

We have been keeping $\delta > 0$ and $z > 0$. But now we can take the limit $\delta \to 0^+$ making the value $-z - i\delta$ get close to the real axis from below, so that $\arg(-z - i\delta) \to -\pi$ [123]. Hence,

$$-\frac{m}{(2\pi)\hbar^2}\ln\left(\frac{2z}{E_a}\right) + i\frac{m}{2\hbar^2} = -\frac{m}{(2\pi)\hbar^2}\ln(2) + \frac{m}{(2\pi)\hbar^2}\ln\left(\sqrt{\mu^2+\Delta^2}-\mu\right) - \frac{m}{(2\pi)\hbar^2}\ln(z) + i\frac{m}{2\hbar^2}. \tag{4.87}$$

We can simplify the equation by canceling terms to arrive at the condition [16, 20]

$$0 = \ln\left(\frac{\sqrt{\mu^2+\Delta^2}-\mu}{E_a}\right). \tag{4.88}$$

Since this is valid for any values of the resonance energy E_a, or for any s-wave scattering length $a_{2D} = \hbar/(mE_a)^{1/2}$, the argument in the logarithm must be equal to one. Then we arrive to the final condition given by the gap equation:

$$E_a = \sqrt{\mu^2+\Delta^2} - \mu. \tag{4.89}$$

Now we return to the number equation, given in equation (4.76). Using the same change of variables as in the renormalized gap equation (4.82), we obtain [16, 20]

$$n = \frac{m}{(2\pi)\hbar^2}\int_0^\infty d\varepsilon\left(1 - \frac{(\varepsilon-\mu)}{\sqrt{(\varepsilon-\mu)^2+\Delta^2}}\right). \tag{4.90}$$

We can perform the integration by means of a table [122] or with elementary integration techniques, similar to the gap equation. Then we get

$$n = \frac{m}{(2\pi)\hbar^2}\left(\mu + \sqrt{\mu^2+\Delta^2}\right) \tag{4.91}$$

Another expression that we can calculate exactly is the grand potential Ω_0. As we are considering an homogeneous system, the value of Ω_0 should diverge in the thermodynamic limit, but its density Ω_0/L^2 must remain finite. Then we have [17, 124]

$$\begin{aligned}\frac{\Omega_0}{L^2} &= \frac{1}{L^2}\sum_{\vec{k}} \xi_{\vec{k}} - E_{\vec{k}} + \frac{\Delta^2}{2E_{\vec{k}}} \\ &= -\frac{m\Delta}{4\pi\hbar^2}\left(\frac{\Delta^2}{2} + \mu^2 - \mu\sqrt{\mu^2+\Delta^2}\right),\end{aligned} \tag{4.92}$$

A nice aspect that we found is that to calculate this expression we do not require to regularize and introduce the scattering length, although the gap is determined by the renormalized equation (4.81) [17]. The steps for calculating the grand potential density are given in the Appendix B.1. This expression, being independent of the renormalization, will hold a property of the non-physical contact interaction that is the so-called scale invariance in the isothermal compressibility [125].

A many-body Hamiltonian of a homogeneous 2D system where the interaction is given by a Dirac delta exhibits an scale invariant behavior under under spatial scaling $\vec{x} \to \lambda\vec{x}$ and time scaling $t \to \lambda^2 t$ [69]. This can be seen by writing the Hamiltonian with one-body operators of momentum $\hat{p}_i = (\hbar/i)\nabla_i$ and two-body operators for the interaction between fermions. In space representation, for a fixed number of particles N, we have the following Hamiltonian[126, 127]:

$$\hat{H}_N = \sum_{i=1}^{N} -\frac{\hbar^2}{2m}\nabla_i^2 + \frac{1}{2}\sum_{i=1}^{N}\sum_{j=1,j\neq i}^{N} g\delta^{(2)}(\vec{x}_i - \vec{x}_j), \tag{4.93}$$

where $\vec{x}_i$ is the position coordinate of the i-th particle and ∇_i^2 is the Laplace operator for the coordinates of the i-th particle. After performing the scaling transformation $\vec{x}_i \to \lambda\vec{x}_i$ we find that the interaction term scales like $g\delta^{(2)}(\lambda\vec{x}_i - \lambda\vec{x}_j) = \lambda^{-2}g\delta^{(2)}(\vec{x}_i - \vec{x}_j)$. The Laplace operator scales in a similar way[17]. Then we find the scale invariant behavior of the Hamiltonian $\hat{H}_N$ of equation (4.93) [128],

$$\hat{H}_N \to \frac{\hat{H}_N}{\lambda^2} \tag{4.94}$$

In general this behavior is not satisfied by the Hamiltonians because the interaction potential can change in a different way under the scale transformation. Here, the property of the Dirac delta function $\delta^{(2)}(\lambda\vec{x}) = |\lambda|^{-2}\delta^{(2)}(\vec{x})$ allows us to find the scaling behavior of equation (4.94). Analogously, we argue that the BCS Hamiltonian (4.6) exhibits the scale invariant behavior, since it also has a contact interaction (delta potential) between fermions of opposite spin.

The same scaling property appears in the Hamiltonian of a non-interacting system $\hat{H}^{\text{Free}}$ where[18] the pressure P^{Free} is given by the density $P^{\text{Free}} = \hbar^2\pi n^2/(2m)$. In our interacting case the pressure P is also given by the density $P = \hbar^2\pi n^2/(2m)$, even after the renormalization procedure, where we introduce a characteristic length of the potential a_{2D} that we expected to (anomalously) break this symmetry [125]. As we will show in Chapter 5 the scale invariance behavior of the mean-field theory is not shown in the density-density correlation functions, where we will find that the interaction generates a characteristic length of the system.

Using the conditions (4.89) and (4.91) of the renormalized theory we find that given the density and the intensity of the attractive interaction, represented by $E_a = \hbar^2/(ma_{2D}^2)$, see Figure 3.2, we

[17] With some informal notation we have

$$\frac{\partial^2}{\partial(\lambda x_i)^2} + \frac{\partial^2}{\partial(\lambda y_i)^2} = \frac{1}{\lambda^2}\left(\frac{\partial^2}{\partial x_i^2} + \frac{\partial^2}{\partial y_i^2}\right)$$

[18] For a non-interacting gas in 2D we can see that from $P = -(\partial E/\partial L^2)_{S,N}$ we get $P = E/L^2$ without the need of performing any sum, because we only have kinetic energy and the wave vectors go like $|\vec{k}| \propto L^{-1}$. See for example [129] for the 3D case.

can determine the gap and chemical potential, and therefore the parameters $u_{\vec{k}}$ and $v_{\vec{k}}$. However, for plotting the thermodynamic properties it is useful to scale the variables with the density and its characteristic energy, which is the Fermi energy of a non-interacting system. For spin 1/2 the Fermi energy ε_F is related to the density n by [124][19]

$$\varepsilon_F = \frac{\hbar^2(2\pi)}{2m}n. \tag{4.95}$$

Accordingly the Fermi wave number is given by

$$n = \frac{k_F^2}{2\pi}. \tag{4.96}$$

Hence we can scale equations (4.89) and (4.91) to find

$$\tilde{\mu} = 1 - \frac{\tilde{E}_a}{2}, \tag{4.97}$$

$$\tilde{\Delta} = \sqrt{2\tilde{E}_a}, \tag{4.98}$$

where the variables scaled with the Fermi energy ε_F will be denoted with a tilde. For example $\tilde{\mu} = \mu/\varepsilon_F$, $\tilde{\Delta} = \Delta/\varepsilon_F$, $\tilde{E}_a = E_a/\varepsilon_F$. Also, using equations (4.97) and (4.98) we can obtain a simple expression for the grand potential in the ground state

$$\frac{\tilde{\Omega}_0}{N} = -\frac{1}{2}\left(1 - \frac{\tilde{E}_a}{2}\right), \tag{4.99}$$

and for the internal energy $E_0 = \langle \hat{H}_{\mathrm{BCS}} \rangle$,

$$\frac{\tilde{E}_0}{N} = \frac{1}{2}(1 - \tilde{E}_a). \tag{4.100}$$

Let us remind that for a contact interaction E_a is the absolute value of an ever-present bound state energy [16], and it represents the real strength of the interaction (not to be confused with g), as illustrated in Figure 3.2. Then, from equations (4.97) and (4.98) we see that for weak interactions the chemical potential is very similar to the Fermi energy of the non-interacting gas $\mu \approx \varepsilon_F$ [16, 20]. Also, for weak interactions, the gap is a small quantity that represents the interaction between fermions (fomenting the formation of pairs at the Fermi surface as shown in the upper panel (a) of Figure 5.1 with large blue dashes). The ground state energy is approximately the one of a non-interacting gas $E_0 \approx N\varepsilon_F/2$, see equation (4.100). This weakly interacting regime is known as the BCS limit. On the other hand, for strong interactions we have a significantly big E_a, such that the chemical potential is half the binding energy of the potential $\mu \approx -E_a/2$ [16, 20]. This is in agreement with the formation of a molecule, where we would have to add two particles with a binding energy of $-E_a$ to form a static molecule. The gap becomes large, but not bigger than the absolute value of the chemical potential $|\mu|$. Also the ground state energy behaves like $E_0 \approx -E_a(N/2)$, the binding energy of a pair multiplied by the number of pairs. From equation

[19] Sometimes a confusion arises when using the Fermi energy. This can be avoided by defining a wave number of the density k_n by $n = k_n^2/(2\pi)$ and an energy $\varepsilon_n = \hbar^2 k_n^2/(2m)$. However, we will keep using k_F and ε_F.

(4.100) we can see that the ground state energy E_0 goes from a positive value on the BCS side to a negative value on the BEC side. Also the chemical potential has a change of sign, being positive on the BCS side and negative on the BEC side, where it is dominated by the two-body binding energy. There are many arbitrary regions used to establish a division between the BEC and BCS sides. The most common is where the chemical potential is zero [30, 130], indicating the lost of a Fermi sphere and the chemical potential being dominated by the bound state energy E_a. The behavior of the chemical potential and the gap can be seen in Figure 4.1.

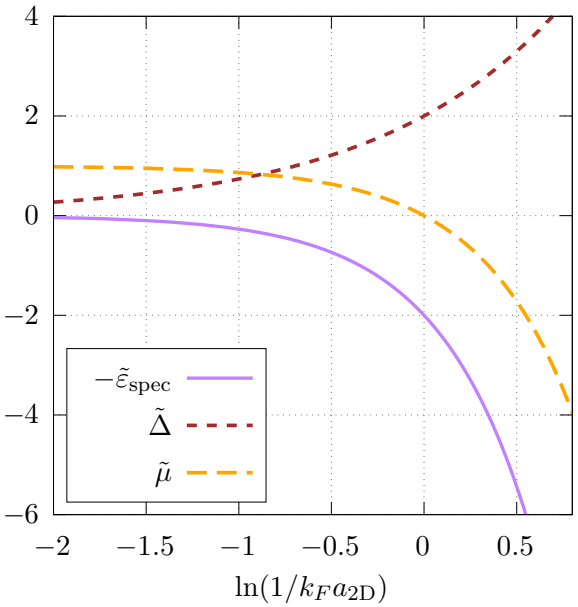

Figure 4.1: Chemical potential μ, gap Δ and threshold energy required to break a pair ε_{spec} [equal to the binding energy per pair $\varepsilon_b = \varepsilon_{spec}$ as shown in equation (4.103)] as functions of the dimensionless parameter $\ln(1/k_F a_{2D})$ (representing the real interaction strength in 2D). Variables are scaled with the Fermi energy ε_F of the non-interacting gas ε_F and with the Fermi wave number k_F. On the left we have the weakly interacting BCS limit, while on the right we have the strongly interacting BEC limit. Differently from the 3D case there is no unitarity limit. In quasi-2D experiments the interactions are analyzed in the interval $-1 < \ln(1/k_F a_{2D}) < 1$ [118, 131]. This figure was taken from [17].

Another quantity that is related to the binding energy of pairs is the so-called condensation energy [16]. At zero temperature we will define it as the difference between the energy of a non-interacting gas (which for the 2D case is $N\varepsilon_F/2$) minus the ground state energy of the interacting gas (internal energy) E_0 [given in equation (4.100)]. Then, the condensation energy is given by [16]

$$E_b = \frac{N}{2}\varepsilon_F - E_0. \tag{4.101}$$

This energy measures the energy associated to the formation of Cooper pairs in the BCS limit [15], while in the BEC limit it measures the energy due to the formation of molecules. In the crossover region it measures a generic energy difference due to the interaction between fermions. However, we will focus on the binding (condensation) energy per pair, which is given by the condensation

energy divided by the number or pairs $N/2$ [17],

$$\varepsilon_b = \frac{2E_b}{N} = E_a. \tag{4.102}$$

As we will show later this is in stark contrast with the 3D case, since for the 2D case we have the following equality [16, 17]

$$\varepsilon_{\text{spec}} = \varepsilon_b = E_a, \tag{4.103}$$

while in 3D we have $\varepsilon_{\text{spec}} \neq |\varepsilon_b|$.

Another thermodynamic quantity that has become important is the Tan's contact $C = m^2\Delta^2/\hbar^4$ which is the thermodynamic quantity[20] given by [99, 120, 132, 133]

$$\left(\frac{\partial E_0}{\partial(\ln a_{2D})}\right)_{A,N} = \frac{\hbar^2 C L^2}{2\pi m}, \tag{4.104}$$

where we are using $\ln(a_{2D})$ as the thermodynamic conjugate variable of the contact. Because the contact C is determined directly by the gap Δ we have not plotted it in Figure 4.1. The contact is an interesting quantity that represents the closeness of opposite spins [30]. This closeness increases as we move from the BCS side to the BEC side (in agreement with the formation of molecules), and a great achievement of the work presented here is that we can show this behavior explicitly with density-density correlation functions, which we will discuss in Chapter 5.

Another thermodynamic property that we can analyze is the isothermal compressibility κ_T, which is given by

$$\kappa_T = \frac{1}{n}\left(\frac{\partial n}{\partial P}\right)_T = \frac{m}{\hbar^2 \pi n^2}. \tag{4.105}$$

This relationship has been related to a scale-invariant behavior [125]. Equation (4.105) shows the same expression of a non-interacting gas. In the literature there can be found other criteria to characterize the deviation of thermodynamic properties from the ones of a scale-invariant behavior. We will not focus on those quantities [125, 128, 134], but in Chapter 5 we will show that the spatial structure of the gas at the mean-field level is not of a scale-invariant system, although the isothermal compressibility (4.105) has a scale invariant behavior [17]. Also we will show that the isothermal compressibility κ_T allows us to identify a failure of the BCS approach which was identified by John Bell [135, 136]. The failure appears in the relation between a non-zero particle fluctuation $\langle(\hat{N} - \langle\hat{N}\rangle)^2\rangle$ and a finite isothermal compressibility [116], which we will discuss in Chapter 5,

$$\kappa_T = L^D \frac{\langle(\hat{N} - \langle\hat{N}\rangle)^2\rangle}{k_B T \langle\hat{N}\rangle^2}, \tag{4.106}$$

where $T \to 0$ is the temperature and k_B is Boltzmann constant. It was assumed that the failure came from the contact interaction [135], since two particles can be annihilated in one region and then created in any other region (arbitrarily separated) with the same probability. However, a general analysis can show that the failure arises from the pairing mechanism (of both approaches,

[20] There are other ways to define the contact C that differ by numerical factors.

mean-field and variational approach), being that the expectation value $\langle c^\dagger_{\vec{k}\uparrow} c^\dagger_{-\vec{k}\downarrow}\rangle$ that corresponds to the interaction between fermions is the quantity that makes $\langle(\hat{N} - \langle\hat{N}\rangle)^2\rangle \neq 0$. A possibility to readdress in the future is the effect of including the interaction between same spins and terms where the pairs can have a wave vector different from zero $\vec{Q} \neq \vec{0}$, see equations (4.1) and (4.6).

4.4.2 Three dimensions

The three-dimensional case poses several difficulties for the calculation of the thermodynamic variables. In this case we cannot solve explicitly the gap and number equations:

$$n = \frac{\langle\hat{N}\rangle}{L^3} = \frac{1}{L^3}\sum_{\vec{k}}\left(1 - \frac{\varepsilon_{\vec{k}} - \mu}{E_{\vec{k}}}\right), \tag{4.107}$$

$$\Delta_{\vec{k}} = -\frac{1}{L^3}\sum_{\vec{k}}\frac{\tilde{U}(\vec{k}_1 - \vec{k})\Delta_{\vec{k}_1}}{2E_{\vec{k}_1}}, \tag{4.108}$$

where $E_{\vec{k}} = \sqrt{(\varepsilon_{\vec{k}} - \mu)^2 + \Delta^2_{\vec{k}}}$, and in the number equation we have made the sum over the spin, using the balanced condition $N_\uparrow = N_\downarrow$. Similarly to the discussion given between equations (4.77) and (4.79), for the contact interaction $\tilde{U}(\vec{k}) = g$ we can conclude that the gap has to be a constant $\Delta_{\vec{k}} = \Delta$ and we find again a divergent expression in equation (4.108) associated to the behavior of the integrand of the gap equation at high values of the wave vector $\vec{k}_1$ (ultraviolet divergence). Again, we know that the divergence is associated to the ill-defined contact interaction, so that we can use the divergence that arises in the scattering problem to cancel the divergence shown in the many-body problem. Differently from the 2D case, we can use the low-energy limit of equation (3.36) or (3.38), by setting $E = 0$ and $\delta = 0$ in those equations. In the thermodynamic limit the resulting integrals can be expressed in terms of associated Legendre functions [26] [18], which are easier to compute, so that a numerical solution can be obtained easily. The steps for obtaining those nice expressions are lengthy, so we will give a general expression for handling the integrals in Appendix B.2. In agreement with [26], the expressions obtained are [18]:

$$\frac{1}{k_F a} = (\tilde{\mu}^2 + \tilde{\Delta}^2)^{1/4} P_{1/2}(x) \tag{4.109}$$

and

$$1 = -\frac{3\pi}{4}(\tilde{\mu}^2 + \tilde{\Delta}^2)^{1/4}[\tilde{\mu}P_{1/2}(x) + (\tilde{\mu}^2 + \tilde{\Delta}^2)^{1/2}P_{3/2}(x)], \tag{4.110}$$

where we have scaled variables with the Fermi energy of a non-interacting gas $\varepsilon_F = \hbar^2 k_F^2/(2m)$, with the density given by $n = k_F^3/(3\pi^2)$. This is denoted by a tilde, $\tilde{\mu} = \mu/\varepsilon_F$, $\tilde{\Delta} = \Delta/\varepsilon_F$. Also we have defined the variable $x = -\mu/\sqrt{\mu^2 + \Delta^2}$ and we have used associated Legendre functions defined by the Hypergeometric function [88]:

$$P_\lambda(x) = {}_2F_1\left(-\lambda, \lambda + 1, 1, \frac{1 - x}{2}\right). \tag{4.111}$$

Equations (4.109) and (4.110) can be obtained without using sophisticated regularization procedures. A technical aspect to point out is the way in which we can scale to get dimensionless variables. In the 2D case we were able to integrate and solve explicitly the gap and number equations without the need to scale variables with the Fermi wave number, which comes from the density[21]. Instead, to solve the gap and number equations numerically in 3D it is natural to scale variables with ε_F and k_F. For example, a characteristic density for ultra cold gases is $n \approx 10^{12}\text{cm}^{-3}$ [137], which is inconvenient to evaluate numerically. Another curious aspect about the scaling of variables is that it turns out that the behavior of the chemical potential dominates the behavior in the extreme limits, weakly (BCS) and strongly (BEC) interacting regimes. Hence, a natural variable that arises in the process of evaluating the integrals of the gap and number equations is $x = -\mu/\sqrt{\mu^2 + \Delta^2}$, which has values in the interval $(-1, 1)$.

Differently, for the contact interaction, the reduced BCS Hamiltonian does not exhibit an scale invariant behavior, as discussed in equation (4.94), the interaction term scales like $1/(\lambda^3 L^3)$. However, we might expect a somewhat small deviation from the scale invariant behavior in the weakly interacting regime (BCS), when the interaction term is very small. A similar observation can be done for a Hamiltonian with finite-range interactions in the BCS limit.

Like for the 2D case, we can calculate an exact relation for the ground state energy $E_0 = \langle \hat{H}_{\text{BCS}} \rangle$ in terms of the gap, chemical potential and scattering length [18, 26]:

$$\frac{\tilde{E}_0}{N} = -\frac{3\pi}{20}\left[\frac{(k_F a)^{-1}\tilde{\Delta}^2}{2} - \frac{4}{\pi}\tilde{\mu}\right] \tag{4.112}$$

Since we do not have explicitly the gap Δ and chemical potential μ as functions of the scattering length a, we cannot analyze the behavior of the ground state energy with the same ease as we did for the 2D case. However, we can still give some not so formal arguments looking at the numerical solutions shown in Figure 4.2. Given that the gap increases proportionally to the real strength of the interaction, in the weakly interacting regime (BCS) we expect that the term $(k_F a)^{-1}\tilde{\Delta}^2$ becomes negligible, so that asymptotically the ground state energy behaves like the non-interacting system $E_0 \approx 3\mu/5$ (with $\mu \approx \varepsilon_F$). In summary the BCS behavior $(k_F a)^{-1} \to -\infty$ is given by

$$\frac{\mu}{\varepsilon_F} \approx 1 \quad , \quad \frac{\Delta}{\varepsilon_F} \approx 8e^{-2}e^{\pi/k_F a}. \tag{4.113}$$

On the other hand, in the strongly interacting regime we expect to obtain a gas of non-interacting molecules condensed in a state with zero momentum. Hence, the energy should be given by the amount of energy required to put the particles in this state $E_0 \approx \mu N$. For the contact potential, we can use the Bethe-Peierls boundary condition [27] to find that the binding energy of the attractive potential is $E_p = \hbar^2/(ma^2)$, so we expect that the variation in energy when we introduce a particle is half the binding energy $\mu \approx -E_p/2$. Then in the BEC limit $(k_F a)^{-1} \to \infty$ we have

$$\frac{\mu}{\varepsilon_F} \approx -\frac{1}{(k_F a)^2} \quad , \quad \frac{\Delta}{\varepsilon_F} \approx (k_F a)^{-1/2}. \tag{4.114}$$

[21] Although we could have scaled variables with k_F and ε_F and then perform the integrals.

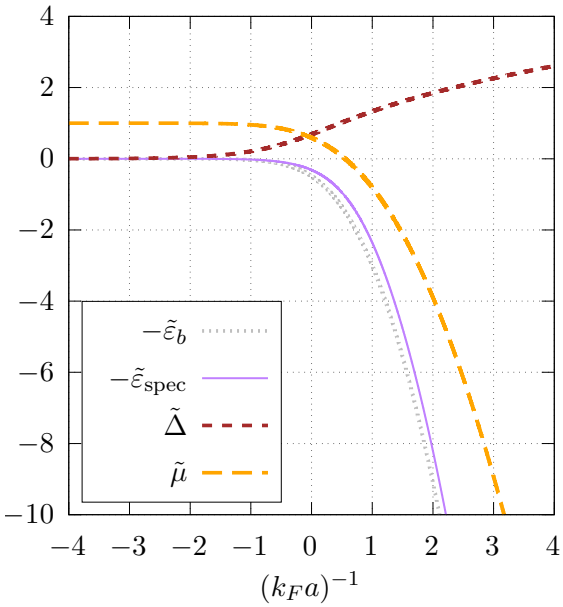

Figure 4.2: Chemical potential μ and gap Δ obtained by solving numerically equations (4.109) and (4.110). Also we show threshold energy required to break a pair $\varepsilon_{\rm spec}$ given in equation (4.74), and binding energy per pair ε_b, given in equation (4.116), as functions of the s-wave scattering length $(k_F a)^{-1}$. Variables are scaled with the Fermi energy of the non-interacting gas ε_F and with the Fermi wave number k_F. On the left we have the weakly interacting BCS limit, while on the right we have the strongly interacting BEC limit. In experiments the interval typically analyzed is $-1 < (k_F a)^{-1} < 1$ [2]. This figure was taken from [18].

Given that for the contact interaction we are assuming that it is enough to characterize the interaction with one parameter, being the scattering length a, we obtain a so-called universal model that can describe a wide amount of different systems [69]. For instance, in ultracold gases like ^{6}Li or ^{40}K, where their broad Feshbach resonances are characterized by the scattering length, we might expect to obtain identical equations of state written in terms of $1/(k_F a)$ and a temperature dependence T/T_F, with T_F the Fermi temperature given by $k_B T_F = \varepsilon_F$ [69], similar to equation (4.112).

Another important aspect of the 3D case is the unitary point, defined as the point where $1/a = 0$. In our present mean-field model it does not show a remarkable behavior in any physical quantity. However, in a more general two-channel Hamiltonian[22], adequate for describing atoms interacting by Feshbach resonances (which reduces to the BCS Hamiltonian (4.6) with a contact

[22] In the two-channel Hamiltonian we consider fermions that can interact to form a molecule (closed channel) and a molecule that can dissociate into two unbounded fermions (open channel). For the molecule state we use a bosonic operator $b_{\vec{q}}$, while for the fermions we use the creation and annihilation operators $c_{\vec{q}\sigma}, c^\dagger_{\vec{q}\sigma}$. The interaction term is of the form

$$\frac{g}{L^{3/2}} \sum_{\vec{k},\vec{q}} \left(b^\dagger_{\vec{q}} c_{\vec{k}+\vec{q}/2\downarrow} c_{-\vec{k}+\vec{q}/2\uparrow} + c^\dagger_{-\vec{k}+\vec{q}/2\uparrow} c^\dagger_{\vec{k}+\vec{q}/2\downarrow} b_{\vec{q}} \right). \tag{4.115}$$

Also we would have kinetic energy terms for each type of particle: $\varepsilon_{\vec{k}} c^\dagger_{\vec{k}\uparrow} c_{\vec{k}\uparrow}$, $\varepsilon_{\vec{k}} c^\dagger_{\vec{k}\downarrow} c_{\vec{k}\downarrow}$, and $(\varepsilon_{\vec{q}}/2) b^\dagger_{\vec{k}} b_{\vec{k}}$. For further details see Ref. [33].

interaction in the case of broad resonances), we find a scale invariant behavior at the unitarity [69], like the one discussed in equation (4.94). Then it is expected to find thermodynamic properties associated to scale invariance at the unitarity, such as an equation of state of the form $P = 2E/(3L^3)$ and a vanishing bulk viscosity [69]. Also, when we include beyond mean-field terms (also known as quantum fluctuations) it is concluded that the unitarity is where the gas becomes "strongly interacting" [69][23]. Also, within a perturbative approximation, higher-order correlations have to be taken into account for describing the unitarity in terms of the scattering length [105]. Let us make an observation for the BCS Hamiltonian given in equation (4.6). From Figure 4.2 we might think that increasing the density allows us to get close to the unitarity. But, by hypothesis, in order to use a contact interaction or an effective two-body interaction, we have to consider a dilute system, so increasing the density would take us outside the regime of our model.

Let us analyze the condensation energy (binding energy) per pair ε_b which is given by the difference between the ground state energy of a non-interacting gas $3N\varepsilon_F/5$ and the ground state energy of the interacting system E_0, given in equation (4.112), divided by the number of pairs,

$$\varepsilon_b = \frac{2}{N}\left(\frac{3}{5}N\varepsilon_F - E_0\right) = \frac{2}{5n}\left[3(\varepsilon_F - \mu)n + \frac{m}{4\pi\hbar^2 a}\Delta^2\right] > 0, \tag{4.116}$$

where on the last equality we used the ground state energy given in equation (4.112). Differently from the 2D case we find that

$$\varepsilon_{\text{spec}} \neq \varepsilon_b. \tag{4.117}$$

This slightly different behavior is shown in Figure 4.2[24].

For the contact interaction case we can obtain a thermodynamic relation for Tan's contact $C = m^2\Delta^2/\hbar^4$ given by [120]

$$\left(\frac{\partial E_0}{\partial a^{-1}}\right)_{S,V,N} = -\frac{\hbar^2 C L^3}{2\pi m}. \tag{4.118}$$

Also we can calculate the isothermal compressibility,

$$\kappa_T = \frac{1}{n^2}\left(\frac{\partial n}{\partial \mu}\right)_{a^{-1}}. \tag{4.119}$$

However, it is not quite direct to perform the partial derivative because we do not know explicitly how the gap Δ depends on the scattering length a, but we can use the following identity:

$$\left(\frac{\partial n}{\partial \mu}\right)_{a^{-1}} = \left(\frac{\partial n}{\partial \mu}\right)_{\Delta} + \left(\frac{\partial n}{\partial \Delta}\right)_{\mu}\left(\frac{\partial \Delta}{\partial \mu}\right)_{a^{-1}}, \tag{4.120}$$

[23] The BCS limit is weakly interacting by construction. The BEC limit is strongly interacting in the sense that we increase the interaction between fermions to form a molecule, but these molecules can interact by a real repulsive potential with a scattering length given by $a_{dd} = 0.6a$ so that relevant dimer-dimer interactions become negligible in the BEC limit ($a \to 0^+$), giving a weakly interacting regime.

[24] At the beginning we thought that the exponential decay at large distances could be determined by ε_b, since numerically it is very similar to $\varepsilon_{\text{spec}}$.

which has the same difficulty in the last derivative $(\partial\Delta/\partial\mu)_{a^{-1}}$. But we can use a jacobian identity to express it in terms of known derivatives:

$$\left(\frac{\partial\Delta}{\partial\mu}\right)_{a^{-1}}\left(\frac{\partial\mu}{\partial a^{-1}}\right)_{\Delta}\left(\frac{\partial a^{-1}}{\partial\Delta}\right)_{\mu} = -1. \tag{4.121}$$

Then, it is enough to use the gap equation (4.109) and number equation (4.110) to calculate the partial derivatives. In Figure 4.3 we show the behavior of the isothermal compressibility throughout the crossover. As expected, in the weakly interacting regime it takes values similar to the one of a non-interacting gas. On the BEC side it diverges, in agreement with the behavior of an ideal Bose-Einstein condensate [138].

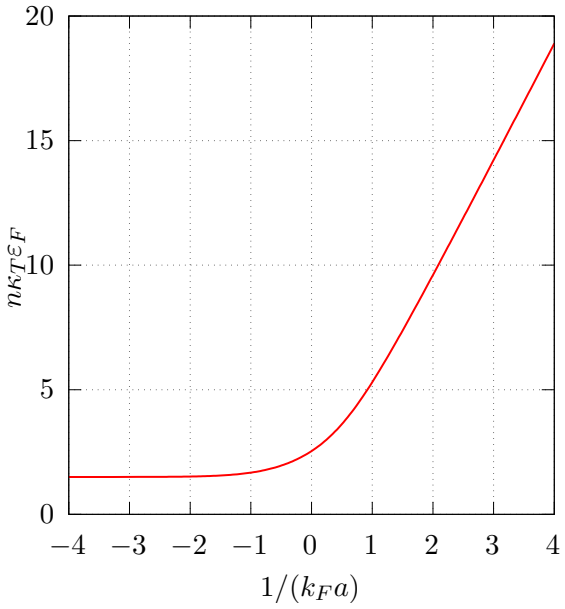

Figure 4.3: Isothermal compressibility κ_T scaled with the density n and the Fermi energy of a non-interacting gas ε_F. In the BCS limit $[(k_Fa)^{-1} \to -\infty]$ the compressibility behaves like the one of a non-interacting gas, while in the BEC limit $[(k_Fa)^{-1} \to +\infty]$ it diverges, in agreement with the behavior of a non-interacting Bose-Einstein condensate [138].

We have determined the thermodynamic properties of the ground state approximation, given by the mean-field method or the BCS-Leggett variational approach. As we have seen, for example in equation (4.36), a quantity that plays an important role is $u_{\vec{k}}v_{\vec{k}}$. It emerges from the interaction between fermions in the mean-field approach. In the next chapter we will analyze the spatial structure of the system, where we will find that $u_{\vec{k}}v_{\vec{k}}$ represents the formation of correlated pairs of opposite spin, which evolve from Cooper pairs in the BCS limit to a bosonic molecule in the BEC limit.

4.4.3 Three dimensions with finite-range interactions

We will present the chemical potential μ and the gap $\Delta_{\vec{k}}$, which depends on the wave vector, for the finite-range interaction potentials given in equations (3.92)-(3.97). Differently from the

contact interaction, the calculations do not require a renormalization procedure to obtain well-defined physical properties. However, these calculations involve more operations and a thorough analysis of numerical calculations. We will follow previous work [92, 103, 104], so we will give a brief review of the behavior of the gap and chemical potential. An extensive analysis of the thermodynamic properties has been presented in the thesis of Eleazar Neri [92].

For finite range potentials we can write the number equation (4.107) in the following form [92, 103]:

$$1 = \frac{3}{4}\int_0^\infty dx\ \sqrt{x}\left(1 - \frac{x-\tilde{\mu}}{\tilde{E}_x}\right), \tag{4.122}$$

where we are using scaled variables with the Fermi energy ε_F and the Fermi wave number k_F: $x = k^2/k_F^2$, $\tilde{\mu} = \mu/\varepsilon_F$, $\tilde{\Delta}_x = \Delta_{\vec{k}}/\varepsilon_F$, $\tilde{E}_x = [(x-\tilde{\mu})^2 + \tilde{\Delta}_x^2]^{1/2}$. The gap equation can be written as [92, 103]:

$$\tilde{\Delta}_x = -\frac{1}{16\pi^3}\int_0^\infty dx'\ \sqrt{x'}\tilde{F}(x,x')\frac{\tilde{\Delta}_{x'}}{2\tilde{E}_{x'}}, \tag{4.123}$$

where we have defined the Kernel of the energy gap $\tilde{F}(x,x')$, which depends on the finite-range potentials. For the potentials of equations (3.92)-(3.97) the Kernels are given by [92, 103]:

$$\tilde{F}_{\rm SW}(x,x') = \frac{8\pi^2\tilde{V}_0\tilde{R}_0}{\sqrt{xx'}}\left(\frac{\sin(Y_2)}{Y_2} - \frac{\sin(Y_1)}{Y_1}\right), \tag{4.124}$$

$$\tilde{F}_{\rm exp}(x,x') = \frac{8\pi^2\tilde{V}_0\tilde{R}_0}{\sqrt{xx'}}\left(\frac{1}{1+Y_2^2} - \frac{1}{1+Y_1^2}\right), \tag{4.125}$$

$$\tilde{F}_{\rm Yuk}(x,x') = \frac{8\pi^2\tilde{V}_0\tilde{R}_0}{\sqrt{xx'}}\ \ln\left(\frac{1+Y_2^2}{1+Y_1^2}\right)^{1/2}, \tag{4.126}$$

$$\begin{aligned}\tilde{F}_{\rm VdW}(x,x') =& \frac{8\pi^2\tilde{V}_0\tilde{R}_0}{\sqrt{xx'}}\left\{\left[\left(\frac{1}{5} - \frac{Y_2^2}{60} + \frac{Y_2^4}{120}\right)\cos(Y_2) + \left(-\frac{Y_2}{20} + \frac{Y_2^3}{120}\right)\sin(Y_2) - \frac{Y_2^5}{120}\left(\frac{\pi}{2} - {\rm Si}(Y_2)\right)\right]\right. \\ &\left. - \left[\left(\frac{1}{5} - \frac{Y_1^2}{60} + \frac{Y_1^4}{120}\right)\cos(Y_1) + \left(-\frac{Y_1}{120} + \frac{Y_1^3}{120}\right)\sin(Y_1) - \frac{Y_1^5}{120}\left(\frac{\pi}{2} - {\rm Si}(Y_2)\right)\right]\right\},\end{aligned} \tag{4.127}$$

with $Y_1 = \tilde{R}_0|\sqrt{x} - \sqrt{x'}|$ and $Y_2 = \tilde{R}_0|\sqrt{x} + \sqrt{x'}|$, where we are using the sine integral [88, 92],

$${\rm Si}(z) = \int_0^z dt\ \frac{\sin(t)}{t}. \tag{4.128}$$

Also, we are scaling the range of the potentials with the Fermi wave number $\tilde{R}_0 = k_F R_0$, and the depth of the potentials $\tilde{V}_0 = V_0/\varepsilon_F$. We can characterize the interaction strength with a parameter $k_F\chi = \tilde{R}_0\tilde{V}_0^{1/2}$. We are interested in describing an interacting gas in the dilute regime. Hence, we have to determine measurable quantities that do not depend strongly on the details of the interaction. Then, we are interested in exploring the properties of interactions with small potential ranges $\tilde{R}_0$. From previous works [94, 103] we have determined that $\tilde{R}_0 = 0.1$ is an adequate upper value for small interaction ranges [19][25]. Also, we will argue that the behavior

[25] An estimate of the order of magnitude of potential ranges can be obtained by using a density $n \approx 10^{12}{\rm cm}^{-3}$ [137] and an atomic range of $R_0 = 5.3\times10^{-7}$ cm [105], which gives $k_F R_0 \approx 0.016$. Then we are using an upper value.

of the chemical potential and gap is similar to the contact interaction case when we decrease the range of interactions.

In Figure 4.4 we show the behavior of the chemical potentials for each potential (pentagons). We can compare their behavior with the chemical potential of the contact interaction (dotted lines). As expected they have the same qualitative behavior, but each potential has a different behavior on the BEC side. For larger potential ranges R we get a further deviation from the contact interaction case[26]. This was expected, since the potential details acquire relevance for the formation of molecules. Each potential has different values of the binding energies as function of the scattering length. In panel (a) of Figure 4.4 we find a good agreement between the contact interaction potential and the square well because the former is renormalized such that we recover the physical properties of the later [77], like the bound state energy $-\hbar^2/(ma^2)$ on the BEC side.

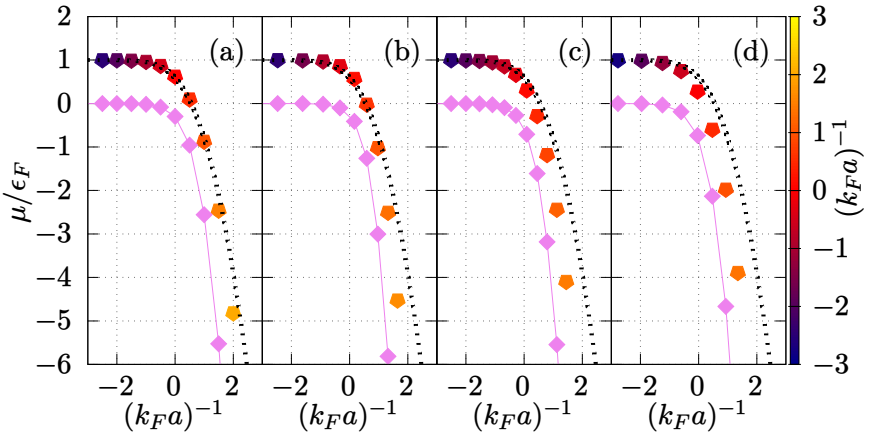

Figure 4.4: Chemical potentials (pentagons) as functions of the inverse of the s-wave scattering length throughout the crossover. (a) corresponds to the square well potential (3.92), (b) to the exponential potential (3.94), (c) to the Yukawa potential (3.96), and (d) to the Van der Waals type potential (3.97). The diamonds (joined with solid lines) correspond to the threshold energy required to break a pair $\varepsilon_{\text{spec}}/\varepsilon_F$ of equation (4.74). For comparison in each panel we show with a dotted line the chemical potential of the contact interaction, as shown in Figure 4.2.

The gaps for each finite-range potential are shown in Figure 4.5. Differently from the contact interaction case the gaps exhibit a non-constant behavior in wave vector space. These behaviors allow the natural convergence of the gap equation without the need of regularization. The discontinuities in the square well and Van der Waals type potentials introduce an inherent oscillatory structure in the gap functions Δ_k [92, 103]. We can see that the gaps are approximately constant near the wave vector $k = 0$, in the low-energy regime. This behavior agrees with the constant behavior of the gaps in the contact interaction. Then we can see that the constant behavior of the gap is adequate for describing the low-energy regime, but fails to describe the high-energy behavior, giving rise to the ultraviolet divergence discussed in subsection 4.4.2.

[26] A curious observation is that the Van der Waals type potential decreases significantly the values of the chemical potential at unitarity $(k_Fa)^{-1} = 0$, as happens with Quantum Monte Carlo simulations and measurements [69]. However, the values depend significantly on the range k_FR_0.

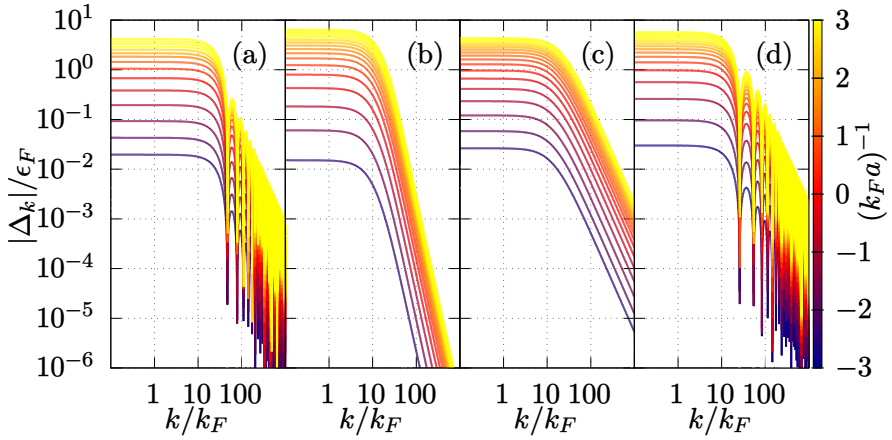

Figure 4.5: Gaps Δ_k as functions of the wave vector k for different values of the inverse scattering lengths $(k_F a)^{-1}$. Each panel corresponds to different potentials. In (a) we have the square well (3.92), in (b) we have the exponential potential (3.94), in (c) we have the Yukawa potential (3.96), and in (d) the Van der Waals type potential (3.97). Notice the constant behavior of each gap for values of $k/k_F \in [0, 5]$. This Figure was taken from [19].

After calculating the threshold energy required to break a pair $\varepsilon_{\text{spec}}$, using equation (4.73), we found that the energy is determined by the value of the gaps at $k = 0$, which we denote by Δ_0. Then we found a general expression for the threshold energy $\varepsilon_{\text{spec}}$ valid for any of the considered potentials, which is given by equation (4.74) [19],

$$\varepsilon_{\text{spec}} = \sqrt{\mu^2 + \Delta_0^2} - \mu.$$

Numerical calculations are shown in Figure 4.4 with diamonds. From equation (4.74) we were able to define a length associated to these many-body binding energies, which we found to be in good agreement with the large-distance correlation lengths calculated numerically, as we will show in the next chapter [19].

Chapter 5

Universality of density correlation functions

Having determined the mean-field ground state of the homogeneous gas of a two-component Fermi gas throughout the BEC-BCS crossover, we can analyze the behavior of pairs of fermions. In this chapter we will introduce the concept of Cooper pair by means of density-density correlation functions, and we will show the evolution from Cooper pairs to molecules as we tune from the BCS side to the BEC side. This will be done by using the position space representation, which allows us to study the spatial structure of our system. Before considering the interacting system we will present the density-density correlation functions of the non-interacting system, the free Fermi gas. Then we will show the behavior of these distributions when the interaction is considered. The particular contribution of the work presented here is that we were able to study the large-distance behavior throughout the crossover. In this regime we found an exponential decay that modulates the amplitude of spatial oscillations. For the density-density correlation function of opposite spins the exponential decay was known only in the extreme limits, BEC and BCS, but not throughout the crossover. Although questionable, the physical intuition that allowed us to find this exponential decay is the relationship between a two-body bound state and its exponential decay. As we have seen, in general there is no two-body bound state (except in 2D), so the binding energy has to be a many-body effect. Then, we were able to readdress the characterization of density fluctuations in an original way that was missing throughout the crossover.

5.1 Spatial structure of the non-interacting gas

Before analyzing the spatial structure of the interacting gas we will show the behavior of the density-density correlation functions of a non-interacting system [139]. This is the typical Fermi gas of two components that is introduced in a condensed matter course [111, 116]. For the balanced case we have $N_\uparrow = N_\downarrow$, such that the total number of particles is $N = N_\uparrow + N_\downarrow$ and the total density is $n = N/L^D$. The ground state is the well-known Fermi sea [111]:

$$|FS\rangle = \prod_{\sigma=\downarrow}^{\uparrow} \prod_{\vec{k}}^{k_F} c^\dagger_{\vec{k}\sigma} |0\rangle \,, \tag{5.1}$$

where again we are using an arbitrary order to make the product over the wave vectors whose norm is less than k_F.

We can analyze the spatial distribution of particles by calculating expectation values of local density operators. Let us define a field operator $\hat{\psi}_\sigma(\vec{x})$, which annihilates a fermion of spin σ in

position $\vec{x}$ [127]:

$$\hat{\psi}_\sigma(\vec{x}) = \frac{1}{L^{D/2}} \sum_{\vec{k}} e^{i\vec{k}\cdot\vec{x}} c_{\vec{k}\sigma}, \tag{5.2}$$

where we are using a linear combination of free fermions with periodic boundary conditions inside a box of size L^D. At the end of calculations we will take the limit of $L \to \infty$. Then, we can define a density operator $\hat{n}_\sigma(\vec{x})$ whose eigenvalues are the local density of particles with spin σ at position $\vec{x}$,

$$\hat{n}_\sigma(\vec{x}) = \hat{\psi}^\dagger_\sigma(\vec{x})\hat{\psi}_\sigma(\vec{x}). \tag{5.3}$$

Naturally, for our homogeneous Fermi sea, given in equation (5.1), the local density of particles is independent of the position, being a fixed quantity that determines our system N_σ/L^D. Similarly, we can define an operator $\hat{n}_\sigma(\vec{x})\hat{n}_{\sigma'}(\vec{y})$ to obtain information about the probability of finding a spin σ in position $\vec{x}$ when there is a spin σ' in position $\vec{y}$, in analogy to its classical definition [139]. We will define a density-density correlation function between spin σ and σ' in the following way:

$$C_{\sigma\sigma'}(\vec{x},\vec{y}) = \langle \hat{n}_\sigma(\vec{x})\hat{n}_{\sigma'}(\vec{y})\rangle - \langle \hat{n}_\sigma(\vec{x})\rangle\langle \hat{n}_{\sigma'}(\vec{y})\rangle. \tag{5.4}$$

This quantity measures the statistically independence of the local densities at position $\vec{x}$ with spin σ and position $\vec{y}$ with spin σ'. The statistical properties of fermions will endow this function with a structure. For non-interacting classical particles the density-density correlation functions are zero [139]. Instead, let us show the structure of the same spins correlation function of the non-interacting quantum gas. Since we are considering a balanced case $N_\uparrow = N_\downarrow$ we have $C_{\uparrow\uparrow}(\vec{x},\vec{y}) = C_{\downarrow\downarrow}(\vec{x},\vec{y})$. Using the definition of field operators (5.2) and (5.3) we get

$$\langle \hat{n}_\uparrow(\vec{x})\hat{n}_\uparrow(\vec{y})\rangle = \frac{1}{L^{2D}} \sum_{\vec{k},\vec{p},\vec{m},\vec{u}} e^{i(\vec{p}-\vec{k})\cdot\vec{x}}\, e^{i(\vec{u}-\vec{m})\cdot\vec{y}}\, \langle c^\dagger_{\vec{k}\uparrow} c_{\vec{p}\uparrow} c^\dagger_{\vec{m}\uparrow} c_{\vec{u}\uparrow}\rangle. \tag{5.5}$$

Since we know the action of the creation and annihilation operators over the Fermi sea, given in equation (5.1), we can identify the combination of wave vectors $\vec{k}$, $\vec{p}$, $\vec{m}$, $\vec{u}$ that give a non-zero contribution [23, 111]. We can identify two cases. One is when $\vec{u} = \vec{m}$ and $\vec{k} = \vec{p}$. The other case is when $\vec{k} = \vec{u}$ and $\vec{p} = \vec{m}$. After rearranging the operators we can use the thermodynamic limit to obtain

$$\begin{aligned}
\langle \hat{n}_\uparrow(\vec{x})\hat{n}_\uparrow(\vec{y})\rangle &= \left(\frac{n}{2}\right)^2 + \frac{1}{L^{2D}} \sum_{\vec{k}} \sum_{\vec{p}} e^{i(\vec{p}-\vec{k})\cdot\vec{x}} e^{i(\vec{k}-\vec{p})\cdot\vec{x}} \langle c^\dagger_{\vec{k}\uparrow} c_{\vec{p}\uparrow} c^\dagger_{\vec{p}\uparrow} c_{\vec{k}\uparrow}\rangle \\
&= \left(\frac{n}{2}\right)^2 + \frac{1}{L^{2D}} \sum_{\vec{p}} e^{i\vec{p}\cdot(\vec{x}-\vec{y})} \sum_{\vec{k}} e^{i\vec{k}\cdot(\vec{y}-\vec{x})} \langle c^\dagger_{\vec{k}\uparrow} c_{\vec{k}\uparrow}\rangle - \left| \frac{1}{L^D} \sum_{\vec{k}} e^{i\vec{k}\cdot(\vec{x}-\vec{y})} \langle c^\dagger_{\vec{k}\uparrow} c_{\vec{k}\uparrow}\rangle \right|^2,
\end{aligned} \tag{5.6}$$

where in the last equality we used the anticommutation relations. We can disregard some restrictions due to the thermodynamic limit, as those will be negligible when $L \to \infty$. We can use the identity

$$\sum_{\vec{p}} e^{i\vec{p}\cdot(\vec{x}-\vec{y})} = L^D\, \delta^{(D)}(\vec{x}-\vec{y}), \tag{5.7}$$

and take explicitly the thermodynamic limit that allows us to turn the sums into integrals. Then we obtain

$$\langle \hat{n}_\uparrow(\vec{x})\hat{n}_\uparrow(\vec{y})\rangle = \left(\frac{n}{2}\right)^2 + \frac{n}{2}\delta^{(D)}(\vec{x}-\vec{y}) - \left|\frac{1}{(2\pi)^D}\int d^D k\; e^{i\vec{k}\cdot(\vec{x}-\vec{y})}\;\theta(k_F - |\vec{k}|)\right|^2, \tag{5.8}$$

where we are using the Heaviside step function $\theta(x)$ and the Fermi wave number and we have used $\langle \hat{n}_\sigma(\vec{x})\rangle = n/2$. We can substitute the expectation value of equation (5.8) into the definition of the same spins correlation function given in equation (5.4) with $\sigma = \sigma' = \uparrow$ to calculate the same spins correlation function:

$$C_{\uparrow\uparrow}(\vec{x},\vec{y}) = \frac{n}{2}\delta^{(D)}(\vec{x}-\vec{y}) - \left|\frac{1}{(2\pi)^D}\int d^D k\; e^{i\vec{k}\cdot(\vec{x}-\vec{y})}\;\theta(k_F - |\vec{k}|)\right|^2. \tag{5.9}$$

For the 3D case we can make a change of variables to use spherical coordinates. After integration we obtain [9, 140]:

$$C^{3D}_{\uparrow\uparrow}(\vec{x},\vec{y}) = \frac{n}{2}\delta^{(3)}(\vec{x}-\vec{y}) - \left|\frac{\sin(k_F|\vec{x}-\vec{y}|) \;-\; k_F|\vec{x}-\vec{y}|\cos(k_F|\vec{x}-\vec{y}|)}{2\pi^2|\vec{x}-\vec{y}|^3}\right|^2, \tag{5.10}$$

where the density defines the 3D Fermi wave number as $n = k_F^3/(3\pi^2)$. For the 2D case we can make a change of variables in equation (5.9) to use polar coordinates. After integration we have [141]

$$C^{2D}_{\uparrow\uparrow}(\vec{x},\vec{y}) = \frac{n}{2}\delta^{(2)}(\vec{x}-\vec{y}) - \left|\frac{k_F J_1(k_F|\vec{x}-\vec{y}|)}{2\pi\; k_F|\vec{x}-\vec{y}|}\right|^2, \tag{5.11}$$

where the relation between the density and the Fermi wave number is $n = k_F^2/(2\pi)$. In both dimensions we have a Dirac delta term which corresponds to the presence of a spin in its own position [139, 142][1]. Another common feature is a negative term, that comes from the anticommutation relations. These terms describe the statistical effect of not finding two spins of the same component close to each other. This property is called Pauli blocking effect. Also, the minus sign corresponds to a so-called anticorrelation because the presence of a spin decreases the probability of finding a spin of the same component very close to it.

For the opposite spins correlation function it can be easily shown that they are zero, in both dimensions,

$$C_{\uparrow\downarrow}(\vec{x},\vec{y}) = 0. \tag{5.12}$$

This is because there is no statistical relation between the location of different spins, and there are no interactions that can modify the probability distribution of the particles. That is

$$\langle \hat{n}_\uparrow(\vec{x})\hat{n}_\downarrow(\vec{y})\rangle = \langle \hat{n}_\uparrow(\vec{x})\rangle\langle \hat{n}_\downarrow(\vec{y})\rangle. \tag{5.13}$$

We must make a warning in our interpretation of the density-density correlation functions. In the following, we will see that the interaction term in the Hamiltonian modifies the behavior of the

[1] If there is a spin $\uparrow$ in position $\vec{x}$, then there is a spin $\uparrow$ in position $\vec{y} = \vec{x}$. If we integrate $\vec{x}$ and $\vec{y}$ of $C_{\uparrow\uparrow}(\vec{x},\vec{y})$ over a small volume, we would count all the particles inside that volume, giving half the density $n/2$ (the coefficient of the Dirac delta), minus a contribution of the Pauli blocking effect [139].

density-density correlation functions, in particular the opposite spins $C_{\uparrow\downarrow}(\vec{x},\vec{y})$. However, this is not an effect of an interaction between two well-identified particles within our many-body system. Rather it is an average effect, as can be seen from the definition in equation (5.4).

We can argue that the density-density correlation functions carry information about local density fluctuations. Let us define an operator that gives the difference from the average density:

$$\delta\hat{n}_\sigma(\vec{x}) = \hat{n}_\sigma(\vec{x}) - \langle\hat{n}_\sigma(\vec{x})\rangle. \tag{5.14}$$

Then, we can write the density-density correlation function, given in equation (5.4), as

$$C_{\sigma\sigma'}(\vec{x},\vec{y}) = \langle\delta\hat{n}_\sigma(\vec{x})\,\delta\hat{n}_{\sigma'}(\vec{y})\rangle. \tag{5.15}$$

Then, we have the expectation value of local deviations of the density at points $\vec{x}$ and $\vec{y}$ for the respective components σ and σ'. In its classical analogue, this form is used to conclude that near a critical point the density fluctuations increase [142].

It is of interest to analyze the relationship between the density-density correlation functions and the thermodynamic properties of the gas. In the grand canonical ensemble we can obtain the relation between the number of particle fluctuations of the ensemble and the isothermal compressibility κ_T, given by [116, 142]

$$\kappa_T = L^D \frac{\langle(\hat{N} - \langle\hat{N}\rangle)^2\rangle}{k_B T \langle\hat{N}\rangle^2}, \tag{5.16}$$

where the average is over statistical ensembles with the respective density matrix, T is the temperature, k_B is the Boltzmann constant and we are considering a homogeneous gas inside a box of size L^D in D dimensions and we are using a total number of particle operator

$$\hat{N} = \sum_\sigma \int d^D x\, \hat{n}_\sigma(\vec{x}). \tag{5.17}$$

We can expand the expectation values in equation (5.16) and use equation (5.17) to obtain

$$\kappa_T n\, k_B T = \frac{1}{\langle\hat{N}\rangle}\left\langle \sum_\sigma \int_{L^D} d^D x\Big[\hat{n}_\sigma(\vec{x}) - \langle\hat{n}_\sigma(\vec{x})\rangle\Big] \sum_{\sigma'} \int_{L^D} d^D y\Big[\hat{n}_{\sigma'}(\vec{y}) - \langle\hat{n}_{\sigma'}(\vec{y})\rangle\Big]\right\rangle, \tag{5.18}$$

where $n = \langle\hat{N}\rangle/L^D$. We can further reduce these products of operators to obtain a relationship between the integrals of density-density correlation functions and the isothermal compressibility:

$$\kappa_T n\, k_B T = \frac{2}{\langle\hat{N}\rangle} \int_{L^D} d^D x \int_{L^D} d^D y\Big[C_{\uparrow\uparrow}(\vec{x},\vec{y}) + C_{\uparrow\downarrow}(\vec{x},\vec{y})\Big], \tag{5.19}$$

where we are assuming a balanced case $N_\uparrow = N_\downarrow$ and we have introduced the definitions of density-density correlation functions between same and different spins (5.4). This expression has been derived for a non-zero temperature and we can notice that it is a general relation that is valid for

interacting systems. However its zero temperature limit $T \to 0$ should be well defined, as can be verified for non-interacting systems. That is, if we use equations (5.10) and (5.11) we get

$$0 = \int_{L^D} d^D x \int_{L^D} d^D y \Big[C_{\uparrow\uparrow}(\vec{x},\vec{y}) + C_{\uparrow\downarrow}(\vec{x},\vec{y}) \Big]. \tag{5.20}$$

However, for the BCS-Legget variational approach, which is the mean-field approach, we will see that we get a contradiction when verifying equation (5.20). Part of the suprise will be that it is the pairing mechanism, represented by the product of parameters $u_{\vec{k}} v_{\vec{k}}$, that contributes to the non-zero value.

5.2 Spatial structure of the crossover with a contact interaction

Having shown the behavior of the density-density correlation functions of the non-interacting system, we can make a comparison with the interacting ones throughout the BEC-BCS crossover. As we have shown in equation (4.53) of Chapter 4 the variational ansatz of BCS introduces a two-particle wave function $\phi_{\mathrm{BCS}}(\vec{r})$. Then, for the ground state we can analyze three quantities (assuming we have the balanced case $N_\uparrow = N_\downarrow$). These are the same spins correlation function $C_{\uparrow\uparrow}(\vec{x},\vec{y})$, the different spins correlation function $C_{\uparrow\downarrow}(\vec{x},\vec{y})$ and the pair wave function $\phi_{\mathrm{BCS}}(\vec{r})$. Taking into account the homogeneity and isotropy of the system we have that the correlation functions depend on the relative position between the points under consideration. That is $C_{\sigma\sigma'}(\vec{x},\vec{y}) = C_{\sigma\sigma'}(\vec{x}-\vec{y})$. To simplify the notation we will define $\vec{r} = \vec{x} - \vec{y}$, with its magnitude given by $r = |\vec{r}|$. Then we have

$$C_{\uparrow\uparrow}(\vec{r}) = \frac{n}{2}\delta^{(D)}(\vec{r}) - |g_{\uparrow\uparrow}(\vec{r})|^2, \tag{5.21}$$

$$C_{\uparrow\downarrow}(\vec{r}) = |g_{\uparrow\downarrow}(\vec{r})|^2, \tag{5.22}$$

where we have defined functions given in terms of Fourier transforms:

$$g_{\uparrow\uparrow}(\vec{r}) = \frac{1}{(2\pi)^D} \int d^D k \; e^{i\vec{k}\cdot\vec{r}} v_{\vec{k}}^2 \tag{5.23}$$

and

$$g_{\uparrow\downarrow}(\vec{r}) = \frac{1}{(2\pi)^D} \int d^D k \; e^{i\vec{k}\cdot\vec{r}} u_{\vec{k}} v_{\vec{k}}. \tag{5.24}$$

To obtain these functional forms we have used the definition of the density-density correlation functions given in equation (5.4). We can calculate the expectation values using the BCS wave function $|\Psi_{\mathrm{BCS}}\rangle$, given in equation (4.31), or we can use the Bogoliubov transformation given in equations (4.13) and (4.14). The later is easier because we know the action of quasiparticle operators $\gamma_{\vec{k}}$ and $\alpha_{\vec{k}}$ over the BCS state $|\Psi_{\mathrm{BCS}}\rangle$. However, calculating the expectation values without quasiparticle operators allows us to perceive the importance of the thermodynamic limit in our calculations. Also, we are interested in analyzing the two-particle probability distribution given by the pair wave function $|\phi_{\mathrm{BCS}}(\vec{r})|^2$. Let us remind that it is given by the Fourier transform in equation (4.50),

$$\phi_{\mathrm{BCS}}(\vec{r}) = \frac{1}{(2\pi)^D} \int d^D k \;\; e^{i\vec{k}\cdot\vec{r}} \; \frac{v_{\vec{k}}}{u_{\vec{k}}}. \tag{5.25}$$

In each dimension we can take advantage of the isotropy and the dependence of the parameters $v_{\vec{k}}$ and $u_{\vec{k}}$ on the norm $|\vec{k}|$ to perform the angular integrals to end with a one-variable integral. In three dimensions we get a one-dimensional Fourier transform [18]. In two dimensions we get a Hankel transform [17]. The functional form of the parameters $u_{\vec{k}}$ and $v_{\vec{k}}$ introduce numerical difficulties for calculating the Fourier or Hankel transforms because of the algebraic decay of the integrands. Hence we will analyze separately the 2D case and then the 3D case. As we will show in the following, being one of the main results of this work, the large-distance behavior of the correlation functions $C_{\uparrow\uparrow}(r)$, $C_{\uparrow\downarrow}(r)$ and pair distribution $|\phi_{\mathrm{BCS}}(r)|^2$ can be written as

$$\rho_\alpha(r) \propto \frac{1}{r^2}\exp\left(\frac{-2r}{\chi_{\mathrm{spec}}}\right)\mathcal{P}_\alpha(\kappa_\alpha r+\varphi_\alpha). \tag{5.26}$$

where $\rho_\alpha(r) = C_{\uparrow\uparrow}(r),\ C_{\uparrow\downarrow}(r),\ |\phi_{\mathrm{BCS}}(r)|^2$. The functions $\mathcal{P}_\alpha$ are oscillatory functions which depend on the dimension of the system. The oscillations are characterized by a wave number κ_α and phases φ_α, which also depend on the dimension of the system. The length χ_{spec} is what we will identify as the large-distance correlation length given in terms of the threshold energy required to break a pair, given in equation (4.74),

$$\chi_{\mathrm{spec}} = \left(\frac{\hbar^2}{m\,\varepsilon_{\mathrm{spec}}}\right)^{1/2}. \tag{5.27}$$

This length depends on the dimension and features of the interaction implicitly by means of the gap $\Delta_{\vec{k}}$ and chemical potential μ, as we have seen previously in Chapter 4 section 4.4. We can analyze the behavior of χ_{spec} by observing figures 4.1, 4.2, 4.4, and 4.5. In the BCS limit the chemical potential is bigger than the gap at zero wave vector $k = 0$, $\mu \gg |\Delta_0|$. Then in the BCS limit we have a highly correlated system, since the correlation length is quite large $k_F\chi_{\mathrm{spec}} \gg 1$. We recover the behavior of Pippard's coherence length, used to describe the size of Cooper pairs in the original BCS theory [15]. That is, we get

$$k_F\chi_{\mathrm{spec}} \approx \frac{2\varepsilon_F}{\Delta_0}, \tag{5.28}$$

where we used equation (5.27) scaled with the Fermi wave number. The important aspect is that the length depends on the inverse of the gap [25][2], since it is the minimum energy required to create an excitation in the BCS limit. We have used that the chemical potential is similar to the non-interacting case $\mu/\varepsilon_F \approx 1$ and that the gap is small $\Delta_0/\varepsilon_F \ll 1$, so that in the BCS limit we can approximate

$$\frac{\varepsilon_{\mathrm{spec}}}{\varepsilon_F} \approx \frac{\Delta_0^2}{2\varepsilon_F^2}. \tag{5.29}$$

As we increase the strength of the interaction, the value of the large-distance correlation length χ_{spec} decreases, indicating the formation of molecules. In the BEC limit, we have $-\mu \gg |\Delta_0|$, so the large-distance correlation length χ_{spec} becomes dominated by the absolute value of chemical potential, leading to a small value of the large-distance correlation length. We have

$$k_F\chi_{\mathrm{spec}} = \left(-\frac{2\varepsilon_F}{\mu}\right)^{1/2}, \tag{5.30}$$

[2] In the work of BCS [15] and in the work of Kadin [25] an additional factor of $\pi \approx 3.14159$ is introduced. Notice that to obtain equation (5.28) we have not used any hypothesis over the density of states around the Fermi wave number.

where we are using that $1 \ll -\mu$. A particular point is where the chemical potential becomes zero, so that χ_{spec} is determined by the gap, which represents the interaction between fermions.

Finally, let us remind that χ_{spec} gives information about the size of local density fluctuations, as commented in equation (5.15). Then, we have characterized the size of density fluctuations in an original way [17, 18, 19], since previous works were based on so-called correlation lengths (coherence lengths) defined as averages, which we will present below. However there is another important length that allows to characterize the behavior between pairs (between molecules in the BEC limit), which is known as healing length ξ_{phase} [143]. We will not report any results about this length, which requires beyond mean-field corrections [8], but we will briefly comment that the healing length is smaller than χ_{spec} and the correlation lengths [to be presented in equation (5.85)] in the BCS limit for the 3D case with contact interaction [8], but in the BEC limit, it becomes larger, showing that the physical properties of the system are dominated by molecules and not by the individual particles.

We will not follow the chronological order in which we obtained the results, but we will briefly describe the development of ideas. First we addressed the large-distance behavior of the 3D case by studying the Fourier transforms of the density-density correlation functions and pair wave function in the complex plane $\mathbb{C}$ [18]. We found an exponential decay that we believed it could be determined by the threshold energy required to break a pair $\varepsilon_{\text{spec}}$ or by the condensation energy per pair ε_b, which is the difference between the ground state energy of the non-interacting system and the interacting system divided by the number of pairs. In that moment we were not able to define if there was a real relationship or just a coincidence in order of magnitudes, see the similarities in Figure 4.2. Later, we realized that our extensions of the Fourier transforms to the complex plane yielded an exponential decay, which explicitly shows its relationship with $\varepsilon_{\text{spec}}$ and not with ε_b for the 3D case with a contact interaction. Then we addressed the 2D case. Following our intuition that a many-body binding energy was present and that it could determine the large-distance behavior, we were able to find explicit expressions for the density-density correlation functions and analyze the large-distance behavior of the pair wave function [17]. Although mean-field is not enough to describe the most significant aspects of 2D systems, those explicit expressions allow us to become familiar with the spatial structure of the mean-field approach (BCS-Legget variational approach). Later, in a joint effort [19], we used previous knowledge and techniques [92, 103, 104, 144] to study the large-distance behavior of the 3D case considering finite-range interactions [92, 103, 104]. This was an interesting task because we wanted to explore the possible changes in the large-distance behavior when using more realistic potentials, instead of the contact interaction. We found generalizations for the threshold energy $\varepsilon_{\text{spec}}$, shown in equation (4.74), and found that it still determines the characteristic length of density fluctuations [19]. Then, this last work determines the universal behavior of the density-density correlation functions at large distances of the mean-field approach. The "universal" adjective comes from the fact that it is a property independent of the interaction details, as used in the literature [69]. Later we will comment on further perspectives when introducing beyond mean-field corrections.

As we have seen in equations (4.50), (5.23) and (5.24), the spatial structure will be obtained from the respective Fourier transforms of $v_{\vec{k}}^2$, $u_{\vec{k}}v_{\vec{k}}$ and $v_{\vec{k}}/u_{\vec{k}}$. Then it is of interest to analyze their behavior throughout the crossover (in wave vector space). We will restrict to the contact

interaction cases in 2D and 3D, which are shown in Figure 5.1. In the BCS limit, shown in panel (a) of Figure 5.1 we see that $v_{\vec{k}}^2$ resembles a step function,

$$v_{\vec{k}}^2 = \frac{1}{2}\left(1 - \frac{\varepsilon_{\vec{k}} - \mu}{\sqrt{(\varepsilon_{\vec{k}} - \mu)^2 + \Delta^2}}\right) \approx \theta(k_F - k), \tag{5.31}$$

showing the presence of a slightly modified Fermi sea, as in the original BCS theory [15]. The variational ansatz $v_{\vec{k}}/u_{\vec{k}}$ behaves like a parabola in the BCS limit,

$$\frac{v_{\vec{k}}}{u_{\vec{k}}} = \frac{\sqrt{(\varepsilon_{\vec{k}} - \mu)^2 + \Delta^2} - (\varepsilon_{\vec{k}} - \mu)}{\Delta} \approx \frac{|\varepsilon_{\vec{k}} - \varepsilon_F| - (\varepsilon_{\vec{k}} - \varepsilon_F)}{\Delta}, \tag{5.32}$$

which has negligible contributions outside the Fermi wave number k_F. In the BCS limit, the distribution $u_{\vec{k}}v_{\vec{k}}$ reveals the formation of pairs of fermions near the boundaries of the Fermi sea with a localized behavior around k_F [15], which we can identify as Cooper pairs,

$$u_{\vec{k}}v_{\vec{k}} = \frac{\Delta}{2\sqrt{(\varepsilon_{\vec{k}} - \mu)^2 + \Delta^2}} \approx \frac{\Delta}{2\sqrt{(\varepsilon_{\vec{k}} - \varepsilon_F)^2 + \Delta^2}}, \tag{5.33}$$

where the smallness of the gap Δ allows us to keep a non-divergent distribution. In panels (b) and (c) of Figure 5.1 we can see that as we increase the interaction strength, moving towards the BEC limit, the distributions $v_{\vec{k}}^2$, $u_{\vec{k}}v_{\vec{k}}$ and $v_{\vec{k}}/u_{\vec{k}}$ become broader, losing their sharp behavior. The maximum of $u_{\vec{k}}v_{\vec{k}}$ shifts from $k = k_F$ towards $k = 0$. Also we can see the vanishing of the Fermi surface in the behavior of $v_{\vec{k}}^2$. In the BEC limit $u_{\vec{k}}v_{\vec{k}}$ and $v_{\vec{k}}/u_{\vec{k}}$ become alike, since $-\mu \gg \Delta$. That is[3]

$$u_{\vec{k}}v_{\vec{k}} \approx \frac{v_{\vec{k}}}{u_{\vec{k}}} \approx \frac{\Delta}{2(\varepsilon_{\vec{k}} - \mu)}. \tag{5.34}$$

A curious observation is that in both dimensions the behavior of combinations of the parameters $u_{\vec{k}}$ and $v_{\vec{k}}$ as functions of $|\vec{k}|$ are similar when we vary the real strength of the interaction, as can be seen in Figure 5.1. Then the structure of our system in wave vector space is not so good for identifying differences between 2D and 3D (with a contact interaction). In contrast we will see that the spatial structure is quite different between 2D and 3D. We will discuss in more detail the behavior in 2D because we were able to calculate explicitly the Hankel transforms that define

[3] In the BEC limit we have $\varepsilon_{\vec{k}} > 0$, $-\mu \gg 1$ and $-\mu/\Delta \gg 1$. Then we have

$$\frac{v_{\vec{k}}}{u_{\vec{k}}} = \frac{\Delta}{\sqrt{(\varepsilon_{\vec{k}} - \mu)^2 + \Delta^2} + (\varepsilon_{\vec{k}} - \mu)} = \frac{1}{\sqrt{(\varepsilon_{\vec{k}} - \mu)^2/\Delta^2 + 1} + (\varepsilon_{\vec{k}} - \mu)/\Delta} \approx \frac{1}{2(\varepsilon_{\vec{k}} - \mu)/\Delta},$$

where in the first equality we used the definitions of the variational parameters, see equations (4.25) and (4.39). In the second equality we moved the gap from the numerator to the denominator. In the third equality we noticed that $-\mu \gg 1$, so $\varepsilon_{\vec{k}} - \mu \gg 1$, regardless of the wave vector k. Hence $(\varepsilon_{\vec{k}} - \mu)/\Delta \gg 1$. Then we can neglect the second term inside the square root, which allows us to verify the approximation. We can perform a similar procedure for $u_{\vec{k}}v_{\vec{k}}$ since

$$u_{\vec{k}}v_{\vec{k}} \approx \frac{\Delta}{2\sqrt{(\varepsilon_{\vec{k}} - \mu)^2 + \Delta^2}} \approx \frac{\Delta}{2(\varepsilon_{\vec{k}} - \mu)}.$$

the correlation functions $C_{\sigma\sigma'}(\vec{r})$. Instead, in 3D some features can only be argued or calculated numerically.

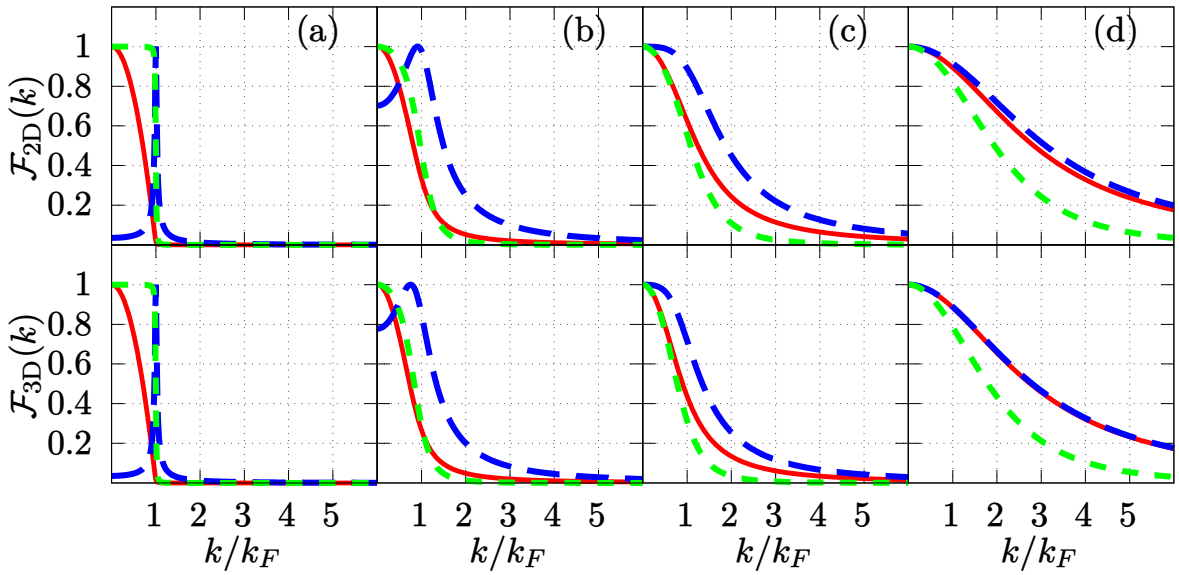

Figure 5.1: Comparison between the 2D (upper panel) and 3D (lower panel) combinations of parameters. The short (green) dashes correspond to $\mathcal{F}(k) = v_{\vec{k}}^2$, the large (blue) dashes correspond to $\mathcal{F}(k) = u_{\vec{k}}v_{\vec{k}}$, and the solid (red) line to $\mathcal{F}(k) = v_{\vec{k}}/u_{\vec{k}}$. There is no strict correspondence between the real strengths of the interaction between 2D and 3D, but each plot corresponds to the same asymptotic limits or regions. In column (a) we have the weakly interacting BCS limit with $\ln(1/k_F a_{2D}) = -8.49$ and $1/(k_F a_{3D}) = -5$. Column (b) is a representative point of the crossover (near unitarity for the 3D case) with $\ln(1/k_F a_{2D}) = -0.891$ and $1/(k_F a_{3D}) = 0.028$. Column (c) corresponds to the region where the chemical potential becomes zero, $\ln(1/k_F a_{2D}) = 0.023$ and $1/(k_F a_{3D}) = 0.578$. The strongly interacting BEC limit corresponds to column (d), with $\ln(1/k_F a_{2D}) = 1.009$ and $1/(k_F a_{3D}) = 2.728$. All curves are normalized to set their maximum equal to one. Figure adapted from [17].

Another interesting quantity is the number of condensed pairs N_0, which is the largest eigenvalue of the two-body density matrix [121],

$$\rho_2(\vec{x}_1, \vec{x}_2, \vec{y}_1, \vec{y}_2) = \langle \hat{\psi}_\uparrow^\dagger(\vec{x}_1)\hat{\psi}_\downarrow^\dagger(\vec{x}_2)\hat{\psi}_\downarrow(\vec{y}_1)\hat{\psi}_\uparrow(\vec{y}_2)\rangle, \tag{5.35}$$

where we are using the field operators given in equation (5.2). The eigenvalues of this two-body density matrix give information about the occupation of two-body states. For the case of fermions we can find a macroscopic occupation of two-body states, like in our present case of BCS-Leggett approach[4]. For a homogeneous gas, the existence of the largest eigenvalue of the density matrix

[4]We do not consider a one-body density matrix $\rho_1(\vec{x}, \vec{y}) = \langle \hat{\psi}^\dagger(\vec{x})\hat{\psi}(\vec{y})\rangle$, whose eigenvalues give information about the occupation of one-body states, since for fermions the Pauli exclusion principle forbids the macroscopic occupation of one-body states. Differently, for bosons, we would consider $\rho_1(\vec{x}, \vec{y})$ to exhibit the condensation.

$\rho_2(\vec{x}_1, \vec{x}_2, \vec{y}_1, \vec{y}_2)$ can be characterized by the density of condensed pairs $n_0 = N_0/L^D$, which is given by [145]

$$n_0 = \frac{N_0}{L^D} = \frac{1}{L^D} \int d^D\vec{x}_1 \int d^D\vec{x}_2 \, |\langle \hat{\psi}_\downarrow(\vec{x}_1)\hat{\psi}_\uparrow(\vec{x}_2)\rangle|^2. \tag{5.36}$$

In the mean-field approach or the BCS-Leggett variational approach this can be calculated using quasiparticle operators or operating directly over the BCS state $|\Psi_{\text{BCS}}\rangle$ [121, 130]. It is found that

$$\begin{aligned} \frac{N_0}{L^D} &= \int d^D\vec{r} \, |g_{\uparrow\downarrow}(\vec{r})|^2 \\ &= \frac{1}{L^D} \sum_{\vec{k}} (u_{\vec{k}} v_{\vec{k}})^2. \end{aligned} \tag{5.37}$$

We can define the condensate fraction as N_0/N, which is a quantity that depends on the behavior of the opposite spins correlation function $C_{\uparrow\downarrow}(\vec{r})$, see equations (5.22), and (5.24). Also we can notice that it depends on the expectation value of the interaction term in the mean-field approximation $u_{\vec{k}} v_{\vec{k}}$, which represents the pairing mechanism of the BCS theory.

After introducing some of the properties given in terms of density-density correlation functions, let us readdress the relationship between fluctuations of particle number and the isothermal compressibility for the interacting system. For the zero temperature limit we have the general condition given in equation (5.20). Then, let us analyze the integrals of density-density correlation functions at the mean-field level. For convenience, to identify the condensate fraction n_0/n, let us consider a non-zero coefficient given by the density $1/n$. Then we have

$$\begin{aligned} \frac{1}{n} \int d^D\vec{r} \, [C_{\uparrow\uparrow}(\vec{r}) + C_{\uparrow\downarrow}(\vec{r})] &= \frac{1}{n}\left[\frac{n}{2} - \int d^D\vec{r} \, |g_{\uparrow\uparrow}(\vec{r})|^2 + |g_{\uparrow\downarrow}(\vec{r})|^2\right] \\ &= \frac{1}{n}\left[\frac{n}{2} - \frac{1}{L^D}\sum_{\vec{k}} (v_{\vec{k}}^2)^2 + \frac{1}{L^D}\sum_{\vec{k}} (u_{\vec{k}} v_{\vec{k}})^2\right], \end{aligned} \tag{5.38}$$

where in the last equality we used (3.11). We can use the normalization condition $u_{\vec{k}}^2 + v_{\vec{k}}^2 = 1$ to find that

$$\frac{1}{n} \int d^2\vec{r} \, [C_{\uparrow\uparrow}(\vec{r}) + C_{\uparrow\downarrow}(\vec{r})] = 2\frac{n_0}{n} \neq 0. \tag{5.39}$$

We were expecting the integral of the correlation functions to be zero [left side of equation (5.39)], see equation (5.20), but the mean-field approximation of the BCS Hamiltonian (4.6) gives us a non-zero value, given by the condensate fraction, which is a quantity that depends on the pairing mechanism given by $u_{\vec{k}} v_{\vec{k}}$. This failure, identified by John Bell [135, 136] has been addressed with beyond mean-field techniques on the integrals of the correlation functions [143]. But still there is the question of how to handle (if possible) beyond mean-field terms in the correlation functions to satisfy the sum rule at zero temperature, given in equation (5.20)[5].

[5] Let us mention that in general the Kubo formula does not allow us to calculate the isothermal compressibility [146].

5.2.1 Two dimensions

Let us explicitly simplify the computation of a two-dimensional Fourier transform of a function $\mathcal{F}(\vec{k})$,

$$f(\vec{r}) = \frac{1}{(2\pi)^2}\int d^2k\, e^{i\vec{k}\cdot\vec{r}}\mathcal{F}(\vec{k}). \tag{5.40}$$

When the function $\mathcal{F}(\vec{k})$ depends on the norm of the wave vector, we can change to polar coordinates and we can perform the integral over the angle to find

$$f(r) = \frac{1}{2\pi}\int_0^\infty dk\, k\mathcal{F}(k)\, J_0(kr), \tag{5.41}$$

where we have used the integral representation of the Bessel function of the first kind of order zero [88]:

$$J_0(kr) = \frac{1}{2\pi}\int_0^{2\pi} d\theta\, e^{ikr\cos(\theta)}. \tag{5.42}$$

Equation (5.41) corresponds to a Hankel transform [88], which for our cases is difficult to compute numerically. The integrands $v_{\vec{k}}^2$, $u_{\vec{k}}v_{\vec{k}}$ and $v_{\vec{k}}/u_{\vec{k}}$ decay algebraically (very slow), and the Bessel function $J_0(kr)$ also oscillates, which makes more difficult the numerical integration [102]. However, after analyzing numerical calculations of $\phi_{\mathrm{BCS}}(r)$, $g_{\uparrow\uparrow}(r)$ and $g_{\uparrow\downarrow}(r)$ we found an oscillatory behavior modulated by an exponential decay at large distances, as shown in equation (5.26) (see also the lower panel of Figure 5.2). We realized that the nodes of $g_{\uparrow\uparrow}(r)$ were the zeros of $J_1(k_Fr)$, while the nodes of $g_{\uparrow\downarrow}(r)$ were the zeros of $J_0(k_Fr)$. Then, it was tempting to find closed-form expressions for the Fourier transforms $g_{\uparrow\uparrow}(r)$ and $g_{\uparrow\downarrow}(r)$. Looking at tables of integrals, like [147, 148, 149], we were not able to identify Hankel transforms of $v_{\vec{k}}^2$, $u_{\vec{k}}v_{\vec{k}}$ and $v_{\vec{k}}/u_{\vec{k}}$. Instead, we looked for (unknown) functions "$g_{\uparrow\uparrow}(r)$" and "$g_{\uparrow\downarrow}(r)$" which could reproduce the large-distance behavior of equation (5.26), in a trial and error way. We looked for their Fourier transforms (Hankel transforms) to see if they agree with $v_{\vec{k}}^2$ and $u_{\vec{k}}v_{\vec{k}}$, respectively. Remarkably, a key aspect that guide us was the hypothesis of an exponential decay, given in equation (5.26), which made easier the search.

The integrals we require to find the Fourier transform of $v_{\vec{k}}^2$ denoted by $g_{\uparrow\uparrow}(r)$ were [17, 147][6]

$$\int_0^\infty x^{\nu+1}K_\mu(ax)\, I_\mu(bx)\, J_\nu(cx)dx = \frac{(ab)^{-\nu-1}c^\nu e^{-(\nu+1/2)\pi i}Q_{\mu-1/2}^{\nu+1/2}(u)}{\sqrt{2\pi}(u^2-1)^{\frac{1}{2}\nu+\frac{1}{4}}} \tag{5.43}$$

where

$$u = \frac{a^2+b^2+c^2}{2ab} \tag{5.44}$$

and $\mathrm{Re}(a) > |\mathrm{Re}(b)| + |\mathrm{Im}(c)|$, $\mathrm{Re}(\nu) > -1$ and $\mathrm{Re}(\mu+\nu) > -1$. The modified Bessel function of the first kind $I_\nu(x)$ is defined by means of the Bessel function of the first kind $J_\nu(x)$ in the following way [88]:

$$I_\nu(x) = e^{-\nu\pi i/2}J_\nu(e^{i\pi/2}x). \tag{5.45}$$

[6] Do not confuse the indices μ with the chemical potential.

The modified Bessel function of the second kind $K_\nu(x)$ is defined in terms of $J_\nu(x)$ and the Bessel function of the second kind $N_\nu(x)$ by [88]

$$K_\nu(x) = \frac{\pi}{2} i^{\nu+1}[J_\nu(ix) + iN_\nu(ix)]. \tag{5.46}$$

The associated Legendre function is defined as [147, 148]

$$Q_\nu^\mu(z) = \frac{e^{\mu\pi i}}{2^{\nu+1}} \frac{\Gamma(\nu+\mu+1)}{\Gamma(\nu+3/2)} \frac{\Gamma(1/2)(z^2-1)^{\mu/2}}{z^{\nu+\mu+1}} \; {}_2F_1\left(\frac{\nu+\mu}{2}+1, \frac{\nu+\mu+1}{2}; \nu+\frac{3}{2}, \frac{1}{z^2}\right), \tag{5.47}$$

where ${}_2F_1$ is the hypergeometric function [88], and $\Gamma(x)$ is the gamma function [88]. The integral representation of the hypergeometric function is a handy expression for our case:

$${}_2F_1(\alpha,\beta,\gamma;z) = \frac{1}{B(\beta,\gamma-\beta)} \int_0^1 t^{\beta-1}(1-t)^{\gamma-\beta-1}(1-tz)^{-\alpha}\, dt, \tag{5.48}$$

which is valid for $\mathrm{Re}(\gamma) > \mathrm{Re}(\beta) > 0$, where $B(\cdot,\cdot)$ is the beta function:

$$B(x,y) = \int_0^1 t^{x-1}(1-t)^{y-1}\, dt. \tag{5.49}$$

For the Fourier transform of $u_{\vec{k}} v_{\vec{k}}$, denoted by $g_{\uparrow\downarrow}(r)$, we used the following integral [147, 149]:

$$\begin{aligned} \int_0^\infty x J_0(ax) K_0(bx) J_0(cx)\, dx &= [a^4 + b^4 + c^4 - 2a^2c^2 + 2a^2b^2 + 2b^2c^2]^{-1/2} \\ &= \{[b^2 + (a-c)^2]\,[b^2 + (a+c)^2]\}^{-1/2}, \end{aligned} \tag{5.50}$$

where $\mathrm{Re}(b) > |\mathrm{Im}(a)|$ and $c > 0$.

The details of the calculations are given in Appendix C.1. For the pair wave function $\phi_{\mathrm{BCS}}(r)$ we were not able to calculate an explicit expression throughout the crossover, but we were able to calculate its asymptotic behavior in both limits, BEC and BCS. We calculated numerically its behavior and we analyzed its Hankel transform representation in the complex plane when considering large distances. Then, the density-density correlation functions are found to be [17]:

$$C_{\uparrow\uparrow}(\vec{r}) = \frac{n}{2}\delta^{(2)}(\vec{r}) - \left|\frac{m\Delta}{2\pi\hbar^2} J_1(k_F r) K_1\left(\frac{r}{\chi_{\mathrm{spec}}}\right)\right|^2, \tag{5.51}$$

$$C_{\uparrow\downarrow}(\vec{r}) = \left|\frac{m\Delta}{2\pi\hbar^2} J_0(k_F r) K_0\left(\frac{r}{\chi_{\mathrm{spec}}}\right)\right|^2, \tag{5.52}$$

where m is the mass of a fermion, Δ is the gap, k_F is the Fermi wave number defined in terms of the density $n = k_F^2/(2\pi)$, and we have introduced the large-distance correlation length χ_{spec} defined in equation (5.27). For the 2D case we find that the large-distance correlation length is given by the s-wave scattering length, differently from the 3D case, see equations (3.63), (4.89), (4.103), and (5.27),

$$\chi_{\mathrm{spec}} = a_{2\mathrm{D}}. \tag{5.53}$$

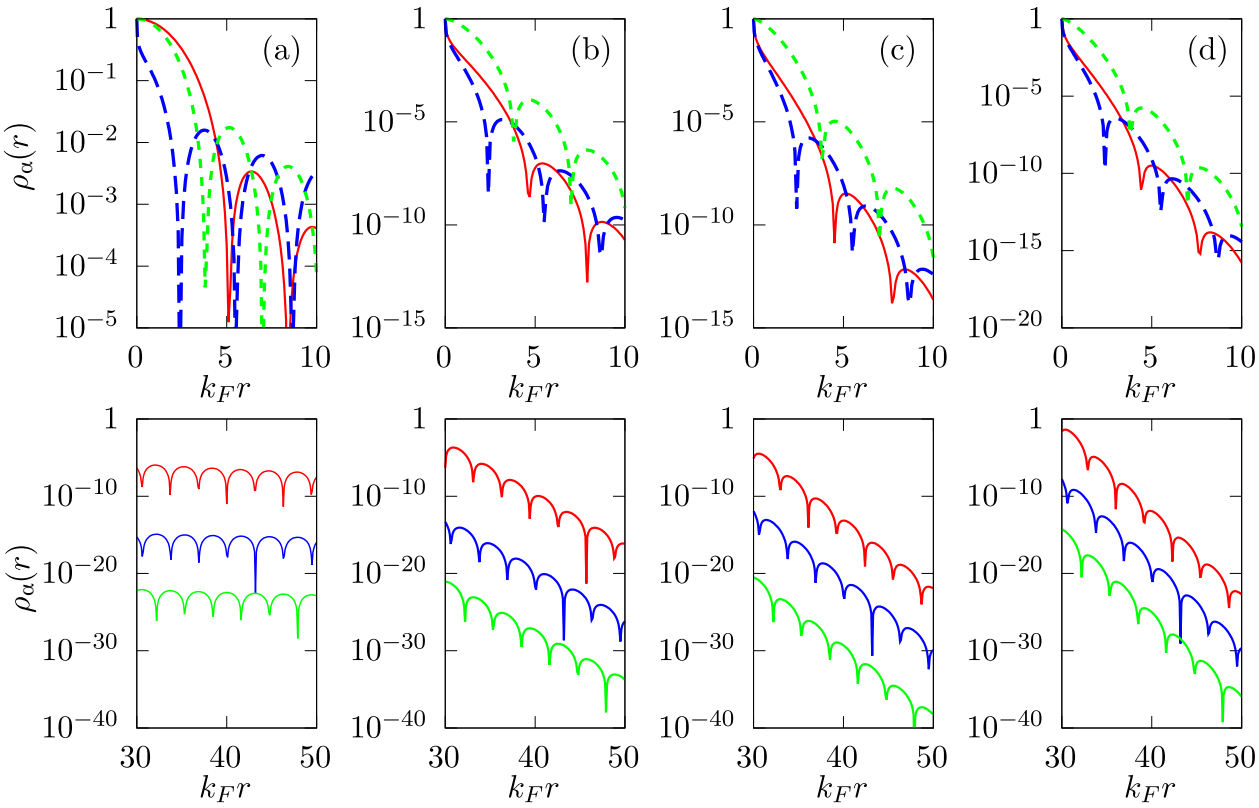

Figure 5.2: Distribution functions throughout the 2D crossover with logarithmic scale. Short (green) dashes correspond to $\rho_\alpha(r) = -C_{\uparrow\uparrow}(r)$ given in equation (5.51), the large (blue) dashes to $\rho_\alpha(r) = C_{\uparrow\downarrow}(r)$ given in equation (5.52), and solid (red) line to $\rho_\alpha(r) = |\phi_{\rm BCS}(r)|^2$. Each column corresponds to different points of the crossover. In the lower panel the upper curves correspond to $|\phi_{\rm BCS}(r)|^2$, the middle ones to $C_{\uparrow\downarrow}(r)$, and the lower ones to $C_{\uparrow\uparrow}(r)$. In (a) we have the weakly interacting BCS limit [$\ln(1/k_F a_{2D}) = -4.95$], in (b) we have a point in the crossover region [$\ln(1/k_F a_{2D}) = -0.34$], (c) is where the chemical potential becomes zero [$\ln(1/k_F a_{2D}) = 0$], and (d) is in the strongly interacting BEC limit [$\ln(1/k_F a_{2D}) = 0.20$]. In the upper panel we show the short distance behavior, where we can see how the functions get localized as we move from the BCS to the BEC limit. The lower panel shows the large-distance behavior, where we see an exponential decay and an oscillatory behavior. This Figure was taken from [17].

Let us discuss the short-distance behavior of the density-density correlation functions. From equations (5.51) and (5.52) we can use the well-known asymptotic behaviors of the Bessel functions $J_\nu(x)$ and $K_\nu(x)$ to find [17, 88]

$$C_{\uparrow\uparrow}(\vec{r}) \approx \frac{n}{2}\delta^{(2)}(\vec{r}) - \left(\frac{m\Delta}{4\pi\hbar^2}\right)^2\left[k_F\, a_{2D} + \frac{(k_F r)^2}{2}\left(\frac{1}{k_F a_{2D}}\ln\left(\frac{e^{\gamma-1/2}\, r}{2a_{2D}}\right) - \frac{k_F a_{2D}}{4}\right)\right]^2. \tag{5.54}$$

$$C_{\uparrow\downarrow}(\vec{r}) \approx \left[\frac{m\Delta}{2\pi\hbar^2}\ln\left(\frac{r}{a_{2D}}\right)\right]^2, \tag{5.55}$$

Hence, at short distances the opposite spins correlation function $C_{\uparrow\downarrow}(\vec{r})$ has a logarithmic divergence that is characterized by Tan's contact $C = m^2\Delta^2/\hbar^4$, see equation (4.104). In contrast, for the 3D

case this divergence is an algebraic one. We can also see that the Pauli blocking effect is also determined by the contact, with the probability of finding same spins near each other diminishing like $[r^2\ln(r)]^2$. In 2D the (radial) Pauli blocking effect is higher, since in 3D it diminishes as r^2. Since in the BCS limit the gap is small $\Delta \ll 1$, the opposite spins correlation function becomes negligible $C_{\uparrow\downarrow}(\vec{r}) \approx 0$. Accordingly, in the BCS limit, the same spins correlation function $C_{\uparrow\uparrow}(\vec{r})$ asymptotically (at short distances) behaves like the non-interacting one, shown in equation (5.11). Part of these behaviors have been reported by Werner and Castin [99], where they assume a zero-energy scattering state for an equivalent of the pair wave function. Differently, in the work presented here we are not assuming a functional form for $\phi_{\mathrm{BCS}}(r)$. The behaviors here emerge naturally from the mean-field approximation of the many-body problem with a contact interaction. To remark the contrast, in the BCS limit, at short distances, we found the asymptotic behavior of the pair wave function:

$$\phi_{\mathrm{BCS}}(r) \approx \frac{2\varepsilon_F}{\pi\Delta} k_F^2 \frac{J_2(k_F r)}{(k_F r)^2}, \tag{5.56}$$

where we can see that there is no logarithmic divergence near the origin, in contrast to Ref. [99]. This can be seen in the upper panel of Figure 5.2 (solid line). However, throughout the crossover and in the BEC limit the squared norm of the pair wave function $|\phi_{\mathrm{BCS}}(r)|^2$ acquires a behavior that resembles equation (5.55) at short distances, as can be seen in Figure 5.2 from (b) to (d). In fact, in the BEC limit when $-\mu \gg \Delta$ we have that $u_{\vec{k}} v_{\vec{k}} \approx v_{\vec{k}}/u_{\vec{k}}$, see equation (5.34), so that

$$\phi_{\mathrm{BCS}}(r)|_{\mathrm{BEC}} \approx g_{\uparrow\downarrow}(r)|_{\mathrm{BEC}}, \tag{5.57}$$

where we have used equations (4.50) and (5.24). Numerically we were not able to exhibit this behavior, see Figure 5.3, but it is an analytical result that follows from equation (5.34).

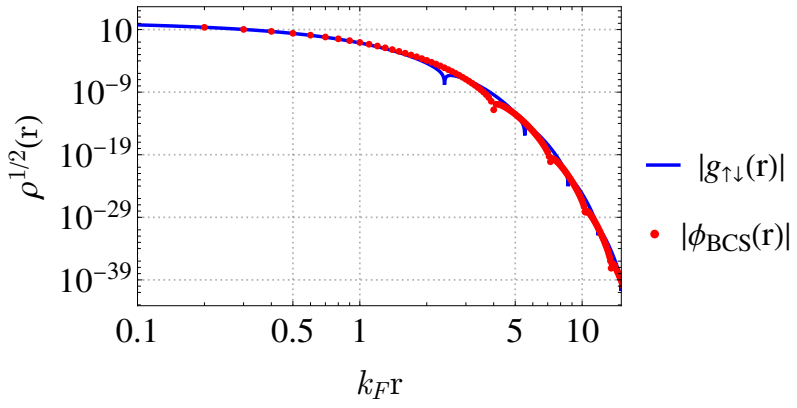

Figure 5.3: We show a comparison between $|g_{\uparrow\downarrow}(r)|$ and $|\phi_{\mathrm{BCS}}(r)|$ in the BEC limit $E_a/\varepsilon_F \approx 70$ with arbitrary normalization. At short distances we find an overlap $\phi_{\mathrm{BCS}}(r) \approx g_{\uparrow\downarrow}(r)$. However, the first nodes of each function (small peaks before $k_F r \approx 5$) have a different position [17].

Before analyzing the large-distance behavior, let us comment on the anomalous breaking of scale invariance, which is of theoretical interest for the contact interaction [125, 128]. In a non-interacting gas the absence of a length other than the interparticle distance k_F^{-1} leads to a scale-invariant system. Hence, the density-density correlation functions of same spins (5.11) have a power law decay, so there is no length to characterize the decay at large distances. Instead, for the

interacting system we have an exponential decay that is given by the s-wave scattering length a_{2D} which is a quantity introduced by renormalizing the theory. Then we see that after renormalization the system loses its scale invariance (anomalous breaking of scale invariance). As expected, the scale invariance is lost due to the scattering length a_{2D} that represents the interaction between fermions.

Part of the novelty of the work presented here is the analysis of the large-distance behavior of the density-density correlation functions. Differently from the 3D case, we can extract this behavior explicitly for the density-density correlation functions. The pair wave function had to be characterized numerically and we will give arguments to exhibit explicitly its exponential decay at large distances. From equations (5.51) and (5.52) we find, for $r \gg 1$,

$$C_{\uparrow\uparrow}(r) \approx -\frac{\text{const}}{r^2}\,\exp\left(-\frac{2r}{a_{2D}}\right)\cos^2\left(k_F r - \frac{3\pi}{4}\right), \tag{5.58}$$

$$C_{\uparrow\downarrow}(r) \approx \frac{\text{const}}{r^2}\,\exp\left(-\frac{2r}{a_{2D}}\right)\cos^2\left(k_F r - \frac{\pi}{4}\right), \tag{5.59}$$

where we have used the exact relation $\chi_{\text{spec}} = a_{2D}$ and the well-known behaviors of the Bessel functions $J_\nu(x)$ and $K_\nu(x)$ for large arguments. The exponential decay comes from the modified Bessel functions of the second kind $K_\nu(x)$, while the oscillatory behavior is due to the Bessel functions of the first kind $J_\nu(x)$. At large distances the Hankel transform of the pair wave function can be approximated by

$$\phi_{\text{BCS}}(r) \approx \frac{1}{2\pi}\int_0^\infty dk\,\frac{v_{\vec{k}}}{u_{\vec{k}}}\left[\frac{e^{i(kr-\pi/4)} + e^{-i(kr-\pi/4)}}{\sqrt{2\pi kr}}\right], \tag{5.60}$$

where we have used the large-argument approximation of the Bessel function $J_0(kr)$ given in equation (3.45), using complex exponential functions. The integral in equation (5.60) can be analyzed in the complex plane. Using a change of variables and choosing a suitable contour of integration to surround the branch cuts of $v_{\vec{k}}/u_{\vec{k}}$ we can obtain an equivalent integral which allows us to conclude that the pair wave function decays exponentially. The steps for this analysis are given in Appendix C.2. We obtained

$$\begin{aligned}\phi_{\text{BCS}}(r) \propto \frac{1}{\sqrt{k_F r}}\int_{\tau_0}^\infty e^{-\tau k_F r}\left(\frac{2\tau^2+\tilde{\mu}}{\tilde{\Delta}}\right)^{1/4}\Bigg[\cos\left(\sqrt{\frac{\tau^2+\tilde{\mu}}{\tilde{\Delta}}}\right)\left(\cos(\theta(\tau)/2) - \frac{\tau\sin(\theta(\tau)/2)}{\sqrt{\tau^2+\tilde{\mu}}}\right)\\ +\sin\left(\sqrt{\frac{\tau^2+\tilde{\mu}}{\tilde{\Delta}}}\right)\left(\frac{\tau\cos(\theta(\tau)/2)}{\sqrt{\tau^2+\tilde{\mu}}} + \sin(\theta(\tau)/2)\right)\Bigg]\left(\frac{\sqrt{4\tau^2(\tau^2+\tilde{\mu}) - \tilde{\Delta}^2}}{\tilde{\Delta}}\right)d\tau,\end{aligned} \tag{5.61}$$

where $\tau_0 = \{[(\tilde{\mu}^2 + \tilde{\Delta}^2)^{1/2} - \tilde{\mu}]/2\}^{1/2}$, we have used the scaled chemical potential $\tilde{\mu} = \mu/\varepsilon_F$ and gap $\tilde{\Delta} = \Delta/\varepsilon_F$ and we have introduced the function

$$\theta(\tau) = \tan^{-1}\left(\frac{\sqrt{\tau^2+\tilde{\mu}}}{\tau}\right). \tag{5.62}$$

To argue that the pair wave function exhibits an exponential decay we notice that in escence the integrand is bounded, and it decays exponentially when $\tau \to \infty$. Then, if we were to find

the antiderivative (indefinite integral), when evaluating the upper limit we would get a zero contribution. When evaluating the lower limit an exponential function will appear, but evaluated at τ_0. Then, we get a behavior of the form

$$\phi_{\mathrm{BCS}}(r) \propto \frac{e^{-r/a_{2\mathrm{D}}}}{\sqrt{r}}. \tag{5.63}$$

This argument lacks strict mathematical formality. However, it is similar to the ones used in Relativistic Quantum Field theory, for example, to illustrate the non-zero value of the propagation amplitude of the Klein-Gordon Field outside the light-cone [150]. The point we want to emphasize is the appearance of an exponential. When we approximate $J_0(kr)$ in the integral of the pair wave function, see equation (5.60), with the asymptotic behavior given in equation (3.45), we remove a very big part of the structure. Mainly, we remove the oscillations and part of the power law decay. To reinforce the argument of an exponential decay we fitted the envelopes of numerical calculations, like the ones shown in Figure 5.2, and found good agreement with the exponential decay given by equation (5.26). The numerical fits are shown with (red) dots in Figure 5.5 (a).

Let us address the oscillatory behavior of the pair distributions under consideration. From our explicit theoretical results, shown in equations (5.58) and (5.59), we can see that the oscillatory behavior of the density-density correlation functions is characterized by the Fermi wave number k_F throughout the whole crossover. As we will see below, this is in stark contrast with the 3D case where the wave vectors of the oscillations decrease as we approach the BEC limit. The oscillatory behavior of the pair wave function was characterized numerically. In Figure 5.4 we show numerical fits to the wave number κ_{BCS}. Then the oscillatory behavior of equation (5.26) is given by the wave vectors

$$\kappa_\alpha = k_F \tag{5.64}$$

for $\alpha = \uparrow\uparrow$, $\uparrow\downarrow$, BCS.

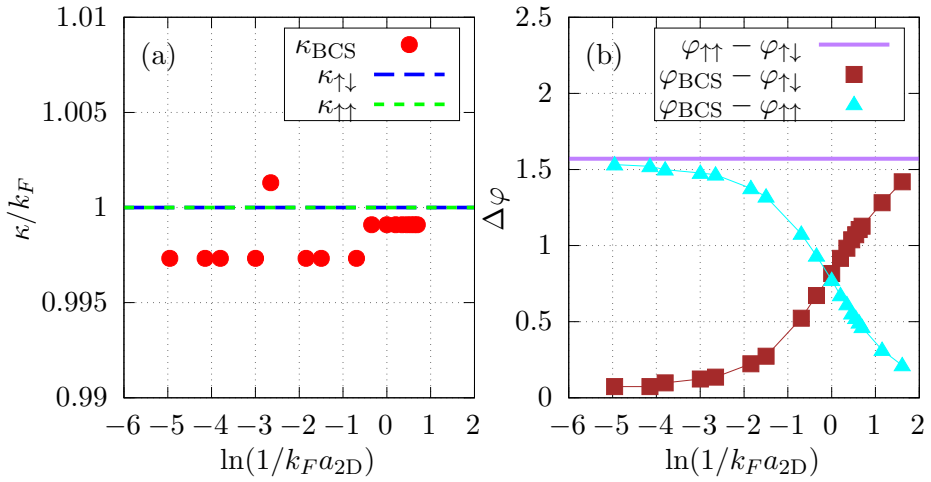

Figure 5.4: (a) Large-distance wave vectors κ_α, with $\alpha = \uparrow\uparrow, \uparrow\downarrow$, BCS of equation (5.26) for the 2D case. The (red) dots correspond to numerical fits of $\kappa_{\rm BCS}$. For comparison we show the wave vectors of the correlation functions $\kappa_{\uparrow\uparrow} = \kappa_{\uparrow\downarrow} = k_F$ [theoretical results extracted from equations (5.58) and (5.59)]. (b) Large-distance phase differences between the distributions. The phases are defined in equation (5.26). The phase difference $\varphi_{\uparrow\uparrow} - \varphi_{\uparrow\downarrow}$ is a theoretical result, see equations (5.58) and (5.59). This Figure was taken from [17].

Characteristic lengths that allow us to study the spatial structure of the gas are the so-called correlation lengths for the correlation functions $C_{\sigma\sigma'}(\vec{r})$ and the mean pair radius for the pair wave function $\phi_{\rm BCS}(r)$. This lengths can be defined in the following way [17]:

$$\xi_\alpha^2 = \frac{|\int r^2 \rho_\alpha(r) d^2 r|}{|\int \rho_\alpha(r) d^2 r|}, \tag{5.65}$$

where $\rho_\alpha(r) = |\phi_{\rm BCS}(r)|^2, C_{\uparrow\downarrow}(r), C_{\uparrow\uparrow}(r)$. The opposite spins correlation function $\xi_{\uparrow\downarrow}$ is also known as pair coherence length (denoted as $\xi_{\rm pair}$ in recent works [8, 143]). Differently from the large-distance correlation length $\chi_{\rm spec}$ of equation (5.26), the correlation lengths ξ_α depend on the short distance behavior, so that they might depend on the interaction details. The integrals of equation (5.65) can be easily done in wave vector space. The correlation length $\xi_{\uparrow\downarrow}$ has been extensively studied in the literature [16, 28, 151, 152, 153]. The integrals can be performed similarly to the integral of the renormalized gap equation (4.82). We were able to find explicit expressions for the three lengths (we include $\xi_{\uparrow\downarrow} = \xi_{\rm pair}$ for completeness, although it is not an original result of the work presented here, see Ref. [52]):

$$\xi_{\rm BCS}^2 = \frac{\hbar^2}{m\Delta} \frac{[-1 + 2x^2 + 2x\sqrt{1+x^2} - x\pi + 2{\rm arcsinh}(x) - 2x\arctan(x) + \ln(4+4x^2)]}{x + \frac{2}{3}x^3 + \frac{2}{3}(1+x^2)^{3/2}}, \tag{5.66}$$

$$\xi_{\uparrow\downarrow}^2 = \frac{\hbar^2}{4m\Delta}\left[x + \frac{2+x^2}{(1+x^2)}\left(\frac{\pi}{2} + \arctan(x)\right)^{-1}\right], \tag{5.67}$$

$$\xi_{\uparrow\uparrow}^2 = \frac{\hbar^2}{8m\Delta} \frac{4 + 3x[\pi + x(2+\pi x)] + 6(x+x^3)\arctan(x)}{(1+x^2)\left(\frac{\pi}{2} + \arctan(x)\right)}, \tag{5.68}$$

where $x = \mu/\Delta$. These lengths are shown in Figure 5.5. We can see that in the BCS limit $\ln(1/k_F a_{2D}) \to -\infty$ the lengths $\xi_{\uparrow\uparrow}$ and $\xi_{\uparrow\downarrow}$ diverge like [17]

$$\begin{aligned} \xi_{\uparrow\downarrow} &\approx \frac{1}{2\sqrt{2}} a_{2D}, \\ \xi_{\uparrow\uparrow} &\approx \frac{1}{2}\sqrt{\frac{3}{2}} a_{2D}. \end{aligned} \tag{5.69}$$

In our renormalized interaction the bound state energy decreases with an increase of a_{2D}. In contrast the mean pair raidus has a finite value in the BCS limit [17]

$$\xi_{BCS} \approx \sqrt{6}\frac{1}{k_F}. \tag{5.70}$$

This indicates that the pair wave function becomes dominated by the interparticle distance, up to a normalization constant, as shown in equation (5.56). This behavior is in agreement with a weak interaction regime, where we would expect small deviations from a non-interacting system with an scale-invariant behavior. However, the pair wave function $\phi_{BCS}(r)$ is unable to describe a non-interacting system. For obtaining the asymptotic limits given in equations (5.69) and (5.70) we have used that $x = \mu/\Delta \gg 1$ in equations (5.66)-(5.68). Then we write the chemical potential μ and gap Δ in terms of the s-wave scattering length a_{2D} using equations (4.97), (4.98), and (3.63).

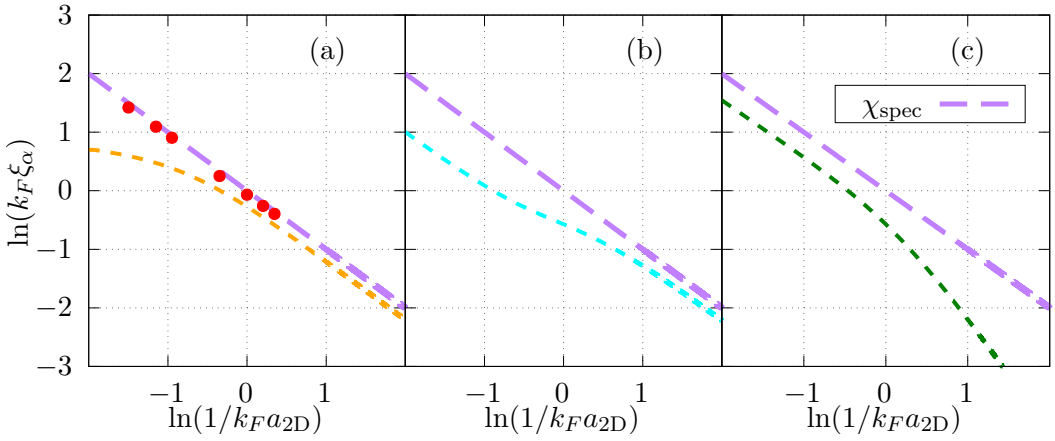

Figure 5.5: Characteristic lengths of two-body distributions throughout the crossover in 2D. Short dashes correspond to the correlation lengths ξ_α of equation (5.65). Large (purple) dashes correspond to the large-distance correlation length χ_{spec}. In (a) we show the lengths of $\phi_{BCS}(\vec{r})$, where the (red) dots are numerical fits extracted from the envelopes shown in the lower panel of Figure 5.2 [upper (red) curves]. In (b) we show the ones of $C_{\uparrow\downarrow}(\vec{r})$. In (c) the ones of $C_{\uparrow\uparrow}(\vec{r})$. This Figure was taken from [17].

On the other side, in the BEC limit $\ln(1/k_F a_{2D}) \to \infty$, the lengths are dominated again by the

s-wave scattering length, but in this limit a_{2D} becomes small. We have [17]

$$\begin{aligned}\xi_{\uparrow\downarrow} &\approx \sqrt{\frac{2}{3}}a_{2D},\\ \xi_{\uparrow\uparrow} &\approx \sqrt{\frac{4}{5}}(k_F a_{2D})a_{2D},\\ \xi_{BCS} &\approx \sqrt{\frac{2}{3}}a_{2D},\end{aligned} \tag{5.71}$$

As expected, from equation (5.34), we see the same behavior between $\xi_{\uparrow\downarrow}$ and ξ_{BCS}. The same spins correlation length $\xi_{\uparrow\uparrow}$ diminishes faster indicating the formation of molecules and the low effect of Pauli-blocking in this limit [17], since it decays like $\xi_{\uparrow\uparrow} \propto a_{2D}^2$. In the 2D case the scattering length is equal to the length associated to the threshold energy required to break a pair $a_{2D} = \chi_{spec}$. Differently from the 3D case, to be presented below, the correlation lengths $\xi_{\uparrow\downarrow}$ and ξ_{BCS} differ from $\chi_{spec} = a_{2D}$ by a numerical factor. For obtaining the asymptotic behaviors of the correlation lengths in the BEC limit given in equation (5.69) we have used $x = \mu/\Delta \ll -1$.

Finally, let us mention that the condensate fraction has been calculated explicitly using wave vector representation [154],

$$\frac{n_0}{n} = \frac{1}{4}\frac{\frac{\pi}{2} + \arctan(\mu/\Delta)}{\frac{\mu}{\Delta} + \sqrt{1+(\mu/\Delta)^2}}, \tag{5.72}$$

which has the nice property of being an expression that depends on the quotient μ/Δ [154]. Another nice aspect of our explicit expressions (5.51) and (5.52) is that we can calculate the condensate fraction using position representation with well-known integrals of Bessel functions [122]. We obtained an equivalent expression:

$$\frac{n_0}{n} = \frac{\tilde{\Delta}^2}{4}\left[\frac{\arctan((1-\tilde{\mu})^{-1/2})}{2\sqrt{1-\tilde{\mu}}}\right], \tag{5.73}$$

where $\tilde{\mu} = \mu/\varepsilon_F$ and $\tilde{\Delta} = \Delta/\varepsilon_F$. From equation (5.72) we can see that in the BEC limit the condensate fraction becomes a constant,

$$\frac{n_0}{n} \approx \frac{1}{2}. \tag{5.74}$$

We can use this limit in the density of condensed pairs given in equation (5.37) and the fact that $u_{\vec{k}}v_{\vec{k}} \approx v_{\vec{k}}/u_{\vec{k}}$ in the BEC limit, as indicated in equation (5.34) to find that

$$\sum_{\vec{k}} \frac{v_{\vec{k}}^2}{u_{\vec{k}}^2}\bigg|_{BEC} \approx N_0. \tag{5.75}$$

This result allows us to verify the boson commutation relations for the operators $b_{\vec{0}}$, given that we have verified equation (4.60).

5.2.2 Three dimensions

The three-dimensional Fourier transforms with spherical symmetry can be converted into one-dimensional Fourier transforms. In spherical coordinates the 3D Fourier transform of a function $\mathcal{F}(k)$ is given by

$$f(\vec{r}) = \frac{1}{(2\pi)^3}\int_{k=0}^{k=\infty}\int_{\varphi=0}^{\varphi=2\pi}\int_{\theta=0}^{\theta=\pi} e^{ikrcos(\theta)}\mathcal{F}(k)k^2\,\mathrm{sen}(\theta)\,dk\,d\theta\,d\varphi. \tag{5.76}$$

Integration over the azimuth angle φ gives us a 2π factor. The integral over the polar angle can be done using

$$\int_{\theta=0}^{\theta=\pi} e^{ikrcos(\theta)}\,\frac{(-ikr)}{(-ir)}\,\mathrm{sen}(\theta)\,d\theta = -\frac{1}{ir}\Big[e^{ikr\,cos(\theta)}\Big]_0^{\pi} = \frac{1}{ir}[e^{ikr} - e^{-ikr}]. \tag{5.77}$$

Then we have

$$\begin{aligned} f(r) &= \frac{1}{ir(2\pi)^2}\int_0^{\infty}\mathcal{F}(k)\,k[e^{ikr} - e^{-ikr}]\,dk \\ &= \frac{1}{ir(2\pi)^2}\left[\int_0^{\infty}\mathcal{F}(k)k\,e^{ikr}dk \;\; + \int_{\infty}^{0}\mathcal{F}(k)(-k)\,e^{-ikr}(-dk)\right], \end{aligned} \tag{5.78}$$

where in the last equality we splitted the integral. In the last term we can make a change of vairable $x = -k$ to join the two terms into one integral that has the form of a one-dimensional Fourier transform:

$$f(r) = \frac{1}{ir(2\pi)^2}\int_{-\infty}^{\infty}\mathcal{F}(k)k\,e^{ikr}\,dk. \tag{5.79}$$

Like in the 2D case we face the same problem of computing this integrals numerically for the correlation functions $C_{\sigma\sigma'}(r)$ and pair wave function $\phi_{\mathrm{BCS}}(r)$. We can take advantage of the branch cuts that appear in the combinations of $v_{\vec{k}}^2$, $u_{\vec{k}}v_{\vec{k}}$ and $v_{\vec{k}}/u_{\vec{k}}$ [123]. When extending the integrals to the complex plane, we can close a contour in the upper half, like the one shown in Figure 5.6.

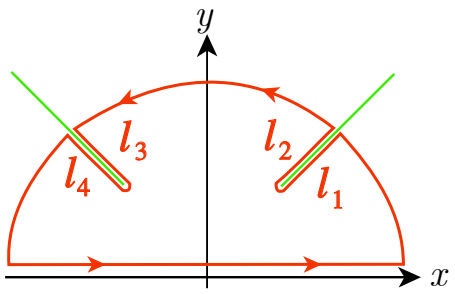

Figure 5.6: Ilustration of the closed integration contour that surrounds the branch cuts of $v_{\vec{k}}^2$, $u_{\vec{k}}v_{\vec{k}}$ and $v_{\vec{k}}/u_{\vec{k}}$. When extending the integrals to the complex plane we have used $k = x + iy$. This figure was taken from [18].

The integral over the whole contour is zero, since there are no poles inside the contour. Then we obtain that the one-dimensional Fourier transform can be calculated by the integrals that surround the branch cuts [7]. The expressions that we found are given by [18, 155]:

$$(k_\Delta r)\phi_{\mathrm{BCS}}(k_\Delta r) = -8\pi(k_\Delta)^3 \int_{t_0}^{\infty} \left(\frac{2t^2-\mu_\Delta}{\sqrt{t^2-\mu_\Delta}}\right) \sqrt{4t^2(t^2-\mu_\Delta)-1}\ \exp\Big[-\sqrt{t^2-\mu_\Delta}(k_\Delta r)\Big]\ \mathrm{sen}(t(k_\Delta r))\,dt, \tag{5.80}$$

$$(k_\Delta r)\, g_{\uparrow\uparrow}(k_\Delta r) = -4\pi(k_\Delta)^3 \int_{t_i}^{\infty} \left(\frac{2t^2-\mu_\Delta}{\sqrt{t^2-\mu_\Delta}}\right) \frac{2t\sqrt{t^2-\mu_\Delta}}{\sqrt{4t^2(t^2-\mu_\Delta)-1}}\ \exp\Big[-\sqrt{t^2-\mu_\Delta}(k_\Delta r)\Big]\ \cos(t(k_\Delta r))\,dt. \tag{5.81}$$

$$(k_\Delta r)\, g_{\uparrow\downarrow}(k_\Delta r) = -4\pi(k_\Delta)^3 \int_{t_i}^{\infty} \left(\frac{2t^2-\mu_\Delta}{\sqrt{t^2-\mu_\Delta}}\right) \frac{1}{\sqrt{4t^2(t^2-\mu_\Delta)-1}}\ \exp\Big[-\sqrt{t^2-\mu_\Delta}(k_\Delta r)\Big]\ \mathrm{sen}(t(k_\Delta r))\,dt, \tag{5.82}$$

where

$$t_0 = \left(\frac{\mu_\Delta + (\mu_\Delta^2+1)^{1/2}}{2}\right)^{1/2}, \tag{5.83}$$

and we have defined $\mu_\Delta = \mu/\Delta$ and the wave vector of the gap $k_\Delta = \sqrt{2m\Delta}/\hbar$. Like for the pair wave function in the 2D case, see equation (5.61), we can see that the integrand has an exponential function. An antiderivative (indefinite integral) should have this same exponential evaluated in the lower limit (the upper limit would give a zero contribution). Hence we can conclude that the correlation functions have an exponential decay of the form [17]

$$\rho_\alpha(r) \propto \frac{e^{-2r/\chi_{\mathrm{spec}}}}{r^2}. \tag{5.84}$$

This verifies the exponential decay stated before in equation (5.26). The large-distance properties have been analyzed numerically [18, 155]. Here we include those results for completeness[8]. Numerical calculations of density-density correlation functions $C_{\sigma\sigma'}(r)$ and the pair distribution $|\phi_{\mathrm{BCS}}(r)|^2$ are shown in the lower panel of Figure 5.7. The straight lines formed by the envelopes with a great decrease in orders of magnitude indicates an exponential decay.

[7] We must declare that the theoretical treatment of the 3D Fourier transforms to obtain equations (5.80), (5.81) and (5.82) was part of the work presented for obtaining the degree of Master in Science (Physics) [155], where we analyzed them numerically. The present work goes further and analyzes these equations analytically.

[8] The analysis of the oscillatory behavior is an original contribution of the work presented here. The exponential decay corresponds to a previous work [155], although the explicit form of equation (5.84) was overlooked.

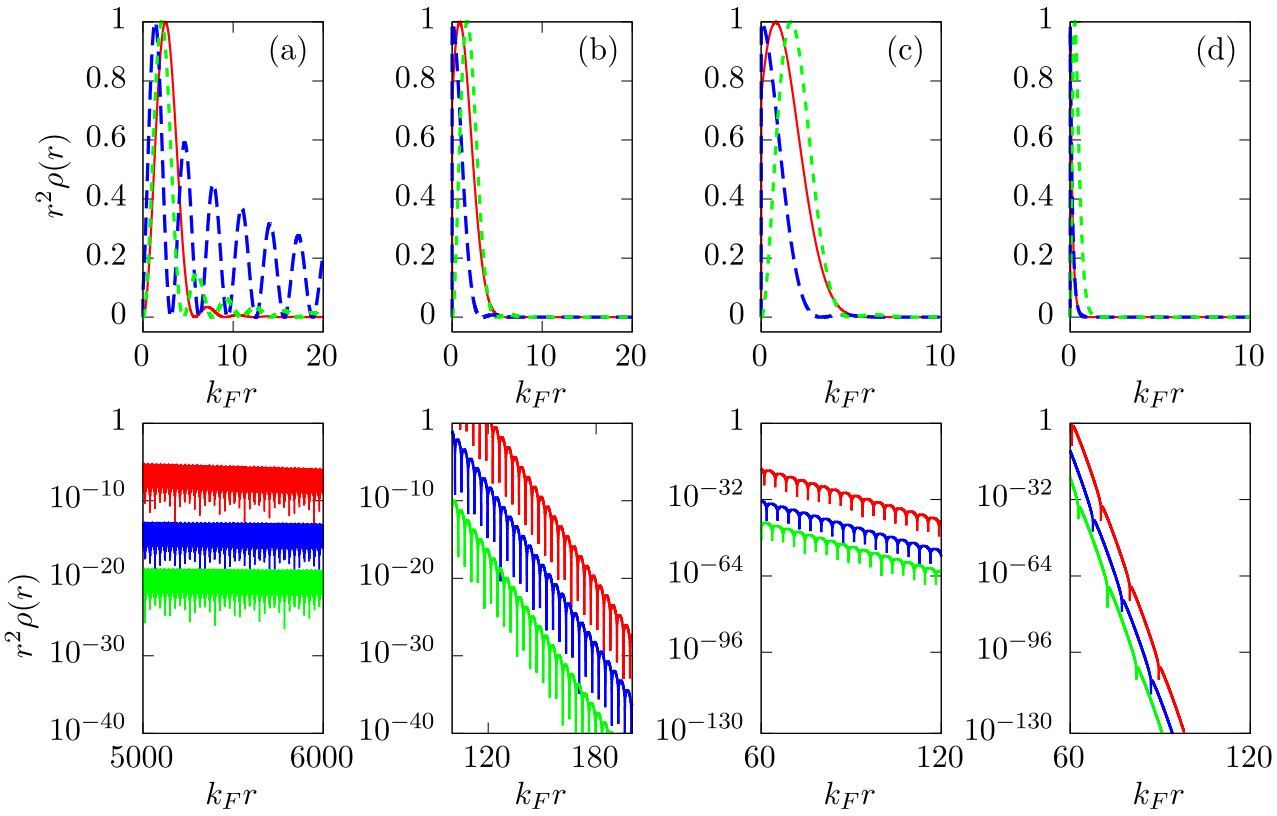

Figure 5.7: Distribution functions throughout the 3D crossover. The upper panel corresponds to the short-distance behavior. Short (green) dashes correspond to $\rho_\alpha(r) = -C_{\uparrow\uparrow}(r)$, the large (blue) dashes to $\rho_\alpha(r) = C_{\uparrow\downarrow}(r)$, and solid (red) line to $\rho_\alpha(r) = |\phi_{\rm BCS}(r)|^2$. Each column corresponds to different points of the crossover. The lower panel has a logarithmic scale to show the large-distance behavior and we have ordered the functions: The upper curves correspond to $|\phi_{\rm BCS}(r)|^2$, the middle ones to $C_{\uparrow\downarrow}(r)$, and the lower ones to $-C_{\uparrow\uparrow}(r)$. In (a) we have the weakly interacting BCS limit $[1/k_F a = -5.0]$, in (b) we have a point near unitarity from the BCS side $[1/k_F a = -0.0046]$, (c) is near unitarity from the BEC side $[1/k_F a = 0.0064]$, and (d) is in the strongly interacting BEC limit $[1/k_F a = 4.0]$. The oscillatory behavior at short distances (upper panel) is modulated by an algebraic decay and the exponential decay, so it cannot be seen. This Figure was taken from [18].

In the lower panel of Figure 5.7 we can see an oscillatory behavior throughout the crossover, that was not studied in the BEC limit [18]. The wave vectors κ_α of equation (5.26) that characterize these oscillations are shown in Figure 5.8. In the BCS limit we have $\kappa_\alpha = k_F$, for $\alpha = \uparrow\uparrow, \uparrow\downarrow$, BCS, in agreement with a weakly interacting regime [15]. As we move to the BEC side the wave vectors diminish, accelerating the convergence of $\phi_{\rm BCS}(r)$ and $g_{\uparrow\downarrow}(r)$ to a bound state distribution (that does not have oscillations), indicating the formation of molecules. This is a behavior very different from the 2D case, see Figure 5.4.

To calculate the wave vectors we found the distance between consecutive nodes for each function. Then we obtained an average distance $\bar{d}_\alpha$, which determines the wave vectors $\kappa_\alpha = 2\pi/(2\bar{d})$. The numerical computations were easier in the 3D case, so comparing Figure 5.4 (b) [17] with Figure 5.8 (b) [18] we can see that we were not able to calculate $\phi^{\rm 2D}_{\rm BCS}(r)$ in the deep BEC regime. Both

plots should exhibit the same behavior, see equation (5.57). In that sense Figure 5.4 (b) is missing an interval with $\ln(1/k_F a_{2D}) > 2$. However, this is not a problem, since in both dimensions we can use equations (4.50) and (5.24) to obtain the BEC asymptotic behavior $\phi_{BCS} \approx g_{\uparrow\downarrow}(r)$ because $u_{\vec{k}} v_{\vec{k}} \approx v_{\vec{k}}/u_{\vec{k}}$ as discussed in equation (5.34)

We can see the evolution of the nodes of the two-body distributions from Figure 5.8 (b), where we show phase differences between the two-body distributions. In the BCS limit the nodes of the pair wave function $\phi_{BCS}(r)$ coincide with the nodes of $g_{\uparrow\downarrow}(r)$, as we move to the BEC side, past the unitarity $1/(k_F a) = 0$ the nodes of $\phi_{BCS}(r)$ coincide with $g_{\uparrow\uparrow}(r)$, but then, in the BEC limit the nodes of $\phi_{BCS}(r)$ approach the ones of $g_{\uparrow\downarrow}(r)$ again. Differently from the 2D case, the nodes of the density-density correlation functions change their positions for different points of the crossover.

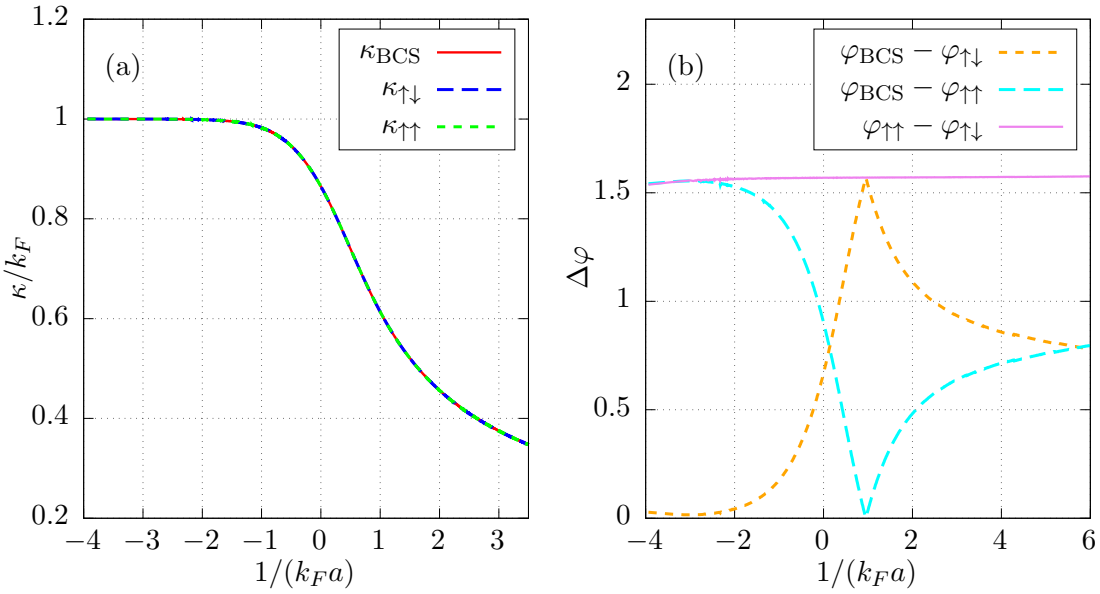

Figure 5.8: (a) Large-distance wave vectors κ_α, with $\alpha = \uparrow\uparrow, \uparrow\downarrow$, BCS of equation (5.26) for the 3D case, the three lines overlap. (b) Large-distance phase differences between the distributions. The phases are defined in equation (5.26). This Figure was taken from [18].

Similarly to the 2D case, the local density fluctuations have been characterized by the correlation lengths defined as second moments of pair distributions,

$$\xi_\alpha^2 = \frac{|\int r^2 \rho_\alpha(r) d^3 r|}{|\int \rho_\alpha(r) d^3 r|}, \tag{5.85}$$

where $\rho_\alpha(r) = |\phi_{BCS}(r)|^2, C_{\uparrow\downarrow}(r), C_{\uparrow\uparrow}(r)$. With the same integral identities used for expressing the gap equation (4.109) and number equation (4.110) in terms of associated Legendre functions, shown in Appendix B.2 we can obtain explicit expressions for these lengths:

$$\xi_{BCS}^2 = \frac{\hbar^2}{m(\mu^2+\Delta^2)^{1/2}} \left\{ \frac{1 + 2z - z^2 - 2z^3 + 2\sqrt{2}(1+z)^{1/2}\left(P_{\frac{5}{2}}(z) - zP_{\frac{3}{2}}(z)\right)}{\left[\sqrt{2}(1-z)(1+z)^{1/2}\right]\left[-{}_2F_1\left(\frac{7}{2}, -\frac{5}{2}; 2, \frac{1-z}{2}\right) + z\,{}_2F_1\left(\frac{5}{2}, -\frac{3}{2}; 2, \frac{1-z}{2}\right)\right]} \right\}. \tag{5.86}$$

$$\xi_{\uparrow\downarrow}^2 = \frac{1}{8}\frac{\hbar^2}{2m}\frac{1}{(\mu^2+\Delta^2)^{1/2}}\frac{5+8z+3z^2}{(1+z)^2}. \tag{5.87}$$

$$\xi_{\uparrow\uparrow}^2 = \frac{3}{8}\frac{\hbar^2}{2m}\frac{1}{(\mu^2+\Delta^2)^{1/2}}\left(\frac{1-z}{1+z}\right), \tag{5.88}$$

where $z = -\mu/\sqrt{\mu^2+\Delta^2}$ and we are using associated Legendre functions which are given in terms of the Hypergeometric function $P_\lambda(z) = {}_2F_1(-\lambda, \lambda+1, 1, (1-z)/2)$. The correlation lengths are illustrated in Figure 5.9.

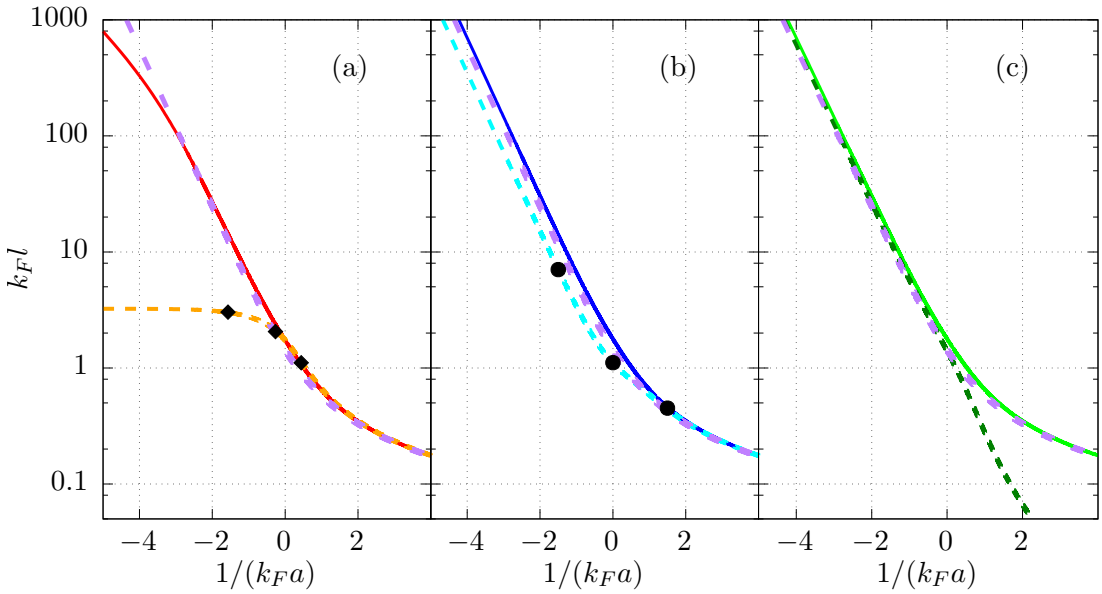

Figure 5.9: In each panel we show the correlation lengths (short dashes) defined as an average in equation (5.85), numerical calculations of the large-distance correlation length with a numerical factor $k_F\chi_{\rm spec}/\sqrt{2}$, and a length associated to the condensation energy per pair $k_F\chi_b = k_F\hbar/(2m\varepsilon_b)^{1/2}$ (separated dashes). Panel (a) corresponds to $|\phi_{\rm BCS}(r)|^2$, panel (b) to $C_{\uparrow\downarrow}(r)$, and panel (c) to $C_{\uparrow\uparrow}(r)$. The diamonds in panel (a) correspond to $k_F\xi_{\rm BCS}$ taken from Ref. [26]. The circles in panel (b) correspond to $k_F\xi_{\uparrow\downarrow}$ extracted from Ref. [143]. This Figure was taken from [18].

We can analyze the asymptotic behaviors in the BCS limit [8, 18, 26]

$$\begin{aligned}\xi_{\uparrow\downarrow} &\approx \frac{1}{\sqrt{2}}\frac{e^2}{8k_F}e^{-\frac{\pi}{2k_F a}}\\ \xi_{\uparrow\uparrow} &\approx \sqrt{\frac{3}{2}}\frac{e^2}{8k_F}e^{-\frac{\pi}{2k_F a}}\end{aligned} \tag{5.89}$$

We can see that the correlation lengths increase in the weakly interacting regime in agreement with a highly correlated system. In fact, the opposite spins correlation length $\xi_{\uparrow\downarrow}$ recovers the Pippard's coherence length, since the gap goes like $\Delta = 8\varepsilon_F e^{-2}e^{\pi/k_F a}$, so that $\xi_{\uparrow\downarrow} \propto 1/\sqrt{\Delta}$ [52]. The

same-spins correlation length $\xi_{\uparrow\uparrow}$ exhibits a similar behavior [18]. The limit of the mean pair radius is a constant determined by the density of the system [26]

$$\xi_{\rm BCS} \approx \sqrt{\frac{21}{2}}\frac{1}{k_F}. \tag{5.90}$$

This length does not agree with the behavior of the Pippard's coherence length [26]. However, we have shown that the pair wave function has a large-distance correlation length which agrees with the behavior of Pippard's coherence length [18].

On the other hand, in the BEC limit the correlation lengths decrease, in agreement with the formation of a bound state,

$$\begin{aligned} \xi_{\uparrow\downarrow} &\approx \frac{a}{\sqrt{2}}, \\ \xi_{\uparrow\uparrow} &\approx \sqrt{\frac{1}{2\pi}}\,(k_F a)^{3/2}\, a, \\ \xi_{\rm BCS} &\approx \frac{a}{\sqrt{2}}. \end{aligned} \tag{5.91}$$

The behavior of the opposite spins correlation function was expected from the gap equation, that takes the form of a Schrödinger equation of a bound state in the BEC limit, with a binding energy given by $-\hbar^2/(ma^2)$ [13]. In the same way as in 2D, the same spins correlation length $\xi_{\uparrow\uparrow}$ decreases faster, indicating the lost of the Pauli blocking effect due to molecule formation. For obtaining the asymptotic limits it is useful to factorize into terms which can be calculated when $z \to \pm 1$ and then use the fact that $|\mu/\Delta| \to \infty$ using the correct sign of the chemical potential, which is positive in the BCS limit and negative in the BEC limit.

Now that we have introduced the correlation lengths in 2D and in 3D, let us discuss the opposite spins correlation length $\xi_{\uparrow\downarrow}$ also called coherence length [143]. With the discovery of high temperature superconductors, it became important to find a way to classify them, so that from experimental observations the mechanisms that enhance superconductivity could be identified [52]. This is still an open problem which is being addressed [156, 157]. One way to obtain a higher temperature superfluid (superconductor) was identified by Nozières and Schmitt-Rink [35], who found that a stronger interaction between electrons would lead to a higher critical temperature [35, 52]. However, in general it is not possible to represent explicitly such interactions, so it was required to find a parameter that could indicate the interaction strength of the material [52]. In Ref. [52] the coherence length $\xi_{\uparrow\downarrow}$ was proposed for characterizing the interaction between fermions. Also the coherence length was proposed to unify the description of a BEC-BCS crossover in such a way that its value determines the BCS and BEC regimes in 2D and in 3D [28]. Our work determines a large-distance correlation length which has an invariant expression between the 2D and 3D cases (for contact interactions) given in equation (5.27). Then, we can contribute to the establishment of another unifying parameter between 2D and 3D, since the large-distance correlation length can be written in terms of thermodynamic quantities without denoting explicitly the spatial dimension, see equation (5.27). Instead, the integrals of the correlation lengths carry a geometric factor that

depends on the spatial dimension, see equations (5.65) and (5.85).

Lastly, the condensate fraction has been reported to be given by [121]

$$\frac{n_0}{n} = \frac{3\pi\tilde{\Delta}^{3/2}}{2^{3/2}8}\sqrt{\frac{\tilde{\mu}}{\tilde{\Delta}} + \sqrt{1+\frac{\tilde{\mu}^2}{\tilde{\Delta}^2}}}\,. \tag{5.92}$$

With the same arguments given in equation (5.72) for the 2D case we can verify the commutation relations for the bosonic-like operators $b_{\vec{0}}$ in the BEC limit, see equation (4.59). It can be shown that in the BEC limit the condensate fraction becomes a constant [121],

$$\frac{n_0}{n} \approx \frac{1}{2}. \tag{5.93}$$

Since in this limit $v_{\vec{k}}u_{\vec{k}} \approx v_{\vec{k}}/u_{\vec{k}}$ we can verify equation (4.60) and hence the bosonic-like commutation relation given in equation (4.59).

5.3 Universal behavior of density fluctuations in three dimensions

For the 3D case we will explore the large-distance behavior of the density-density correlation functions $C_{\sigma\sigma'}(r)$ and the pair wave function distribution $|\phi_{\mathrm{BCS}}(r)|^2$ for the finite-range potentials presented in equations (3.92)-(3.97) of Chapter 3. We found that their large-distance behavior is given again by an oscillatory behavior and an exponential decay, as presented in equation (5.26), which we can compare with the results obtained for the contact interaction.

One of the main motivations for exploring the cases with finite-range potentials was to test whether the relationship between the large-distance correlation length and the threshold energy required to break a pair, as given in equation (5.26), holds for finite-range interactions [19]. We have verified numerically the validity of this relation for the four finite-range potentials, which have different representative features. Then the profound implication is that this relationship is a property of the mean-field approach to the BCS Hamiltonian (4.6), and is independent on the details of the interaction (provided it is an attractive interaction). Therefore, we found a universal property of the mean-field approach. It will be interesting to explore if this behavior remains when using beyond mean-field techniques. In analogy with the behavior of the opposite spins correlation length (coherence length) $\xi_{\uparrow\downarrow}$ we believe some approaches will introduce a power law decay [8].

We should remember that when we set our model Hamiltonian, as a BCS Hamiltonian in equation (4.6) we had the hope of finding properties that do not depend strongly on the interaction details. The finding of a universal property should call our attention, since it becomes a strong property that is worth to examine if it survives corrections or generalizations. For example, including finite temperature effects (at the mean-field level there is still an exponential decay that agrees with our results for the 3D contact interaction case, see Ref. [158]), beyond mean-field terms [8], testing it in a two-channel Hamiltonian [12], or considering an unbalance between fermion components [33]. Universal properties are highly valued, since they allow us to group models that share those properties, like happened in critical phenomena, where universality classes appeared

[159, 160]. Also the finding of alternative models where a universal property breaks down allows us to enrich or change our understanding of nature.

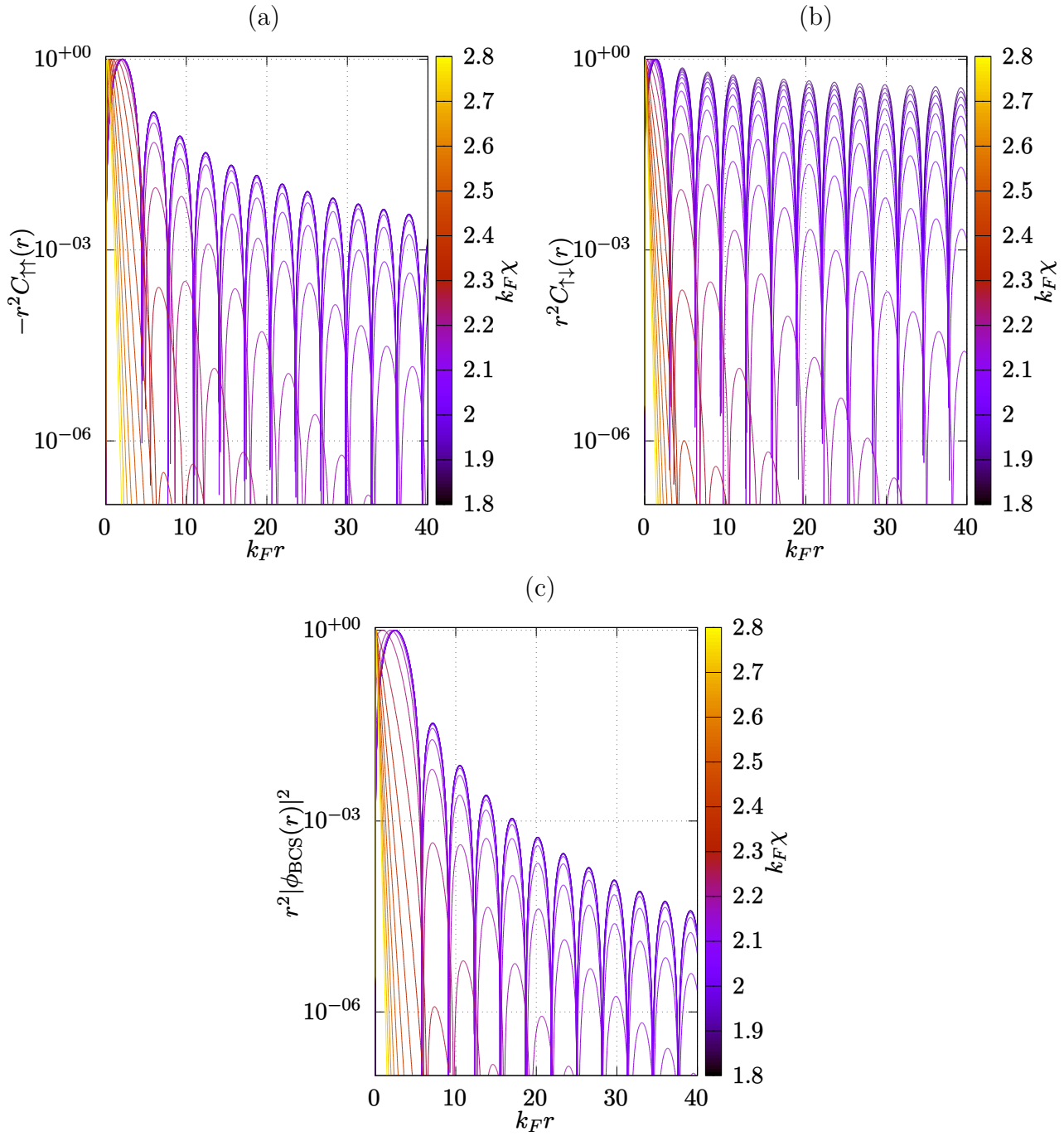

Figure 5.10: Two-body distributions for the square well potential (3.92). (a) shows the behavior of $C_{\uparrow\uparrow}(r)$, (b) the behavior of $C_{\uparrow\downarrow}(r)$ and (c) the behavior of $|\phi_{\rm BCS}(r)|^2$. All functions are arbitrarily normalized such that their maximum is equal to one. The vertical axis has a logarithmic scale. Colors or intensity correspond to different values of interaction strength $k_F\chi$. In each plot the upper curves correspond to the weakly interacting BCS limit (dark curves), and the lower curves to the strongly interacting BEC limit (yellow-light curves). These plots show an exponential decay and an oscillatory behavior [17]. The relation of $k_F\chi$ with the s-wave scattering length can be seen in Figure 3.3 (a).

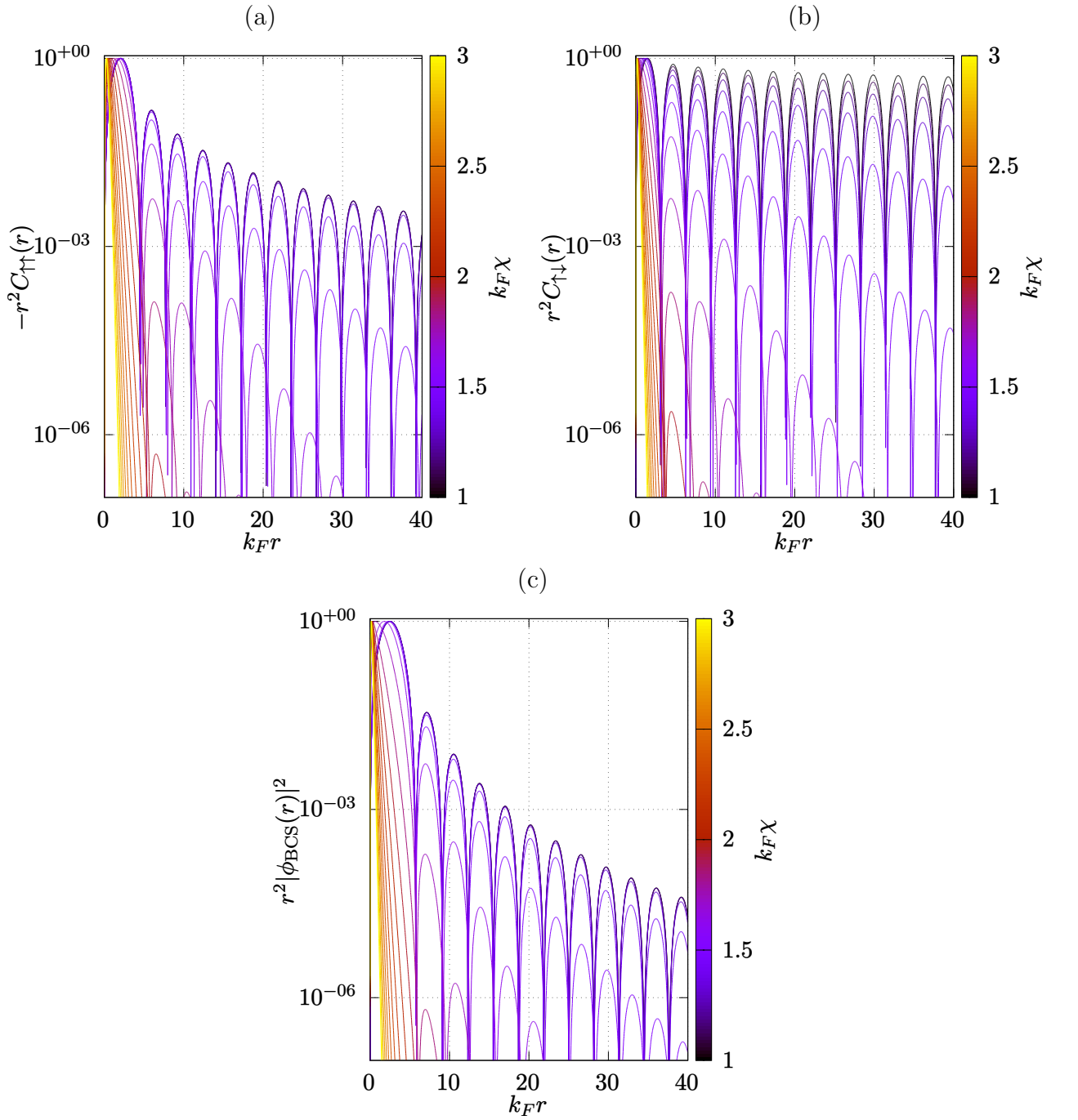

Figure 5.11: Two-body distributions for the exponential potential (3.94). (a) shows the behavior of $C_{\uparrow\uparrow}(r)$, (b) the behavior of $C_{\uparrow\downarrow}(r)$ and (c) the behavior of $|\phi_{\mathrm{BCS}}(r)|^2$. All functions are arbitrarily normalized such that their maximum is equal to one. The vertical axis has a logarithmic scale. Colors or intensity correspond to different values of interaction strength $k_F\chi$. In each plot the upper curves correspond to the weakly interacting BCS limit (dark curves), and the lower curves to the strongly interacting BEC limit (yellow-light curves). These plots show an exponential decay and an oscillatory behavior [17]. The relation of $k_F\chi$ with the s-wave scattering length can be seen in Figure 3.3 (b).

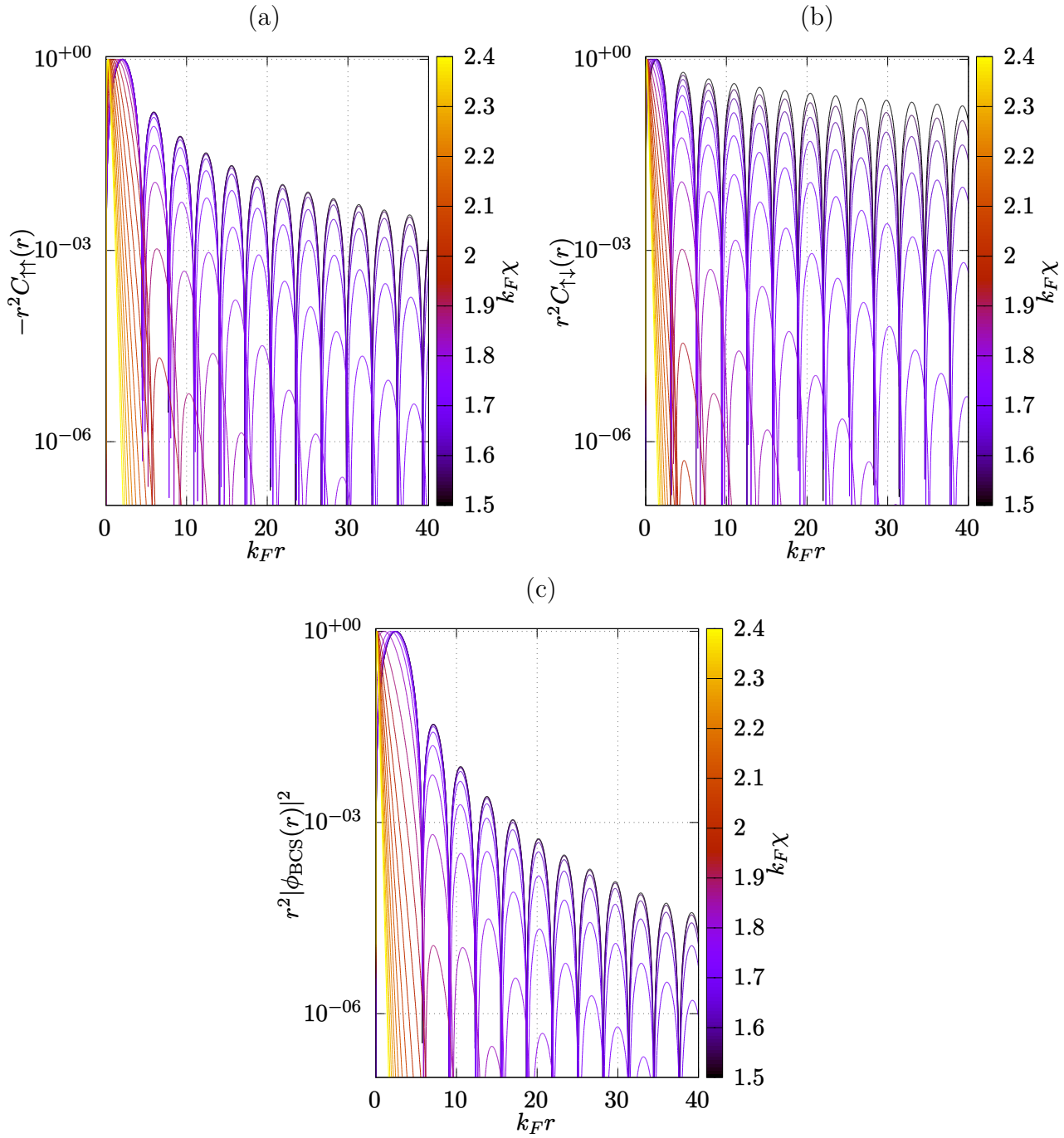

Figure 5.12: Two-body distributions for the Yukawa potential (3.96). (a) shows the behavior of $C_{\uparrow\uparrow}(r)$, (b) the behavior of $C_{\uparrow\downarrow}(r)$ and (c) the behavior of $|\phi_{\mathrm{BCS}}(r)|^2$. All functions are arbitrarily normalized such that their maximum is equal to one. The vertical axis has a logarithmic scale. Colors or intensity correspond to different values of interaction strength $k_F\chi$. In each plot the upper curves correspond to the weakly interacting BCS limit (dark curves), and the lower curves to the strongly interacting BEC limit (yellow-light curves). These plots show an exponential decay and an oscillatory behavior [17]. The relation of $k_F\chi$ with the s-wave scattering length can be seen in Figure 3.3 (c).

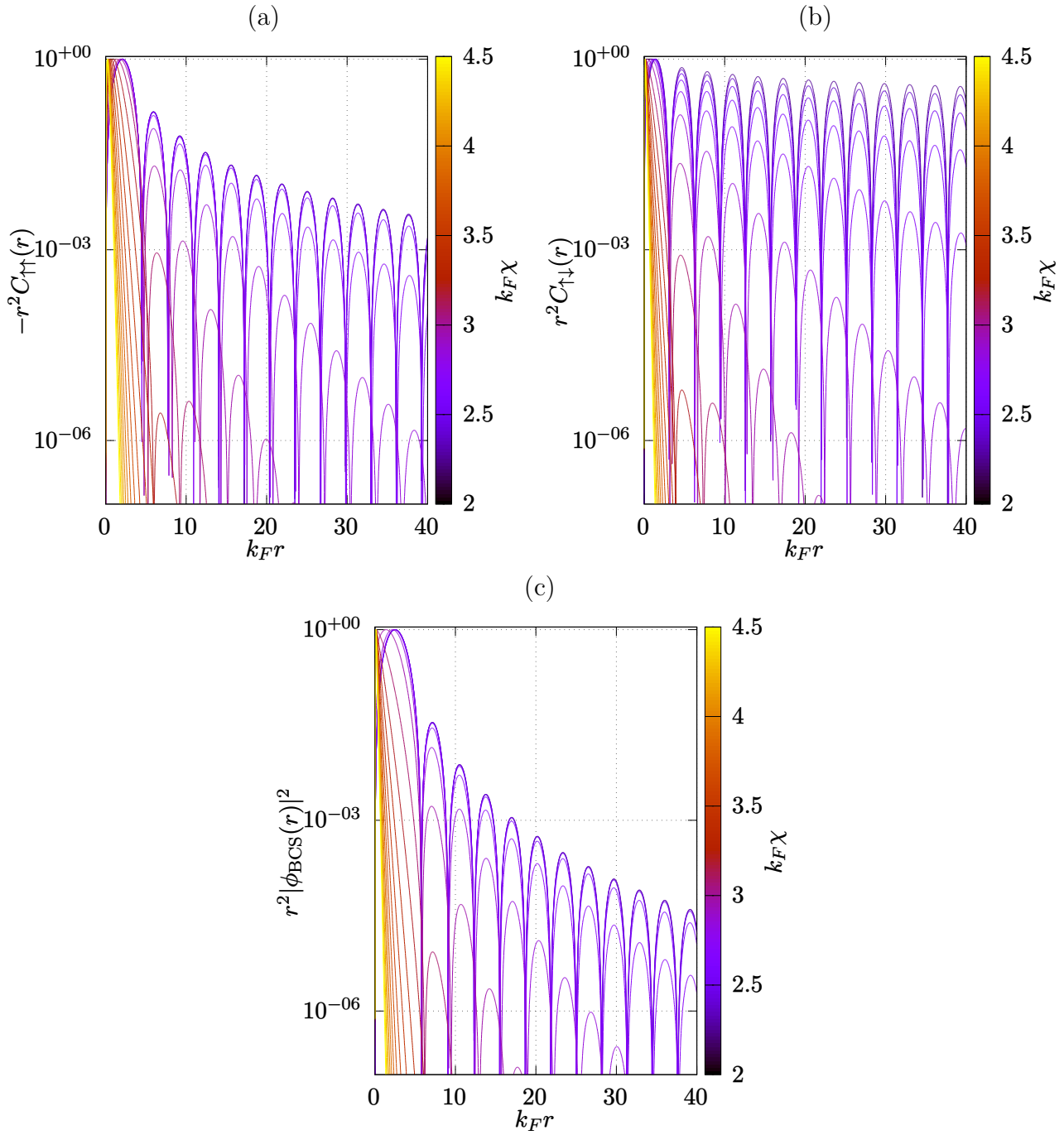

Figure 5.13: Two-body distributions for the Van der Waals type potential (3.97). (a) shows the behavior of $C_{\uparrow\uparrow}(r)$, (b) the behavior of $C_{\uparrow\downarrow}(r)$ and (c) the behavior of $|\phi_{\rm BCS}(r)|^2$. All functions are arbitrarily normalized such that their maximum is equal to one. The vertical axis has a logarithmic scale. Colors or intensity correspond to different values of interaction strength $k_F\chi$. In each plot the upper curves correspond to the weakly interacting BCS limit (dark curves), and the lower curves to the strongly interacting BEC limit (yellow-light curves). These plots show an exponential decay and an oscillatory behavior [17]. The relation of $k_F\chi$ with the s-wave scattering length can be seen in Figure 3.3 (d).

From Figure 5.10 to Figure 5.13 we can see the behaviors of the density-density correlation functions $C_{\sigma\sigma'}(r)$ and the pair wave function $|\phi_{\rm BCS}(r)|^2$ for each finite-range potential. These numerical calculations were performed with a basic numerical integration method such as the trapezoidal rule [102]. We can see the oscillatory behavior and an exponential decay for the majority of the functions, given that the envelopes form straight lines with a rapid decay as we increase the distance $k_F r$. From Figure 5.10 to Figure 5.13 the three upper curves are not in an interval where they exhibit an exponential decay. That is why those curves of $r^2 C_{\uparrow\downarrow}(r)$ seem to decay slower than the other functions. For the deep BCS limit we had to use a different interval of $k_F r \in [200, 300]$ to find the exponential decay, although this was done with less numerical accuracy.

The calculation of the large-distance correlation lengths involve some simple steps, although these calculations take a long time. The local maximums of $\ln(|r^2\rho_\alpha(r)|)$ were extracted for $\rho_\alpha(r) = C_{\uparrow\uparrow}(r),\ C_{\uparrow\downarrow}(r),\ |\phi_{\rm BCS}(r)|^2$. Then, using those points we fitted a function of the form

$$f(k_F r) = m(k_F r) + b. \tag{5.94}$$

The slope m gives us the large-distance correlation length in the following way:

$$m = -\frac{2}{k_F \chi_\alpha}, \tag{5.95}$$

where the subindex α is for different two-body distributions $\alpha = \uparrow\uparrow,\ \uparrow\downarrow,$ BCS. In Figure 5.14 we show the large-distance correlation lengths calculated numerically, as reported in [19]. It is to be noted that there is a good agreement between numerical fits (squares, triangles and asterisks) and the length associated to the threshold energy required to break a pair $\chi_{\rm spec}$ (solid line), given in equation (5.27).

Qualitatively, the large-distance correlation lengths show the same behaviors (for finite-range interactions and contact interaction). Particularly, in Figure 5.14 (a) we find almost an overlap between the large-distance correlation length of the contact interaction and the one of the square well. This could have been expected, since the renormalization process aims to recover the behavior of potentials such as the square well [13, 105]. The large-distance correlation lengths of the exponential potential (b) and Yukawa potential (c) exhibit their own behavior, with much similarities to the contact interaction. Differently, the case of the Van der Waals type potential has a large-distance correlation length smaller than the contact interaction case. This might be a good indicator, since it tells us that the power law decay of a potential does not affect drastically the range of density correlations, in comparison with the contact interaction. However, this is a tentative conclusion which requires further analysis to ensure its validity. We have shown calculations for a fixed range $k_F R_0 = 0.1$, which is a very high value for experimental situations[9]. When decreasing this range we expect to recover the contact interaction case, so at the moment we believe these calculations show an enhanced effect of finite-range interactions over the large-distance behavior.

[9] An estimate of the order of magnitude can be obtained by using a density $n \approx 10^{12}\text{cm}^{-3}$ [137] and an atomic range of $R_0 = 5.3 \times 10^{-7}$ cm [105], which gives $k_F R_0 \approx 0.016$.

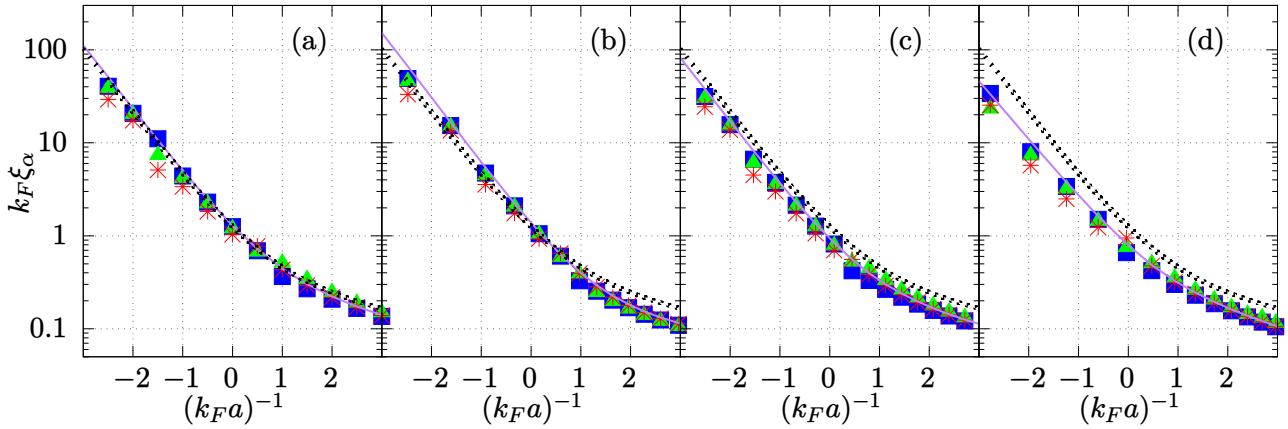

Figure 5.14: Large-distance correlation lengths $\xi_\alpha = \chi_\alpha/2$ as functions of the scattering length a for different interaction potentials: (a) square well, (b) exponential potential, (c) Yukawa potential, and (d) Van der Waals type potential. Lengths are scaled with the Fermi wave number k_F. Numerical calculations are shown with squares (blue) for the opposite spins correlation function $C_{\uparrow\downarrow}(r)$, triangles (green) for the same spins correlation function $C_{\uparrow\uparrow}(r)$, and asterisks (red) for the pair wave function $|\phi_{\mathrm{BCS}}(r)|^2$. It is found an overlap with the length associated to the threshold energy required to break a pair $\xi_{\mathrm{spec}} = \chi_{\mathrm{spec}}/2$ (solid line). For comparison in each panel we show the large-distance correlation length of the contact interaction with dotted lines. Hence, this Figure verifies the exponential decay given in equation (5.26). This Figure was taken from [19].

The oscillatory behavior was also characterized numerically. We calculated the wave vectors κ_α for each distribution using the separation between nodes in the plots shown from Figure 5.10 to Figure 5.13. The wave vectors turned out to behave similarly to the contact interaction case, but we were not able to characterize the difference in the deep BEC limit due to numerical difficulties. The wave vectors are shown in Figure 5.15.

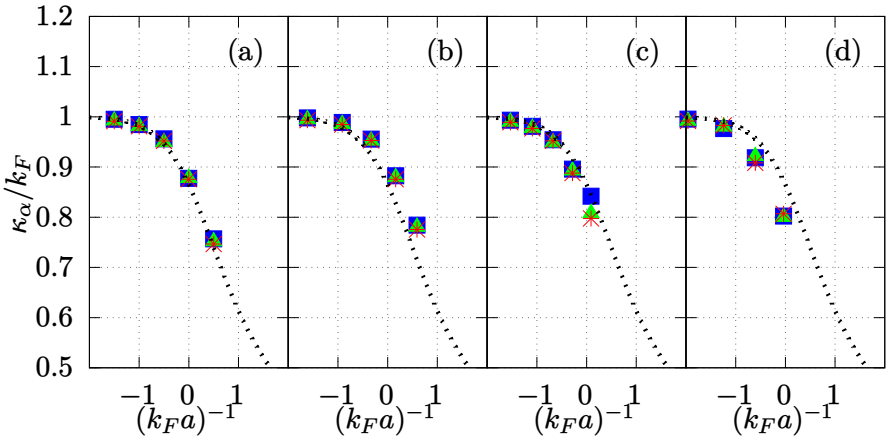

Figure 5.15: Large-distance wave vectors κ_α as functions of the scattering length a for different interaction potentials: (a) square well, (b) exponential potential, (c) Yukawa potential, and (d) Van der Waals type potential. We have used the Fermi wave number k_F to scale variables. Numerical calculations are shown with squares (blue) for the opposite spins correlation function $C_{\uparrow\downarrow}(r)$, triangles (green) for the same spins correlation function $C_{\uparrow\uparrow}(r)$, and asterisks (red) for the pair wave function $|\phi_{\mathrm{BCS}}(r)|^2$. The dotted lines correspond to the contact interaction case, shown in Figure 5.8. This Figure was taken from [19].

Chapter 6

Conclusions and perspectives

We have analyzed the large-distance behavior of the density-density correlation functions $C_{\uparrow\uparrow}(r)$, $C_{\uparrow\downarrow}(r)$ and the pair wave function $|\phi_{\mathrm{BCS}}(r)|^2$ of the BEC-BCS crossover of a homogeneous Fermi gas of two components, in the balanced case. We addressed the two-dimensional (2D) case with a contact interaction [17], the three-dimensional (3D) case with a contact interaction [18], and the 3D case with finite-range interactions [19]. In those three cases we found that at large distances the functions exhibit an oscillatory behavior and an exponential decay [17, 18, 19], given in equation (5.26). Mainly, one of our findings was that the exponential decays χ_{spec} are determined by a many-body binding energy $\varepsilon_{\mathrm{spec}}$, for which we found a general expression given in equation (4.74)

$$\varepsilon_{\mathrm{spec}} = \sqrt{\mu^2 + \Delta_0^2} - \mu, \tag{6.1}$$

where Δ_0 is the value of the gap at zero wave vector. Hence, we found $\chi_{\mathrm{spec}} = \hbar/(m\varepsilon_{\mathrm{spec}})^{1/2}$, with m the mass of a fermion.

Notably, for the 3D cases, we determined that the relationship between the large-distance exponential decay and the many-body binding energy $\varepsilon_{\mathrm{spec}}$ is universal within the mean-field approach, since it holds for different finite-range potentials, although the numerical values are different for each potential, as shown in Figure 5.14. The universal character should call our attention, since it might offer a property that joins different models, as in critical phenomena, where distinct models belong to a universality class [159]. Also it should be interesting to explore conditions that break this universal property, or to explore how robust is this property. We have also determined that the relation between the large-distance exponential decay χ_{spec} and the binding energy $\varepsilon_{\mathrm{spec}}$ is invariant between 2D and 3D for the contact interaction. It might be interesting to explore this relation in other types of geometry, like one dimension [161] or quasi-2D [30].

The other main contribution was the characterization of the large-distance oscillatory wave vectors of equation (5.26). We were not able to relate them to another physical quantity, as happened between the exponential decay and the binding energy, but we believe the oscillations might be related to the many-body distribution in wave vector space. However, a relation between the wave vectors and the presence of a Fermi surface in the BCS limit was already established in Ref. [29]. Also it might be interesting to explore a possible relationship with Friedel's oscillations that emerge when an impurity is placed in a superfluid of the BCS type [158, 162].

The ability to study the large-distance behavior in the 2D case allowed us to find analytical expressions for the density-density correlation functions $C_{\sigma\sigma'}(r)$, given in equations (5.51) and

(5.52). Although they belong to the mean-field approach, these analytical expressions give a wide view of the spatial structure throughout the crossover. As we have shown, they exhibit the relation between the short distance behavior and Tan's contact, see equations (5.54) and (5.55). They show the evolution of the Pauli blocking effect. They allowed us to calculate the condensate fraction, shown in equation (5.73), and they allowed us to exhibit the failure of the BCS approach in fulfilling the relation between the isothermal compressibility and the integrals of density-density correlation functions in the zero temperature case, see equation (5.39).

Let us comment on the exponential decay at large distances. The density-density correlation functions $C_{\sigma\sigma'}(r)$ carry information about the local density fluctuations separated by a distance r, see equation (5.15). Then we have addressed the problem of determining characteristic sizes of density fluctuations. Our general approach also addresses, as a particular case, the size of the pairs that become Cooper pairs on the BCS side or molecules on the BEC side, since the opposite spins correlation function $C_{\uparrow\downarrow}(r)$ determines them. Previous work had only been able to estimate the opposite spin pair sizes in the deep BCS limit [15, 25, 143] or in the deep BEC limit [9, 13]. It is important to mention that an experimental system that exhibits the physical properties associated to the homogeneous BEC-BCS crossover requires to have a minimum size given by the large-distance correlation length $(\chi_{\text{spec}}/2)^D$, see equations (5.26) and (5.27). Remarkably, on the BCS side these sizes are very large [18], which corresponds to a highly correlated system. Insted in the BEC limit the large-distance correlation lengths decrease, indicating a low correlated system.

Part of the initial motivation for finding the large-distance exponential decay rests in the search for a description of the normal to superfluid transition. This transition has been identified as belonging to the XY-universality class within the renormalization group formalism [163]. However, we believe that sometimes it is not quite clear how to chose the order parameters to describe adequately the phase transitions. An important example has been shown by Ignacio Reyes Ayala, Jackson Poveda Cuevas and Víctor Romero Rochín in Ref. [164, 165], where they found that the ideal Bose-Einstein condensation has critical exponents of a different universality class than the accepted one (spherical model) [116, 166], exhibiting the importance of extracting the order parameter from thermodynamic variables, and establishing a different approach to critical phenomena[1]. Focusing on the BEC-BCS crossover, we thought that the isothermal compressibility could diverge at the critical temperature, as it happens in the normal to superfluid transition in helium-4 [168]. Some theoretical models predicted a divergence of the isothermal compressibility [169], where the large-distance correlation length would exhibit a behavior of the critical phenomena, giving a critical exponent [170]. However, experimental data suggested that the isothermal compressibility remains finite at the normal-superfluid phase transition of the BEC-BCS crossover [171]. Recently, other models have predicted a non-divergent behavior of the isothermal compressibility [172, 173], ruling out the critical exponent in the large-distance correlation length. Nevertheless, the finding of a large-distance exponential has become an interesting feature. For example the large-distance correlation length has been analyzed for small temperatures in the 3D case with a contact interaction for the opposite spins correlation function [158], finding a good agreement with the work presented here.

[1]Following the aforementioned work, we have made an exploration of the critical phenomena of the liquid-vapor critical point, where we found conditions that lead to the scaling behavior of the entropy, and therefore to the manifestation of critical phenomena [167].

Let us give some comments about the information contained in the correlation length defined as a second moment, see equations (5.65) and (5.85). The integral that defines the correlation lengths averages over all distances, particularly the short distance regime, which is a regime that we should avoid by hypotheses because we are neglecting the details of the interaction considering a dilute gas. However, the short-distance contribution is small, allowing to adequately condense information of the spatial structure in the correlation lengths. Then we find a qualitative similarity between the large-distance correlation length and the correlation length for the opposite spins. However, the averaging at short distances makes difference between both lengths for the pair wave function and the same spins correlation function, as can be seen in Figures 5.5 and 5.9, panels (a) and (c).

Let us remark some differences between the 2D case and the 3D case, since we have exploited the similarities that arise in the mean-field approach. The first ones are about the Cooper instability, two fermions interacting in the presence of a fixed Fermi sea can form a bound state. In 2D a necessary and sufficient condition is the existence of a bound state in the two-body interaction potential [16]. Instead in 3D an attractive interaction without a bound state is enough to show the instability [174]. The definition of a s-wave scattering length is quite different between both dimensions. Although in 2D there exist scattering resonances, they do not mark an important point in the crossover region [20]. In contrast, for the 3D case, the scattering resonance defines the unitarity, an important point of the crossover [69]. Other aspect related to the definitions of the scattering lengths is the fact that the (non-physical) coupling constant that precedes the Dirac delta of the contact interaction is unable to introduce a length in 2D, leading to the natural appearance of a logarithm $\ln(a_{2\mathrm{D}})$. Another difference is that in 2D beyond mean-field terms are necessary for describing the presence of superfluidity by means of the Berezinskii–Kosterlitz–Thouless mechanism [175]. Also we expect a drastic change in the 2D case when describing finite temperature properties, since the BCS-Leggett approach describes a Bose-Einstein condensate at zero temperature, but in 2D the condensate can not be reached at finite temperatures. However, it might be interesting to analyze the quasi-2D case to find if the large-distance behaviors persist when approaching a 2D confinement [30]. A great difference arose in the large-distance oscillatory behavior. In 2D the wave vectors that characterize the oscillations are constant throughout the crossover, while in 3D they decrease as we move from the BCS side to the BEC side. We believe the constant behavior is a property of the contact interaction in 2D, but further calculations are required to arrive to a conclusion.

The great variety of physical phenomena that arises in many-body systems allows for a natural continuation of the work presented here. As we have mentioned, the quest to find clear signatures of the Fulde-Ferrell-Larkin-Ovchinnikov phase in ultracold gases [176] and superconductors [177] is still of interest. We believe the theoretical characterization of sizes of density fluctuations will provide a necessary condition to observe this exotic phase. We have some preliminary results in addressing the unbalanced Sarma state [33, 44], where we believe there is a competition between paired fermions and unpaired fermions. Paired fermions might give an exponential decay, but the unpaired fermions might give a power law decay, thus giving a highly correlated system (like in the BCS limit of the cases presented here). For the unbalanced case it will be useful to consider the correlation length, given as a second moment, to characterize density fluctuations. There are quantum critical points in the unbalanced case, where it might be worth analyzing the large-

distance behavior of the density-density correlation functions [33]. Also, even if it is not directly related to critical phenomena, it is interesting to address the large-distance behavior near the normal to superfluid phase transition. For the 2D case it is necessary to consider beyond mean-field corrections to describe the presence of a superfluid by means of a Berezinskii–Kosterlitz–Thouless mechanism [175, 178, 179]. Then it might be interesting to compare the behavior of density-density correlation functions and phase-phase correlation functions[2], which exhibit the transition from an exponential decay to an algebraic decay when decreasing the temperature below the transition temperature T_{BKT}. Another important aspect that should be analyzed is the relationship between the integrals of density-density correlation functions and the isothermal compressibility at zero temperature [135], shown in equations (5.20) and (5.39). The failure to fulfill this relation can be regarded as a deviation from the real ground state. Then, a further analysis of this relation might give a clue for including beyond mean-field corrections that allow for a better description of the ground state. Also, it might be interesting the analysis of density-density correlation functions in inhomogeneous systems, which describe more adequately the experimental situations in ultracold gases and superconductors [34, 181]. The large-distance correlation length between opposite spins (in 3D for a contact interaction) has been addressed in Ref. [158] for small finite temperature within the mean-field approach, where they recover the behavior reported here. It remains to see how beyond mean-field approximations modify the large-distance behavior [158]. Other prospective is the consideration of a more general Hamiltonian, see equation (4.1), it might exhibit different large-distance behaviors and it might fulfill the relationship between the isothermal compressibility and the integrals of density-density correlation functions (5.19). Also, we might think about a way of removing the condensate fraction from the calculation of particle number fluctuations[3]. It might be interesting to study density-density correlation functions considering p-wave pairing [16]. Also, we might explore the BEC-BCS crossover in nuclear matter [8]. Recently multiband models are being explored [54, 55], so it might be interesting to analyze their spatial structure.

[2]Experimental measurements of density-density correlation functions of opposite spins have been performed [180], but further improvements might be achieved in the future.

[3]Thanks to Santiago Francisco Caballero Benítez for this suggestion.

Appendix A

Atomic scattering at low energies

This is the appendix of Chapter 3. We calculate an approximate expression for the absolute value of the s-wave bound state energy of a circular potential (2D).

A.1 Bound state of the circular potential

In this section we will follow the notation and conventions defined in subsection 3.2.1.

The circular potential is defined by:

$$U(r) = \begin{cases} -U_0 & \text{si } r \leq r_0 \text{ (region } I\text{)}, \\ 0 & \text{si } r > r_0 \text{ (region } II\text{)}, \end{cases} \tag{A.1}$$

where $r_0 > 0$ is the radius of the potential, shown in the inset of Figure 3.2.

The radial equation in region I is

$$r^2 \frac{d^2R}{dr^2} + r\frac{dR}{dr} + \left[\frac{2m_r}{\hbar^2}(E_{\text{bound}} + U_0)r^2 - l^2\right]R = 0, \tag{A.2}$$

where $E_{\text{bound}} + U_0 > 0$. Then we can define

$$\kappa^2 = \frac{2m_r}{\hbar^2}(E_{\text{bound}} + U_0) \geq 0. \tag{A.3}$$

Let us comment on the solutions of the Bessel differential equation. When l is a semi-integer it is enough to consider both Bessel functions: $J_l(\kappa r)$ y $J_{-l}(\kappa r)$, as linearly independent solutions. When $\kappa \geq 0$, and l is an integer, we have $J_l(\kappa r) = (-1)^l J_{-l}(\kappa r)$, so we need to consider another linearly independent solution. In this case we use Neumann functions $N_l(\kappa r)$ defined by

$$N_l(x) = \begin{cases} \dfrac{\cos(l\pi)J_l(x) - J_{-l}(x)}{\text{sen}(l\pi)} & \text{si } l \notin \mathbb{Z}, \\ \\ \lim\limits_{\beta \to l} \dfrac{\cos(\beta\pi)J_\beta(x) - J_{-\beta}(x)}{\text{sen}(\beta\pi)} & \text{si } l \in \mathbb{Z}. \end{cases} \tag{A.4}$$

Going back to the radial equation, we have $l = 0, 1, 2, \ldots$ since the angular part must be single valued, which restricts the values of l. The Neumann function of order zero has a logarithmic

divergence at zero, so that it is not square integrable. That is, for small arguments we have [88]

$$N_0(x) = \frac{2}{\pi}(\ln(x) + \gamma - \ln(2)) + O(x^2), \tag{A.5}$$

where $\gamma \approx 0.5772$ is the Euler-Mascheroni constant. Then we can conclude that the solution if region I is

$$R_I(\kappa r) = AJ_l(\kappa r). \tag{A.6}$$

Instead, outside of the potential, in region II we have

$$r^2\frac{d^2R}{dr^2} + r\frac{dR}{dr} + \left[\frac{2m_r}{\hbar^2}E_b r^2 - l^2\right]R = 0. \tag{A.7}$$

In this case, by analogy with the spherical well (in 3D) the solution is given by Hankel functions of the first kind

$$R_{II}(kr) = H_l^{(1)}(ikr), \tag{A.8}$$

where we have defined

$$k = \frac{\sqrt{2m_r|E_{\text{bound}}|}}{\hbar}. \tag{A.9}$$

Then, the boundary conditions (continuity of the wave function and its derivatives) give us

$$\frac{A\kappa J_l'(\kappa r_0)}{AJ_l(\kappa r_0)} = \frac{ikB\frac{d}{dx}H_l^{(1)}(x)|_{x=ikr_0}}{BH_l^{(1)}(ikr_0)}. \tag{A.10}$$

Writing explicitly the parameters of the potential and the energy we have

$$\frac{r_0\frac{\sqrt{2m_r(E_b+U_0)}}{\hbar}J_l'\left(\frac{\sqrt{2m_r(E_{\text{bound}}+U_0)}}{\hbar}r_0\right)}{J_l\left(\frac{\sqrt{2m_r(E_{\text{bound}}+U_0)}}{\hbar}r_0\right)} = \frac{ir_0\frac{\sqrt{2m_r|E_{\text{bound}}|}}{\hbar}DH_l^{(1)}\left(ir_0\frac{\sqrt{2m_r|E_{\text{bound}}|}}{\hbar}\right)}{H_l^{(1)}\left(ir_0\frac{\sqrt{2m_r|E_{\text{bound}}|}}{\hbar}\right)}, \tag{A.11}$$

where $DH_l^{(1)}$ is the first derivative. We can define

$$E'_{\text{bound}} = \frac{2m_rE_{\text{bound}}}{\hbar^2}r_0^2 < 0 \tag{A.12}$$

and

$$U'_0 = \frac{2m_rU_0}{\hbar^2}r_0^2 > 0. \tag{A.13}$$

Hence we need to solve numerically

$$\frac{\sqrt{E'_{\text{bound}}+U'_0}\,J_l'(\sqrt{E'_{\text{bound}}+U'_0})}{J_l(\sqrt{E'_{\text{bound}}+U'_0})} = \frac{i\sqrt{|E'_{\text{bound}}|}\,DH_l^{(1)}(i\sqrt{|E'_{\text{bound}}|})}{H_l^{(1)}(i\sqrt{|E'_{\text{bound}}|})}. \tag{A.14}$$

To obtain E_{bound} shown in Figure 3.2 we used Mathematica [122].

Analytical approximation

We will consider the case when $E'_{\text{bound}} \to 0^-$ en la ecuación (A.14) to find an approximate expression for the bound state energy in the case of shallow potentials.

The boundary condition for the bound state problem, given in equation (A.11) is

$$\frac{\kappa r_0 R'_I(\kappa r_0)}{R_I(\kappa r_0)} = \frac{k r_0 R'_{II}(k r_0)}{R_{II}(k r_0)}. \tag{A.15}$$

In analogy to the scattering problem at low energies, where we were using $E \to 0^+$ [or $E \to V(\infty)$], we can define

$$\alpha^- = \frac{\kappa r_0 R'_I(\kappa r_0)}{R_I(\kappa r_0)}. \tag{A.16}$$

This constant α^- will carry the information of the structure inside the potential (region I). Then we have the condition

$$\alpha^- = \frac{i\sqrt{|E'_{\text{bound}}|}\, DH_l^{(1)}(i\sqrt{|E'_{\text{bound}}|})}{H_l^{(1)}(i\sqrt{|E'_{\text{bound}}|})}. \tag{A.17}$$

When considering $E'_{\text{bound}} \to 0^-$, the right hand side the dominant term has a divergent behavior given by

$$\frac{i\sqrt{|E'_{\text{bound}}|}\, DH_l^{(1)}(i\sqrt{|E'_{\text{bound}}|})}{H_l^{(1)}(i\sqrt{|E'_{\text{bound}}|})} = \frac{2}{2\gamma - 2\ln(2) + \ln(|E'_{\text{bound}}|)} + O(|E'_{\text{bound}}|). \tag{A.18}$$

It can be noticed that this is a general condition, that does not show the explicit structure of the potential in region I, although the information is contained in the constant α^-. Then, for shallow potentials we have

$$\alpha_{0^-} \approx \frac{2}{2\gamma - 2\ln(2) + \ln(|E'_{\text{bound}}|)}. \tag{A.19}$$

Rearranging the equation we have

$$2\gamma + \ln(|E'_{\text{bound}}|/4) = \frac{2}{\alpha_{0^-}}, \tag{A.20}$$

so that

$$|E'_{\text{bound}}| = 4\exp\left(\frac{2}{\alpha_{0^-}} - 2\gamma\right). \tag{A.21}$$

Going back to the definitions, we had $|E'_{\text{bound}}| = (kr_0)^2 = |E_{\text{bound}}|/\varepsilon_0$, where $\varepsilon_0 = \hbar^2/(2m_r r_0^2)$. Hence, the s-wave bound state energy for shallow potentials is

$$|E_{\text{bound}}| = 4\varepsilon_0\exp\left(\frac{2}{\alpha_{0^-}} - 2\gamma\right). \tag{A.22}$$

We can notice the similarity with E_a given in equation (3.62). However the difference is in the constant that contains the information of the boundaries α. As shown in Figure 3.2, the approximation $E_a = |E_{\text{bound}}|$ is valid for shallow potentials.

Appendix B

BEC-BCS crossover of ultracold Fermi gases

This is the appendix of Chapter 4. In section B.1 we give the details for calculating the gran potential energy in 2D. Also, in section B.2 we give the integral identities for handling integrals that appear in the 3D case with contact interaction.

B.1 Grand potential in 2D

Here we will show explicitly the calculation of the gran potential energy Ω_0 for the ground state in 2D, using the contact interaction. We start from the expression:

$$\frac{\Omega_0}{L^2} = \frac{1}{(2\pi)^2}\int d^2k\left(\varepsilon - \mu - \frac{(\varepsilon-\mu)^2}{\sqrt{(\varepsilon-\mu)^2+\Delta^2}} - \frac{\Delta^2}{2\sqrt{(\varepsilon-\mu)^2+\Delta^2}}\right) \tag{B.1}$$

Changing to polar coordinates and integrating the angular variable we obtain

$$\frac{\Omega_0}{L^2} = \frac{1}{2\pi}\int dk\, k\left(\varepsilon - \mu - \frac{(\varepsilon-\mu)^2}{\sqrt{(\varepsilon-\mu)^2+\Delta^2}} - \frac{\Delta^2}{2\sqrt{(\varepsilon-\mu)^2+\Delta^2}}\right) \tag{B.2}$$

We can scale the grand potential with the gap, provided that it is not zero, and make a change of variable to $y = \varepsilon/\Delta$, with $k_\Delta = (2m\Delta)^{1/2}/\hbar$, to get

$$\frac{\Omega_0}{\Delta L^2} = \frac{k_\Delta^2}{2\pi}\int_0^\infty \frac{dy}{2}\left(y - \mu_\Delta - \frac{(y-\mu_\Delta)^2}{\sqrt{(y-\mu_\Delta)^2+1}} - \frac{1}{2\sqrt{(y-\mu_\Delta)^2+1}}\right). \tag{B.3}$$

Then we can make another change of variables $z = y - \mu_\Delta$ to get

$$\frac{\Omega_0}{\Delta L^2} = \frac{k_\Delta^2}{2\pi}\int_{\mu_\Delta}^\infty \frac{dz}{2}\left(z - \frac{z^2}{\sqrt{z^2+1}} - \frac{1}{2\sqrt{z^2+1}}\right). \tag{B.4}$$

Each term can be integrated separately,

$$\begin{aligned}\frac{\Omega_0}{\Delta L^2} &= \frac{k_\Delta^2}{2(2\pi)}\left[\frac{z^2}{2} - \frac{1}{2}\left(z\sqrt{z^2+1} - \operatorname{arcsinh}(z)\right) - \frac{1}{2}\operatorname{arcsinh}(z)\right]_{\mu_\Delta}^\infty \\ &= \frac{k_\Delta^2}{4(2\pi)}\left[z^2 - z\sqrt{z^2+1}\right]_{\mu_\Delta}^\infty,\end{aligned} \tag{B.5}$$

where in the last equation we canceled the arcsinh(z). To evaluate the upper limit of the integral we need to use L'Hôpital's rule,

$$\lim_{z\to\infty} z^2\left(1-\frac{\sqrt{z^2+1}}{z}\right) = \lim_{z\to\infty}\frac{\left(1-\frac{\sqrt{z^2+1}}{z}\right)}{1/z^2} = \lim_{z\to\infty}\frac{-\left(\frac{z^2}{\sqrt{z^2+1}}-\sqrt{z^2+1}\right)}{z^2}}{-2z^{-3}} \\ = \lim_{z\to\infty}\left(\frac{z^2}{\sqrt{z^2+1}}-\sqrt{z^2+1}\right)\frac{z}{2} = \lim_{z\to\infty}\left(\frac{-1}{\sqrt{z^2+1}}\right)\frac{z}{2} = -\frac{1}{2} \tag{B.6}$$

where in the last equality we identified a well-known limit (also obtained from L'Hôpital's rule). The calculation of this limit allows us to perform the integral without using the renormalization procedure. Therefore, we have

$$\frac{\Omega_0}{\Delta L^2} = \frac{k_\Delta^2}{4(2\pi)}\left[-\frac{1}{2}-\left(\mu_\Delta^2-\mu_\Delta\sqrt{\mu_\Delta^2+1}\right)\right] \tag{B.7}$$

We can now multiply by Δ and substitute $k_\Delta = (2m\Delta)^{1/2}/\hbar$ to obtain equation (4.92).

B.2 Integral identities

In several calculation we find the following integral:

$$\int_0^\infty \frac{\kappa^\lambda}{[(\kappa^2-\tilde{\mu})^2+\tilde{\Delta}^2]^\beta}\,d\kappa. \tag{B.8}$$

By means of a change of variable we obtain

$$\int_0^\infty \frac{\kappa^\lambda}{[(\kappa^2-\tilde{\mu})^2+\tilde{\Delta}^2]^\beta}\,d\kappa = \frac{(\tilde{\mu}^2+\tilde{\Delta}^2)^{\lambda/4+1/4-\beta}}{2}\int_0^\infty \frac{x^{\lambda/2-1/2}}{[x^2+2zx+1]^\beta}dx, \tag{B.9}$$

where $z = -\tilde{\mu}/\sqrt{\tilde{\mu}^2+\tilde{\Delta}^2}$ and we have made the change of variable $\kappa = (\tilde{\mu}^2+\tilde{\Delta}^2)^{1/4}x^{1/2}$. Hence, we are interested in calculating

$$I(\alpha,\beta,z) = \int_0^\infty \frac{x^\alpha}{(x^2+2xz+1)^\beta}dx, \tag{B.10}$$

where $\alpha = \lambda/2-1/2$. Analyzing the dominant terms of the integrand, we can see that the integral converges when

$$\alpha - 2\beta + 1 < 0, \tag{B.11}$$

which corresponds to the power of the dominant term when $x\to\infty$. In the limit $x\to 0$ the integrand is well behaved. However, in some cases we have

$$\alpha - 2\beta + 1 \geq 0 \tag{B.12}$$

so that the integral diverges. Nevertheless, we can separate those divergent terms allowing us to join them with others so as to obtain well defined physical quantities. For this, we have to note that there exists a positive integer $n_0 \geq 1$, such that

$$n_0 > \alpha - 2\beta + 1 > n_0 - 1, \tag{B.13}$$

when α and β are of the form

$$\alpha = \frac{1}{2}, \frac{3}{2}, \cdots = \frac{2m+1}{2} \tag{B.14}$$

$$\beta = \frac{1}{2}, 1, \frac{3}{2}, 2, \cdots = \frac{l}{2}. \tag{B.15}$$

Hence, equation (B.10) can be written in the following way:

$$I(\alpha,\beta,z) = \int_0^\infty \frac{x^\alpha}{(1+x)^{2\beta}} \left(1 - \frac{2(1-z)x}{(1+x)^2}\right)^{-\beta} dx. \tag{B.16}$$

Noticing that $x/(1+x)^2 < 1$ and that

$$\lim_{x\to 0} \frac{x}{(1+x)^2} \to 0, \tag{B.17}$$

$$\lim_{x\to \infty} \frac{x}{(1+x)^2} \to 0, \tag{B.18}$$

we can introduce a series expansion in equation (B.16),

$$(1-y)^{-\beta} = \sum_{n=0}^{\infty} \frac{(\beta)_n}{n!} y^n, \tag{B.19}$$

where $(\beta)_n$ is the Pochamer symbol, such that $(\beta)_0 = 1$. Integrating each term of the series we obtain

$$\begin{aligned} I(\alpha,\beta,z) &= \sum_{n=0}^{n_0-1} \frac{(\beta)_n}{n!} 2^n (1-z)^n \int_0^\infty \frac{x^{\alpha+n}}{(1+x)^{2n+2\beta}} dx + \\ &+ \sum_{n=n_0}^{\infty} \frac{(\beta)_n}{n!} 2^n (1-z)^n \int_0^\infty \frac{x^{\alpha+n}}{(1+x)^{2n+2\beta}} dx, \end{aligned} \tag{B.20}$$

where we have performed an explicit division between the divergent terms, which are the ones of the first sum, and the convergent one, which are in the second sum. In this last sum we can identify the definition of the Beta function $\mathrm{B}(\mathrm{p},\mathrm{q})$ defined as

$$\mathrm{B}(p,q) = \int_0^\infty \frac{x^{p-1}}{(1+x)^{p+q}} dx. \tag{B.21}$$

Using its properties we can find that (only for the second sum in equation (B.20))

$$\begin{aligned} \int_0^\infty \frac{x^{\alpha+n}}{(1+x)^{2n+2\beta}} dx &= \mathrm{B}(\alpha+n+1, n+2\beta-\alpha-1) \\ &= \Gamma(\alpha+1)\Gamma(2\beta-\alpha-1)\frac{(\alpha+1)_n (2\beta-\alpha-1)_n}{\Gamma(2\beta+2n)}. \end{aligned} \tag{B.22}$$

Another required property pertains to the Pochamer symbol:

$$(2\beta)_n = 2^{2n} (\beta)_n \, (\beta+1/2)_n. \tag{B.23}$$

Hence the second sum in equation (B.20) can be completed to obtain an hypergeometric function ${}_2F_1$, by identification:

$$\begin{aligned}
&\sum_{n=n_0}^{\infty} \frac{(\beta)_n}{n!} 2^n (1-z)^n \int_0^{\infty} \frac{x^{\alpha+n}}{(1+x)^{2n+2\beta}} dx \\
&= \mathrm{B}(\alpha+1, 2\beta-\alpha-1)\ {}_2\mathrm{F}_1(\alpha+1, 2\beta-\alpha-1; \beta+\frac{1}{2}, \frac{1-z}{2}) \\
&- \sum_{n=0}^{n_0-1} \mathrm{B}(\alpha+1, 2\beta-\alpha-1) \frac{(\alpha+1)_n\,(2\beta-\alpha-1)_n}{n!\left(\beta+\frac{1}{2}\right)_n} \left(\frac{1-z}{2}\right)^n,
\end{aligned} \tag{B.24}$$

where we completed the hypergeometri function, given by

$$\mathrm{F}(a, b; c, y) = \sum_{n=0}^{\infty} \frac{(a)_n (b)_n}{n!(c)_n} y^n. \tag{B.25}$$

With equation (B.24) we can complete all the integrals that appear in the gap equation, number equation, grand potential, and correlation lengths of the 3D case with a contact interaction. When summing all the terms that diverge individually in the first sum of equation (B.20) with the ones of another integral, we obtain finite physical results. That is:

$$\left| \sum_{n=0}^{n_0-1} \frac{(\beta)_n}{n!} 2^n (1-z)^n \int_0^{\infty} \frac{x^{\alpha+n}}{(1+x)^{2n+2\beta}} dx \ + \ \Big[\text{Divergent terms from another integral}\Big] \right| < \infty. \tag{B.26}$$

Appendix C

Universality of density correlation functions

This is the appendix of Chapter 5. In section C.1 we give the details for calculating the analytical expressions the density-density correlation functions $C_{\uparrow\uparrow}(r)$ and $C_{\uparrow\downarrow}(r)$ for the 2D case. In section C.2 we give the steps for approximating the large-distance behavior of the pair wave function $\phi_{\mathrm{BCS}}(r)$ in 2D.

C.1 Calculation of density correlation functions in 2D

C.1.1 Same spins

We will obtain explictly the function $g_{\uparrow\uparrow}(r)$ that corresponds to the Fourier transform of $v_{\vec{k}}^2$. We will use equation (5.43) with the parameters $\nu = 0$, $\mu = 1$

$$\begin{aligned} c &= \kappa, \\ b &= i, \\ a &= \left[\frac{\sqrt{\tilde{\mu}^2 + \tilde{\Delta}^2} - \tilde{\mu}}{2}\right]^{1/2} = \sqrt{1-\tilde{\mu}}. \end{aligned} \tag{C.1}$$

The coefficient k is correct by definition, since we want to calculate a Hankel transform. The coefficient b was deduced from numerical calculations of $g_{\uparrow\uparrow}$, we expected to have an oscillatory function with a phase shift of $\pi/2$ relative to $g_{\uparrow\downarrow}(r)$, as shown in Figure 5.4. The coefficient b was chosen so as to agree with the large-distance exponential decay that we were trying to find. Then we have

$$\begin{aligned} \int_0^\infty x\, K_1(\sqrt{1-\tilde{\mu}}x)\, I_1(ix)\, J_0(\kappa x)\, dx &= -\frac{1}{i}\int_0^\infty x\, K_1(\sqrt{1-\tilde{\mu}}x)\, J_1(x)\, J_0(\kappa x)\, dx \\ &= \frac{e^{-i\pi/2}}{i\sqrt{2\pi(1-\tilde{\mu})}}\,\frac{Q_{1/2}^{1/2}(u)}{(u^2-1)^{1/4}} \end{aligned} \tag{C.2}$$

with

$$u = \frac{\kappa^2 - \tilde{\mu}}{2i\sqrt{1-\tilde{\mu}}} \tag{C.3}$$

Now we will show the form of the associated Legendre function of the second kind $Q_{1/2}^{1/2}(u)$. From equation (5.47) we have

$$\begin{aligned} Q_{1/2}^{1/2}(u) &= \frac{e^{i\pi/2}}{2^{3/2}}\frac{\Gamma(2)}{\Gamma(2)}\frac{\Gamma(1/2)(u^2-1)^{1/4}}{u^2}\ {}_2F_1\left(\frac{3}{2},1,2;\frac{1}{u^2}\right) \\ &= \frac{e^{i\pi/2}}{2^{3/2}}\frac{\sqrt{\pi}(u^2-1)^{1/4}}{u^2}\ {}_2F_1\left(\frac{3}{2},1,2;\frac{1}{u^2}\right), \end{aligned} \tag{C.4}$$

where we have introduced the hypergeometric function ${}_2F_1$. Then, it is necessary to obtain an explicit form for the hypergeometric function. To achieve this we will use its integral representation given in equation (5.48). If we set $z = 1/u^2$ we have

$$\begin{aligned} {}_2F_1\left(\frac{3}{2},1,2;z\right) &= \frac{1}{B(1,1)}\int_0^1 t^0(1-t)^0(1-tz)^{-3/2}dt \\ &= \int_0^1 (1-tz)^{-3/2}dt \\ &= \frac{2}{z}\left(\frac{1}{\sqrt{1-z}}-1\right), \end{aligned} \tag{C.5}$$

where we used the particular value of the beta function $B(1,1) = 1$. Rewriting our expressions with the variable u we have

$${}_2F_1\left(\frac{3}{2},1,2;\frac{1}{u^2}\right) = 2u^2\left(\frac{1}{\sqrt{1-\frac{1}{u^2}}}-1\right). \tag{C.6}$$

An important comment is in order. It is highly recommended to use the right side of equation (C.6) as it is. The reason is because we should be careful that when relating the Fourier transform and the Hankel transform, the functions with finite norm should have a transform with the same finite norm[1]. When extending the square root to the complex plane we must be cautious of not changing the logarithmic branch. Then, we must be careful when using operations like $z = 1/z^{-1}$ inside the square root, since a change of branch introduces phases. Going back to the associated Legendre function of the second kind in equation (C.4) we have

$$\begin{aligned} Q_{1/2}^{1/2}(u) &= \frac{e^{i\pi/2}}{2^{3/2}}\frac{\sqrt{\pi}(u^2-1)^{1/4}}{u^2}\ {}_2F_1\left(\frac{3}{2},1,2;\frac{1}{u^2}\right) \\ &= \frac{e^{i\pi/2}}{2^{3/2}}\frac{\sqrt{\pi}(u^2-1)^{1/4}}{u^2}\left[2u^2\left(\frac{1}{\sqrt{1-\frac{1}{u^2}}}-1\right)\right] \\ &= \frac{e^{i\pi/2}}{2^{1/2}}\sqrt{\pi}(u^2-1)^{1/4}\left(\frac{1}{\sqrt{1-\frac{1}{u^2}}}-1\right) \end{aligned} \tag{C.7}$$

[1]This affirmation is not so rigorous, but intuitive. We should use Plancherel theorem to see that if a function is integrable and square integrable, then its Fourier transform should be square integrable.

Then, returning to the Hankel transform, we have

$$\begin{aligned}\int_0^\infty x\, K_1(\sqrt{1-\tilde{\mu}}x)\, I_1(ix)\, J_0(\kappa x)\, dx &= -\frac{1}{i}\int_0^\infty x\, K_1((1-\tilde{\mu})^{1/2}x)\, J_1(x)\, J_0(\kappa x)\, dx \\ &= \frac{e^{-i\pi/2}}{i\sqrt{2\pi(1-\tilde{\mu})}}\,\frac{Q_{1/2}^{1/2}(u)}{(u^2-1)^{1/4}} \\ &= \frac{e^{-i\pi/2}}{i\sqrt{2\pi(1-\tilde{\mu})}}\,\frac{1}{(u^2-1)^{1/4}}\left[\frac{e^{i\pi/2}}{2^{1/2}}\sqrt{\pi}(u^2-1)^{1/4}\left(\frac{1}{\sqrt{1-\frac{1}{u^2}}}-1\right)\right] \\ &= \frac{1}{i2\sqrt{(1-\tilde{\mu})}}\left(\frac{1}{\sqrt{1-\frac{1}{u^2}}}-1\right).\end{aligned} \tag{C.8}$$

Hence we can substitute the value of $u = (\kappa^2-\tilde{\mu})/(2i\sqrt{1-\tilde{\mu}})$ to find that

$$\begin{aligned}\int_0^\infty x\, K_1(\sqrt{1-\tilde{\mu}}x)\, I_1(ix)\, J_0(\kappa x)\, dx &= -\frac{1}{i}\int_0^\infty x\, K_1((1-\tilde{\mu})^{1/2}x)\, J_1(x)\, J_0(\kappa x)\, dx \\ &= \frac{1}{i2\sqrt{(1-\tilde{\mu})}}\left(\frac{1}{\left(1-\frac{1}{u^2}\right)^{1/2}}-1\right) \\ &= \frac{1}{i2\sqrt{(1-\tilde{\mu})}}\left(\frac{\kappa^2-\tilde{\mu}}{[(\kappa^2-\tilde{\mu})^2+4(1-\tilde{\mu})]^{1/2}}-1\right)\end{aligned} \tag{C.9}$$

where we have used

$$1-\frac{1}{u^2} = 1-\frac{1}{-(\kappa^2-\tilde{\mu})^2/(4(1-\tilde{\mu}))} = 1+\frac{4(1-\tilde{\mu})}{(\kappa^2-\tilde{\mu})^2} = \frac{(\kappa^2-\tilde{\mu})^2+4(1-\tilde{\mu})}{(\kappa^2-\tilde{\mu})^2}. \tag{C.10}$$

Hence, from equation (C.9) we can identify the integral over the real numbers:

$$\int_0^\infty x\, K_1((1-\tilde{\mu})^{1/2}x)\, J_1(x)\, J_0(\kappa x)\, dx = \frac{1}{2\sqrt{(1-\tilde{\mu})}}\left(1-\frac{\kappa^2-\tilde{\mu}}{[(\kappa^2-\tilde{\mu})^2+4(1-\tilde{\mu})]^{1/2}}\right). \tag{C.11}$$

The relationship between v_κ^2 and $g_{\uparrow\uparrow}(\rho)$ is given by the following integral:

$$v_\kappa^2 = \frac{(2\pi)}{k_F^2}\int_0^\infty g_{\uparrow\uparrow}(\rho)\rho J_0(\kappa\rho)d\rho, \tag{C.12}$$

where we have scaled quantities with k_F, and we have performed the change of variables $\kappa = k/k_F$ and $\rho = k_F r$. What we will do is to find a suitable function $g_{\uparrow\uparrow}(\rho)$ using equation (C.11). Let

$$g_{\uparrow\uparrow}(\rho) = \Theta K_1((1-\tilde{\mu})^{1/2}\rho)\, J_1(\rho), \tag{C.13}$$

with Θ a constant to be determined. Then we should have

$$\begin{aligned} v_\kappa^2 &= \frac{(2\pi)}{k_F^2}\int_0^\infty g_{\uparrow\uparrow}(\rho)\rho J_0(\kappa\rho)d\rho \\ &= \frac{(2\pi)}{k_F^2}\Theta\int_0^\infty K_1((1-\tilde{\mu})^{1/2}\rho)\,J_1(\rho)\rho J_0(\kappa\rho)d\rho \\ &= \frac{(2\pi)}{k_F^2}\Theta\frac{1}{\sqrt{(1-\tilde{\mu})}}\left[\frac{1}{2}\left(1-\frac{\kappa^2-\tilde{\mu}}{[(\kappa^2-\tilde{\mu})^2+4(1-\tilde{\mu})]^{1/2}}\right)\right]. \end{aligned} \tag{C.14}$$

Since

$$v_\kappa^2 = \frac{1}{2}\left(1-\frac{\kappa^2-\tilde{\mu}}{[(\kappa^2-\tilde{\mu})^2+4(1-\tilde{\mu})]^{1/2}}\right), \tag{C.15}$$

we can use $\tilde{\Delta}^2 = 4(1-\tilde{\mu})$ to obtain from equation (C.14) the following condition:

$$1 = \frac{(2\pi)}{k_F^2}\Theta\frac{1}{\sqrt{(1-\tilde{\mu})}}, \tag{C.16}$$

from where we can determine Θ,

$$\Theta = \frac{k_F^2}{(2\pi)}\sqrt{1-\tilde{\mu}} = \frac{k_F^2\tilde{\Delta}}{4\pi}. \tag{C.17}$$

Hence we obtain

$$g_{\uparrow\uparrow}(\rho) = \frac{\tilde{\Delta}k_F^2}{4\pi}K_1((1-\tilde{\mu})^{1/2}\rho)\,J_1(\rho), \tag{C.18}$$

where $\rho = k_F r$.

C.1.2 Opposite spins

We will address the opposite spins correlation function. Given that we have polar symmetry, $u_{\vec{k}}v_{\vec{k}}$ depends on the norm of the wave vector k, and the Fourier transform can be expressed as a Hankel transform [88]

$$g_{\uparrow\downarrow}(\vec{r}) = g_{\uparrow\downarrow}(r) = \frac{1}{(2\pi)}\int_0^\infty dk\,k\,u_{\vec{k}}v_{\vec{k}}\,J_0(kr). \tag{C.19}$$

Also, it is worth remembering how to obtain $u_{\vec{k}}v_{\vec{k}}$ when we know $g_{\uparrow\downarrow}(r)$ since this integral will be the one found in a table of integrals [147],

$$u_{\vec{k}}v_{\vec{k}} = \int d^2\vec{r}e^{-i\vec{k}\cdot\vec{r}}g_{\uparrow\downarrow}(r). \tag{C.20}$$

If we express this integral in polar coordinates we obtain

$$\begin{aligned} u_{\vec{k}}v_{\vec{k}} &= \int_0^\infty r\,dr\int_0^{2\pi}d\theta e^{-ikr\cos(\theta)}g_{\uparrow\downarrow}(r) \\ &= \int_0^\infty rg_{\uparrow\downarrow}(r)(2\pi)J_0(-kr)\,dr, \end{aligned} \tag{C.21}$$

where we have used the integral representation of the Bessel function of the first kind of order zero

$$(2\pi)J_0(-kr) = \int_0^{2\pi} d\theta e^{-ikr\cos(\theta)}. \tag{C.22}$$

Using the parity property of the Bessel function, $J_0(kr) = J_0(-kr)$, we get

$$u_{\vec{k}}v_{\vec{k}} = (2\pi)\int_0^{\infty} g_{\uparrow\downarrow}(r) r J_0(kr)\, dr. \tag{C.23}$$

Scaling with k_F and performing a change of variable $\kappa = k/k_F$ and $\rho = k_F r$ we have

$$u_\kappa v_\kappa = \frac{(2\pi)}{k_F^2}\int_0^{\infty} g_{\uparrow\downarrow}(\rho)\rho J_0(\kappa\rho) d\rho. \tag{C.24}$$

We will find a function $g_{\uparrow\downarrow}(\rho)$ that allows us to obtain $u_\kappa v_\kappa = \tilde{\Delta}2^{-1}[(\kappa^2 - \tilde{\mu})^2 + \tilde{\Delta}^2]^{-1/2}$. The search for this function is based in the special case of equation (C.19) when the chemical potential is zero [122]. We will use the following result, obtained from Ref. [147],

$$\begin{aligned}\int_0^{\infty} x J_0(ax)K_0(bx)J_0(cx)\, dx &= [a^4 + b^4 + c^4 - 2a^2c^2 + 2a^2b^2 + 2b^2c^2]^{-1/2} \\ &= \{[b^2 + (a-c)^2]\,[b^2 + (a+c)^2]\}^{-1/2},\end{aligned} \tag{C.25}$$

where $\mathrm{Re}[b] > |\mathrm{Im}[a]|$ y $c > 0$. This result can also be found in [149]. The analysis of the large-distance behavior allowed us to choose correctly the coefficientes in the following way[2]

$$a = 1, \tag{C.26}$$

$$b = \left[\frac{\sqrt{\tilde{\mu}^2 + \tilde{\Delta}^2} - \tilde{\mu}}{2}\right]^{1/2}, \tag{C.27}$$

$$c = \kappa. \tag{C.28}$$

Remarkably, the value of b is the one that determines the large-distance behavior, so we will verify that it is correct. The value of c is correct by definition, since we want to calculate a Hankel transform. The value of $a = 1$ was chosen since the nodes of $g_{\uparrow\downarrow}(r)$ in numerical calculations, agree with the zeros of $J_0(k_F r)$. Let us compare the right side of equation (C.25) with the square root in the denominator of $u_\kappa v_\kappa$. We should have

$$(\kappa^2 - \tilde{\mu})^2 + \tilde{\Delta}^2 = [b^2 + (1-\kappa)^2][b^2 + (1+\kappa)^2] \tag{C.29}$$

Expanding both sides we have

$$\begin{aligned}\kappa^4 + \tilde{\mu}^2 - 2\tilde{\mu}\kappa^2 + \tilde{\Delta}^2 &= b^4 + b^2(1 + \kappa^2 + 2\kappa) + b^2(1 + \kappa^2 - 2\kappa) + (1-\kappa^2)^2 \\ &= b^4 + 2b^2 + 1 + 2(b^2 - 1)\kappa^2 + \kappa^4\end{aligned} \tag{C.30}$$

[2]Despite the simplicity of the final calculation presented here, we must mention that the search for this integral was not so easy, since we analyzed several integrals given in Ref. [147].

From the coefficients of κ^2 we find:

$$2(b^2 - 1) = -2\tilde{\mu} \tag{C.31}$$

Then

$$b^2 = -\tilde{\mu} + 1. \tag{C.32}$$

Using the condition obtained from the number equation, given in equation (4.91),

$$1 = \frac{\tilde{\mu}}{2} + \frac{\sqrt{\tilde{\mu}^2 + \tilde{\Delta}^2}}{2}, \tag{C.33}$$

we find that

$$b^2 = \frac{\sqrt{\tilde{\mu}^2 + \tilde{\Delta}^2} - \tilde{\mu}}{2}. \tag{C.34}$$

Also we can verify that the constant terms in equation (C.30) agree:

$$b^4 + 2b^2 + 1 = \tilde{\mu}^2 + \tilde{\Delta}^2 \tag{C.35}$$

If we substitute the value of b given in equation (C.34) se find

$$\begin{aligned} b^4 + 2b^2 + 1 &= (-\tilde{\mu} + 1)^2 + 2(1 - \tilde{\mu}) + 1 \\ &= \tilde{\mu}^2 - 4\tilde{\mu} + 4 \\ &= \tilde{\mu}^2 + \tilde{\Delta}^2, \end{aligned} \tag{C.36}$$

where in the last equality we used $\tilde{\mu} = 1 - \tilde{\Delta}^2/4$, which can be obtained combining the conditions of the gap and number equations, shown in equations (4.97) and (4.98). Then we can conclude that the value of b is right. We can go back to equation (C.25) which explicitly is

$$\int_0^\infty \rho J_0(\rho) K_0\left(\left[\frac{(\tilde{\mu}^2 + \tilde{\Delta}^2)^{1/2} - \tilde{\mu}}{2}\right]^{1/2} \rho\right) J_0(\kappa\rho)\, d\rho = [(\kappa^2 - \tilde{\mu})^2 + \tilde{\Delta}^2]^{-1/2} \tag{C.37}$$

With this equation we can determine the functional form of $g_{\uparrow\downarrow}(\rho)$ in equation (C.24). Let

$$g_{\uparrow\downarrow}(\rho) = \Theta J_0(\rho) K_0\left(\left[\frac{(\tilde{\mu}^2 + \tilde{\Delta}^2)^{1/2} - \tilde{\mu}}{2}\right]^{1/2} \rho\right), \tag{C.38}$$

where Θ is a constant to be determined. When substituting in equation (C.24) and using equation (C.37) we have

$$\frac{\tilde{\Delta}}{2\sqrt{(\kappa^2 - \tilde{\mu})^2 + \tilde{\Delta}^2}} = \frac{(2\pi)}{k_F^2} \frac{\Theta}{[(\kappa^2 - \tilde{\mu})^2 + \tilde{\Delta}^2]^{1/2}}. \tag{C.39}$$

Then

$$\Theta = \frac{\tilde{\Delta} k_F^2}{4\pi} = \frac{2m}{\hbar^2 k_F^2} \frac{k_F^2 \Delta}{4\pi} = \frac{m\Delta}{2\pi\hbar^2}. \tag{C.40}$$

Hence we obtain

$$g_{\uparrow\downarrow}(\rho) = \frac{\tilde{\Delta} k_F^2}{4\pi} J_0(\rho) K_0\left(\left[\frac{(\tilde{\mu}^2 + \tilde{\Delta}^2)^{1/2} - \tilde{\mu}}{2}\right]^{1/2} \rho\right) = \frac{\tilde{\Delta} k_F^2}{4\pi} J_0(\rho) K_0\left(\frac{\rho}{\sqrt{2} k_F \chi_b}\right), \tag{C.41}$$

where $\rho = k_F r$. Rearranging terms, and substituting into equation (5.24) we obtain equation (5.52).

C.2 Large-distance approximation of the pair wave function in 2D

The following was taken from Ref. [17]. For large arguments we can approximate the Bessel function $J_0(kr)$, by [123]

$$J_0(kr) \approx \frac{e^{i(kr-\pi/4)} + e^{-i(kr-\pi/4)}}{\sqrt{2\pi kr}}. \tag{C.42}$$

We can substitute this approximation into the definition of the Hankel transform (5.41) to obtain

$$\phi_{\mathrm{BCS}}(r) \approx \frac{k_\Delta^{3/2}}{\sqrt{2\pi^3 r}}\left[\frac{S_+(r)e^{-i\pi/4} + S_-(r)e^{i\pi/4}}{2}\right], \tag{C.43}$$

where we divided the integrals using the following definition:

$$S_\pm(r) = \int_0^\infty \sqrt{p}\mathcal{F}(p)e^{\pm ipk_\Delta r}dp. \tag{C.44}$$

Also we have scaled the lengths with the wave vector k_Δ associated to the gap $\Delta = \hbar^2 k_\Delta^2/2m$. Since we will focus on the pair wave function we have

$$\mathcal{F}(p) = \sqrt{(p^2-\mu_\Delta)^2+1} - (p^2-\mu_\Delta), \tag{C.45}$$

where $\mu_\Delta = \mu/\Delta$. Performing the change of variable $p = e^{i\pi/2}x$ in $S_+(r)$ and $p = e^{-i\pi/2}x$ in $S_-(r)$ we obtain

$$\phi_{\mathrm{BCS}}(r) \approx -\frac{ik_\Delta^{3/2}}{2^{3/2}\sqrt{\pi^3 r}}\left[\int_{\mathbb{I}} \sqrt{x}\mathcal{F}(ix)e^{-xk_\Delta r}dx\right], \tag{C.46}$$

where we have joined the two integrals into one which is over the imaginary axis, from $x = -i\infty$ to $x = i\infty$. The integrand has five branch cuts, associated to the square roots, see equations (C.45) and (C.46). The one associated to $\sqrt{x}$ is a spurious branch cut that comes from the approximation of the Bessel function $J_0(kr)$. The other four branch cuts are determined by:

$$\mathrm{Re}[(x^2+\mu_\Delta)^2+1] \le 0, \text{ and } \mathrm{Im}[(x^2+\mu_\Delta)^2+1] = 0. \tag{C.47}$$

Using $x = a + ib$ we can find that those branch cuts are given by the points of the hyperbola $b^2 - a^2 = \mu_\Delta$ whose magnitude satisfies $|x|^2 \ge (\mu_\Delta^2+1)^{1/2}$. Since the integrand on the right side of equation (C.46) decreases exponentially for $\mathrm{Re}\, x \to \infty$, we can close a contour to the right side of the complex plane with a semicircle-like contour, which surrounds infinitesimally two branch cuts, as illustrated in Figure C.1.

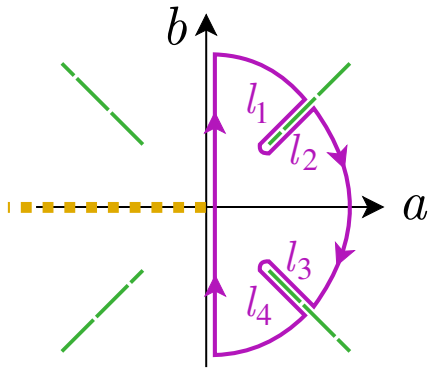

Figure C.1: Qualitative illustration of the branch cuts of the integrand in equation (C.46). The large dashes (green) correspond to the branch cuts of $\mathcal{F}(ix)$, see equation (C.45), while the short dashes (orange) to the branch cut of $\sqrt{x}$. The solid line (purple) represents the contour used in the Cauchy's integral formula in equation (C.48). Close to the branch cuts we have four paths denoted by l_i, with $i = 1, 2, 3, 4$. Figure taken from [17].

Given that we have a closed contour $\mathcal{C}$, we can use Cauchy's integral formula to obtain [123]

$$\oint_{\mathcal{C}} \sqrt{x}\mathcal{F}(ix)e^{-xk_\Delta r}dx = 0, \tag{C.48}$$

Taking the radius of the semicircle to infinity, we get

$$\begin{aligned}\int_{\mathbb{I}} \sqrt{x}\mathcal{F}(ix)e^{-xk_\Delta r}dx =& 2\int_{l_2} \sqrt{x}\sqrt{|(x^2+\mu_\Delta)^2+1|}e^{-i\pi/2}e^{-xk_\Delta r}dx \\ &+ 2\int_{l_4} \sqrt{x}\sqrt{|(x^2+\mu_\Delta)^2+1|}e^{-i\pi/2}e^{-xk_\Delta r}dx,\end{aligned} \tag{C.49}$$

where l_2 and l_4 are the paths shown in Figure C.1. The parametrization of l_2 is given by $\gamma_2(t) = t + i(t^2+\mu_\Delta)^{1/2}$, while the parametrization of l_4 is $\gamma_4(t) = t - i(t^2+\mu_\Delta)^{1/2}$, with $t \in [t_0, \infty)$, where

$$t_0 = \left(\frac{(\mu_\Delta^2+1)^{1/2} - \mu_\Delta}{2}\right)^{1/2}. \tag{C.50}$$

Using the explicit parametrizations $\gamma_2(t)$ and $\gamma_4(t)$ we can join the two integrals in equation (C.49) into one integral:

$$\int_{\mathbb{I}} \sqrt{x}\mathcal{F}(ix)e^{-xk_\Delta r}dx = 4\int_{t_0}^{\infty} \sqrt{4t^2(t^2+\mu_\Delta)-1}e^{-i\pi/2}e^{-tk_\Delta r}\mathrm{Re}[e^{-i\sqrt{t^2+\mu_\Delta}}\sqrt{\gamma_2(t)}\gamma_2'(t)]dt. \tag{C.51}$$

Noticing that the branch cuts always remain in their own quadrant we can obtain an alternative expression for $\gamma_2(t)$ and its derivative. We can use de Moivre's formula to obtain

$$\gamma_2(t) = (2t^2+\mu_\Delta)^{1/2}[\cos\,\theta(t) + i\sin\,\theta(t)], \tag{C.52}$$

where we have defined the function

$$\theta(t) = \arctan\left(\frac{\sqrt{t^2+\mu_\Delta}}{t}\right). \tag{C.53}$$

This form allows us to handle the factor $\sqrt{\gamma_2(t)}$ in equation (C.51), since we can divide the respective angle $\theta(t)$. Then we get

$$\begin{aligned}\int_{\mathbb{I}} \sqrt{x}\mathcal{F}(ix)e^{-xk_\Delta r}dx =& 4\int_{t_0}^{\infty} \sqrt{4t^2(t^2+\mu_\Delta)-1}\; e^{-i\pi/2}e^{-tk_\Delta r}(2t^2+\mu_\Delta)^{1/4} \\ &\times\left\{\cos(\sqrt{t^2+\mu_\Delta})\left[\cos(\theta(t)/2)-\frac{t\sin(\theta(t)/2)}{\sqrt{t^2+\mu_\Delta}}\right]\right. \\ &\left.+\sin(\sqrt{t^2+\mu_\Delta})\left[\frac{t\cos(\theta(t)/2)}{\sqrt{t^2+\mu_\Delta}}+\sin(\theta(t)/2)\right]\right\}dt.\end{aligned} \tag{C.54}$$

After substituting equation (C.54) into equation (C.46) and scaling variables with the Fermi wave number k_F instead of k_Δ we obtain the desired result, corresponding to equation (5.61),

$$\begin{aligned}\phi_{\mathrm{BCS}}(r) \propto \frac{1}{\sqrt{k_F r}}\int_{\tau_0}^{\infty} e^{-\tau k_F r}\left(\frac{2\tau^2+\tilde{\mu}}{\tilde{\Delta}}\right)^{1/4}&\left[\cos\left(\sqrt{\frac{\tau^2+\tilde{\mu}}{\tilde{\Delta}}}\right)\left(\cos(\theta(\tau)/2)-\frac{\tau\sin(\theta(\tau)/2)}{\sqrt{\tau^2+\tilde{\mu}}}\right)\right. \\ &\left.+\sin\left(\sqrt{\frac{\tau^2+\tilde{\mu}}{\tilde{\Delta}}}\right)\left(\frac{\tau\cos(\theta(\tau)/2)}{\sqrt{\tau^2+\tilde{\mu}}}+\sin(\theta(\tau)/2)\right)\right]\left(\frac{\sqrt{4\tau^2(\tau^2+\tilde{\mu})-\tilde{\Delta}^2}}{\tilde{\Delta}}\right)d\tau,\end{aligned} \tag{C.55}$$

where $\tau_0 = \{[(\tilde{\mu}^2+\tilde{\Delta}^2)^{1/2}-\tilde{\mu}]/2\}^{1/2}$, and we have redefined the function

$$\theta(\tau) = \tan^{-1}\left(\frac{\sqrt{\tau^2+\tilde{\mu}}}{\tau}\right). \tag{C.56}$$

Bibliography

[1] Quantum technologies in a nutshell, https://qt.eu/about-quantum-flagship/quantum-technologies-in-a-nutshell (Consultado el 26 de abril de 2023).

[2] W. Ketterle and M. W. Zwierlein, Making, probing and understanding ultracold fermi gases, arXiv preprint arXiv:0801.2500 (2008).

[3] D. Hernández-Rajkov, J. Padilla-Castillo, M. Mendoza-López, R. Colín-Rodríguez, A. Gutiérrez-Valdés, S. Morales-Ramírez, R. Gutiérrez-Arenas, C. Gardea-Flores, R. Jáuregui-Renaud, J. Seman, *et al.*, Experimental setup for the production of ultracold strongly correlated fermionic superfluids of 6li, Revista mexicana de física **66**, 388 (2020).

[4] J. A. Sobota, Y. He, and Z.-X. Shen, Angle-resolved photoemission studies of quantum materials, Rev. Mod. Phys. **93**, 025006 (2021).

[5] S. Gupta, Z. Hadzibabic, M. W. Zwierlein, C. A. Stan, K. Dieckmann, C. H. Schunck, E. G. M. van Kempen, B. J. Verhaar, and W. Ketterle, Radio-frequency spectroscopy of ultracold fermions, Science **300**, 1723 (2003), https://www.science.org/doi/pdf/10.1126/science.1085335 .

[6] J. M. Jasinski, B. S. Meyerson, and B. A. Scott, Mechanistic studies of chemical vapor deposition, Annual Review of Physical Chemistry **38**, 109 (1987), https://doi.org/10.1146/annurev.pc.38.100187.000545 .

[7] I. Bloch, J. Dalibard, and W. Zwerger, Many-body physics with ultracold gases, Rev. Mod. Phys. **80**, 885 (2008).

[8] G. C. Strinati, P. Pieri, G. Roepke, P. Schuck, and M. Urban, The BCS–BEC crossover: From ultra-cold fermi gases to nuclear systems, Physics Reports **738**, 1 (2018).

[9] S. Giorgini, L. P. Pitaevskii, and S. Stringari, Theory of ultracold atomic fermi gases, Rev. Mod. Phys. **80**, 1215 (2008).

[10] C. J. Pethick and H. Smith, *Bose–Einstein condensation in dilute gases* (Cambridge university press, 2008).

[11] J. E. Padilla Castillo, *Time-averaged optical potentials for trapping and manipulating ultracold quantum 6Li gases*, Master's thesis, PCF-UNAM (2021).

[12] Y. Ohashi, H. Tajima, and P. van Wyk, Bcs–bec crossover in cold atomic and in nuclear systems, Progress in Particle and Nuclear Physics **111**, 103739 (2020).

[13] A. J. Leggett, Diatomic molecules and cooper pairs, in *Modern Trends in the Theory of Condensed Matter*, edited by A. Pękalski and J. A. Przystawa (Springer Berlin Heidelberg, Berlin, Heidelberg, 1980) pp. 13–27.

[14] C. H. Schunck, Y.-i. Shin, A. Schirotzek, and W. Ketterle, Determination of the fermion pair size in a resonantly interacting superfluid, Nature **454**, 739 (2008).

[15] J. Bardeen, L. N. Cooper, and J. R. Schrieffer, Theory of superconductivity, Phys. Rev. **108**, 1175 (1957).

[16] M. Randeria, J.-M. Duan, and L.-Y. Shieh, Superconductivity in a two-dimensional fermi gas: Evolution from cooper pairing to bose condensation, Phys. Rev. B **41**, 327 (1990).

[17] J. C. Obeso-Jureidini and V. Romero-Rochín, Density correlation functions and the spatial structure of the two-dimensional bec-bcs crossover, Phys. Rev. A **105**, 043307 (2022).

[18] J. C. Obeso-Jureidini and V. Romero-Rochín, Spatial structure of the pair wave function and the density correlation functions throughout the bec-bcs crossover, Phys. Rev. A **101**, 033619 (2020).

[19] J. C. Obeso-Jureidini, G. A. Dominguez-Castro, E. Neri, R. Paredes, and V. Romero-Rochín, Universal correlations along the bec-bcs crossover, (submitted to New Journal of Physics) arXiv preprint arXiv:2211.03832 (2022).

[20] K. Miyake, Fermi Liquid Theory of Dilute Submonolayer 3He on Thin 4He II Film: Dimer Bound State and Cooper Pairs, Progress of Theoretical Physics **69**, 1794 (1983), https://academic.oup.com/ptp/article-pdf/69/6/1794/5161819/69-6-1794.pdf .

[21] M. L. Cohen, The Fermi atomic pseudopotential, American Journal of Physics **52**, 695 (1984), https://pubs.aip.org/aapt/ajp/article-pdf/52/8/695/8503373/695_1_online.pdf .

[22] T.-L. Ho and R. B. Diener, Fermion superfluids of nonzero orbital angular momentum near resonance, Phys. Rev. Lett. **94**, 090402 (2005).

[23] A. L. Fetter and J. D. Walecka, *Quantum theory of many-particle systems* (Courier Corporation, 2012).

[24] M. Tinkham, *Introduction to superconductivity* (Courier Corporation, 2004).

[25] A. M. Kadin, Spatial structure of the cooper pair, Journal of superconductivity and novel magnetism **20**, 285 (2007).

[26] G. Ortiz and J. Dukelsky, BCS-to-BEC crossover from the exact bcs solution, Phys. Rev. A **72**, 043611 (2005).

[27] H. Bethe and R. Peierls, Quantum theory of the diplon, Proceedings of the Royal Society of London. Series A-Mathematical and Physical Sciences **148**, 146 (1935).

[28] F. Marsiglio, P. Pieri, A. Perali, F. Palestini, and G. C. Strinati, Pairing effects in the normal phase of a two-dimensional fermi gas, Phys. Rev. B **91**, 054509 (2015).

[29] A. Perali, F. Palestini, P. Pieri, G. C. Strinati, J. T. Stewart, J. P. Gaebler, T. E. Drake, and D. S. Jin, Evolution of the normal state of a strongly interacting fermi gas from a pseudogap phase to a molecular bose gas, Phys. Rev. Lett. **106**, 060402 (2011).

[30] J. Levinsen and M. M. Parish, Strongly interacting two-dimensional fermi gases, in *Annual Review of Cold Atoms and Molecules*, Chap. 1, pp. 1–75.

[31] D. M. Eagles, Possible pairing without superconductivity at low carrier concentrations in bulk and thin-film superconducting semiconductors, Phys. Rev. **186**, 456 (1969).

[32] G. Zhu and A. J. Leggett, BEC-BCS crossover with feshbach resonance for a three-hyperfine-species model, Phys. Rev. A **87**, 023627 (2013).

[33] D. E. Sheehy and L. Radzihovsky, Bec–bcs crossover, phase transitions and phase separation in polarized resonantly-paired superfluids, Annals of Physics **322**, 1790 (2007).

[34] J. J. Kinnunen, J. E. Baarsma, J.-P. Martikainen, and P. Törmä, The Fulde–Ferrell–Larkin–Ovchinnikov state for ultracold fermions in lattice and harmonic potentials: a review, Reports on Progress in Physics **81**, 046401 (2018).

[35] P. Nozieres and S. Schmitt-Rink, Bose condensation in an attractive fermion gas: From weak to strong coupling superconductivity, Journal of Low Temperature Physics **59**, 195 (1985).

[36] C. A. R. Sá de Melo, M. Randeria, and J. R. Engelbrecht, Crossover from bcs to bose superconductivity: Transition temperature and time-dependent ginzburg-landau theory, Phys. Rev. Lett. **71**, 3202 (1993).

[37] L. He, S. Mao, and P. Zhuang, Bcs–bec crossover in relativistic fermi systems, International Journal of Modern Physics A **28**, 1330054 (2013).

[38] B. DeMarco and D. S. Jin, Onset of fermi degeneracy in a trapped atomic gas, Science **285**, 1703 (1999), https://www.science.org/doi/pdf/10.1126/science.285.5434.1703 .

[39] C. A. Regal, M. Greiner, and D. S. Jin, Observation of resonance condensation of fermionic atom pairs, Phys. Rev. Lett. **92**, 040403 (2004).

[40] N. Chamel and P. Haensel, Physics of neutron star crusts, Living Reviews in relativity **11**, 1 (2008).

[41] Q. Chen, K. Levin, and J. Stajic, Applying bcs–bec crossover theory to high-temperature superconductors and ultracold atomic fermi gases (review article), Low Temperature Physics **32**, 406 (2006), https://doi.org/10.1063/1.2199443 .

[42] G. Sun, L. He, and P. Zhuang, Bec-bcs crossover in the nambu-jona-lasinio model of qcd, Phys. Rev. D **75**, 096004 (2007).

[43] M. Randeria, Crossover from bcs theory to bose–einstein condensation, in *Bose-Einstein Condensation*, edited by A. Griffin, D. W. Snoke, and S. Stringari (Cambridge University Press, 1995) p. 355–392.

[44] G. Sarma, On the influence of a uniform exchange field acting on the spins of the conduction electrons in a superconductor, Journal of Physics and Chemistry of Solids **24**, 1029 (1963).

[45] P. Fulde and R. A. Ferrell, Superconductivity in a strong spin-exchange field, Phys. Rev. **135**, A550 (1964).

[46] A. Larkin and Y. N. Ovchinnikov, Nonuniform state of superconductors, Soviet Physics-JETP **20**, 762 (1965).

[47] C. C. Tsuei and J. R. Kirtley, Pairing symmetry in cuprate superconductors, Rev. Mod. Phys. **72**, 969 (2000).

[48] J. G. Bednorz and K. A. Müller, Possible high t c superconductivity in the ba- la- cu- o system, Zeitschrift für Physik B Condensed Matter **64**, 189 (1986).

[49] S. Rinott, K. B. Chashka, A. Ribak, E. D. L. Rienks, A. Taleb-Ibrahimi, P. L. Fevre, F. Bertran, M. Randeria, and A. Kanigel, Tuning across the bcs-bec crossover in the multiband superconductor fe1+ y se x te1- x: An angle-resolved photoemission study, Science Advances **3**, e1602372 (2017), https://www.science.org/doi/pdf/10.1126/sciadv.1602372 .

[50] Y. Cao, V. Fatemi, S. Fang, K. Watanabe, T. Taniguchi, E. Kaxiras, and P. Jarillo-Herrero, Unconventional superconductivity in magic-angle graphene superlattices, Nature **556**, 43 (2018).

[51] Y. Nakagawa, Y. Kasahara, T. Nomoto, R. Arita, T. Nojima, and Y. Iwasa, Gate-controlled bcs-bec crossover in a two-dimensional superconductor, Science **372**, 190 (2021), https://www.science.org/doi/pdf/10.1126/science.abb9860 .

[52] F. Pistolesi and G. C. Strinati, Evolution from bcs superconductivity to bose condensation: Role of the parameter $k_f\xi$, Phys. Rev. B **49**, 6356 (1994).

[53] M. de Llano, Unificación de la condensación de bose-einstein con la teoría bcs de superconductore, RECEN-Revista Ciências Exatas e Naturais **5**, 09 (2003).

[54] A. A. Shanenko, T. T. Saraiva, A. Vagov, A. S. Vasenko, and A. Perali, Suppression of fluctuations in a two-band superconductor with a quasi-one-dimensional band, Phys. Rev. B **105**, 214527 (2022).

[55] T. T. Saraiva, P. J. F. Cavalcanti, A. Vagov, A. S. Vasenko, A. Perali, L. Dell'Anna, and A. A. Shanenko, Multiband material with a quasi-1d band as a robust high-temperature superconductor, Phys. Rev. Lett. **125**, 217003 (2020).

[56] K. Ochi, H. Tajima, K. Iida, and H. Aoki, Resonant pair-exchange scattering and bcs-bec crossover in a system composed of dispersive and heavy incipient bands: A feshbach analogy, Phys. Rev. Res. **4**, 013032 (2022).

[57] Laboratorio Nacional de Materia Cuántica, `https://lanmac.org.mx/es` (Consultado el 26 de abril de 2023).

[58] The Nobel Prize in Physics 1997,
https : //*www.nobelprize.org*/*prizes*/*physics*/1997/*summary*/ (Consulted in abril 13, 2023.).

[59] The Nobel Prize in Physics 2001,
https : //*www.nobelprize.org*/*prizes*/*physics*/2001/*summary*/ (Consulted in abril 13, 2023.).

[60] A. Schmitt, Introduction to superfluidity, Lect. Notes Phys **888** (2015).

[61] P. Törmä, Physics of ultracold fermi gases revealed by spectroscopies, Physica Scripta **91**, 043006 (2016).

[62] S. Baier, M. J. Mark, D. Petter, K. Aikawa, L. Chomaz, Z. Cai, M. Baranov, P. Zoller, and F. Ferlaino, Extended bose-hubbard models with ultracold magnetic atoms, Science **352**, 201 (2016), https://www.science.org/doi/pdf/10.1126/science.aac9812 .

[63] J. Ibañez Azpiroz, A. Eiguren, A. Bergara, G. Pettini, and M. Modugno, Tight-binding models for ultracold atoms in honeycomb optical lattices, Phys. Rev. A **87**, 011602 (2013).

[64] G. Roati, C. D'Errico, L. Fallani, M. Fattori, C. Fort, M. Zaccanti, G. Modugno, M. Modugno, and M. Inguscio, Anderson localization of a non-interacting bose–einstein condensate, Nature **453**, 895 (2008).

[65] G. A. Domínguez-Castro and R. Paredes, The aubry–andré model as a hobbyhorse for understanding the localization phenomenon, European Journal of Physics **40**, 045403 (2019).

[66] M. G. Skou, K. K. Nielsen, T. G. Skov, A. M. Morgen, N. B. Jørgensen, A. Camacho-Guardian, T. Pohl, G. M. Bruun, and J. J. Arlt, Life and death of the bose polaron, Phys. Rev. Res. **4**, 043093 (2022).

[67] F. Scazza, G. Valtolina, P. Massignan, A. Recati, A. Amico, A. Burchianti, C. Fort, M. Inguscio, M. Zaccanti, and G. Roati, Repulsive fermi polarons in a resonant mixture of ultracold ^{6}Li atoms, Phys. Rev. Lett. **118**, 083602 (2017).

[68] A. Celi, A. Sanpera, V. Ahufinger, and M. Lewenstein, Quantum optics and frontiers of physics: the third quantum revolution, Physica Scripta **92**, 013003 (2016).

[69] W. Zwerger, *The BCS-BEC crossover and the unitary Fermi gas*, Vol. 836 (Springer Science & Business Media, 2011).

[70] H. T. Stoof, K. B. Gubbels, and D. Dickerscheid, *Ultracold quantum fields* (Springer, 2009).

[71] D. Hernández Rajkov, *Non-destructive and high resolution imaging techniques for studying ultracold quantum gases*, Master's thesis, PCF-UNAM (2021).

[72] R. A. Zamora Zamora, *Excitaciones cuánticas macroscópicas en condensados de Bose-Einstein: vórtices, skyrmiones y turbulencia*, Ph.D. thesis, PCF-UNAM (2018).

[73] M. E. Gehm, *Preparation of an optically-trapped degenerate Fermi gas of 6Li: Finding the route to degeneracy*, Ph.D. thesis, Duke University, North Carolina (2003).

[74] E. Arimondo, M. Inguscio, and P. Violino, Experimental determinations of the hyperfine structure in the alkali atoms, Rev. Mod. Phys. **49**, 31 (1977).

[75] G. Breit and I. I. Rabi, Measurement of nuclear spin, Phys. Rev. **38**, 2082 (1931).

[76] N. Ramsey, *Molecular beams*, Vol. 20 (Oxford University Press, 1956).

[77] C. Chin, R. Grimm, P. Julienne, and E. Tiesinga, Feshbach resonances in ultracold gases, Rev. Mod. Phys. **82**, 1225 (2010).

[78] M.-O. Mewes, G. Ferrari, F. Schreck, A. Sinatra, and C. Salomon, Simultaneous magneto-optical trapping of two lithium isotopes, Phys. Rev. A **61**, 011403 (1999).

[79] W. Demtröder, *Atoms, Molecules and Photons: An Introduction to Atomic-, Molecular- and Quantum Physics*, Graduate Texts in Physics (Springer Berlin Heidelberg, 2010).

[80] A. J. Moerdijk, B. J. Verhaar, and A. Axelsson, Resonances in ultracold collisions of ^{6}Li, ^{7}Li, and ^{23}Na, Phys. Rev. A **51**, 4852 (1995).

[81] G. Andrade-Sanchez and V. Romero-Rochin, Potential and feshbach *s*-wave resonances in coupled atomic collision channels, arXiv preprint arXiv:2306.09236 (2023).

[82] M. Bartenstein, A. Altmeyer, S. Riedl, R. Geursen, S. Jochim, C. Chin, J. H. Denschlag, R. Grimm, A. Simoni, E. Tiesinga, C. J. Williams, and P. S. Julienne, Precise determination of ^{6}Li cold collision parameters by radio-frequency spectroscopy on weakly bound molecules, Phys. Rev. Lett. **94**, 103201 (2005).

[83] L. E. Ballentine, *Quantum mechanics: a modern development* (World Scientific Publishing Company, 1998).

[84] R. G. Newton, *Scattering Theory of Waves and Particles* (Springer Berlin, Heidelberg, 1982).

[85] J. Taylor, *Scattering Theory: Quantum Theory on Nonrelativistic Collisions* (Wiley, 1972).

[86] P. Jeszenszki, A. Y. Cherny, and J. Brand, s-wave scattering length of a gaussian potential, Phys. Rev. A **97**, 042708 (2018).

[87] D. Griffiths, *Introduction to Quantum Mechanics*, Pearson international edition (Pearson Prentice Hall, 2005).

[88] G. B. Arfken and H. Weber, *Mathematical Methods for Physicists, Burlington, MA* (Elsevier, 2005).

[89] J. J. Sakurai, J. Napolitano, *et al.*, *Modern quantum mechanics* (Pearson Harlow, 2014).

[90] S. K. Adhikari, Quantum scattering in two dimensions, American Journal of Physics **54**, 362 (1986), https://doi.org/10.1119/1.14623 .

[91] S. A. Morgan, M. D. Lee, and K. Burnett, Off-shell t matrices in one, two, and three dimensions, Phys. Rev. A **65**, 022706 (2002).

[92] E. Neri Medina, *Termodinámica de un gas de fermiones con interacción en el régimen de bajas temperaturas, Cruce BEC-BCS*, Ph.D. thesis, PCF-UNAM (2011).

[93] T. Wu and T. Ohmura, *Quantum Theory of Scattering*, International series in physics (Prentice-Hall, 1962).

[94] M. Bartenstein, *From Molecules to Cooper pairs: Experiments in the BEC-BCS Crossover*, Ph.D. thesis, Fakultät für Mathematik, Informatik und Physik der Leopold-Franzens-Universität Innsbruck (2005).

[95] L. R. Mead and J. Godines, An analytical example of renormalization in two-dimensional quantum mechanics, American Journal of Physics **59**, 935 (1991), https://doi.org/10.1119/1.16675 .

[96] N. Ashcroft and N. Mermin, *Solid State Physics* (Saunders College Publishing, Fort Worth, 1976).

[97] I. R. Lapidus, Quantum-mechanical scattering in two dimensions, American Journal of Physics **50**, 45 (1982), https://doi.org/10.1119/1.13004 .

[98] L. D. Landau and E. M. Lifshitz, *Quantum mechanics: non-relativistic theory*, Vol. 3 (Elsevier, 2013).

[99] F. Werner and Y. Castin, General relations for quantum gases in two and three dimensions: Two-component fermions, Phys. Rev. A **86**, 013626 (2012).

[100] E. Merzbacher, *Quantum Mechanics* (Wiley, 1998).

[101] H. R. Sadeghpour, J. L. Bohn, M. J. Cavagnero, B. D. Esry, I. I. Fabrikant, J. H. Macek, and A. R. P. Rau, Collisions near threshold in atomic and molecular physics, Journal of Physics B: Atomic, Molecular and Optical Physics **33**, R93 (2000).

[102] W. H. Press, S. A. Teukolsky, W. T. Vetterling, and B. P. Flannery, *Numerical recipes 3rd edition: The art of scientific computing* (Cambridge university press, 2007).

[103] E. Neri, S. F. Caballero-Benítez, V. Romero-Rochín, and R. Paredes, Pairing and molecule formation along the BCS-BEC crossover for finite range potentials, Physica Scripta **95**, 034013 (2020).

[104] S. F. Caballero-Benítez, R. Paredes, and V. Romero-Rochín, The contact in the BCS–BEC crossover for finite range interacting ultracold fermi gases, Physics Letters A **377**, 1756 (2013).

[105] S. J. J. M. F. Kokkelmans, J. N. Milstein, M. L. Chiofalo, R. Walser, and M. J. Holland, Resonance superfluidity: Renormalization of resonance scattering theory, Phys. Rev. A **65**, 053617 (2002).

[106] W. Rarita and R. D. Present, On the nuclear two-, three- and four-body problems, Phys. Rev. **51**, 788 (1937).

[107] J. Rowlinson, The yukawa potential, Physica A: Statistical Mechanics and its Applications **156**, 15 (1989).

[108] P. C. Hohenberg, Existence of long-range order in one and two dimensions, Phys. Rev. **158**, 383 (1967).

[109] R. Paredes and V. Romero-Rochín, Teoría BCS, Consulted in august 6, 2018 (www.fisica.unam.mx/personales/romero/MC/FERMI.pdf).

[110] A. Abrikosov, L. Gorkov, I. Dzyaloshinski, and R. Silverman, *Methods of Quantum Field Theory in Statistical Physics*, Dover Books on Physics (Dover Publications, 2012).

[111] H. Bruus, K. Flensberg, and Ø. Flensberg, *Many-Body Quantum Theory in Condensed Matter Physics: An Introduction*, Oxford Graduate Texts (OUP Oxford, 2004).

[112] N. N. Bogoljubov, On a new method in the theory of superconductivity, Il Nuovo Cimento **7**, 794 (1958).

[113] J. G. Valatin, Comments on the theory of superconductivity, Il Nuovo Cimento **7**, 843 (1958).

[114] A. J. Leggett, A theoretical description of the new phases of liquid ^{3}He, Rev. Mod. Phys. **47**, 331 (1975).

[115] H. Stoof, D. Dickerscheid, and K. Gubbels, *Ultracold Quantum Fields*, Theoretical and Mathematical Physics (Springer Netherlands, 2008).

[116] R. K. Pathria, *Statistical Mechanics*, International series of monographs in natural philosophy (Elsevier Science & Technology Books, 1972).

[117] J. M. Blatt, Electron Pairs in the Theory of Superconductivity, Progress of Theoretical Physics **23**, 447 (1960), https://academic.oup.com/ptp/article-pdf/23/3/447/5206014/23-3-447.pdf .

[118] M. Feld, B. Fröhlich, E. Vogt, M. Koschorreck, and M. Köhl, Observation of a pairing pseudogap in a two-dimensional fermi gas, Nature **480**, 75 (2011).

[119] C. Chin, M. Bartenstein, A. Altmeyer, S. Riedl, S. Jochim, J. H. Denschlag, and R. Grimm, Observation of the pairing gap in a strongly interacting fermi gas, Science **305**, 1128 (2004), https://www.science.org/doi/pdf/10.1126/science.1100818 .

[120] V. Romero-Rochín, Thermodynamic origin of the contact, Journal of Physics B: Atomic, Molecular and Optical Physics **44**, 095302 (2011).

[121] L. Salasnich, N. Manini, and A. Parola, Condensate fraction of a fermi gas in the bcs-bec crossover, Phys. Rev. A **72**, 023621 (2005).

[122] Wolfram Research, Inc., Wolfram mathematica 13 student edition (13.2.0.0, (2023)).

[123] J. E. Marsden and M. J. Hoffman, *Análisis básico de variable compleja* (Trillas, 1996).

[124] L. Salasnich and F. Toigo, Composite bosons in the two-dimensional bcs-bec crossover from gaussian fluctuations, Phys. Rev. A **91**, 011604 (2015).

[125] E. Taylor and M. Randeria, Apparent low-energy scale invariance in two-dimensional fermi gases, Phys. Rev. Lett. **109**, 135301 (2012).

[126] V. Romero-Rochín, Notes on many body theory of bose and fermi gases at low temperatures, Consultado 25 de mayo de 2019 (http://www.fisica.unam.mx/personales/romero/MC/Many-body.pdf).

[127] J. Negele and H. Orland, *Quantum Many Particle Systems* (Basic Books, 1995).

[128] M. Holten, L. Bayha, A. C. Klein, P. A. Murthy, P. M. Preiss, and S. Jochim, Anomalous breaking of scale invariance in a two-dimensional fermi gas, Phys. Rev. Lett. **121**, 120401 (2018).

[129] F. Reif, *Fundamentals of Statistical and Thermal Physics* (Waveland Press, Long Grove, Illinois, 2009).

[130] L. Salasnich, Condensate fraction of a two-dimensional attractive fermi gas, Phys. Rev. A **76**, 015601 (2007).

[131] A. T. Sommer, L. W. Cheuk, M. J. H. Ku, W. S. Bakr, and M. W. Zwierlein, Evolution of fermion pairing from three to two dimensions, Phys. Rev. Lett. **108**, 045302 (2012).

[132] S. Tan, Large momentum part of a strongly correlated fermi gas, Annals of Physics **323**, 2971 (2008).

[133] V. Ngampruetikorn, J. Levinsen, and M. M. Parish, Pair correlations in the two-dimensional fermi gas, Phys. Rev. Lett. **111**, 265301 (2013).

[134] M. Olshanii, H. Perrin, and V. Lorent, Example of a quantum anomaly in the physics of ultracold gases, Phys. Rev. Lett. **105**, 095302 (2010).

[135] J. S. Bell, Fluctuation compressibility theorem and its application to the pairing model, Phys. Rev. **129**, 1896 (1963).

[136] J. S. Bell, On the einstein podolsky rosen paradox, Physics Physique Fizika **1**, 195 (1964).

[137] B. Mukherjee, Z. Yan, P. B. Patel, Z. Hadzibabic, T. Yefsah, J. Struck, and M. W. Zwierlein, Homogeneous atomic fermi gases, Phys. Rev. Lett. **118**, 123401 (2017).

[138] Pitaevskiĭ, *Bose-Einstein Condensation and Superfluidity*.

[139] L. Landau and E. Lifshitz, *Statistical Physics, Part 1*, v. 5 (Elsevier Science, 2013).

[140] J. Eisert, Advanced quantum mechanics (20104301), Consultado 23 de marzo de 2023 (https://www.physik.fu-berlin.de/en/einrichtungen/ag/ag-eisert/teaching/ws18-19/AdvancedQuantumMechanicsChapter5.pdf).

[141] U. de Freitas, L. C. Ioriatti, and N. Studart, Theoretical study of a two-dimensional quantum system: electrons on a helium film, Journal of Physics C: Solid State Physics **20**, 5983 (1987).

[142] H. Stanley, *Introduction to Phase Transitions and Critical Phenomena*, International series of monographs on physics (Oxford University Press, 1971).

[143] F. Palestini and G. C. Strinati, Temperature dependence of the pair coherence and healing lengths for a fermionic superfluid throughout the bcs-bec crossover, Phys. Rev. B **89**, 224508 (2014).

[144] G. A. Dominguez Castro, *Desorden en sistemas con interacciones de largo y corto alcance*, Ph.D. thesis, PCF-UNAM (2022).

[145] C. N. Yang, Concept of off-diagonal long-range order and the quantum phases of liquid he and of superconductors, Rev. Mod. Phys. **34**, 694 (1962).

[146] T. Morita and S. Katsura, Calculation of the isothermal susceptibility by the kubo formula, Journal of Physics C: Solid State Physics **2**, 1030 (1969).

[147] I. Gradshteyn and I. Ryzhik, *Table of integrals, series, and products*, edited by D. Zwillinger and V. Moll (Academic press, 2014).

[148] H. Bateman, A. Erdélyi, W. Magnus, F. Oberhettinger, and F. G. Tricomi, *Higher transcendental functions* (McGraw-Hill, New York, 1953) volumes I and II.

[149] H. Bateman, A. Erdélyi, W. Magnus, F. Oberhettinger, and F. G. Tricomi, *Tables of integral transforms*, Vol. II (McGraw-Hill Book Company, New York, 1954).

[150] M. Peskin and D. Schroeder, *An Introduction To Quantum Field Theory*, Frontiers in Physics (Avalon Publishing, 1995).

[151] M. Marini, F. Pistolesi, and G. Strinati, Evolution from bcs superconductivity to bose condensation: analytic results for the crossover in three dimensions, The European Physical Journal B - Condensed Matter and Complex Systems **1**, 151 (1998).

[152] M. Casas, J. M. Getino, M. de Llano, A. Puente, R. M. Quick, H. Rubio, and D. M. van der Walt, Bcs-bose model of exotic superconductors: Generalized coherence length, Phys. Rev. B **50**, 15945 (1994).

[153] Y. Yerin, H. Tajima, P. Pieri, and A. Perali, Coexistence of giant cooper pairs with a bosonic condensate and anomalous behavior of energy gaps in the bcs-bec crossover of a two-band superfluid fermi gas, Phys. Rev. B **100**, 104528 (2019).

[154] L. Salasnich, Condensate formation with three-component ultracold fermions, Phys. Rev. A **83**, 033630 (2011).

[155] J. C. Obeso Jureidini, *Sistemas fermiónicos ultrafríos con cruce BEC-BCS*, Master's thesis, PCF-UNAM (2019).

[156] B. Lilia, R. Hennig, P. Hirschfeld, G. Profeta, A. Sanna, E. Zurek, W. E. Pickett, M. Amsler, R. Dias, M. I. Eremets, *et al.*, The 2021 room-temperature superconductivity roadmap, Journal of Physics: Condensed Matter **34**, 183002 (2022).

[157] D. Rybicki, M. Jurkutat, S. Reichardt, C. Kapusta, and J. Haase, Perspective on the phase diagram of cuprate high-temperature superconductors, Nature communications **7**, 11413 (2016).

[158] L. Pisani, P. Pieri, and G. C. Strinati, Spatial emergence of off-diagonal long-range order throughout the bcs-bec crossover, Phys. Rev. B **105**, 054505 (2022).

[159] A. Pelissetto and E. Vicari, Critical phenomena and renormalization-group theory, Physics Reports **368**, 549 (2002).

[160] D. J. Amit and V. Martin-Mayor, *Field theory, the renormalization group, and critical phenomena: graphs to computers* (World Scientific Publishing Company, 2005).

[161] C. Rylands, P. Calabrese, and B. Bertini, Solution of the bec to bcs quench in one dimension, Phys. Rev. Lett. **130**, 023001 (2023).

[162] A. L. Fetter, Spherical impurity in an infinite superconductor, Phys. Rev. **140**, A1921 (1965).

[163] S. Kamal, D. A. Bonn, N. Goldenfeld, P. J. Hirschfeld, R. Liang, and W. N. Hardy, Penetration depth measurements of 3d XY critical behavior in $\mathrm{yba_2cu_3o_{6.95}}$ crystals, Phys. Rev. Lett. **73**, 1845 (1994).

[164] I. Reyes-Ayala, F. J. Poveda-Cuevas, and V. Romero-Rochín, Non-classical critical exponents at bose–einstein condensation, Journal of Statistical Mechanics: Theory and Experiment **2019**, 113102 (2019).

[165] I. Reyes Ayala, *Transiciones de fase y fenómenos críticos en gases de bose ultrafríos*, Ph.D. thesis, PCF-UNAM (2019).

[166] J. D. Gunton and M. J. Buckingham, Condensation of the ideal bose gas as a cooperative transition, Phys. Rev. **166**, 152 (1968).

[167] J. C. Obeso-Jureidini, D. Olascoaga, and V. Romero-Rochín, Thermodynamic derivation of scaling at the liquid–vapor critical point, Entropy **23**, 10.3390/e23060720 (2021).

[168] M. Barmatz, I. Hahn, J. A. Lipa, and R. V. Duncan, Critical phenomena in microgravity: Past, present, and future, Rev. Mod. Phys. **79**, 1 (2007).

[169] F. Palestini, P. Pieri, and G. C. Strinati, Density and spin response of a strongly interacting fermi gas in the attractive and quasirepulsive regime, Phys. Rev. Lett. **108**, 080401 (2012).

[170] S. Ma, *Modern Theory Of Critical Phenomena* (Taylor & Francis, 2018).

[171] M. J. H. Ku, A. T. Sommer, L. W. Cheuk, and M. W. Zwierlein, Revealing the superfluid lambda transition in the universal thermodynamics of a unitary fermi gas, Science **335**, 563 (2012), https://www.science.org/doi/pdf/10.1126/science.1214987 .

[172] R. Sato, D. Kagamihara, K. Manabe, D. Inotani, and Y. Ohashi, Isothermal compressibility of an ultracold fermi gas in the bcs–bec crossover, Journal of Low Temperature Physics **196**, 119 (2019).

[173] D. Kagamihara, R. Sato, K. Manabe, H. Tajima, and Y. Ohashi, Isothermal compressibility and effects of multibody molecular interactions in a strongly interacting ultracold fermi gas, Phys. Rev. A **106**, 033308 (2022).

[174] L. N. Cooper, Bound electron pairs in a degenerate fermi gas, Phys. Rev. **104**, 1189 (1956).

[175] G. Bighin and L. Salasnich, Vortices and antivortices in two-dimensional ultracold fermi gases, Scientific Reports **7**, 1 (2017).

[176] M. Pini, P. Pieri, and G. Calvanese Strinati, Strong fulde-ferrell larkin-ovchinnikov pairing fluctuations in polarized fermi systems, Phys. Rev. Res. **3**, 043068 (2021).

[177] M. D. Croitoru and A. I. Buzdin, In search of unambiguous evidence of the fulde–ferrell–larkin–ovchinnikov state in quasi-low dimensional superconductors, Condensed Matter **2**, 10.3390/condmat2030030 (2017).

[178] E. Taylor, A. Griffin, N. Fukushima, and Y. Ohashi, Pairing fluctuations and the superfluid density through the bcs-bec crossover, Phys. Rev. A **74**, 063626 (2006).

[179] B. C. Mulkerin, L. He, P. Dyke, C. J. Vale, X.-J. Liu, and H. Hu, Superfluid density and critical velocity near the berezinskii-kosterlitz-thouless transition in a two-dimensional strongly interacting fermi gas, Phys. Rev. A **96**, 053608 (2017).

[180] P. A. Murthy, I. Boettcher, L. Bayha, M. Holzmann, D. Kedar, M. Neidig, M. G. Ries, A. N. Wenz, G. Zürn, and S. Jochim, Observation of the berezinskii-kosterlitz-thouless phase transition in an ultracold fermi gas, Phys. Rev. Lett. **115**, 010401 (2015).

[181] P. de Gennes, *Superconductivity of Metals and Alloys*, Advanced book classics (W.A. Benjamin, 1966).